Synthesis, group 10 metal-catalyzed cyclization reactions and hydroboration of polyynes

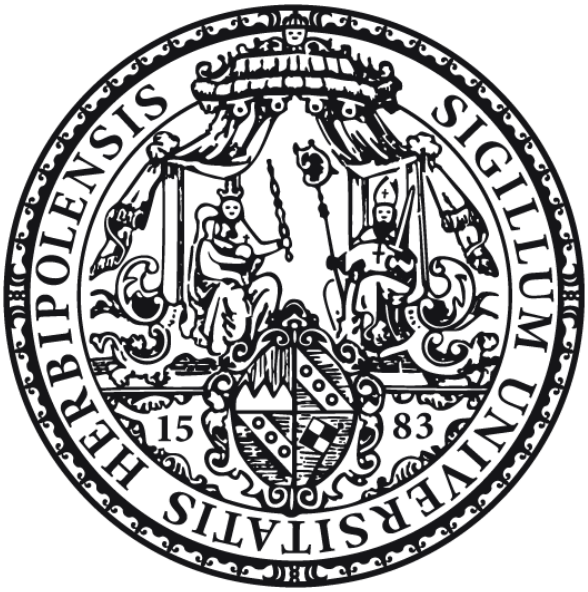

Dissertation zur Erlangung des naturwissenschaftlichen Doktorgrades

an der Fakultät für Chemie und Pharmazie

der Julius-Maximilians-Universität Würzburg

vorgelegt

von

Robert Ricker

aus Schwäbisch-Hall

Würzburg, im August 2022

Eingereicht bei der Fakultät für Chemie und Pharmazie am

_____

Gutachter der Dissertation

1. Gutachter: Prof. Dr. Dr. h.c. Todd B. Marder

2. Gutachter: Prof. Dr. Qing Ye

Prüfer des öffentlichen Promotionskolloquiums

1. Prüfer: Prof. Dr. Dr. h.c. Todd B. Marder

2. Prüfer: Prof. Dr. Qing Ye

3. Prüfer: _____

Tag des öffentlichen Promotionskolloquiums

_____

Doktorurkunde ausgehändigt am

_____

AFFIDAVIT

I hereby confirm that my thesis entitled “Synthesis, group 10 metal-catalyzed cyclization reactions and hydroboration of polyynes” is the result of my own work. I did not receive any help or support from commercial consultants. All sources and/or materials applied are listed and specified in the thesis.

Furthermore, I confirm that this thesis has not yet been submitted as part of another examination process neither in identical nor in similar form.

Würzburg, 2022 _____

EIDESSTATTLICHE ERKLÄRUNG

Hiermit erkläre ich an Eides statt, die Dissertation „Synthesis, group 10 metal-catalyzed cyclization reactions and hydroboration of polyynes“ eigenständig, d.h. insbesondere selbstständig und ohne Hilfe eines kommerziellen Promotionspartners angefertigt und keine anderen als die von mir angegebenen Quellen und Hilfsmittel verwendet zu haben.

Ich erkläre außerdem, dass die Dissertation weder in gleicher noch in ähnlicher Form bereits in einem anderen Prüfungsverfahren vorgelegen hat.

Würzburg, 2022 _____

List of Abbreviations

abs absorption
acac acetylacetonato
APCI atmospheric-pressure chemical ionization
ASAP atmospheric solids analysis probe
COSY correlation spectroscopy
CT charge-transfer
DA Diels-Alder
dba dibenzylideneacetone
DFT density-function theory
DMAD dimethylacetylene dicarboxylate
em emission
eq equivalent
ESI electrospray ionization
FWHM full width at half maximum
HDDA hexadehydro-Diels-Alder
HMBC heteronuclear multiple bond correlation
HOMO highest occupied molecular orbital
HPLC high performance liquid chromatography
HRMS high-resolution mass spectrometry
IC internal conversion
IRF instrument response function
ISC intersystem crossing
LIFDI liquid injection field desorption/ionization
LUMO lowest unoccupied molecular orbital
LE locally excited
NMR nuclear magnetic resonance
o- ortho
p- para
THF tetrahydrofuran
TLC thin-layer chromatography
TMS trimethylsilyl
TOF time of flight
TS transition state

Table of Contents

1. Palladium(0)-catalyzed bisdiyne annulations and photophysical characterization of the resulting naphthalene, azulene and 1,3-cylohexadiene derivatives.

Introduction

Metal-catalyzed cyclization reactions of alkynes provide convenient access to cyclic scaffolds from simple precursors.[1] The involvement of alkenes in alkyne cyclizations is of interest as an atom efficient method for the construction of cyclohexadienes, cyclohexenes and other cyclic products.[2] Cobalt-catalyzed [2+2+2] cycloaddition of *1,7*-diynes to (cyclo)alkenes has recently been used for the synthesis of 6,10-dihydroanthracyclinone structures, as precursors of several anthracycline derivatives, used as antineoplastics and antibiotics (Figure 1).[3] The most prominent palladium-catalyzed cyclizations involve electron deficient alkynes, such as dimethyl acetylenedicarboxylate (DMAD) and cyclizations of *in situ* generated benzynes.[4, 5]

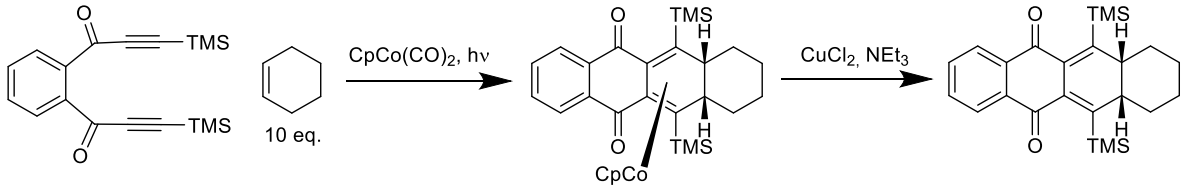

Figure 1: Synthesis of a dihydroanthracyclinone core by Co-catalyzed 1,7-diyne-olefin cyclization and oxidative demetallation by Whitener et al.[3]

Mechanistically, transition-metal catalyzed cycloadditions of alkynes are generally considered to start from the coordination and then oxidative addition of two alkynes to the metal, to form metallacyclopentadiene, or metallacyclopentatriene intermediates following coordination of a third alkyne (Figure 2). This is followed by (a) insertion to seven-membered metallacycloheptatriene or metallacycloheptatetraene rings, or (b) [2+2] cycloaddition to give metallabicycloheptatriene intermediates, or (c) [4+2] cycloaddition. The final step is the reductive elimination and generation of the arene products.[6]

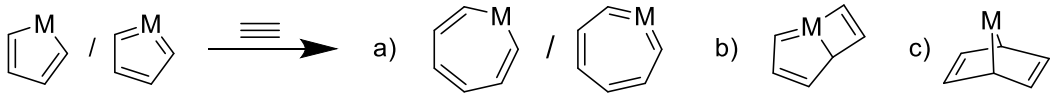

Figure 2: Intermediates of transition metal (M) catalyzed [2+2+2] cyclization of alkynes.[6]

In a recent DFT study, Yamamoto found that the palladium(0)-catalyzed [2+2+2] cross-cycloaddition of a 1,6-diyne with dimethyl acetylenedicarboxylate (DMAD) proceeds *via* the formation of a palladacyclopentadiene, followed by the insertion of DMAD to give a

palladacycloheptatriene intermediate, leading to the benzene product.[7] For alkyne-alkene cyclizations, Aubert and co-workers conducted DFT calculations on cobalt, which propose the initial formation of a metallacycle with two alkynes.[8] The olefin then inserts into the cobaltacycle, resulting to the 1,3-cyclohexadiene product or a hexatriene product, formed by β-H elimination. For bimetallic alkyne trimerizations, a dimetallacyclopentadiene is considered to be the key intermediate, whereby a metallacyclopentadiene coordinates to a second metal centre. The dimetallacyclopentadiene may then undergo [4+2] cycloaddition with a third alkyne.[9]

Our group has studied the interactions of 1,3-butadiynes and bisdiynes with rhodium and characterized the resulting rhodacyclopentadienes and organic products.[10-16] We recently found that when reacting bisdiyne **1-1** with [$(PPh_3)_2Pt(CO_3)$] or other platinum(0) catalysts, we cannot isolate the expected platinacyclopentadiene, but obtain fully substituted azulene (**1-2**) and naphthalene (**1-3**) derivatives as the products (Figure 3).[17] The reaction always produced both derivatives in low to moderate yields, resulting in a challenging separation of the products. Varying the temperature, catalyst, catalyst loading, and ligand type altered product distribution but did not lead to a single product. In this work, we replaced platinum with a palladium catalyst to study the influence thereof. Furthermore, we wanted to achieve selectivity for a single product and improve the yields. As alkynylated conjugated compounds, in particular substituted azulene and naphthalene derivatives, are of interest for application as materials, we also collected spectroscopic data of the isolated compounds.[18-22]

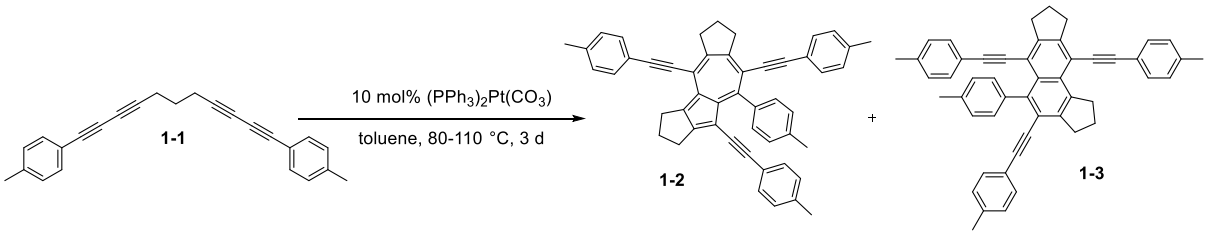

Figure 3: Platinum-catalyzed bisdiyne cyclization reaction.[17]

Discussion

Synthesis

Based on our findings on platinum, we tested several palladium(0) systems for their ability to catalyze cyclization reactions of bisdiyne **1-1**. The precatalyst tris(dibenzylideneacetone) dipalladium(0) ($Pd_2(dba)_3{\cdot}CHCl_3$), with one equivalent of PPh_3 added, turned out to be the most active Pd source, while others such as $Pd(PPh_3)_4$ gave much lower conversions, or no conversion at all for palladium(II) acetate, with one equivalent of PPh_3 added. When using $Pd_2(dba)_3{\cdot}CHCl_3$, substrate **1-1** was converted at 60 °C within few hours, forming azulene derivative **1-2** and naphthalene derivative **1-3** in a 9:1 ratio (Figure 4), determined by NMR spectroscopy. Due to the nature of $Pd_2(dba)_3{\cdot}CHCl_3$, the reaction mixture contained 0.15 equivalents of dibenzylideneacetone (dba), which readily reacted with the bisdiyne substrate **1-1** to give the 1,3-cyclohexadiene **1-4** as a byproduct.

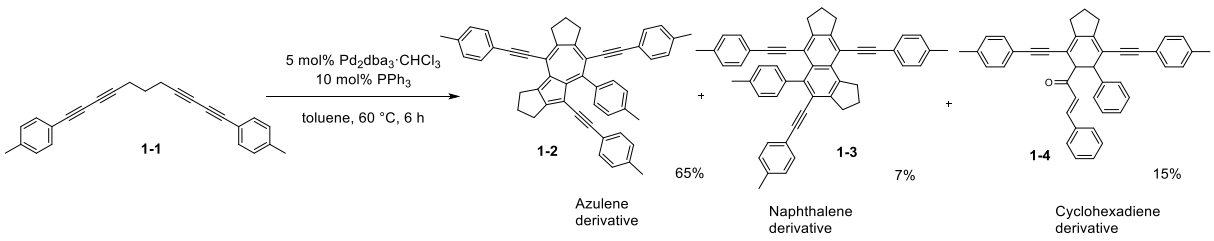

Figure 4: The palladium-catalyzed bisdiyne cyclization reaction (yields determined by ^{1}H NMR spectroscopy).

Screening of different solvents for the reaction showed that tetrahydrofuran shifts the azulene-naphthalene ratio to 20:1 while dimethylformamide gives a ratio of 3:4 and without formation of **1-4**, while reducing the overall yield (experimental chapter, Table 4). Using acetonitrile, as the solvent, gave only the naphthalene derivative and not the azulene or 1,3-cyclohexadiene derivatives, which facilitated product isolation. To increase substrate solubility, 1,2-dichloroethane was added to acetonitrile (Figure 5).

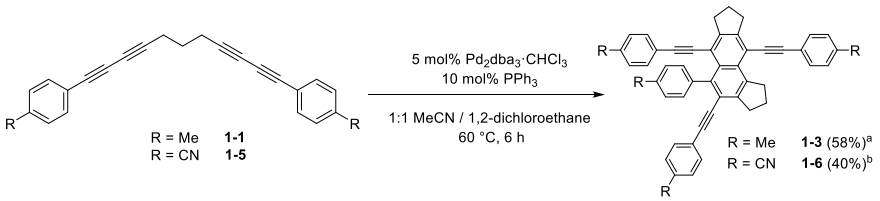

Figure 5: Solvent-controlled selectivity in the palladium-catalyzed bisdiyne annulation reaction. [a]NMR yield, [b]Isolated yield.

To elucidate further the effect of the ligand, different phosphines, NHCs, bipyridyl and phenanthroline ligands were screened, using toluene as the solvent (experimental chapter, Table 4). Bulkier ligands such as P(*o*-tol)$_3$ gave less azulene/naphthalene, while the amount of

1,3-cyclohexadiene remained unchanged. Bulkier and more electron-donating phosphine ligands such as Sphos or Xphos gave mostly the 1,3-cyclohexadiene product, while weakly donating ligands (bipy, $P(OPh)_3$ or dba) showed no or low conversions (see experimental chapter, Table 5).

As there are only few examples of palladium-catalyzed alkyne-alkene cyclizations in the literature,[23-28] we performed follow-up experiments concerning the [2+2+2] 1,3-cyclohexadiene side-product formation. When 0.85 equivalents of dba were added to the mixture, resulting in a 1:1 ratio of dba to bisdiyne, the 1,3-cyclohexadiene derivative became the preferred product and was isolated for four different bisdiyne substrates (Figure 6).

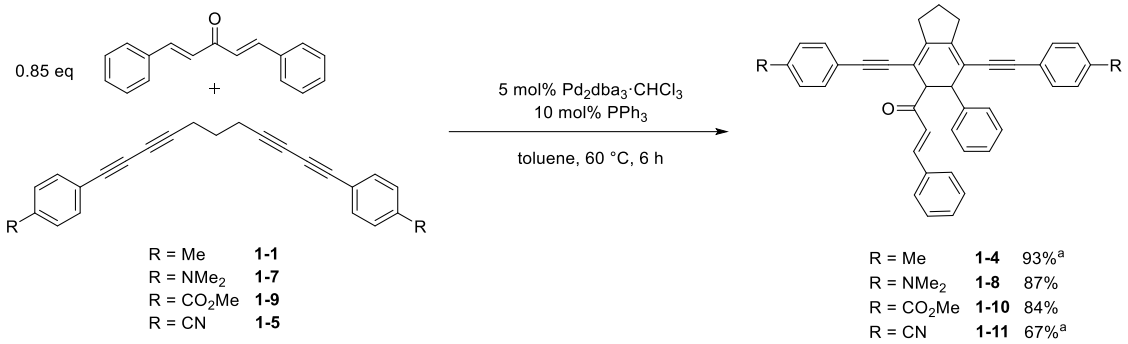

Figure 6: Palladium-catalyzed [2+2+2] cyclization of bisdiynes with dibenzylideneacetone. Isolated yields. [a]SPhos was used instead of PPh_3, which slightly improved the yield.

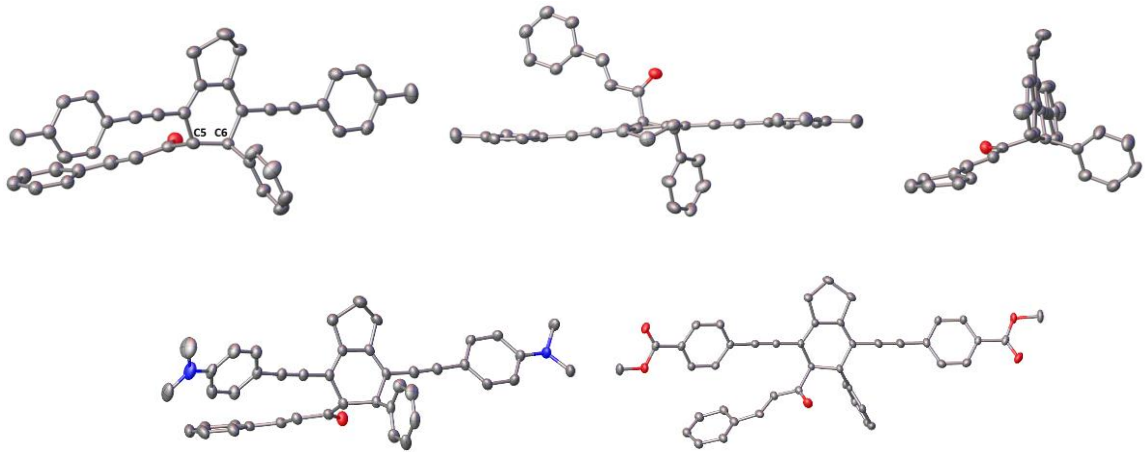

*Figure 7: Solid state structures of **1-4** (top row with front view, top view, and side view) and of **1-8** and **1-10** (bottom row) with thermal ellipsoids drawn at the 50% probability level. Hydrogen atoms are omitted for clarity. Carbons C5 and C6 are labeled in the top left image.*

Compounds **1-4**, **1-8** and **1-10** were crystallized and their structures were obtained *via* single-crystal X-ray diffraction (Figure 7). The angle, obtained from the crystal structure, for compound **1-4** between the cinnamoyl and phenyl moiety at carbons C5 and C6 is 142.64(17)° (labeled in the top left image in Figure 7), which shows that the *trans*-orientation of the substituents at the double bond of the dba substrate is preserved in the product. Similar

results were obtained for the other derivatives. The reaction produces two enantiomers, resulting from the stereocenters at carbons C5 and C6, which were both present in the crystal structures and could not be separated *via* chromatography on silica. We further tried to react bisdiyne **1-1** with other olefins (*trans*-stilbene, ethyl acrylate, acrylonitrile, cyclohex-2-en-1-one, 4-methylpent-3-en-2-one) using the reaction conditions in Figure 6, but the [2+2+2] co-cycloaddition with **1-1** was not observed for any of them (see experimental chapter). Attempts to co-cyclizate bisdiyne **1-1** with several acetylenes ((dibenzonitrile ethyne, di(methyl benzoate) ethyne, dimethyl-acetylenedicarboxylate (DMAD)) were also unsuccessful or gave the cyclotrimerization product hexamethyl benzenehexacarboxylate in the case of DMAD (see experimental chapter).

Theoretical study[1]

Density functional theory (DFT) calculations were conducted in order to propose a mechanism of the Pd-catalyzed cyclization of bisdiyne **1-1** with dba towards cyclohexadiene product **1-4**, which is shown in Figure 8. The calculated free energy profile of the transformation is depicted in Figure 9. Firstly, bisdiynes substrate **1-1** coordinates to palladium, giving rise to ***B*** (exergonic by 24.5 kcal/mol). Then the two C≡C bonds undergo oxidative addition via transition state $\boldsymbol{TS_{BC}}$ with a barrier of 29.2 kcal/mol, along with the formation of a new C-C bond resulting in the irreversible formation of cyclopentadienylpalladium(II) compound ***C***. This process is strongly exergonic by 42.7 kcal/mol. After coordination of dba to give **D**, subsequently migratory insertion of dba via transition state $\boldsymbol{TS_{DE}}$ forms cycloheptadienylpalladium intermediate ***E***, followed by reductive elimination via $\boldsymbol{TS_{EA}}$. Cyclohexadiene product **1-4** is finally obtained by reductive elimination (exergonic by 57.2 kcal/mol). The activation free energies of the migratory insertion and reductive elimination steps are 19.2 and 7.7 kcal/mol, respectively. Alternatively, the transformation can possibly also be completed by Diels-Alder reaction from **C** via transition state $\boldsymbol{TS_{CA}}$, the relative free energy of which is 4.2 kcal/mol higher than that of $\boldsymbol{TS_{DE}}$ (dashed red line in Figure 9). The oxidative cyclization of bisdiynes **1-1** is rate determining, bearing the highest energy barrier.

[1] The theoretical study was conducted by Dr. Xiaoling Luo, Chongqing Key Laboratory of Inorganic Functional Materials, Chongqing Normal University.

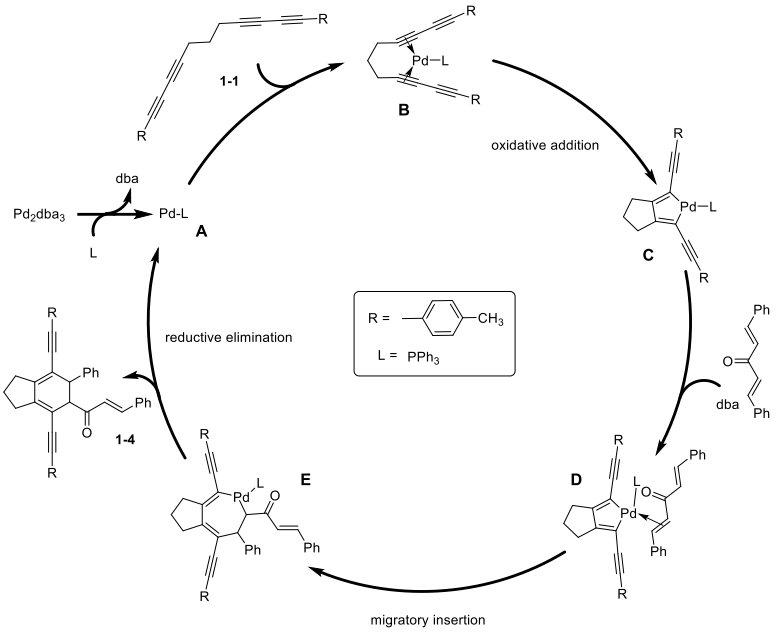

Figure 8: Proposed mechanism of Pd-catalyzed bisdiyne-olefin co-cyclization.

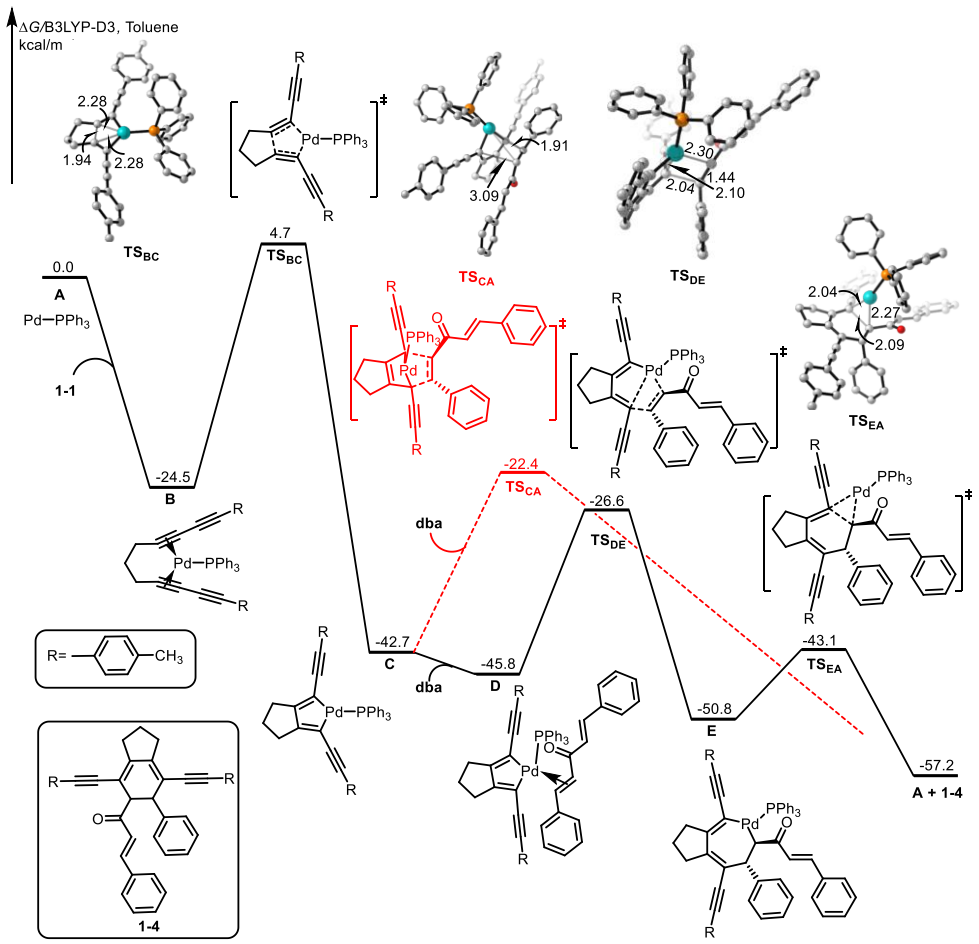

*Figure 9: Free energy profiles of Pd-catalyzed [2+2+2] cycloaddition of bisdiyne **1-1** with dibenzylideneacetone (dba). The energies are in kcal/mol and represent the relative free energies calculated with the DFT/B3LYP-D3(BJ) method in toluene. The bond distances are given in Ångstroms. The C–H bonds are omitted for clarity.*

Photophysical properties

Absorption and emission spectra of naphthalene **1-6** were measured in toluene and CH_2Cl_2 and compared to the previously[17] recorded data of **1-3** (Figure 10 and Table 1). The absorption spectrum in toluene of **1-6** shows an intense absorption band at 349 nm, as well as two more bands at 410 nm and 433 nm. The emission maximum of **1-6** is redshifted from toluene to CH_2Cl_2 by only 200 cm^{-1}. The extinction coefficient of **1-6** in CH_2Cl_2 is 43000 $mol^{-1} \cdot cm^{-1}$.

The absorption maximum of **1-6** is redshifted by 1467 cm^{-1}, in comparison to **1-3** and the emission by is redshifted by 762 cm^{-1}. Both compounds show emission maxima with a vibrational progression. The quantum yield of **1-6** (Φ = 0.72) is slightly higher than that of **1-3** (Φ = 0.6). The absorption and emission spectra of **1-3** and **1-6** are redshifted, compared to unsubstituted naphthalene, which absorbs with maxima at 220 nm and 275 nm and emits at 320 nm in cyclohexane. The fluorescence quantum yield of **1-3** and **1-6** is strongly increased compared to unsubstituted naphthalene (Φ = 0.23).[29]

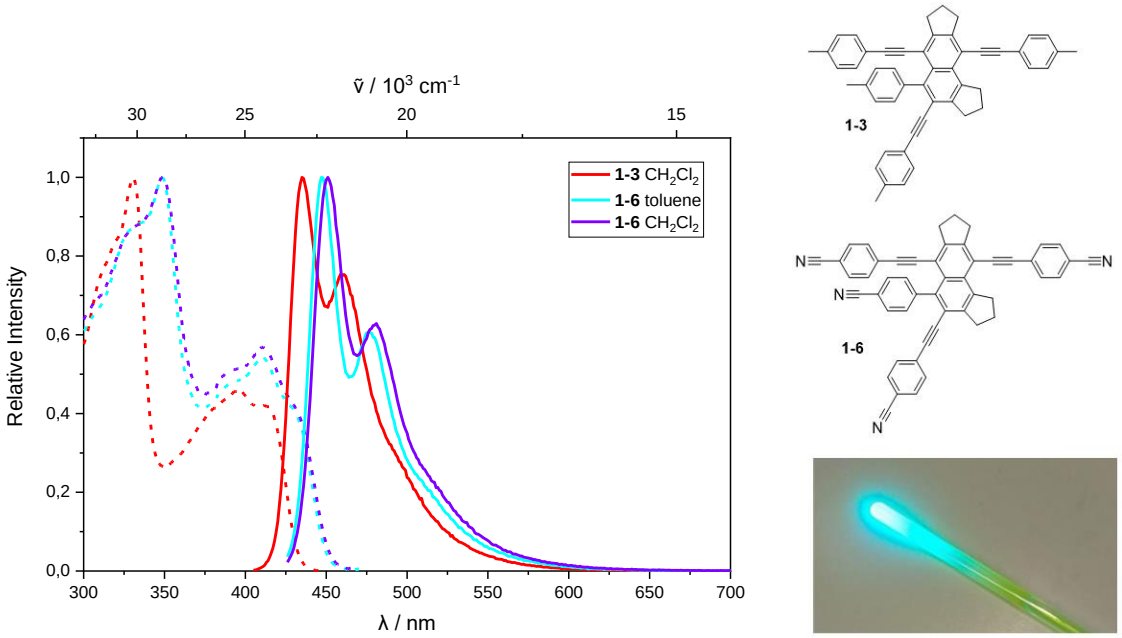

*Figure 10: UV/Vis absorption (dashed line) and emission (solid line) spectra of **1-3** and **1-6** and a $CDCl_3$ solution of **1-6**, irradiated at 365 nm.*

*Table 1: Photophysical data for compounds **1-3**[17] and **1-6**.*									
#	**solvent**	**λ_{max} abs (nm)**	**λ_{max} em (nm)**	**Stokes shift (cm^{-1})**	**Φ**	**τ (ns)**	**τ_0 (ns)**	**$k_{nr}/10^7 s^{-1}$**	**$k_r/10^7 s^{-1}$**
1-3	CH_2Cl_2	332 399 417	436 461	1045	0.60	1.8	3.0	22.2	33.3
1-6	CH_2Cl_2	349 410 433	451 481	921	0.72	1.69	2.3	16.6	42.6
1-6	toluene	349 411 433	447 477	723	0.73	1.68	2.3	16.1	43.5

We further obtained absorption and emission spectra of 1,3-cyclohexadiene derivatives **1-4**, **1-8**, **1-10** and **1-11** in toluene, which are unstable when irradiated in dilute solution (see experimental chapter). Most likely, a photoinduced conrotatory electrocyclic reaction will take place to form hexatrienes, a common reaction for 1,3-cyclohexadienes under irradiation (Figure 11).[30-32]

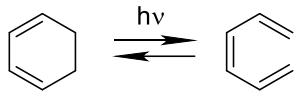

Figure 11: Light-induced electrocyclic ring-opening of cyclohexadienes.[31]

Vibrational spectroscopy

The IR and Raman spectra of compound **1-6** were measured in the solid state (Figure 12). The fingerprint region (500-1500 cm^{-1}) is predominant in the IR, whereas the C≡C stretching vibration at 2187 cm^{-1} is the strongest signal in the Raman spectrum. The IR spectrum further exhibits C-H stretching bands at ca. 2900 cm^{-1} which are not present in the Raman spectrum. From the magnified section of the spectrum in Figure 12 (right side), it can be seen that in the IR spectrum, the C≡N band at 2225 cm^{-1} is stronger relative to the C≡C band at 2187 cm^{-1}; the opposite is true for the Raman spectrum. During the C≡C vibration, predominantly the polarizability of the molecule changes, leading to a strong signal in the Raman spectrum. In the IR however, the C≡N band is stronger, as this vibration changes the dipole moment of the molecule.[33]

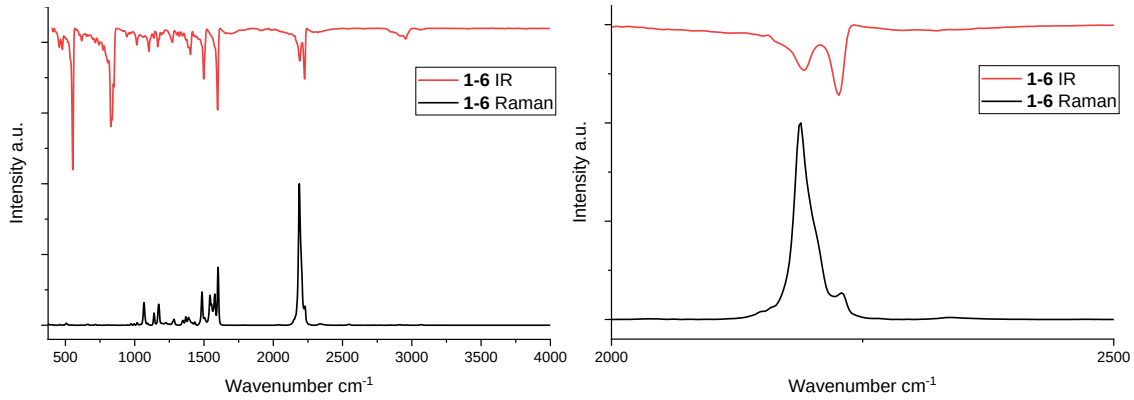

*Figure 12: Solid state Raman and IR spectra of **1-6** (left) and magnified section of the same spectra (right).*

Conclusions

Palladium(0), like platinum(0), catalyzes the annulative dimerization of two bisdiynes. The catalyst $Pd_2(dba)_3{\cdot}CHCl_3$, with one equivalent of PPh_3 added, was the most active Pd(0)-source for the reaction. The dba ligand of the latter precatalyst reacts with the bisdiyne as well, to give a 1,3-cyclohexadiene derivative as the side product. When 0.85 equivalents of dba are added to the reaction, resulting in a 1:1 ratio of dba to bisdiyne, the 1,3-cyclohexadiene derivative is the major product, which was isolated for four different bisdiyne substrates. The solvent has significant influence on the reaction. When the reaction is conducted in acetonitrile, only the naphthalene product and none of the other products are obtained. DFT calculations gave insight in the mechanism of the formation of the 1,3-cyclohexadiene product, which is likely formed *via* insertion of dba into a palladayclopentadiene intermediate. The isolated nitrile-substituted naphthalene derivative shows strong blue fluorescence and a distinctive C≡C absorption band in the Raman spectrum.

2. Nickel(0)-catalyzed [2+2+2] cycloaddition of bisdiynes giving rise to alkynylated o-terphenyl chromophores

Introduction

Cycloaddition reactions are a convenient tool to construct complex organic molecules.[34] These redox-neutral and atom economical transformations are used in many areas of chemistry, such as for the creation of new functional materials[35] or in biological applications.[36] In material chemistry, cyclization reactions of unsaturated precursors represent one of the best ways to create carbon-rich scaffolds.[19] Today, the most common metals used for [2+2+2] cyclizations are Co and Rh.[37-39] A common synthetic strategy is to tether two or more of the alkynes units to achieve a higher degree of selectivity.[40-42] Alkynylated aromatics can be used as materials for non-linear optics, as fluorescent dyes and in optoelectronic devices, examples of this being ethynylated naphthalenes and bis(phenylethynyl)anthracenes.[20, 43-45] The incorporation of alkyne units into conjugated systems provides good electronic communication along with structural rigidity and stability.[46, 47] The substitution of aromatic cores with amine-based donors and strong acceptor moieties, such as nitriles, can give rise to thermally activated delayed fluorescence (TADF) and hot exciton emitters, which are able to utilize triplet states efficiently. If a molecule combines the strong radiative relaxation of a local-excitation with the hot reversed intersystem crossing (hRISC) capability of a charge-transfer state, these hybridized local and charge-transfer excited state (HLCT) compounds can potentially be used as efficient OLED materials.[48-50] Our group has recently studied group 9 and 10 metal-catalyzed and also metal-free cyclization reactions of diynes and bisdiynes and characterized the resulting (luminescent) products.[16, 17, 51] Although in recent years, many efforts were made in the field of metal free bisdiyne cyclizations,[52] there is not much to be found in the literature about metal catalyzed bisdiyne cyclizations. In previous work, our group found that [Rh(κ^2-*S,S*`-S_2CNEt_2)(PPh_3)$_2$] catalyzes the formation of dimers and trimers of bisdiynes in varying ratios, depending on the substituents on the bisdiyne and the amount of catalyst used (Figure 13, top).[53] In contrast, we found that platinum(0) and palladium(0) systems catalyze the formation of azulene and naphthalene products from bisdiynes, as previously demonstrated in Chapter 1 (Figure 13, bottom). Nickel, while also being substantially cheaper than its counterparts in group 10, can access more oxidation states (+I and +III) and facilitates oxidative addition due to it being less electronegative, compared to palladium.[54] Thus, after

our results with rhodium, platinum, and palladium, we wanted to explore the reactivity of nickel towards bisdiynes.

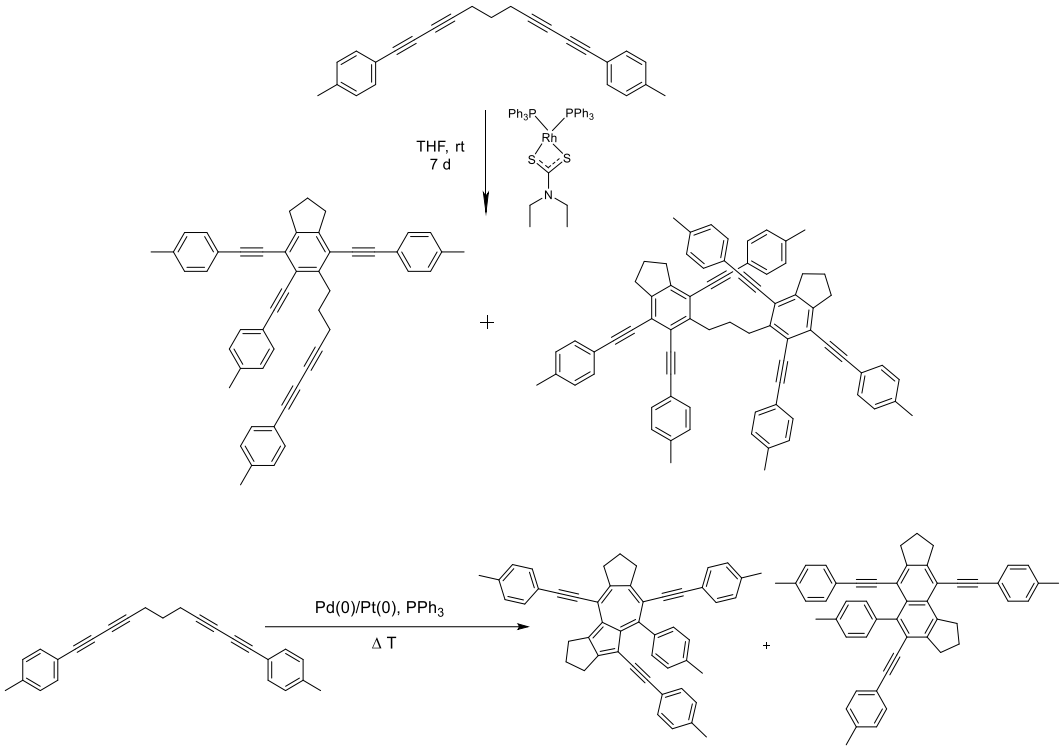

Figure 13: Examples of cyclization products, previously isolated by our group, formed by Rh (top)[53] *and Pt or Pd (bottom) catalysts.*

Discussion

Synthesis

When attempting the cyclization of bisdiyne **2-1** with Ni(0) as the metal catalyst, in the form of the Ni(II) catalyst precursor [(TMEDA)Ni(*o*-tolyl)Cl],[55, 56] the formation of [2+2+2] product **2-2** was observed, when conducting the reaction in toluene at 100 °C (Figure 14). Interestingly, the same product was previously found when using a rhodium (I) catalyst (Figure 13, top).[53] The azulene and naphthalene products that were formed under Pt and Pd catalysis (Figure 13, bottom and Chapter 1) were not observed. The reaction does not show any conversion when run below 60 °C. In addition to the main product, trimers of **2-1** were also detected in the reaction mixture *via* mass spectrometry, which were not characterized further.

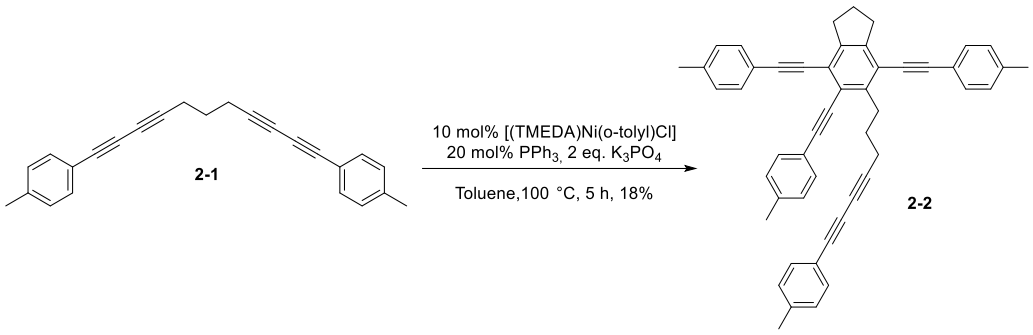

Figure 14: Nickel-catalyzed bisdiyne cyclization reaction (isolated yield).

In the next step, dibenzonitrile acetylene **2-3** was added to the reaction to see whether the dimerization of the bisdiyne **2-1** would still be the prominent reaction or whether a cross-cyclization product would be observed. Indeed, now, a [2+2+2] cyclization between the two substrates took place to form the diethynyl *ortho*-terphenyl derivative **2-4**, while **2-2** was also detected in trace amounts in the reaction mixture (Figure 15).

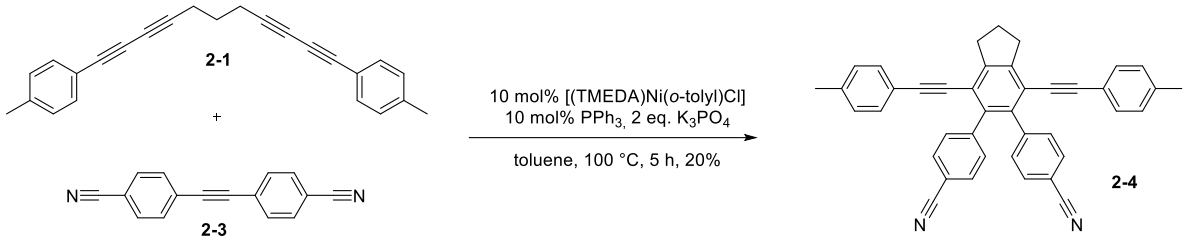

Figure 15: Nickel-catalyzed bisdiyne-diphenylacetylene cyclization reaction (isolated yield).

To elucidate the effects of different substitution patterns, an N,N-dimethylaniline-substituted bisdiyne was combined with acetylenes bearing benzonitrile, methyl benzoate or pyridine moieties, to obtain the diethynyl *o*-terphenyl derivatives **2-5**, **2-6** and dipyridinyl benzene derivative **2-7** (Figure 16), whereby the electron-rich bisdiyne significantly increased the yields of the reaction. To study the effect of a weaker donor moiety on the electrochemical and photophysical properties of the system, a triphenylamine-substituted bisdiyne was then combined with *p*-benzonitrile- and *p*-pyridinyl substituted acetylenes, to generate compounds **2-8** and **2-9** (Figure 16). The cyclization of the two *inner* alkynes of the bisdiyne with the added diphenylacetylenes seems to be the preferred mode of reaction out of all possible ways in which the available triple bonds in the reaction could cyclize. While the dimer of two bisdiynes was often detect as a minor side product, the cyclotrimerization of the diphenylacetylenes was never encountered under the conditions applied.

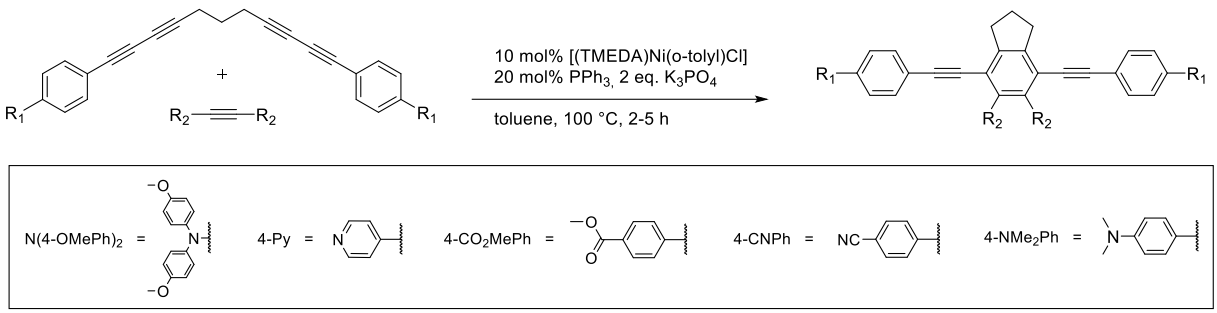

Entry	Compound	R_1	R_2	Yield (%)[a]
1	**2-5**	NMe_2	4-CNPh	74[b]
2	**2-6**	NMe_2	4-CO_2MePh	51[b]
3	**2-7**	NMe_2	4-Py	51[c]
4	**2-8**	N(4-OMePh)$_2$	4-CNPh	23[c]
5	**2-9**	N(4-OMePh)$_2$	4-Py	26[c]
		Unsuccessful attempts		
6		CN	4-CNPh	<10[b]
7		NMe_2	4-NMe_2Ph	– [b]
8		CN	4-NMe_2Ph	traces[b]

Figure 16: Nickel-catalyzed bisdiyne-diphenylacetylene cyclization reactions. [a] isolated yields, [b] 100 °C for 5 h, oil bath heating, [c] at 100 °C for 2 h, microwave reactor.

Some of the reactions were carried out in a microwave reactor in less time. The yields of the procedure were low to moderate, as the conditions were not optimized for every combination of substituents, and some loss of product was encountered during chromatography. When investigating the substrate scope, we noticed a trend. The reaction only worked well when an electron-rich bisdiyne was combined with an electron-poor acetylene. When combining bisdiynes and diphenylacetylenes with both components only bearing either NMe_2 or nitrile substituents, the desired tetra-N,N-dimethylaniline substituted derivative was not observed (Figure 16, entry 7), while the tetra-benzonitrile substituted product was observed, but only in very low yields (Figure 16, entry 6). When the substitution pattern of the substrates was inverted, with the bisdiyne substrate bearing benzonitrile substituents and the diphenylacetylene bearing NMe_2 substituents, only traces of the desired intermolecular cyclization product were observed (Figure 16, entry 8). In these unsuccessful attempts, the dimer of two bisdiynes was detected in the mixtures, while the diphenylacetylene component remained unreacted. When the reaction was conducted without the Ni-precatalyst, with all other reagents present, no reaction was observed. When the diphenylacetylene component was replaced with several different olefin derivatives, the conditions used for the Ni-catalyzed cyclizations above showed no reaction, the formation of the respective cyclopentadiene derivatives was not observed (see experimental chapter). A test reaction, to reproduce the

results using common conditions for cobalt-catalyzed [2+2+2] cyclizations, gave the desired bisdiyne-alkyne cyclization product in trace amounts (see experimental chapter).[57] As there are no recent mechanistic studies of Ni-catalyzed [2+2+2] cycloadditions, we can only propose, based on other systems, that the reaction starts with the formation of a metallacycle from Ni(0) and the bisdiyne. This step is accepted to be the first and rate determining one for several metals in alkyne cyclization reactions. The metallacyclopentadiene can then insert another alkyne or undergo intermolecular or intramolecular Diels-Alder cyclization with another coordinated alkyne.[37, 41, 58, 59] While oxidative addition is facilitated by an electron-rich bisdiyne, an electron-poor diphenylacetylene likely favors the subsequent annulation. This would explain why the reaction only works well with certain substitution patterns, similar to the Diels-Alder reaction, which favors electron-rich dienes and electron-poor dienophiles.[60]

In a follow-up experiment to obtain a water-soluble chromophore, compound **2-9** was treated with methyl triflate to afford the triflate salt **2-10,** with the color of the compound changing from yellow to red (Figure 17). The methylation occurs only on the pyridine and not at the triarylamine moieties, confirmed via ^{15}N-HMBC spectroscopy, which may be due to steric effects (see experimental chapter).

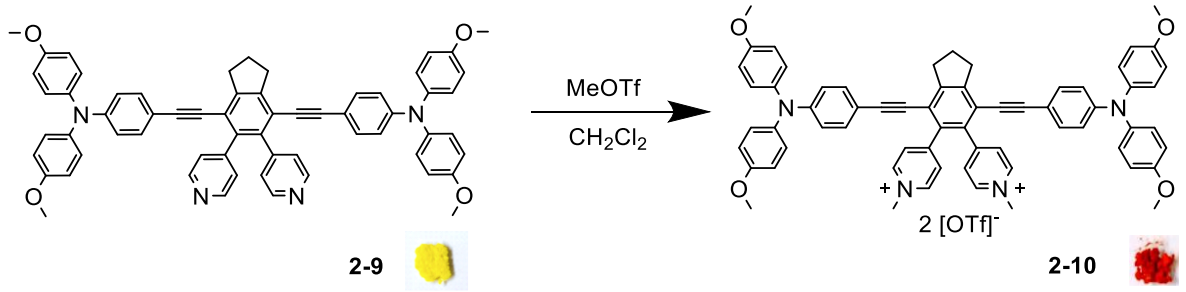

*Figure 17: Selective methylation of pyridine moieties in compound **2-9** to give **2-10** along with pictures of the compounds as powders.*

Single-crystal X-ray diffraction

Compounds **2-4**, **2-5**, **2-6, 2-8** and **2-9** were crystallized and their structures were obtained *via* single-crystal X-ray diffraction. In the solid state, the two phenyl moieties, formerly belonging to the diphenylacetylenes, are twisted with respect to the rest of the molecule (Figure 18). The triphenylamine moieties of **2-8** and **2-9** exhibit a typical *propellor-like* shape. All compounds show antiparallel stacking in the solid state, which is associated with reducing the dipolar disorder, which may be beneficial for charge transport in the material.[61] The twisted arrangement of the donor and acceptor moieties also benefits efficient charge-transfer

transitions and the spaced out habitus may suppress quenching of excited states via the dexter mechanism.[62]

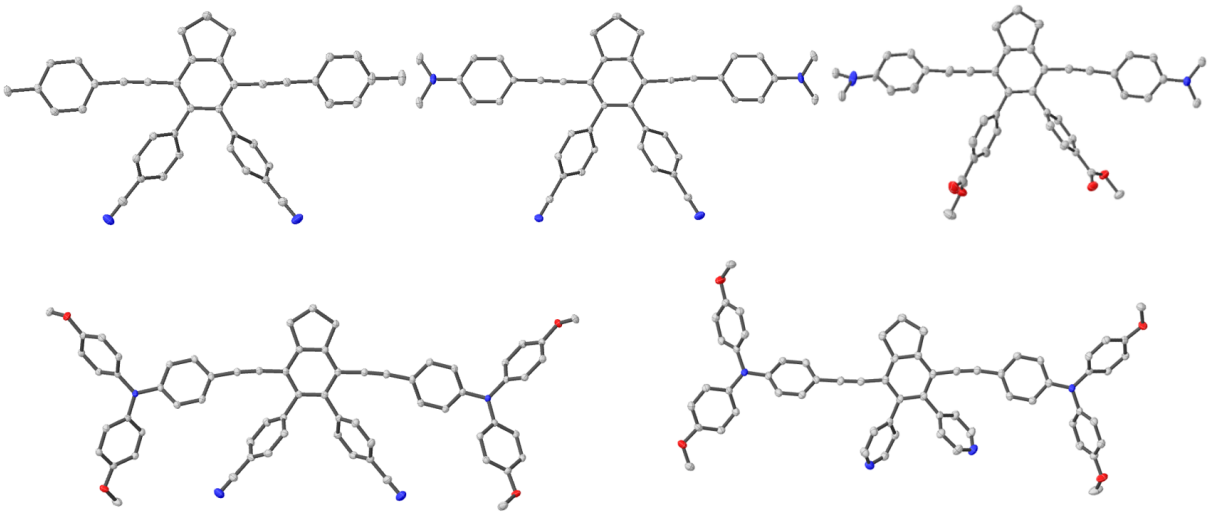

Figure 18: Structures *of **2-4**, **2-5**, **2-6** (top row) and **2-8** and **2-9** (bottom row) with thermal ellipsoids drawn at the 50% probability level* in the solid state. *Hydrogen atoms are omitted for clarity.*

Photophysical properties

The linear photophysical properties of compounds **2-4**, **2-5**, **2-6** and **2-7** were studied. The spectra of **2-4** are drastically different from **2-5**, **2-6** and **2-7,** with the latter donor-acceptor compounds showing redshifted absorption and broad, structureless emission bands, a typical charge-transfer (CT) behavior (Figure 19). In contrast, compound **2-4** displays vibronic resolution, suggesting a locally excited (LE) state, even in CH_2Cl_2. The compounds feature good to excellent fluorescence quantum yields in non-polar solvents; all the compounds exhibit short lifetimes of only a few nanoseconds.

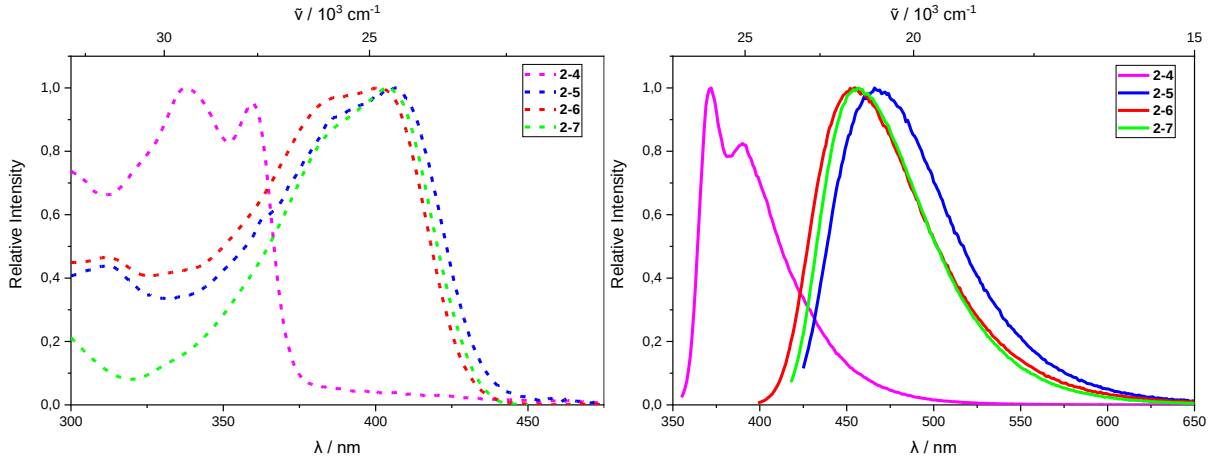

*Figure 19: Absorption (left) and emission (right) spectra of **2-4**, **2-5**, **2-6** and **2-7** in CH_2Cl_2.*

Absorption and emission spectra of **2-5**, **2-6** and **2-7** were also recorded in solvents of different polarity, and the compounds exhibit solvatochromic fluorescence, typical of donor-acceptor

systems (Figures 20 & 21).[63, 64] The emission redshift from toluene to MeCN is 3451 cm^{-1} for **2-5**, 3011 cm^{-1} for **2-6**, and 3256 cm^{-1} for **2-7**. In the locally-excited state of compounds bearing aniline type donors, a rotation of the NR_2 moiety can occur in the excited state in polar solvents, leading to a twisted intramolecular charge transfer (TICT) state.[65] If this TICT state is present, the compounds can exhibit dual fluorescence in polar solvents, which they do *not*.

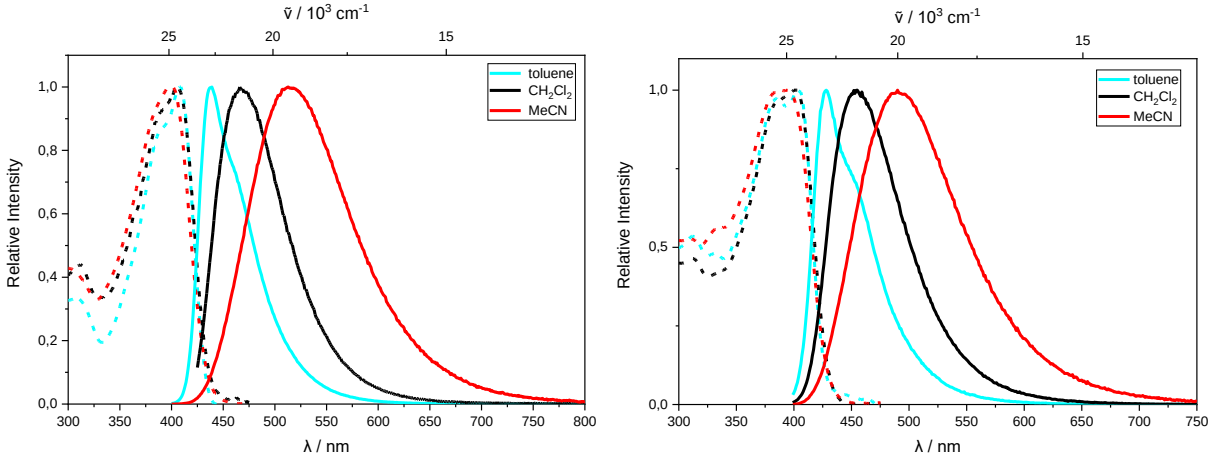

*Figure 20: Absorption (dashed) and emission (solid) spectra of **2-5** and **2-6** in three solvents.*

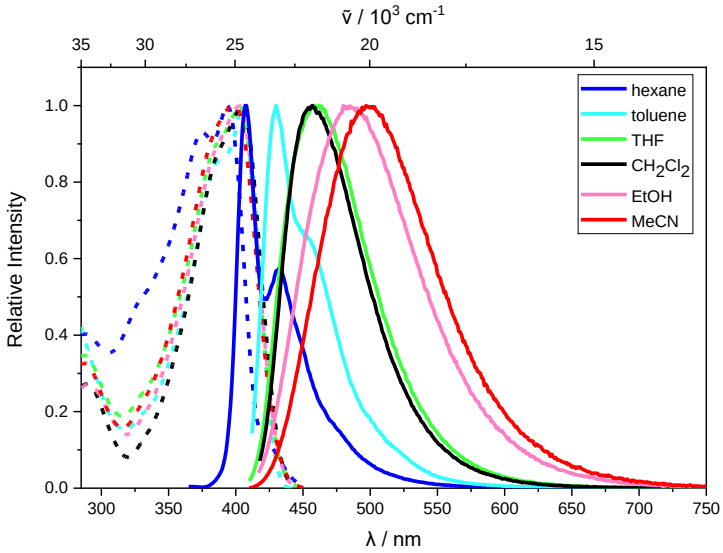

*Figure 21: Absorption (dashed) and emission (solid) **2-7** (right) in six solvents.*

Triphenylamine compounds **2-8** and **2-9** are also solvatochromic, with redshifts of the emission from toluene to MeCN of 4520 cm^{-1} for **2-8** and 4563 cm^{-1} for **2-9**. They absorb strongly, with extinction coefficients of 83000 mol^{-1} cm^{-1} (**2-8**) and 88000 mol^{-1} cm^{-1} (**2-9**) in THF (Figures 22 & 23). Similarly to the dimethylamino-substituted compounds, both triphenylamine-substituted dyes do not show dual fluorescence. All of the D-π-A-π-D

compounds exhibit locally-excited and charge transfer (HLCT) character, with the transition being LE-type in non-polar solvents with considerable CT-character in polar solvents.

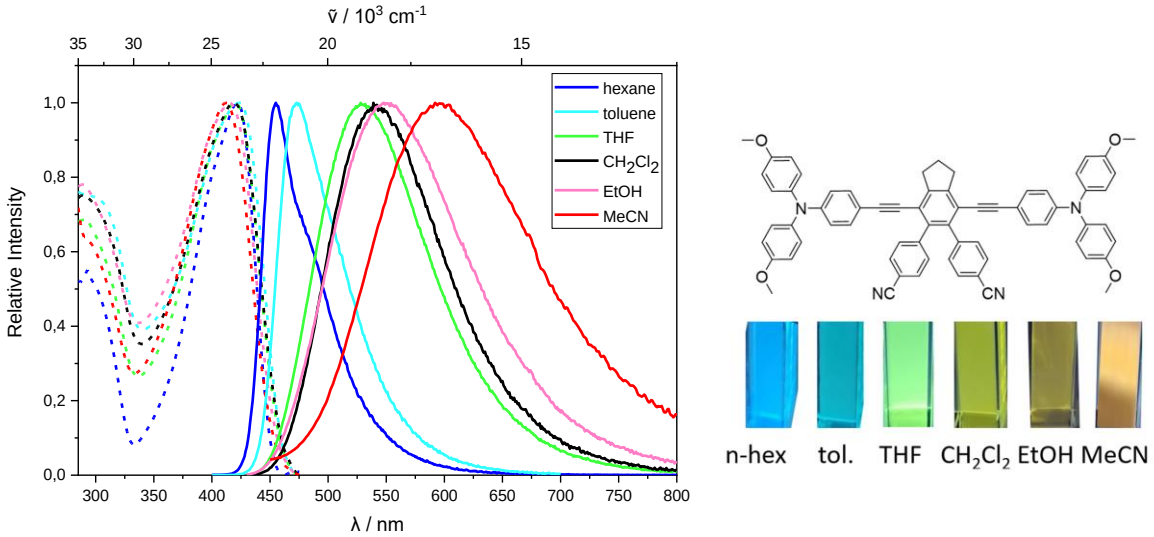

*Figure 22: Absorption (dashed) and emission (solid) spectra of **2-8** in several different solvents and photos of the emission in cuvettes with an absorbance of 0.1, irradiated at 365 nm.*

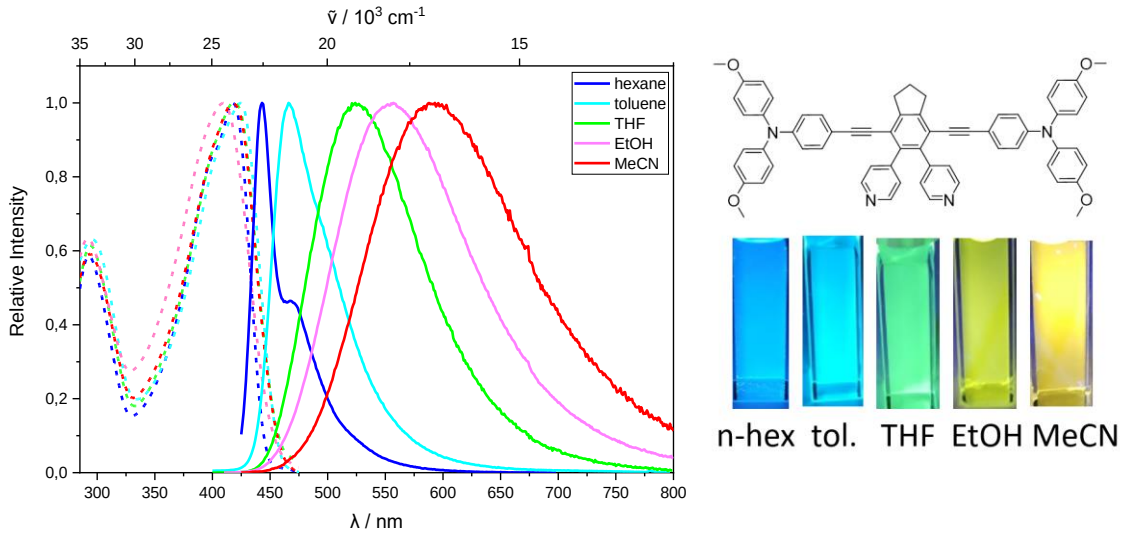

*Figure 23: Absorption (dashed) and emission (solid) spectra of **2-9** in several different solvents and photos of the emission in cuvettes with an absorbance of 0.1, irradiated at 365 nm.*

Table 2: Photophysical data. Extinction coefficients were determined at the absorption band of lowest energy.

#	Solvent	ε (mol^{-1} cm^{-1})	λ_{max} abs (nm)	λ_{max} em (nm)	Stokes shift (cm^{-1})	Φ	τ (ns)	τ_0 (ns)	$k_{nr}/10^7 s^{-1}$	$k_r/10^7 s^{-1}$
2-4	CH_2Cl_2	34000	340, 360	372, 390	896	0.67	3.00	4.5	11.0	22.3
2-5	toluene		383, 398	438	2295	0.83	1.10	1.3	15.5	75.5
2-5	CH_2Cl_2	53000	393, 406	468	3263	0.90	1.95	2.2	5.1	46.2
2-5	MeCN		390, 408	516	5130	0.38	3.27	8.6	19.0	11.6
2-6	toluene		384, 401	427	1518	0.84	1.15	1.4	13.9	73.0
2-6	CH_2Cl_2	50000	384, 401	455	2960	0.83	1.84	2.2	9.2	45.1
2-6	MeCN		384, 396	490	4844	0.50	2.84	5.7	17.6	17.6
2-7	n-hexane		375, 395	407, 432	746	0.91	0.83	0.9	10.8	109.6
2-7	toluene		386, 404	430	1497	0.97	0.92	0.9	3.3	105.4
2-7	THF	68000	386, 402	459	3089	0.99	1.34	1.4	0.7	73.9
2-7	CH_2Cl_2		386, 402	456	2946	1	1.28	1.3	0.0	78.1
2-7	EtOH		386, 402	485	4257	0.17	0.4	2.4	207.5	42.5
2-7	MeCN		380, 397	500	5189	0.61	2.14	2.8	11.2	35.5
2-8	n-hexane		293, 422	455	1719	0.86	1.42	1.7	9.9	60.6
2-8	toluene		298, 423	472	2454	0.93	1.64	1.8	4.3	56.7
2-8	THF	83000	293, 420	530	4942	0.95	3.04	3.2	1.6	31.3
2-8	CH_2Cl_2		289, 418	540	5405	0.86	3.18	3.7	4.4	27.0
2-8	EtOH		289, 415	551	5948	0.36	1.75	4.9	36.6	20.6
2-8	MeCN		293, 412	600	7605	0.16	0.96	6.0	87.5	16.7
2-9	n-hexane		292, 417	442	1356	0.84	1.16	1.4	13.8	72.4
2-9	toluene		295, 424	466	2126	1	1.44	1.4	0.0	69.4
2-9	THF	88000	294, 418	525	4876	0.84	3.06	3.6	5.2	27.5
2-9	EtOH		291, 409	556	6464	0.26	1.18	4.5	62.7	22.0
2-9	MeCN		293, 417	595	7174	0.13	0.94	7.2	92.6	13.8

We further studied the photophysical properties of compound **2-10** and found that it does not show any emission in solution. The bright red substance absorbs strongly in the UV and into the visible region of the spectrum up to ca. 600 nm, with an extinction coefficient of 73000 mol^{-1} cm^{-1} in THF (Figure 24). The lack of emissive relaxation may be explained by the donor and acceptor moieties of the compound being *too strong*, which reduces the HOMO/LUMO gap. This may prevent fluorescence, as explained by the energy gap law, which states that the nonradiative decay rate (k_{nr}) of a transition increases exponentially with decreasing energy gap between two states.[66-68]

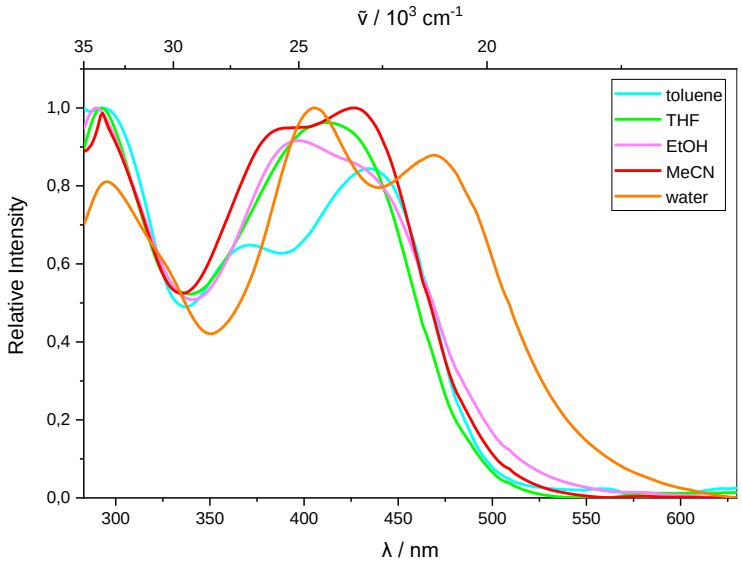

*Figure 24: Absorption spectra of **2-10** in several different solvents.*

Electrochemistry

Compounds **2-5** and **2-8**, were studied using cyclic voltammetry. The values are given with respect to Fc/Fc^+ in THF. Compound **2-5** is irreversibly oxidized starting at 0.01 V, and is irreversibly reduced in a multi-step process starting at 2.76 V. For **2-8**, irreversible oxidation occurs at 0 V, and a reduction was not observed within the solvent window. Both compounds bear two benzonitrile units as the acceptor moiety, with **2-5** having two dimethyl aniline groups, while **2-8** bears two anisole groups on the amine nitrogen. While both compounds have similar oxidation behavior, the bis-*p*-methoxyphenyl aniline groups seem to shift the reduction potential of **2-8** significantly.

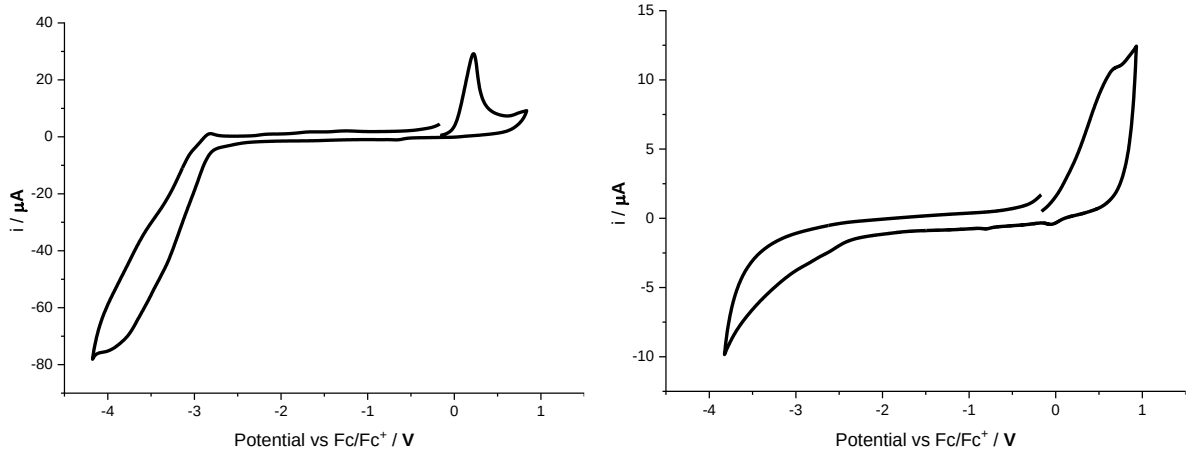

*Figure 25: Cyclic voltammograms of **2-5** (left) and **2-8** (right) in THF/ 0.1M [n-Bu_4N][PF_6].*

Vibrational spectroscopy

IR and Raman spectra were recorded of solid-state samples of **2-8**, **2-9** and **2-10**. The Raman and IR spectra show aromatic C=C vibrations at ca. 1600 cm^{-1} and a characteristic C≡C stretch band at 2194 cm^{-1} (Figure 26). The IR spectra of all compounds contain C-H-stretch bands at 2750 cm^{-1} and above, which are not observed in the Raman spectra. The signals in the fingerprint area from 500 - 1500 cm^{-1} are much stronger than the rest of the spectrum in the IR-spectra in comparison to the Raman-spectra. For **2-8**, the C≡N-stretch vibration at 2226 cm^{-1} is visible in the Raman spectrum, but much stronger in the IR spectrum in relation to the C≡C band (Figure 27). The IR intensity of aromatic nitriles is known to be enhanced when the molecule also bears electron donating groups, further this vibration changes the dipole moment more than the polarizability.[69] The reverse is the case for the C≡C stretch, which is generally stronger in Raman spectra, and only significant in IR spectra, when the moiety is located at the outer positions of a molecule.[33]

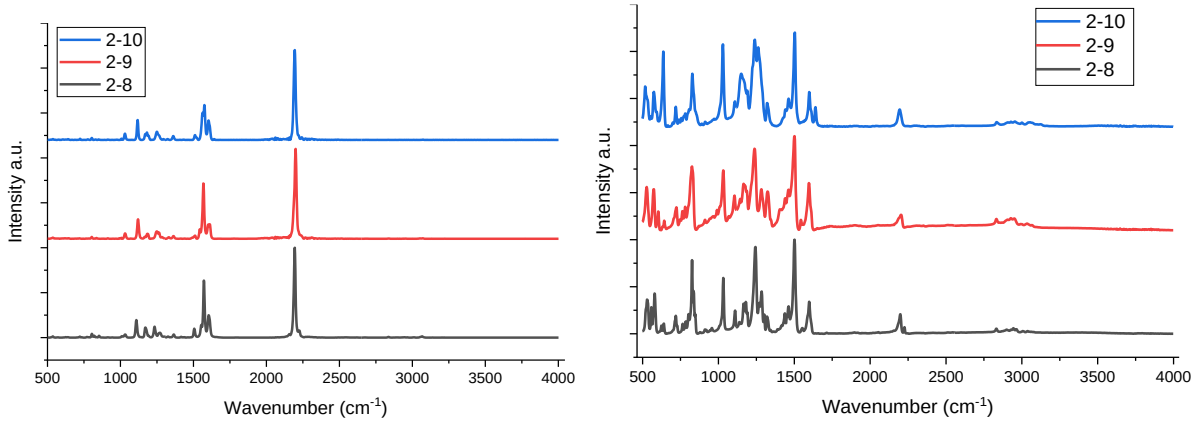

*Figure 26: Raman (left) and IR spectra (right) of **2-8**, **2-9** and **2-10.***

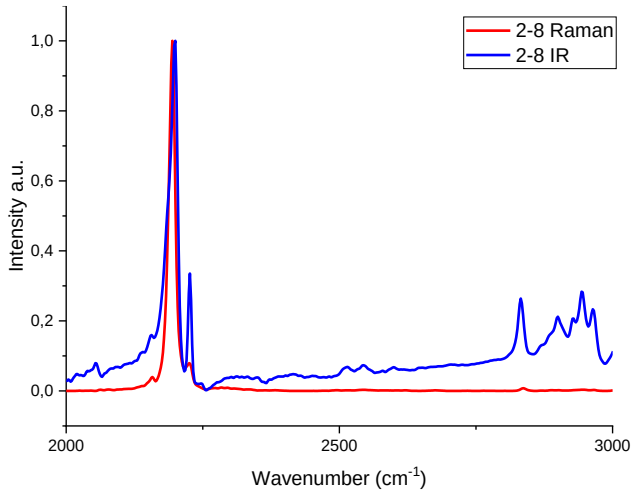

*Figure 27: Comparison of an excerpt of the Raman (red) and IR (blue) spectra of compound **2-8**, normalized to the C≡C stretching band.*

Conclusions

We conducted nickel-catalyzed [2+2+2] cycloadditions of bisdiynes with diaryl acetylenes and studied the resulting air-stable organic products. The reaction works best with the bisdiyne bearing electron donating groups and the diphenylacetylene bearing electron accepting substituents. The C_{2v}-symmetric D-π-A-π-D *o*-terphenyl dyes were studied by UV/Vis and fluorescence spectroscopy. They show solvatochromic emission with good to excellent quantum yields in solution. The vibrational spectra of the triarylamine dyes were studied, which all show a strong characteristic alkyne stretching band in the Raman and IR spectra.

3. Synthesis and characterization of a tetracationic bis-triarylborane tetrayne

Introduction

There have long been efforts to synthesize polyynes with different sizes and end groups, consisting of up to 44 carbon atoms linked in a row.[70] Shorter polyynes, such as diynes, triynes and tetraynes, are a common class of natural products and are found even in vegetables, e.g., diynes in carrots, celery and parsley, which show various biological activities.[71, 72] Polyynes can be potentially applied as pharmaceuticals[73] or functional materials.[74] They can serve as molecular wires[75, 76] or as a component of dyes, such as the red-emitting tetrayne in Figure 28, by Tang and coworkers, that can be used for cancer cell imaging.[77, 78] However, the main remaining challenges for the application of polyynes are selective synthesis and purification.[79]

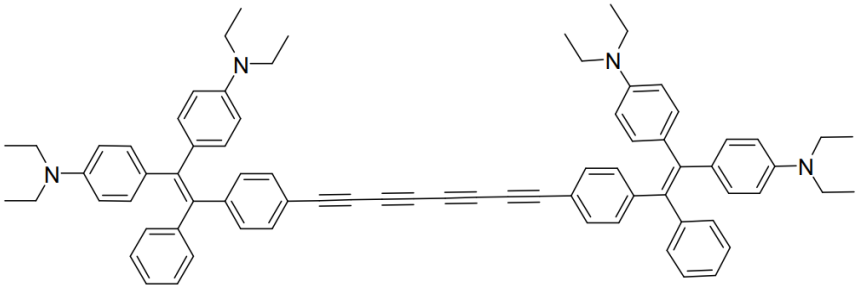

Figure 28: Example of a red-emitting tetrayne dye by Tang and coworkers.[77]

To synthesize polyynes with even numbers of ethyne units (e.g. diynes and tetraynes), which bear the same end-cap on both sides, the copper-catalyzed oxidative Glaser, Hay, and Eglinton coupling reactions are commonly used.[80-82] The oxidative dimerization of terminal acetylenes can also be conducted in a co-catalyzed manner, using palladium and copper catalysts.[83] When the target polyynes bear two different end-caps, or contain an uneven number of ethyne units, they can be obtained via the Cadiot-Chodkiewitz reaction, the Fritsch–Buttenberg–Wiechell rearrangement, or *via* molybdenum-catalyzed alkyne metathesis.[84-87] End-capping polyynes with bulky groups contributes to their stability, by preventing the chains from cross-linking.[88-91] Polyynes end-capped with hydrogen (*terminal*) or halogens may be very reactive or prone to explosion, and have caused injuries and damage in the laboratory in the past.[92, 93] The possibilities for further functionalization of polyynes are broad. They can, for example, be catalytically hydrogenated and borylated or serve as precursors for metallacycles and σ-polyyne complexes, or be converted *via* cyclization chemistry.[79, 94] Triarylboranes have been developed over time, with regard to their synthetic access and optical properties, enabling

their potential application in dyes, sensors, and optoelectronic materials.[95-99] Their most prominent properties are based on the empty p-orbital on the boron center, which leads to strong π-electron acceptor ability when connected to a π-system, enabling the design of charge-transfer compounds.[100] Triarylboranes can be water-soluble when substituted with trimethylammonium groups, and water-stable, when the central boron is protected with at least five *o*-methyl groups.[101-103] Alkynylated triarylboranes have previously been incorporated in several materials such as BODIPY-dyes, rhenium acetylide complexes used as chemosensors, and in platinum acetylide complexes for optical power limiting.[104-106] Our group recently studied the interaction of rod-like triarylborane compounds with DNAs and RNAs.[102, 107, 108] Small molecules can interact with DNA/RNA via external binding, intercalation and groove binding, with the latter one typically taking place for the systems we reported.[109] Our group recently studied a tetracationic bis-triarylborane 1,3-butadiyne chromophore (Figure 29).[110] This compound interacts with DNA/RNA and proteins and can be probed *via* fluorescence and surface-enhanced Raman spectroscopy (SERS).[111, 112] The polyyne motif was selected as a linker in our current research, as polyynes are excellent Raman probes. The motif has even been used for spectral barcoding, as Raman absorption is distinctively influenced by the substitution pattern and length of the polyyne chain.[113]

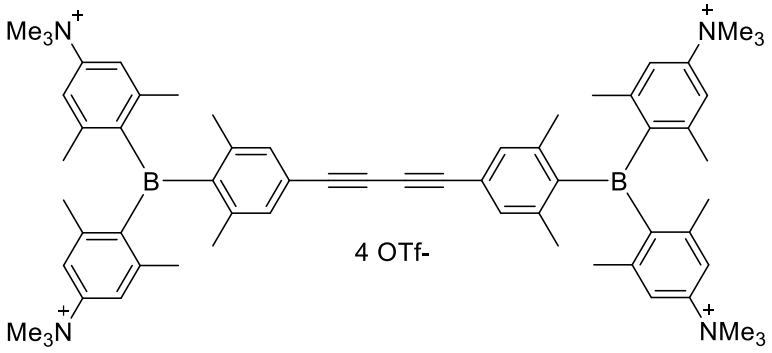

Figure 29: Recently developed tetracationic triarylborane-diyne dye from Marder et al. for optical probing via SERS and fluorescence.

Based on our recent work on bis-triarylborane-diyne dyes, we extended the polyyne system to prepare the analogous tetrayne. As Raman intensity rises exponentially with the length of the conjugated alkyne system, a longer linker can result in a better and more sensitive imaging dye.[113, 114] We also expected to achieve effective groove binding in DNA/RNA strands by increasing the distance between the bulky triarylborane moieties.

Discussion

Synthesis

In the first step, N,N,3,5-tetramethylaniline **3-1** was brominated with NBS to obtain **3-2**. Next, fluoroborane **3-3** was synthesized *via* a Grignard reaction with $BF_3{\cdot}Et_2O$ (Figure 30).

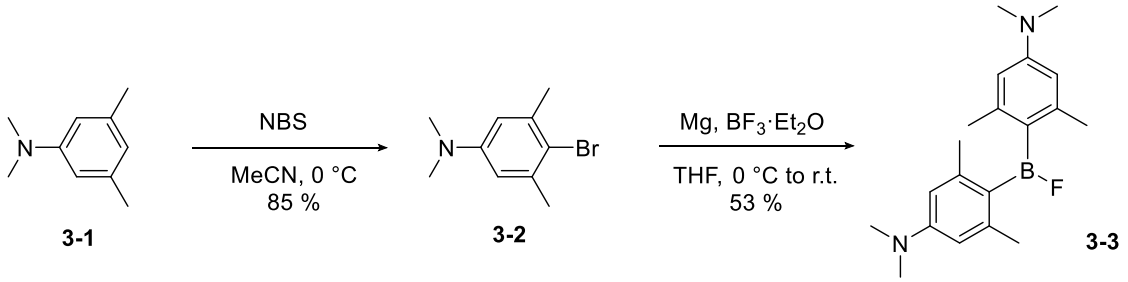

*Figure 30: Grignard-based synthesis of the fluoroborane **3-3**.*

To prepare precursor **3-6**, first **3-4** was subjected to Ir-catalyzed borylation, followed by conversion of the Bpin moiety to bromine to obtain **3-5**. In a Sonogashira reaction, this aryl dibromide was coupled selectively with trimethylsilylacetylene (TMSA) at the less sterically hindered position (Figure 31).

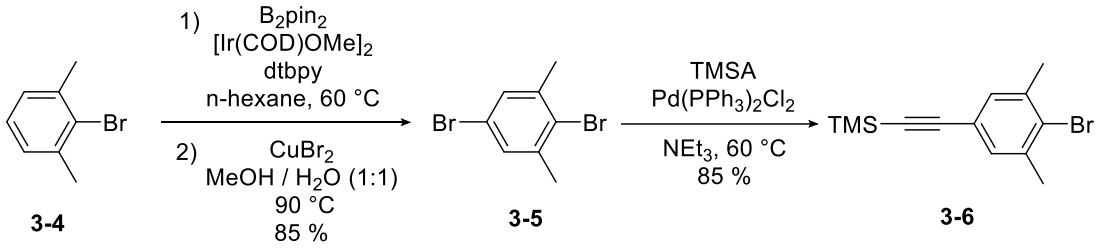

*Figure 31: Synthesis of **3-6** by a series of borylation, bromination and Sonogashira reactions.*

To prepare the triarylborane moiety, **3-6** was lithiated with *t*BuLi and reacted with fluoroborane **3-3**. The crude triarylborane product **3-7** was deprotected with KOH, to obtain the terminal alkyne **3-8** (Figure 32). The synthetic strategy for the preparation of ethynyl precursor **3-8** followed the route reported by our group in 2020.[110]

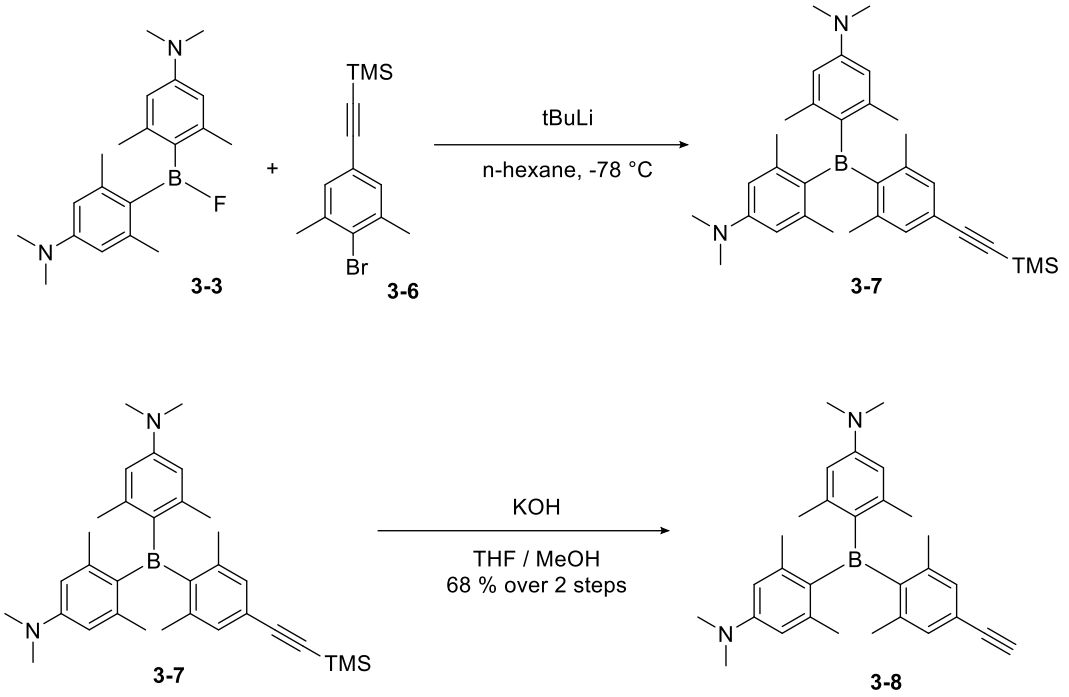

*Figure 32: Synthesis of triarylborane **3-7**, followed by alkaline deprotection yielding **3-8**.*

To obtain 1,3-butadiyne **3-9**, a modified, stepwise, Cadiot-Chodkiewicz protocol was used, because the electrophilic alkyne reagent (bromoethynyl)trimethylsilane would decompose under normal one-step Cadiot-Chodkiewicz conditions. In the first step, terminal alkyne **3-8** was deprotonated by *n*BuLi, followed by treatment with 1.1 eq. of CuI to form the copper acetylide, which was not isolated. The Cu-acetylide was then reacted with (bromoethynyl)trimethylsilane to give **3-9** (Figure 33). Another possible route, starting from the brominated triarylborane alkyne was not feasible, as the bromination of **3-8** could not be achieved selectively, using NBS. Alkaline deprotection of **3-9** gave the terminal 1,3-butadiyne derivative **3-10**, which is quite unstable, and was stored at -30 °C or used immediately after preparation.

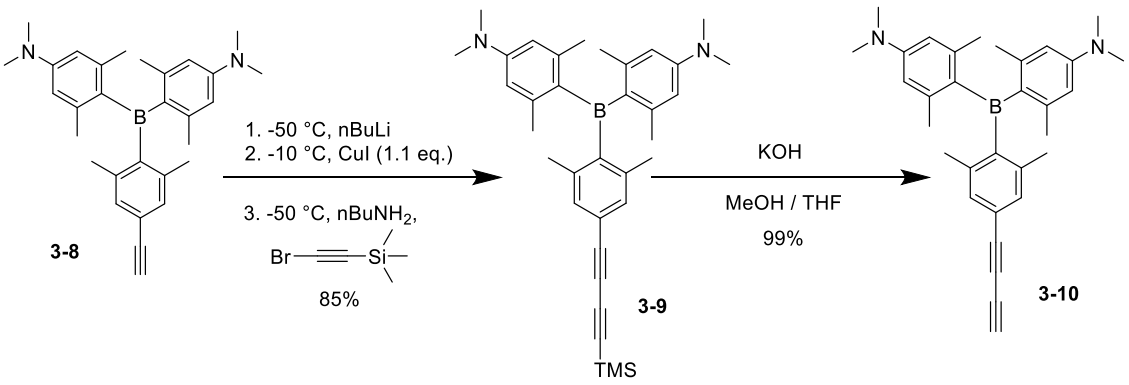

*Figure 33: Stepwise Cadiot-Chodkiewicz-coupling towards **3-9** followed by alkaline deprotection to obtain **3-10**.*

In a Pd/Cu co-catalyzed Glaser-type reaction, **3-10** was then homo-coupled yielding tetrayne **3-11.** To obtain a water-soluble dye, **3-11** was then methylated at all four nitrogens, to obtain the triflate salt **3-12**. (Figure 34).

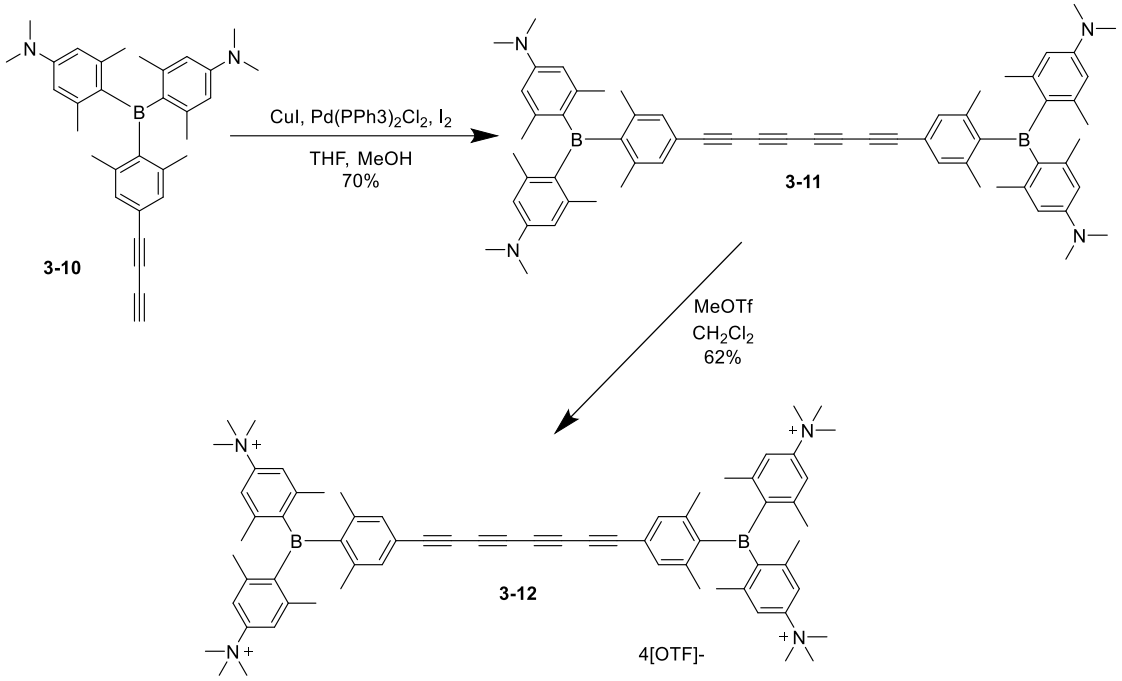

*Figure 34: Oxidative Cu/Pd-catalyzed diyne homo-coupling to give tetrayne **3-11**, and subsequent methylation yielding the triflate salt **3-12.***

Single-crystal X-ray diffraction

The molecular structure of compound **3-11** was obtained by single crystal X-ray diffraction (Figure 35). The distance from one alkyne rod to the next is 4.4443(20) Å, whereby they are kept apart by the bulky end-caps. The rods display a parallel staggered orientation (see experimental chapter, Figure 75). The length of the chain, measured between the two boron atoms, is 20.382(2) Å, while the rod is slightly bent in an S-shape with varying angles C-C-C angles of ca. 3°. The dihedral angle between the two aryl rings attached to the tetrayne rod is 74.46(4)°.

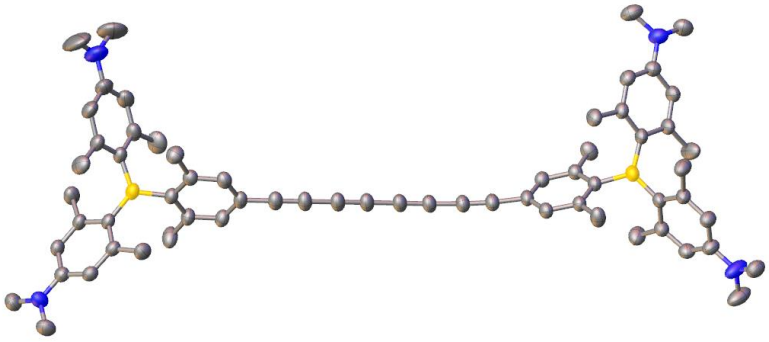

Figure 35: Structure of **3-11** in the solid state with thermal ellipsoids drawn at the 50% probability level. Hydrogen atoms are omitted for clarity.

Photophysical properties

The linear optical properties of **3-11** and **3-12** were investigated in solution (Figure 36 and Table 3). Both compounds absorb in the UV and to ca. 475 nm in the visible region of the spectrum; the absorption is barely affected by the solvent polarity. The emission spectra of neutral tetrayne **3-11** are broad and featureless, being dominated by characteristic local charge-transfer bands, arising from the NMe_2-π-B moieties. For **3-12**, the emission shows vibronic fine structure, along with a reduced quantum yield. Compound **3-11** exhibits a solvatochromic emission redshift of 3825 cm^{-1} from toluene to acetonitrile solutions, while for **3-12** the emission redshift from EtOH to water is only 410 cm^{-1}; the methylation of the amines shuts off the charge transfer process.

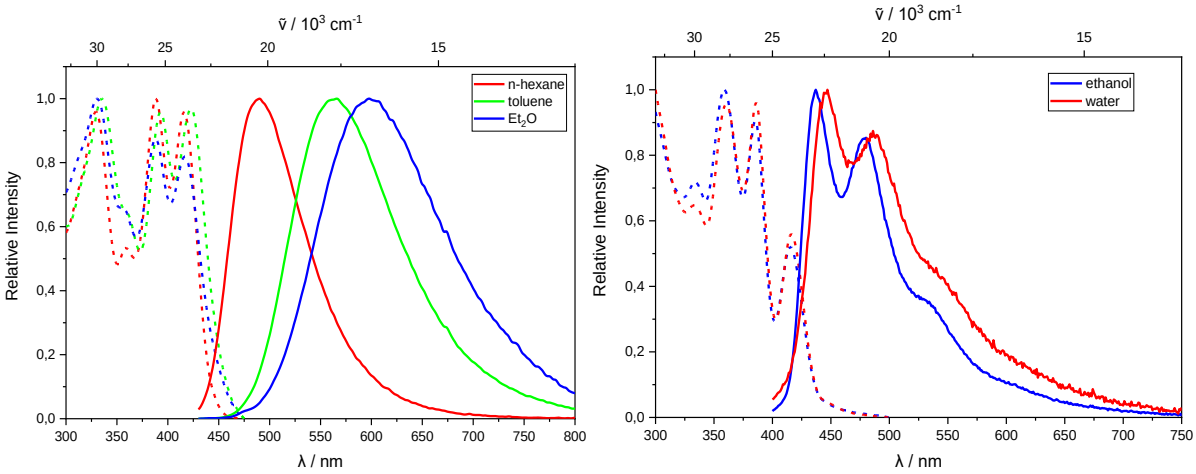

*Figure 36: Normalized absorption (dashed) and emission (solid) spectra of **3-11** in n-hexane, toluene, and diethyl ether solutions (left) and of **3-12** in ethanol and water solution (right).*

*Table 3: Photophysical data of **3-11** and **3-12**. Extinction coefficients were determined at the absorption band of lowest energy.*

#	Solvent	ε (mol^{-1} cm^{-1})	λ_{max} abs (nm)	λ_{max} em (nm)	Stokes shift (cm^{-1})	Φ	τ (ns)	τ_0 (ns)	$k_{nr}/10^7 s^{-1}$	$k_r/10^7 s^{-1}$
3-11	n-hexane	-	329 388 416	488	3547	0.09	1.27	14.1	71.7	7.1
3-11	toluene	56000	335 393 423	563	5879	0.12	3.96	33.0	22.2	3.0
3-11	Et_2O	-	330 387 416	600	7372	0.07	2.15	30.7	43.3	3.3
3-12	EtOH	-	359 385 415	438 478 530	1265	0.02	0.69	34.5	142.0	2.9
3-12	water	47000	359 385 415	446 487 540	1675	0.01	1.24	124.0	79.8	0.8

Vibrational spectroscopy

IR and Raman spectra of solid samples of **3-11** and **3-12** were recorded. In the Raman spectrum, the most prominent bands are at 1590 cm^{-1} (aromatic C=C stretches) and 2127 cm^{-1} (symmetric C≡C stretch) for both compounds (Figure 37, left). In the IR spectra, the C=C stretch is observed at 1587 cm^{-1} and the much weaker antisymmetric C≡C stretch at 2190 cm^{-1} (Figure 37, right). The IR spectra show considerably stronger signals in the fingerprint area (500 - 1500 cm^{-1}), and the C-H stretch signals at ca. 2900 cm^{-1} are visible. Additionally, in the IR spectra of compound **3-12** at ca. 3500 cm^{-1} a broad trimethylammonium band is visible.[115] It is common for symmetric acetylenes, especially when the C≡C unit is not located on the outer parts of the molecule, that the corresponding Raman bands are much more intense than the ones in the IR spectra, which is consistent with our data.[33]

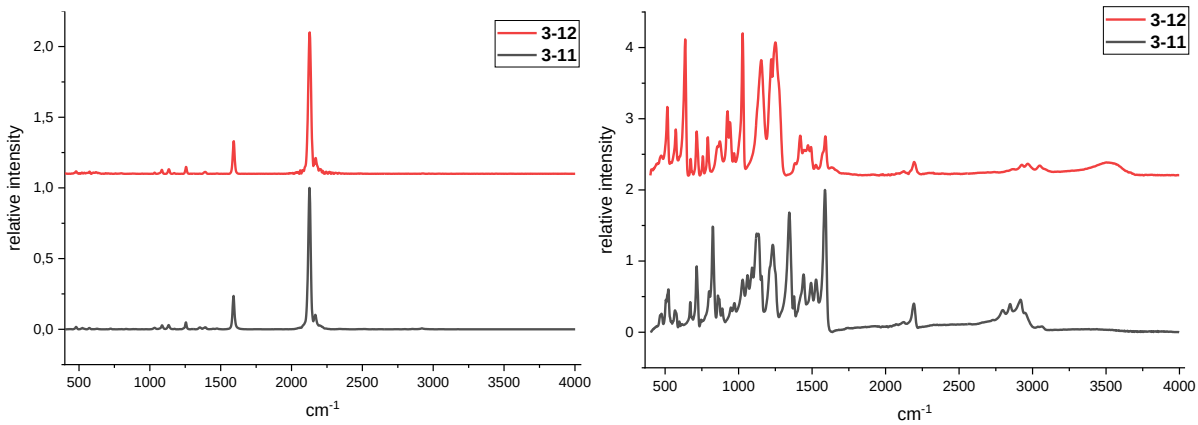

*Figure 37: Raman (left) and IR (right) spectra of **3-11** (black) and **3-12** (red) in the solid state.*

Conclusions

Rod-like bis-triarylborane tetrayne dyes were synthesized in both neutral and tetracationic forms, which may find application in cell imaging and as sensors for DNA, RNA, or other biomolecules. The molecular structure of the neutral compound in the solid state is slightly bent and, in the crystal lattice the alkyne rods are staggered and kept apart by the bulky end-caps. Both molecules are weakly fluorescent in solution and exhibit characteristic alkyne stretching absorptions in the IR and Raman spectra.

4. In situ NMR studies of the phosphine-catalyzed *trans*-hydroboration of 1,3-diynes

Introduction

Transformations of borylated, unsaturated organic building blocks are a major aspect of modern synthetic chemistry, with the Suzuki-Miyaura reaction being among the most commonly used methods to construct C-C bonds.[116-118] The hydroboration of unsaturated scaffolds is an important route towards boronic esters, featuring good atom economy and low toxicity of the involved and produced compounds. The *cis*-hydroboration of olefins and alkynes is typically catalyzed by transition metals, with rhodium being utilized most often.[119-121] The *trans*-hydroboration of internal alkynes, however, remains a synthetic challenge with the only broadly applicable method having been developed by Fürstner using $[Cp^*Ru(MeCN)_3]PF_6$ ($Cp^* = \eta^5\text{-}C_5Me_5$) as the catalyst.[122] Furthermore, the organocatalytic *trans*-hydroboration of alkynes was investigated previously; protocols exist for the phosphine-catalyzed *trans*-hydroboration of propiolates and propiolonitriles.[123-125] *cis*-Hydroborations of 1,3-butadiynes using Co, Ru and Cu catalysts as well as without catalysts were studied previously, whereby good selectivity was achieved, while enabling the boron moiety to be placed at the inner or outer carbon of the diyne.[126-130] Recently, *trans*-borylation of 1,3-butadiynes was achieved for the first time by Taniguchi et al., using N-heterocyclic carbene (NHC) boranes under radical conditions, providing NHC-(E)-alkynylalkenylboranes.[131] The latter protocol was successfully for 1,3-diynes bearing alkyl, propargyl ether, and silyl moieties, but was unsuitable for 1,4-diphenylbuta-1,3-diyne. Recently, our collaboration partners, Santos et al., developed a protocol for the selective *trans* hydroboration of 1,3-diynes with pinacolborane (HBpin), catalyzed by tri-*n*-butylphosphine ($PnBu_3$) to give (*E*)-1-boryl-1,3-enynes, featuring a wide substrate scope (Figure 38). The reaction is regioselective for borylation at the terminal carbon and works faster with electron withdrawing groups at the aryl substituents.

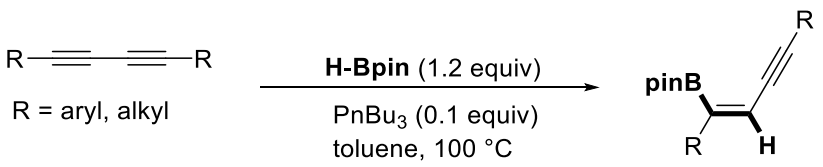

Figure 38: Reaction scheme of the transition metal-free method for the trans hydroboration of 1,3-diynes, developed by Santos et al., Virginia Tech, Department of Chemistry.

To elucidate the mechanism of the reaction, DFT studies were conducted, which led to the proposed catalytic cycle in Figure 39.[2] The first step of the reaction is the nucleophilic attack of the phosphine on the diyne, leading to zwitterionic intermediate **B**, which then reacts with HBpin to form **C**. After a 1,2-hydride shift in **C**, forming **D**, a rearrangement to **E** takes places and the product is released. The highest points in the energy profile in Figure 40 are the addition of phosphine to the diyne, followed by addition of HBpin, which are thus rate-determining. In order to rule out alternative mechanistic pathways, and to accompany the theoretical study, we conducted a series of *in situ* NMR experiments.

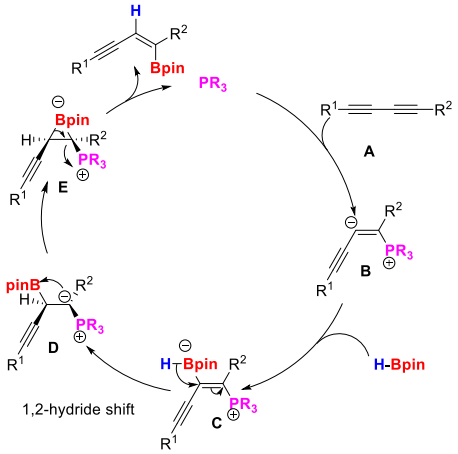

Figure 39: Proposed catalytic cycle for the phosphine-catalyzed 1,3-butadiyne hydroboration.

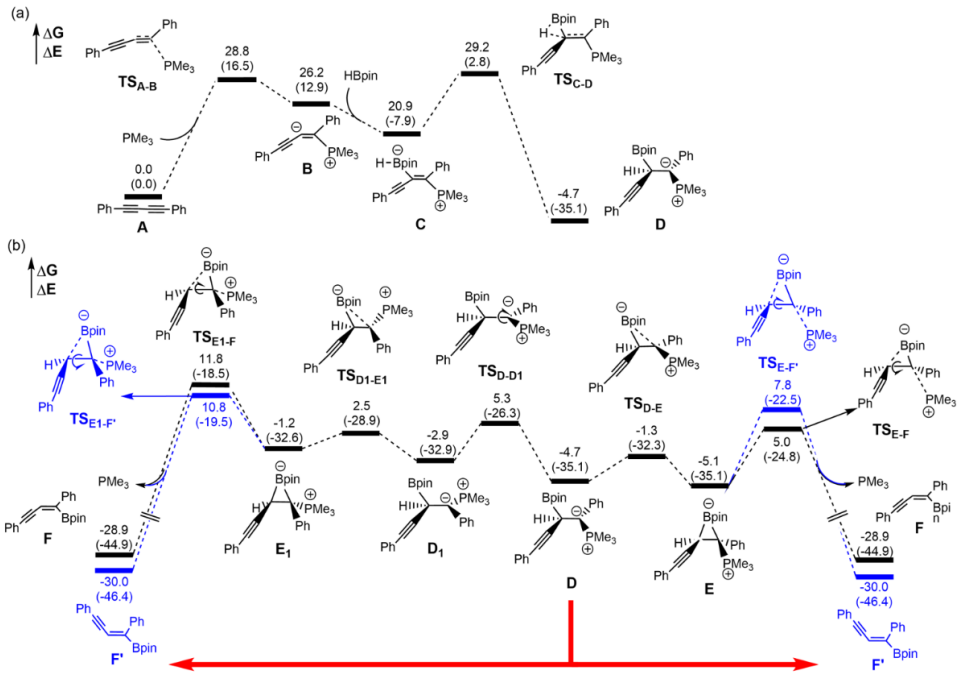

Figure 40: DFT-calculated energy profile of the phosphine-catalyzed hydroboration of 1,3-butadiynes. (M06-2x/6-31(d,p)). Relative free energies and electronic energies (in parentheses) given in kcal/mol. The black colored pathway is for the trans product and blue is for the cis product.

[2] The presented DFT study was conducted by Prof. Dr. Zhenyang Lin et al., Hong Kong University of Science & Technology, Department of Chemistry.

Discussion

As the model reaction, we chose the hydroboration of 1,3-butadiyne **4-1** with HBpin **4-2**, yielding the major *trans*-product **4-4**, with *cis*-hydroboration byproduct **4-5** and the Z-isomer of **4-4** being formed as well (Figure 41). $PnBu_3$ **4-3** was chosen as the phosphine catalyst and all experiments were conducted in toluene-d_8, which provided good selectivity and yield for the reaction.

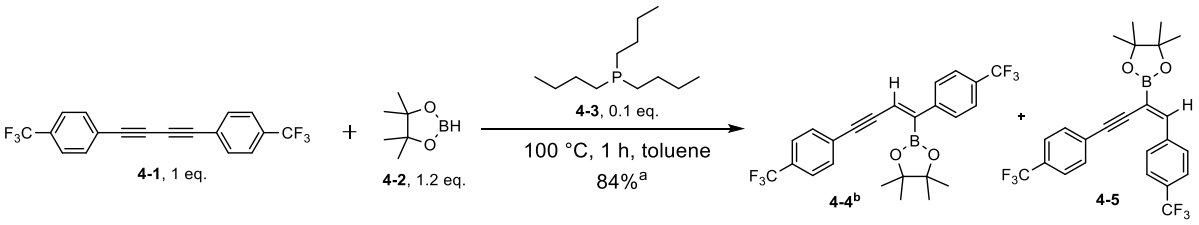

*Figure 41: Model reaction for further studies on the phosphine-catalyzed hydroboration reaction of 1,3-butadiynes. [a]Isolated yield, [b]The cis-hydroboration isomer **4-5** was present in traces of <1%, the Z isomer of **4-4** was formed as well with an E/Z ratio of 89:11 (based on GC-MS analysis).*

1. We conducted a control experiment to see whether the reaction in Figure 41 would work on the NMR scale. Full conversion of the substrate towards the desired products was achieved in 1 hour at 100 °C (see experimental chapter for GC-MS (Figure 77), ^{19}F (Figure 78) and ^{31}P (Figure 79) NMR spectra).

2. To rule out that HBpin would undergo substituent redistribution,[132] or decompose under the conditions applied, we heated a sample of HBpin in toluene-d_8 at 100 °C for 1 day. No additional peaks were found in the ^{11}B or ^{1}H NMR spectra (Figure 42 and experimental chapter Figure 80), which implies that HBpin is stable under the reaction conditions.

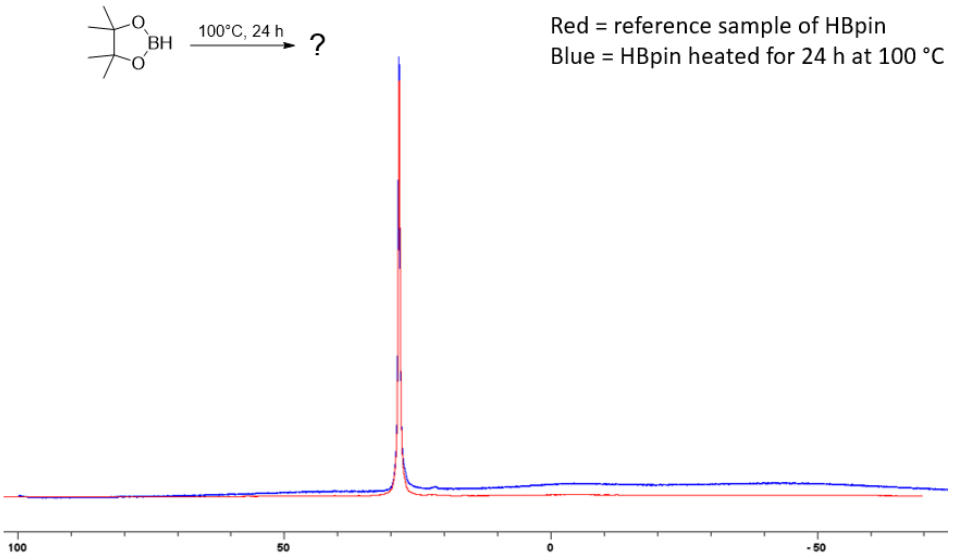

Figure 42: $^{11}B\{^{1}H\}$ (96 MHz) NMR spectra of HBpin (0.1 mmol, 12.8 mg) after 1 d at 100 °C (blue) and HBpin reference sample (red).

3. To see whether the hydroboration would take place without the addition of the phosphine catalyst, a control experiment was conducted. Diyne **4-1** and HBpin, in a 1:1 ratio, were heated at 100 °C for 1 day. The ^{19}F NMR spectrum of the mixture showed no sign of newly formed products or adducts (Figure 43) and, in the GC-MS and ^{11}B NMR spectrum of the mixture only the starting material and no new products were observed (experimental chapter, Figures 81 & 82). Thus, it can be concluded that the hydroboration does not work without adding the catalyst.

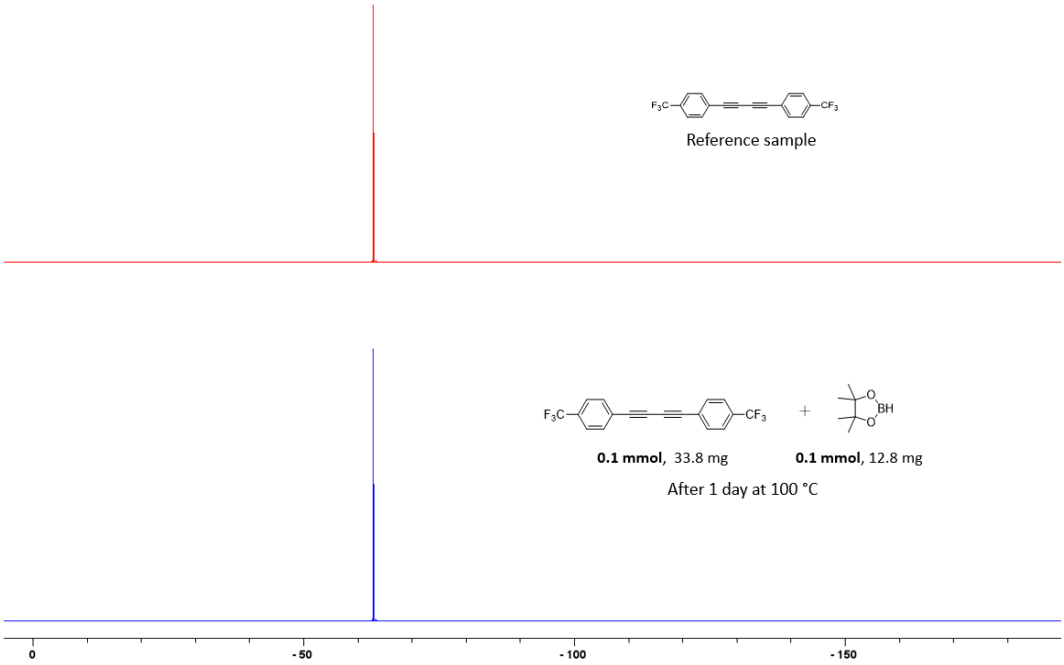

*Figure 43: $^{19}F\{^1H\}$ (470 MHz) NMR spectrum of the mixture of 1,3-butadiyne **4-1** and HBpin (blue) and reference spectrum of **4-1** (red).*

4. To rule out a redistribution reaction or adduct formation, HBpin was combined with the $PnBu_3$ catalyst. No significant new signals were observed in the ^{31}P spectrum when measuring the sample at room temperature or at -40 °C (Figure 44). The same conclusion was drawn from the ^{11}B and ^1H spectra, measured at room temperature and at -40 °C, and from the ^{13}C NMR spectrum (experimental chapter, Figures 83, 84 & 86). In addition, no adducts were detected in the GC-MS and LIFDI HRMS spectra (Figure 85). This observation is in contrast to our previous observations, wherein PPh_3 and other phosphines slowly induced catecholborane (HBcat) redistribution to give $H_3B\text{-}PPh_3$ and $B_2(cat)_3$, whereas smaller phosphines (PMe_3, PEt_3, PMe_2Ph) reacted with HBcat to give $[(PR_3)_2BH_2]^+$ $[B(cat)_2]^-$.[133]

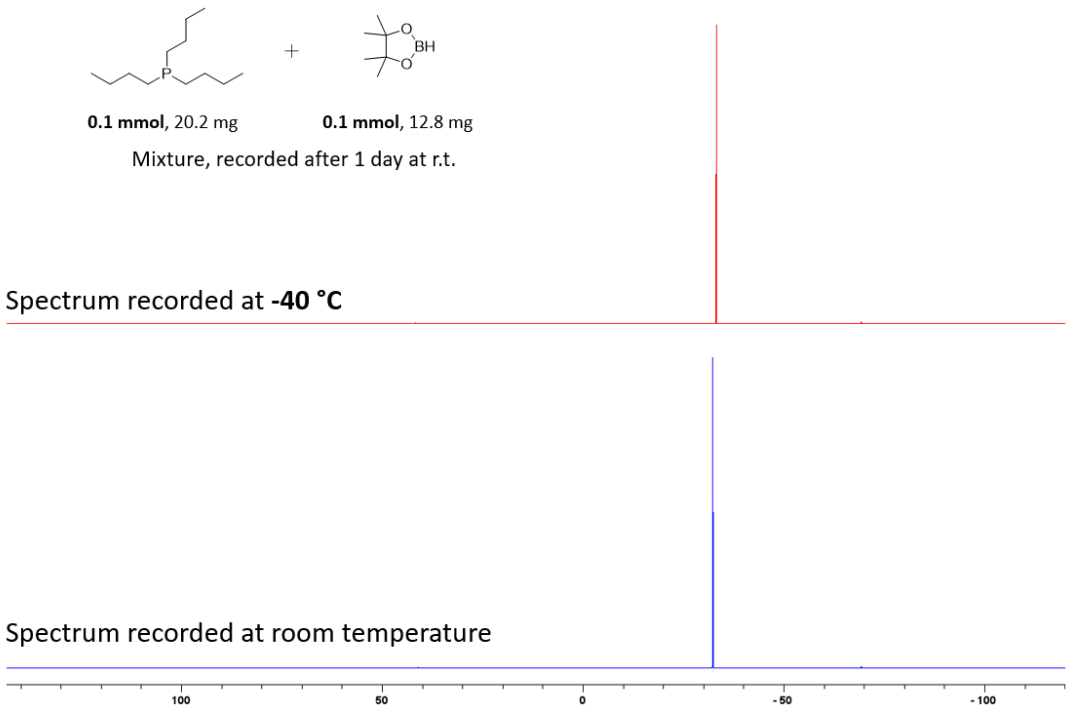

Figure 44: $^{31}P\{^{1}H\}$ (202 MHz) NMR spectra of a solution of a mixture of $PnBu_3$ and HBpin, after 1 d at room temperature. Spectra were recorded at room temperature (blue) and at -40 °C (red). The signal is the unchanged phosphine.

5. Next, diyne **4-1** was combined with $PnBu_3$ in a 1:1 ratio and then analyzed after 3 days at room temperature. The color of the mixture became dark-red, and a number of new signals were observed in the NMR spectra, with the major one being at 17 ppm (Figure 45) in the ^{31}P NMR, and at -60 ppm in the ^{19}F NMR (experimental chapter, Figure 87). The new signals did not increase when the NMR spectrum of the sample was recorded at -40 °C, which suggests that the adducts are not in an equilibrium with the starting material (experimental chapter, Figure 88). We compared the new signals in the ^{31}P spectrum with a methy(tributyl)phosphonium iodide reference sample, which is also strongly downfield shifted (31.4 ppm) in comparison to $PnBu_3$ (-32.3 ppm) and in a similar region with the newly formed signals we encountered (experimental chapter, Figure 93). Thus, we concluded that the new signals likely belong to a zwitterionic adduct intermediate, with a positive charge at P, similar to intermediate **B** in the proposed catalytic cycle in Figure 39.

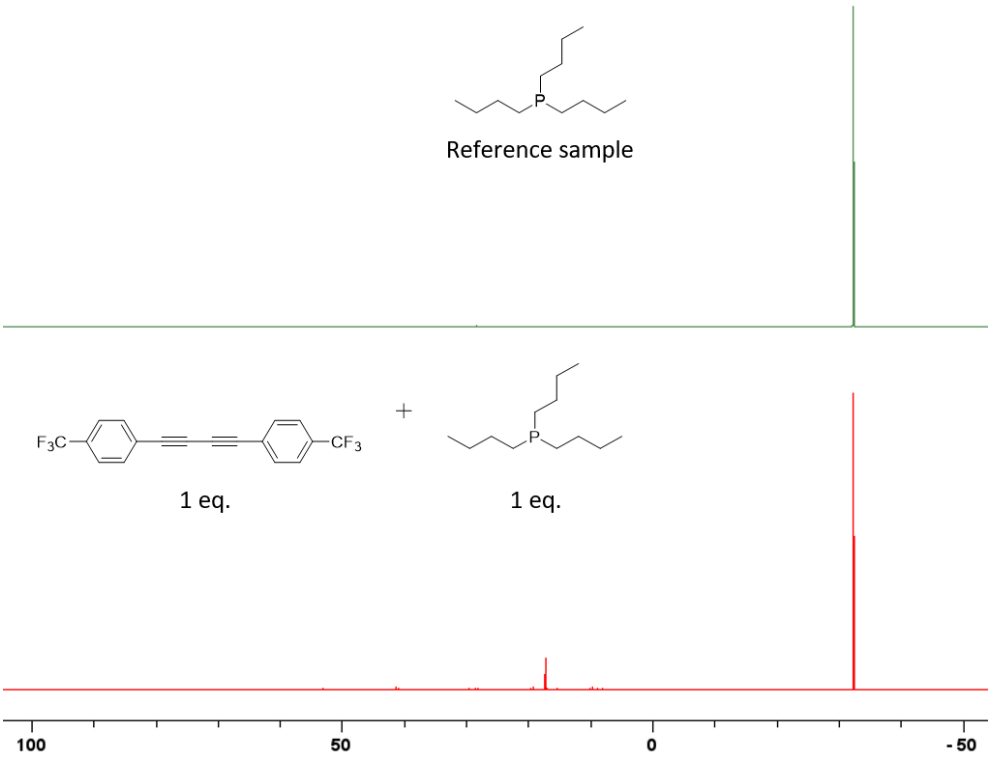

*Figure 45: $^{31}P\{^{1}H\}$ (121 MHz) NMR spectra of a mixture of $PnBu_3$ (0.1 mmol) and diyne **4-1** (0.1 mmol), after 3 d at room temperature (bottom) and a $PnBu_3$ reference sample (top).*

Furthermore, the mass of the phosphine-diyne adduct was identified, along with further adducts containing varying number of phosphines and diynes **4-1**, in the LIFDI-HRMS spectrum of the sample (Figure 46). The products of the reaction seem to contain, in general, more diyne than phosphine, but the HRMS spectrum does not allow quantification of the products. We then compared the reaction with ratios of 1:1 and 10:1 of $PnBu_3$ and diyne **4-1** after 3 days at room temperature. When adding $PnBu_3$ in a 10:1 excess to diyne **4-1**, we found that almost all of the diyne was consumed, while, in the 1:1 mixture, both substrates were still present, and the reaction is thus incomplete (see experimental chapter, Figures 89, 90 & 91). In the ^{19}F NMR spectrum of the mixture, with the phosphine used in 10:1 excess, the signal of substrate **4-1** at -63 ppm diminishes and the new signal at -60 ppm becomes the major one (experimental chapter Figure 87). The disappearance of the diyne in the 10:1 mixture of $PnBu_3$ with diyne **4-1** suggests the possibility of the formation of products that contain more diyne than phosphine. The HRMS of the 10:1 mixture of phosphine with diyne **4-1**, shows mostly signals for the same adducts as the 1:1 mixture (experimental chapter Figure 92). We obtained UV/Vis absorption spectra of mixtures of diyne **4-1**, and of the compound in a 1:1 mixture with $PnBu_3$, and also with a large excess of $PnBu_3$ (Figure 47). The adducts formed in the diyne-

phosphine mixtures absorb in the near-UV, violet, blue, and green region of the visible spectrum, which corresponds with the dark red color of the samples.

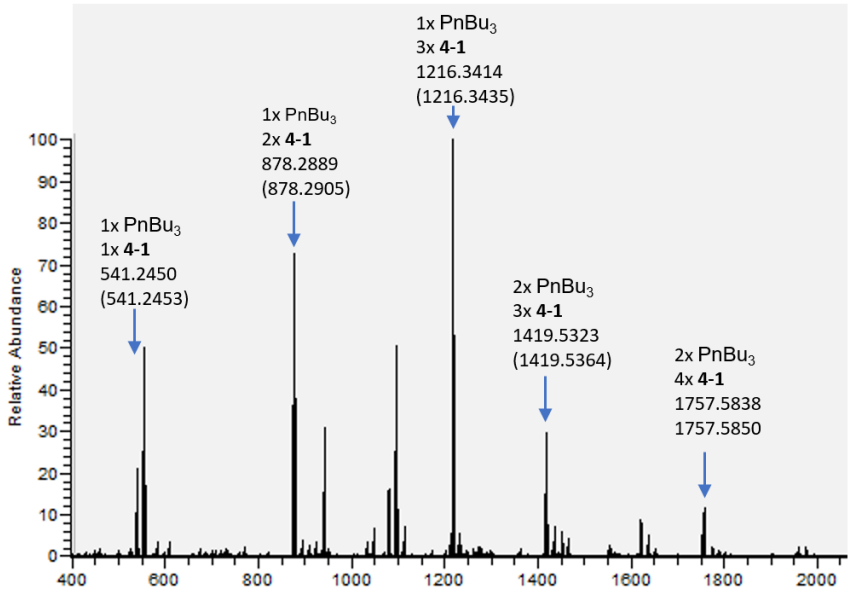

*Figure 46: LIFDI-HRMS of a 1:1 mixture of $PnBu_3$ and diyne **4-1** after 3 d at r.t. The 1:1 adduct of the substrates is marked on the left, and there are several other, heavier, adducts of different composition present.*

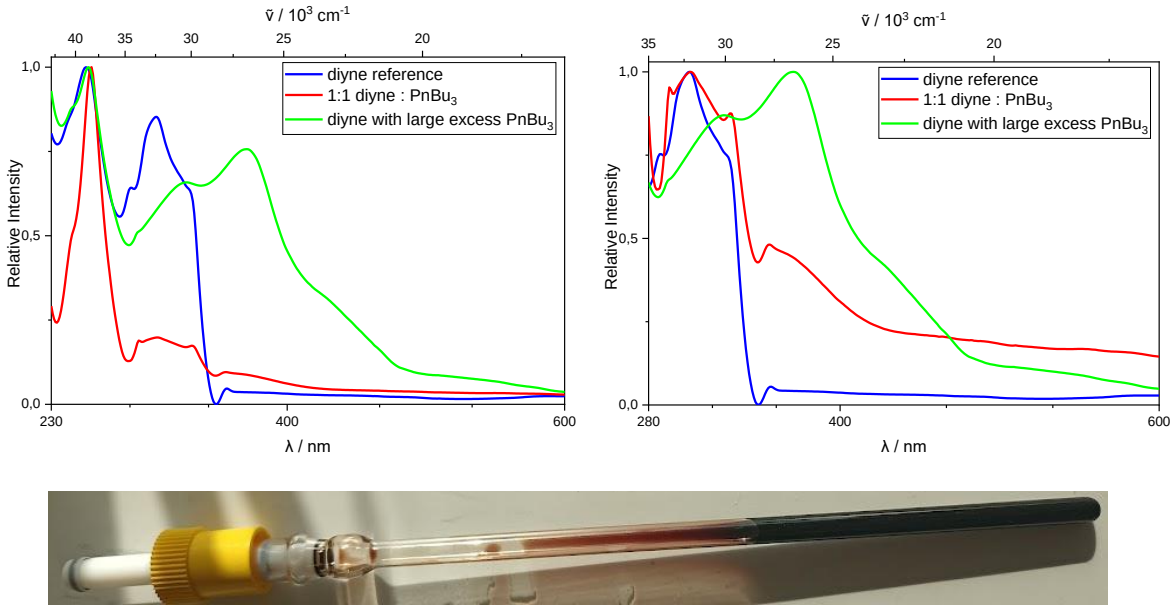

*Figure 47: Above: UV/VIS-Spectra recorded after 7 d at r. t. of a reference sample of diyne **4-1** (blue), of a 1:1 mixture of diyne **4-1**, of $PnBu_3$ (red) and of **4-1** with a large excess of $PnBu_3$ (green) in n-hexane. Below: NMR tube containing a 1:1 mixture of diyne **4-1** and $PnBu_3$. The spectra were normalized within the depicted area. The absorption of diyne **4-1** in the visible region of the spectrum is potentially caused by aggregation.*

6. Hydroboration was also slowly taking place when diyne **4-1** was combined with HBpin and tributylphosphine oxide ($O{=}PnBu_3$) instead of $PnBu_3$ (see GC-MS in Figure 48 and NMR spectra in experimental chapter, Figures 95, 96, 97, 98 and 99). To investigate the cause of this finding,

we combined O=PnBu$_3$ with HBpin and found that O=PnBu$_3$ is partially reduced by HBpin, to generate PnBu$_3$ *in situ* (Figure 49). This *in situ* generation of the catalyst potentially enables the use of O=PnBu$_3$ as a precatalyst, which is air stable and may be more suitable when scaling up the reaction. The phosphine oxide does also not seem to form an adduct with HBpin (see GC-MS, HRMS & NMR spectra in experimental chapter, Figures 100, 101 & 102). The phosphine oxide does not seem to react with diyne **4-1**; when they were combined, no adducts were detected in the ^{19}F or ^{31}P NMR spectra and no PnBu$_3$ was formed (experimental chapter, Figures 104 & 105).

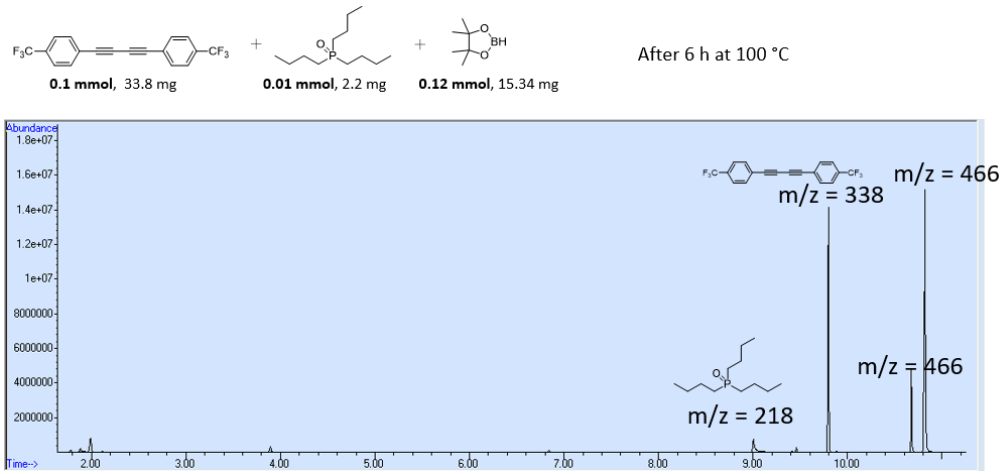

*Figure 48: GC-MS of a 1 : 0.1 : 1.2 mixture of diyne **4-1**, O=PnBu$_3$ and HBpin after 6 h at 100 °C. Hydroboration product signals (m/z= 466) can be detected, but there is still starting material left.*

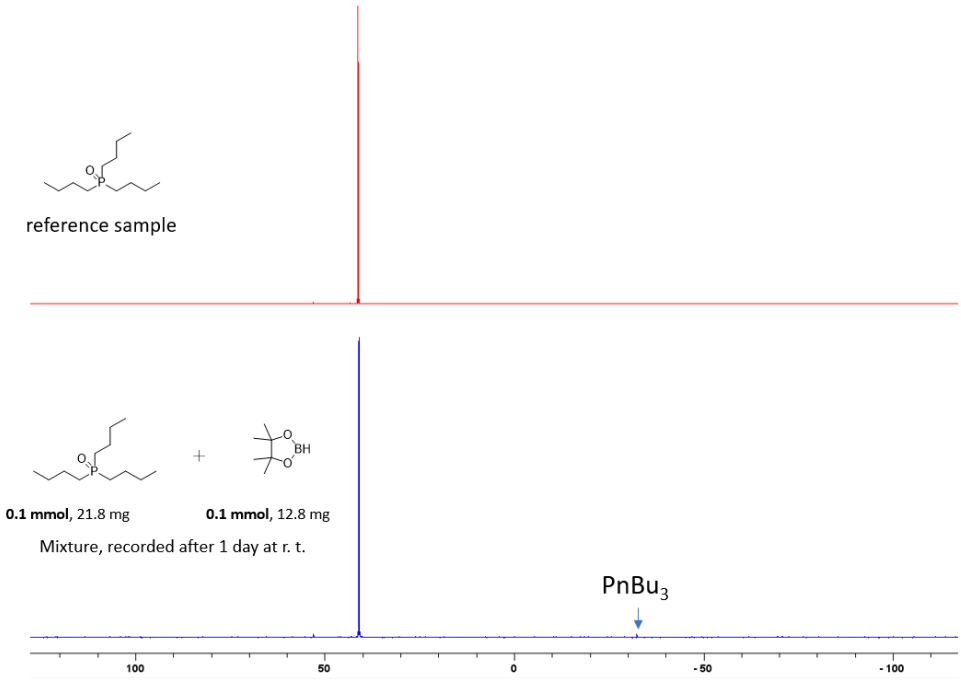

Figure 49: ^{31}P{^{1}H} (121 MHz) NMR spectra of a mixture of O=PnBu$_3$ and HBpin after 1 d at r. t. (blue) and of a O=PnBu$_3$ reference sample. The signal of the newly formed PnBu$_3$ is marked in the bottom spectrum. The signal at 53 ppm is an impurity that was already present in the substrate.

Conclusions

Tributyl phosphine catalyzes the *trans*-hydroboration of 1,3-butadiynes with HBpin. Previously, the substrate scope of the reaction was screened and DFT calculations were conducted by our collaboration partners Lin et al., to elucidate the mechanism. A series of *in situ* NMR experiments were conducted to support the proposed mechanism and to rule out alternative reaction pathways. We confirmed, experimentally, that hydroboration of diyne **4-1** with HBpin does not occur without the phosphine catalyst. We combined HBpin and $PnBu_3$ and did not observe any adducts or other reaction between these two components. When combined at room temperature, the diyne and tributyl phosphine react to generate what appears to be a zwitterionic adduct, as well as species containing multiple phosphines and diynes. Most of these products contain more diyne than phosphine. Hydroboration of the diyne with HBpin also proceeds with tributyl phosphine oxide ($O{=}PnBu_3$) as the precatalyst. The phosphine oxide is thereby reduced to the phosphine during the reaction, which may then act as the catalyst. Phosphine oxide ($O{=}PnBu_3$) did not react with diyne **4-1**, in contrast to $PnBu_3$. The reaction is slower when using phosphine oxide instead of phosphine.

Summary

English Summary

Chapter 1

Palladium(0) catalyzes the cyclization of two equivalents of bisdiyne **1-1**, to give fully-substituted azulene (**1-2**) and naphthalene (**1-3**) (Figure 50) in a single process. The precatalyst $Pd_2(dba)_3{\cdot}CHCl_3$ was found to be the most active Pd(0) source for the reaction, to which 1 equivalent of PPh_3 per Pd was added. The dibenzylideneacetone (dba) ligand reacts with bisdiyne **1-1** as well, to give 1,3-cyclohexadiene **1-4** as a side product. The solvent has a significant influence on the reaction. Thus, when the reaction was conducted in acetonitrile, only the naphthalene product **1-3** is formed.

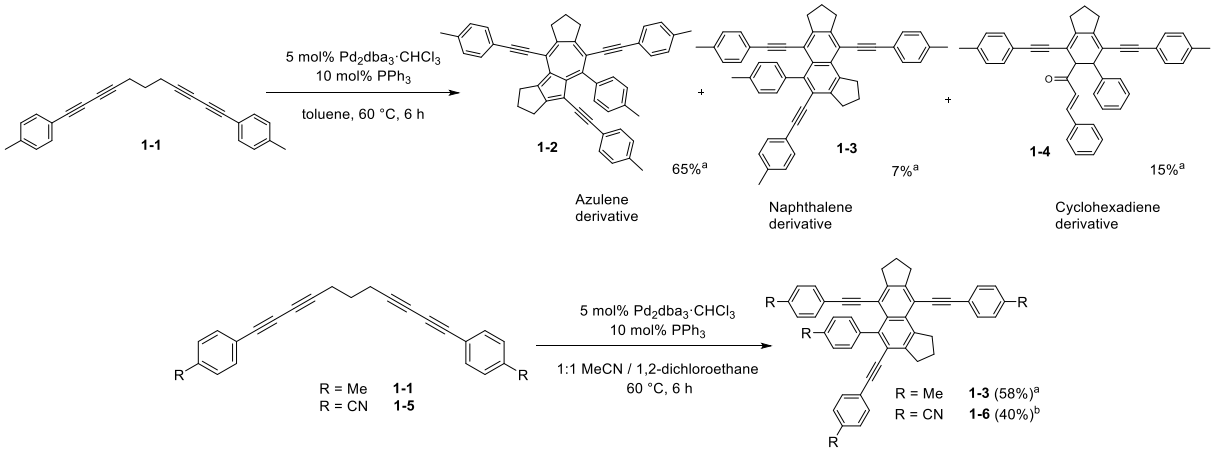

Figure 50: Palladium-catalyzed bisdiyne cyclization reaction (above), and the achieved solvent-controlled selectivity of the reaction (below). [a]NMR yield, [b]Isolated yield.

When 0.85 equivalents of dba are added to the reaction, resulting in a 1:1 ratio of dba to bisdiyne, the 1,3-cyclohexadiene derivative is the major product, which was isolated for four different bisdiyne substrates (Figure 51).

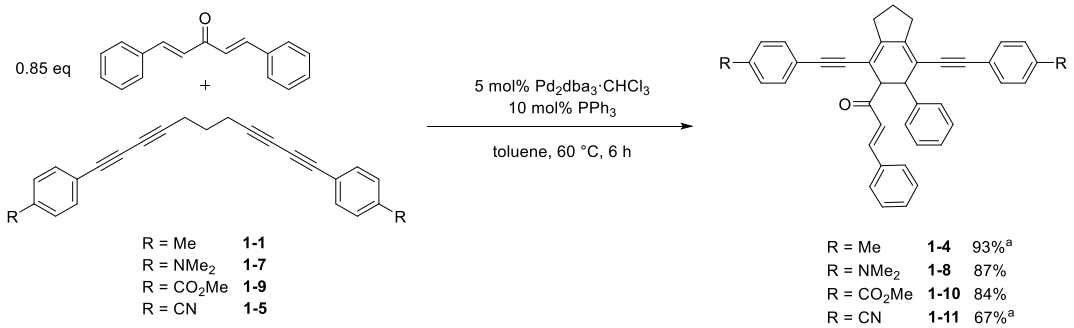

Figure 51: Palladium-catalyzed [2+2+2] co-cyclization of bisdiynes with dibenzylideneacetone. Isolated yields. [a]SPhos was used instead of PPh_3, which slightly improved the yield.

The photophysical properties of nitrile-substituted naphthalene derivative **1-6** were compared to those of the methyl substituted derivative **1-3** (Figure 52). Both compounds absorb in the UV and to ca. 450 nm in the visible region of the spectrum and show emission maxima with a vibrational progression. The quantum yield of **1-6** (Φ = 0.72) is slightly higher than that of **1-3** (Φ = 0.6), with both compounds emitting stronger and bathochromically shifted compared to unsubstituted naphthalene, which emits in the near UV at 320 nm with Φ = 0.23 in cyclohexane.[29] The 1,3-cyclohexadiene derivatives are unstable when irradiated in dilute solution. In the IR spectrum of **1-6**, the C≡N band at 2225 cm^{-1} is stronger relative to the C≡C band at 2187 cm^{-1}; the opposite is true for the Raman spectrum (Figure 53).

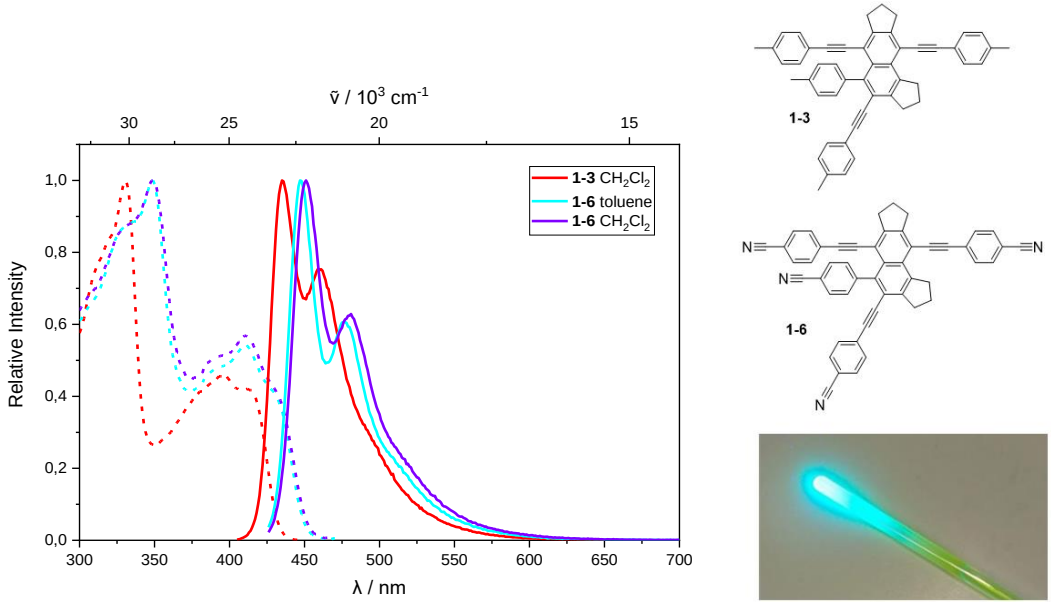

*Figure 52: UV/Vis (dashed line) and emission (solid line) spectra of **1-3** and **1-6** and a $CDCl_3$ solution of **1-6**, irradiated at 365 nm. Data for **1-3** were obtained previously.[17]*

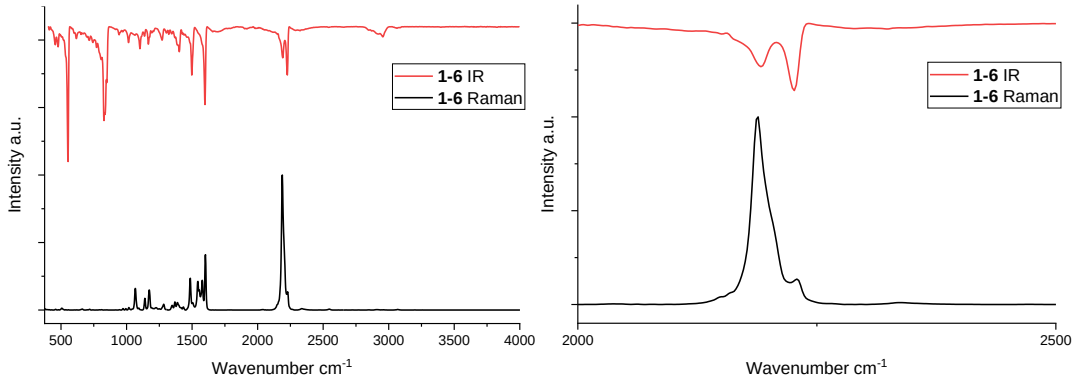

*Figure 53: Solid state Raman and IR spectra of **1-6** (left) and magnified section of the same spectra (right).*

Chapter 2

Nickel(0)-catalyzed [2+2+2] cycloadditions of bisdiynes with diphenylacetylenes were conducted, using the Ni(II) catalyst precursor [(TMEDA)Ni(*o*-tolyl)Cl] as the Ni(0) source, whereas two equivalents of PPh_3 per Ni were added (Figure 54). The reaction worked best with the bisdiyne bearing electron donating groups and the diphenylacetylene bearing electron accepting substituents. The azulene and naphthalene products that were formed under Pd catalysis (Chapter 1) were not observed.

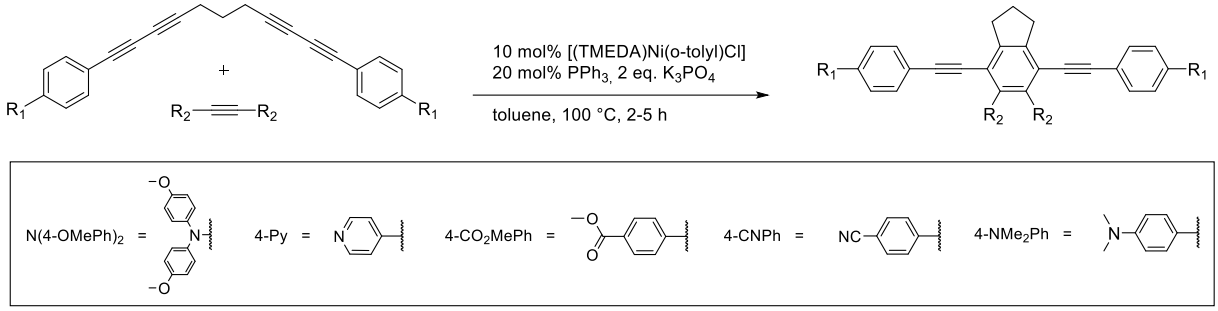

Entry	Compound	R_1	R_2	Yield (%)[a]
1	**2-5**	NMe_2	4-CNPh	74[b]
2	**2-6**	NMe_2	4-CO_2MePh	51[b]
3	**2-7**	NMe_2	4-Py	51[c]
4	**2-8**	N(4-OMePh)$_2$	4-CNPh	23[c]
5	**2-9**	N(4-OMePh)$_2$	4-Py	26[c]
		Unsuccessful attempts		
6		CN	4-CNPh	<10[b]
7		NMe_2	4-NMe_2Ph	– [b]
8		CN	4-NMe_2Ph	traces[b]

Figure 54: Nickel-catalyzed bisdiyne-diphenylacetylene cyclization reactions. [a]Isolated yields, [b]100 °C for 5 h, oil bath heating, [c]At 100 °C for 2 h, microwave reactor.

The C_{2v}-symmetric D-π-A-π-D *o*-terphenyl dyes were studied by UV/Vis and fluorescence spectroscopy. The compounds absorb in the UV and in the visible region of the spectrum to ca. 475 nm. (The spectra of **2-8** are shown as an example in Figure 55). The compounds exhibit solvatochromic emission with good to excellent fluorescence quantum yields in non-polar solvents (e.g. ranging from Φ = 0.83 – 1.00 in toluene). All of the compounds exhibit short lifetimes of only a few nanoseconds. All of the D-π-A-π-D compounds exhibit locally-excited (LE) and charge transfer (CT) character, with the emission being LE-type in non-polar solvents with considerable CT-character in polar solvents.

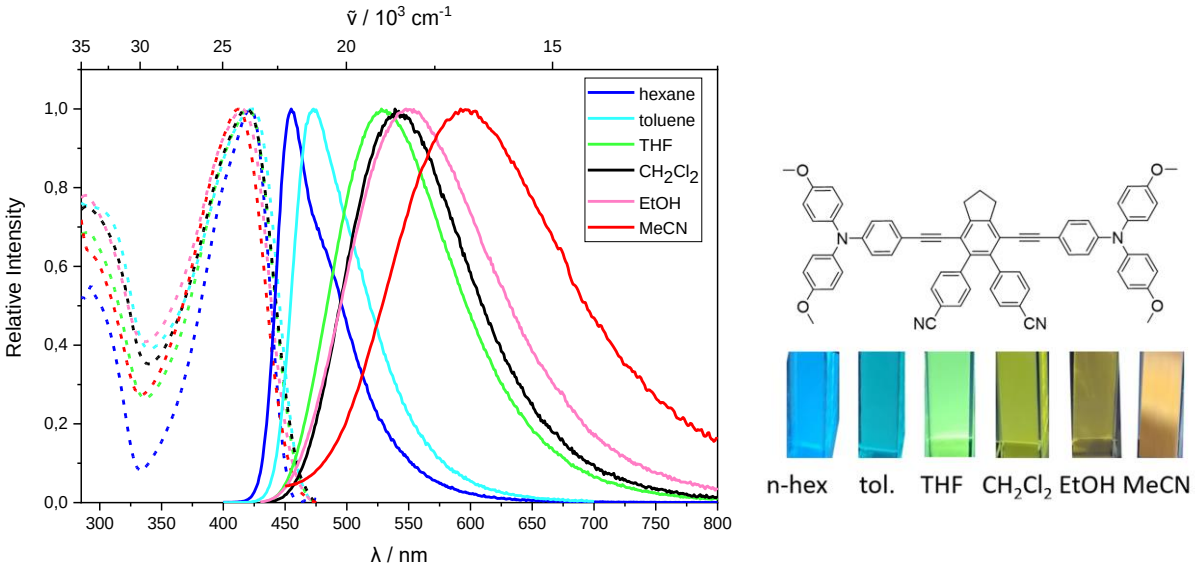

*Figure 55: Absorption (dashed) and emission (solid) spectra of **2-8** in several different solvents and photos of the emission in cuvettes with an absorbance of 0.1, irradiated at 365 nm.*

The vibrational spectra of the triarylamine dyes exhibit a characteristic C≡C stretching band in the Raman and IR spectra at ca. 2194 cm^{-1} (Figure 56); the band is considerably stronger in the Raman spectra compared to the IR spectra.

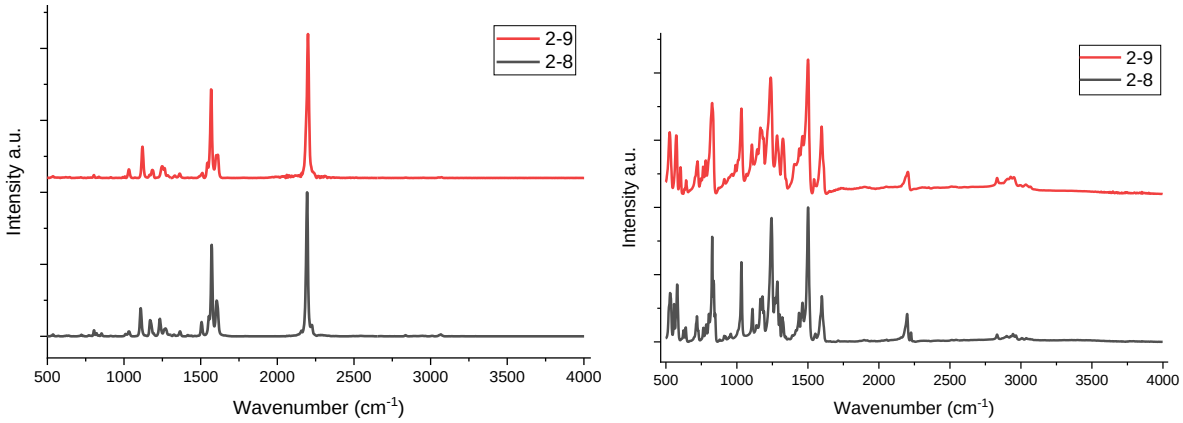

*Figure 56: Raman (left) and IR spectra (right) of **2-8** and **2-9**.*

Chapter 3

Rod-like bis-triarylborane tetrayne dyes were synthesized in both neutral and tetracationic forms, which may find applications in cell imaging and as sensors for DNA, RNA, or other biomolecules. First, trimethylsilyl 1,3-butadiyne **3-9** was synthesized *via* a modified, stepwise, Cadiot-Chodkiewicz protocol, which then underwent deprotection with base to afford **3-10** (Figure 57). In a Pd/Cu co-catalyzed Glaser-type reaction, 1,3-butadiyne **3-10** was then homocoupled, yielding tetrayne **3-11.** To obtain a water-soluble dye, **3-11** was then methylated at all four nitrogens, to obtain the triflate salt **3-12**.

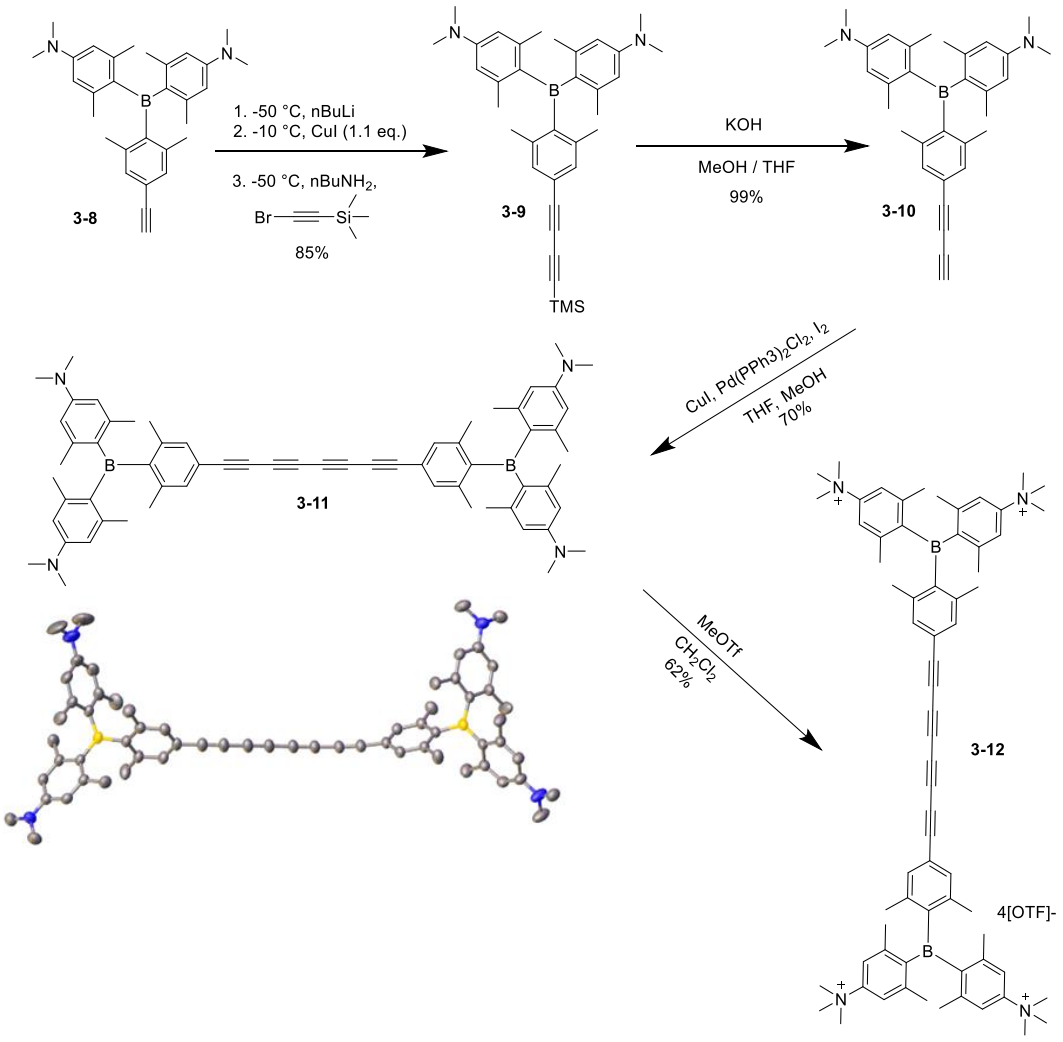

*Figure 57: Synthetic route to neutral and charged tetraynes **3-11** and **3-12**.*

The molecular structure of the neutral compound **3-11** in the solid state is slightly bent (see structure in Figure 57). In the crystal lattice, the alkyne rods are staggered and kept apart by the bulky end-caps. The length of the chain, measured between the two boron atoms, is 20.382(2) Å. Both tetrayne dyes absorb in the near-UV and into the blue region of the visible spectrum and are weakly fluorescent in solution. The charged version **3-12** exhibits a reduced quantum yield, and the methylation of the amines shuts off the charge transfer process. IR and Raman spectra of solid samples of **3-11** and **3-12** were recorded, both exhibit characteristic C≡C stretching absorptions at 2125 cm^{-1} (Figure 58). In the Raman spectra the C≡C bands are significantly more intense compared to those in the IR spectra.

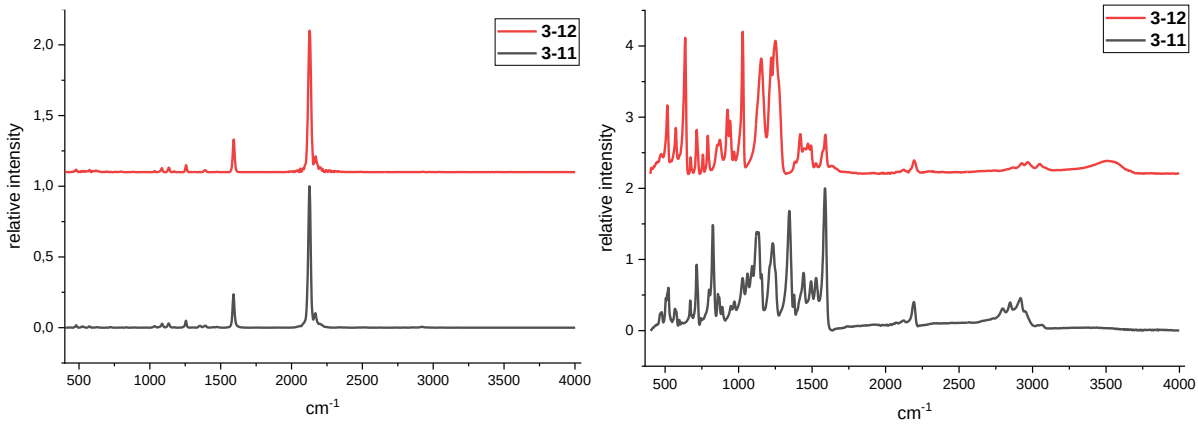

*Figure 58: Raman (left) and IR (right) spectra of **3-11** (black) and **3-12** (red) in the solid state.*

Chapter 4

A protocol for the selective *trans*-hydroboration of 1,3-diynes with pinacolborane (HBpin), catalyzed by tri-*n*-butylphosphine ($PnBu_3$) to give (*E*)-1-boryl-1,3-enynes, featuring a wide substrate scope was developed in collaboration with Santos et al. The reaction is regioselective for borylation at the terminal carbon and works faster with electron withdrawing groups at the aryl substituents. Previously, DFT calculations were conducted by our other collaboration partners Lin et al., to elucidate the mechanism, leading to the proposed catalytic cycle below in Figure 59. A series of *in situ* NMR experiments were conducted, based on the model reaction in Figure 59, to support the proposed mechanism and to rule out alternative reaction pathways.

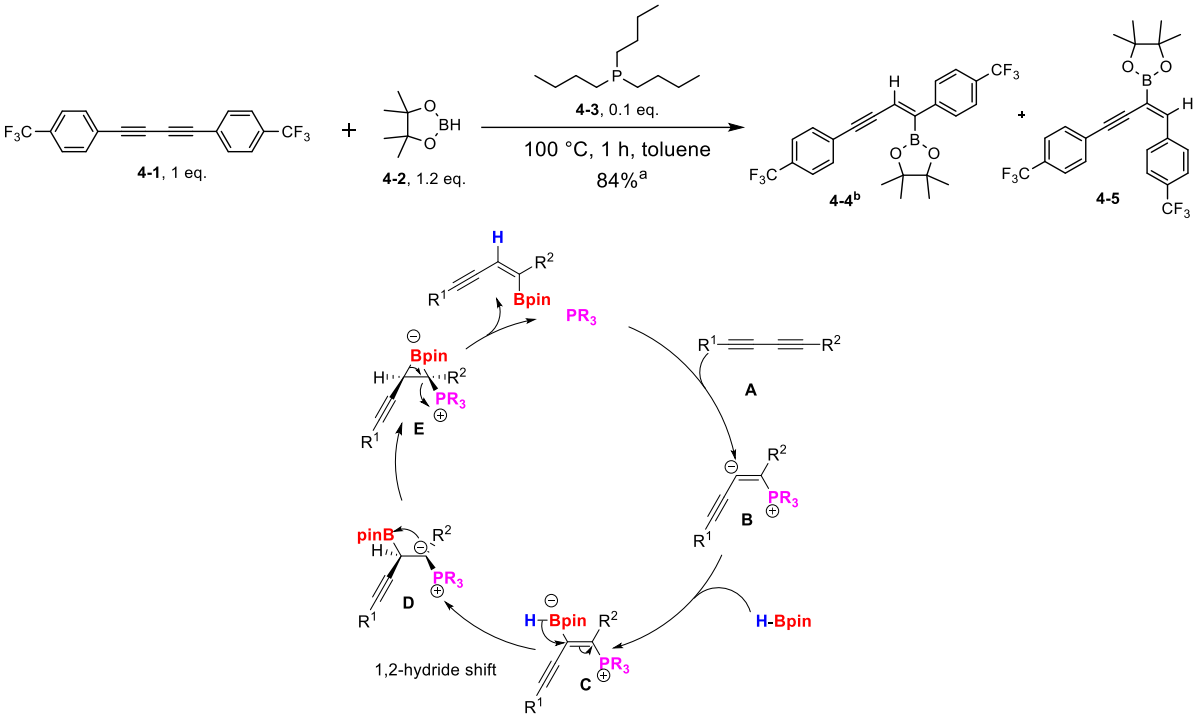

*Figure 59: Above: Model reaction for further studies on the phosphine-catalyzed hydroboration reaction of 1,3-butadiynes. [a]Isolated yield, [b]The cis-hydroboration isomer **4-5** was present in traces of <1%, the Z isomer of **4-4** was formed as well with an E/Z ratio of 89:11 (based on GC-MS analysis).*
Below: Proposed catalytic cycle for the phosphine-catalyzed 1,3-butadiyne hydroboration.

We confirmed, experimentally, that hydroboration of diyne **4-1** with HBpin does not occur without the phosphine catalyst. We combined HBpin and $PnBu_3$ and did not observe any adducts or other reaction between these two components. When combined at room temperature, the diyne **4-1** and $PnBu_3$ react to generate what appears to be a zwitterionic adduct, as well as adducts containing multiple phosphines and diynes (see $^{31}P\{^{1}H\}$ NMR spectrum in Figure 60 and LIFDI HRMS in Figure 61). Most of these adducts contain more diyne than phosphine. Hydroboration of the diyne with HBpin also proceeds with tributyl phosphine

oxide (O=PnBu$_3$) as the precatalyst. The phosphine oxide is thereby reduced to the phosphine during the reaction, which may then act as the catalyst. The phosphine oxide (O=PnBu$_3$) did not react with diyne **4-1**, in contrast to PnBu$_3$. The reaction is slower when using phosphine oxide instead of phosphine. Taken together, experimental evidence supports the catalytic cycle in Figure 59.

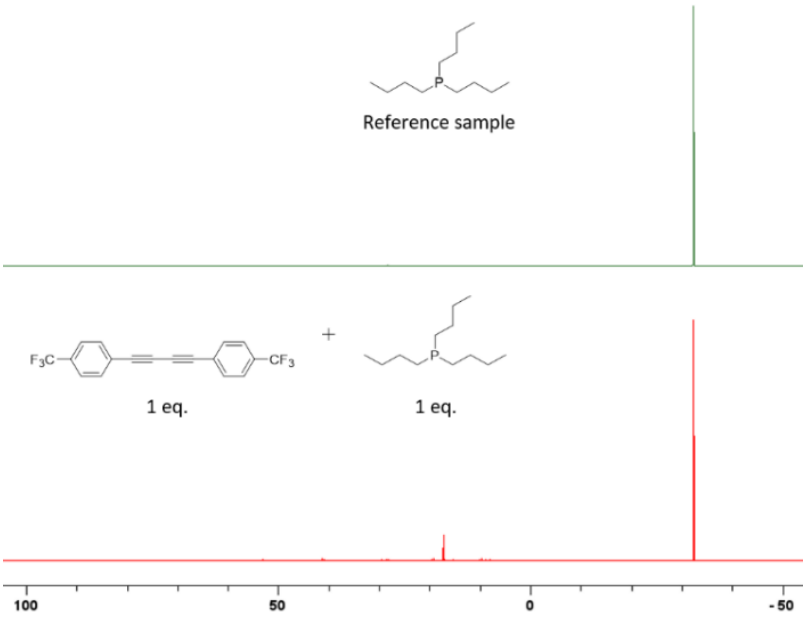

*Figure 60: $^{31}P\{^1H\}$ (121 MHz, scale in ppm) NMR spectra of a mixture of PnBu$_3$ (0.1 mmol) and diyne **4-1** (0.1 mmol), after 3 d at room temperature (bottom) and a PnBu$_3$ reference sample (top). A number of new signals are observed in the bottom spectrum, with the major one being at 17 ppm.*

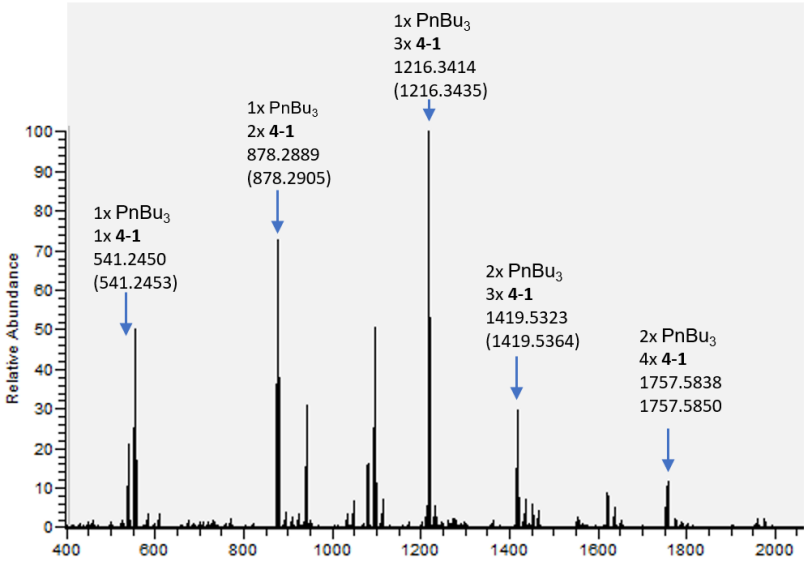

*Figure 61: LIFDI-HRMS of a 1:1 mixture of PnBu$_3$ and diyne **4-1** after 3 d at r.t. The 1:1 adduct of the substrates is marked on the left, and there are several other, heavier, adducts of different composition present.*

Deutsche Zusammenfassung

Kapitel 1

Palladium(0) katalysiert die Zyklisierung von zwei Äquivalenten des Bisdiins **1-1**, um die vollständig substituierten Azulen- (**1-2**) und Naphthalen-Derivate (**1-3**) zu erhalten (Abbildung 62). Der Präkatalysator $Pd_2(dba)_3$-$CHCl_3$ erwies sich als die aktivste Pd(0)-Quelle für die Reaktion, zu der 1 Äquivalent PPh_3 pro Pd hinzugefügt wurde. Der Dibenzylidenaceton (dba)-Ligand reagiert auch mit Bisdiin **1-1**, wobei 1,3-Cyclohexadien **1-4** als Nebenprodukt entsteht. Das Lösungsmittel hat einen erheblichen Einfluss auf die Reaktion. So wird bei der Reaktion in Acetonitril nur das Naphthalenprodukt **1-3** gebildet.

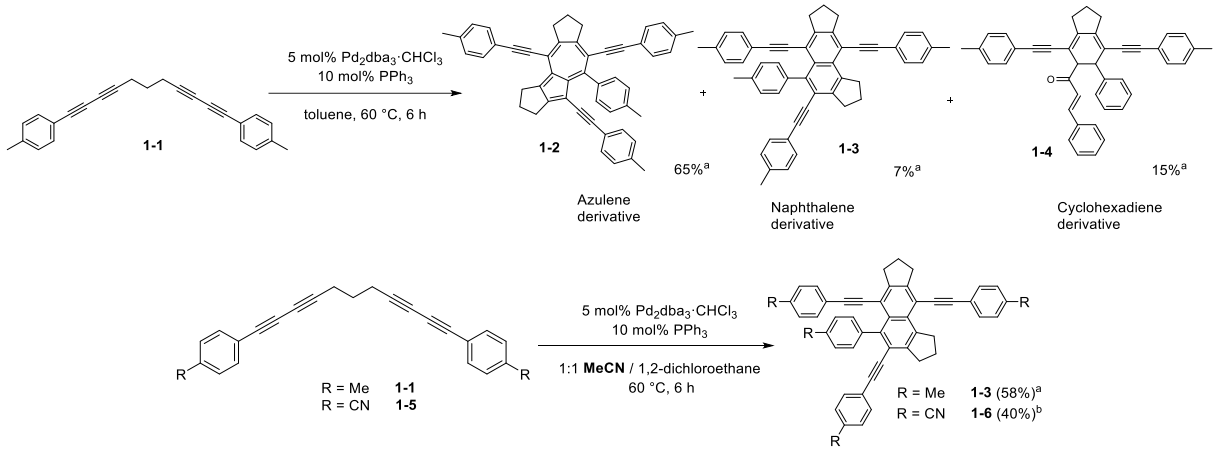

Figure 62: Palladium-katalysierte Bisdiin-Cyclisierungsreaktion (oben) und die erzielte lösungsmittelgesteuerte Selektivität der Reaktion (unten). [a]NMR Ausbeute, [b]Isolierte Ausbeute.

Bei Zugabe von 0.85 Äquivalenten dba zu der Reaktion, was einem Verhältnis von dba zu Bisdiin von 1:1 entspricht, ist das 1,3-Cyclohexadien-Derivat das Hauptprodukt, welches für vier verschiedene Bisdiin-Substrate isoliert wurde (Figure 63).

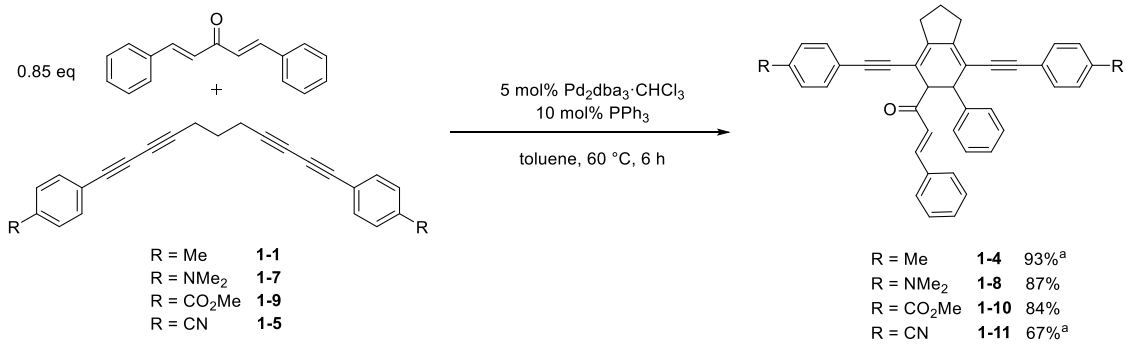

Figure 63: Palladium-katalysierte [2+2+2]-Cocyclisierung von Bisdiinen mit Dibenzylidenaceton. Isolierte Ausbeuten. [a]SPhos wurde anstelle von PPh_3 verwendet, was die Ausbeute leicht verbesserte.

Die photophysikalischen Eigenschaften des nitrilsubstituierten Naphthalen-Derivats **1-6** wurden mit denen des methylsubstituierten Derivats **1-3** verglichen (Abbildung 64). Beide Verbindungen absorbieren im UV und bis ca. 450 nm im sichtbaren Bereich des Spektrums und zeigen Emissionsmaxima mit einer Schwingungsprogression. Die Quantenausbeute von **1-6** (Φ = 0.72) ist etwas höher als die von **1-3** (Φ = 0.6), wobei beide Verbindungen stärker emittieren und bathochrom verschoben sind im Vergleich zu unsubstituiertem Naphthalen, welches im nahen UV bei 320 nm mit Φ = 0.23 in Cyclohexan emittiert.[29] Die 1,3-Cyclohexadien-Derivate sind bei Bestrahlung in verdünnter Lösung instabil. Im IR-Spektrum von **1-6** ist die C≡N-Bande bei 2225 cm^{-1} gegenüber der C≡C-Bande bei 2187 cm^{-1} stärker ausgeprägt; für das Raman-Spektrum gilt das Gegenteil (Abbildung 65).

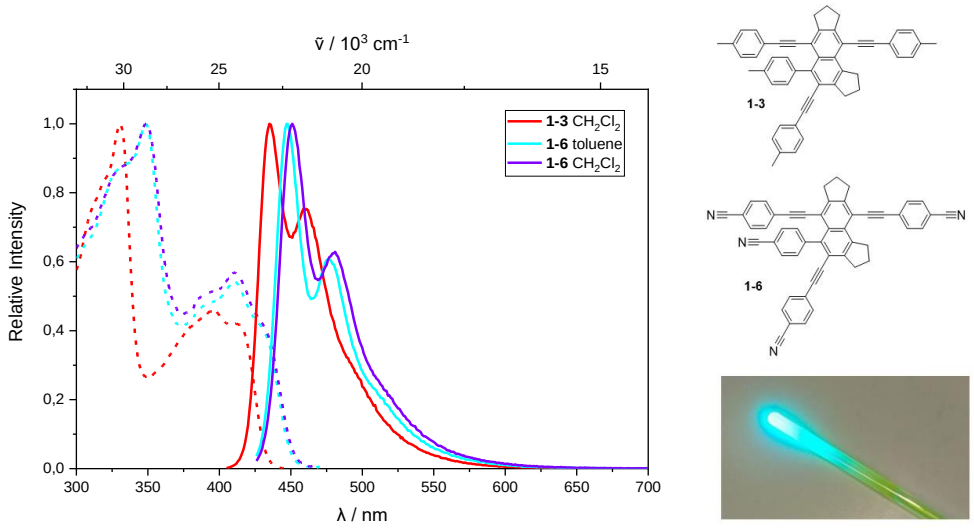

*Figure 64: UV/Vis- (gestrichelte Linie) und Emissionsspektren (durchgezogene Linie) von **1-3** und **1-6** sowie eine $CDCl_3$-Lösung von **1-6**, bestrahlt bei 365 nm. Die Daten für **1-3** wurden zuvor ermittelt.[17]*

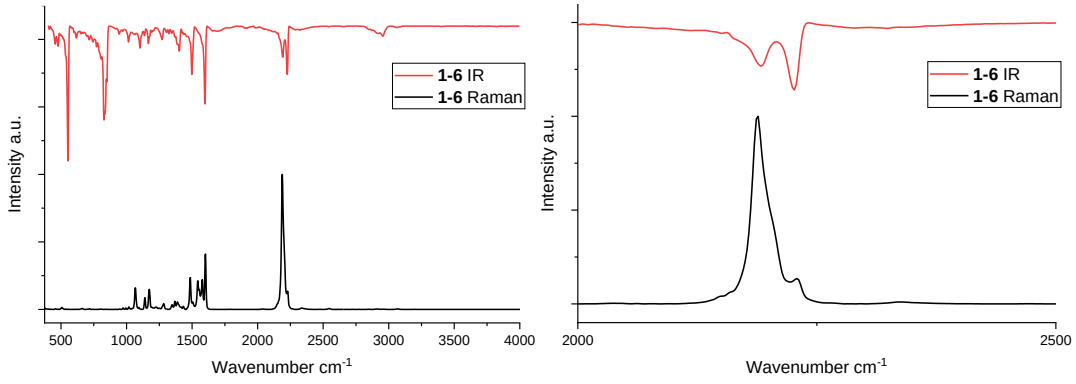

*Figure 65: Raman- und IR-Spektren von **1-6** (links) und vergrößerter Ausschnitt desselben Spektrums (rechts).*

Kapitel 2

Nickel(0)-katalysierte [2+2+2]-Cycloadditionen von Bisdiinen mit Diphenylacetylenen wurden unter Verwendung der Ni(II)-Katalysatorvorstufe [(TMEDA)Ni(o-tolyl)Cl] als Ni(0)-Quelle durchgeführt, wobei zwei Äquivalente PPh_3 pro Ni zugegeben wurden (Abbildung 66). Die Reaktion funktionierte am besten mit Bisdiinen, welche elektronenschiebend substituiert sind, und mit Diphenylacetylenen, mit elektronenziehenden Substituenten. Die Azulen- und Naphthalenprodukte, die unter Pd-Katalyse von Bisdiinen gebildet wurden (Kapitel 1), wurden nicht beobachtet.

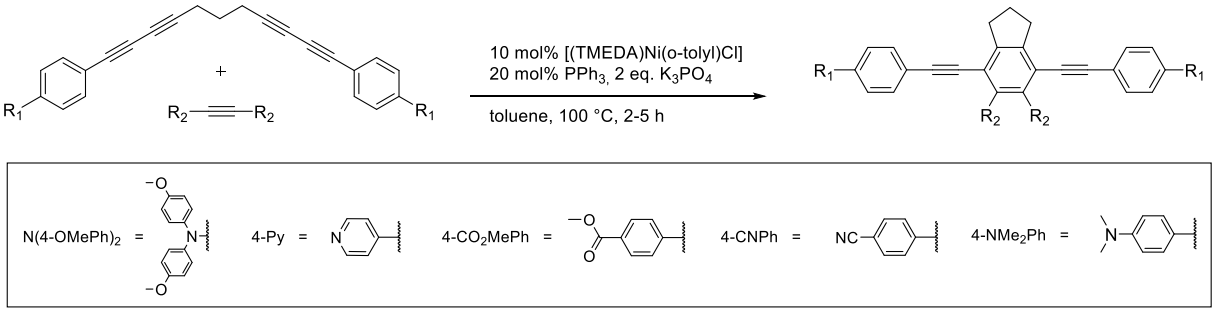

#	Verbindung	R_1	R_2	Ausbeute (%)[a]
1	**2-5**	NMe_2	4-CNPh	74[b]
2	**2-6**	NMe_2	4-CO_2MePh	51[b]
3	**2-7**	NMe_2	4-Py	51[c]
4	**2-8**	N(4-OMePh)$_2$	4-CNPh	23[c]
5	**2-9**	N(4-OMePh)$_2$	4-Py	26[c]
	unerfolgreiche Versuche			
6		CN	4-CNPh	<10[b]
7		NMe_2	4-NMe_2Ph	– [b]
8		CN	4-NMe_2Ph	traces[b]

Figure 66: Nickel-katalysierte Bisdiin-Diphenylacetylen-Cyclisierungsreaktionen. [a]Isolierte Ausbeuten, [b]100 °C für 5 h, Ölbad, [c]Bei 100 °C für 2 h, Mikrowellenreaktor.

Die C_{2v}-symmetrischen D-π-A-π-D o-Terphenyl-Farbstoffe wurden mittels UV/Vis- und Fluoreszenzspektroskopie untersucht. Die Verbindungen absorbieren im UV und im sichtbaren Bereich des Spektrums bis ca. 475 nm. (Die Spektren von **2-8** sind als Beispiel in Abbildung 67 gezeigt). Die Verbindungen zeigen solvatochrome Emission mit guten bis ausgezeichneten Fluoreszenzquantenausbeuten in unpolaren Lösungsmitteln (z. B. im Bereich von $\Phi = 0.83 – 1.00$ in Toluol). Alle Verbindungen weisen kurze Lebensdauern von nur wenigen Nanosekunden auf. Alle D-π-A-π-D-Verbindungen weisen lokal angeregten (LE) und Ladungstransfer-Charakter (CT) auf, wobei die Emission in unpolaren Lösungsmitteln vom LE-Typ ist und in polaren Lösungsmitteln einen erheblichen CT-Charakter aufweist.

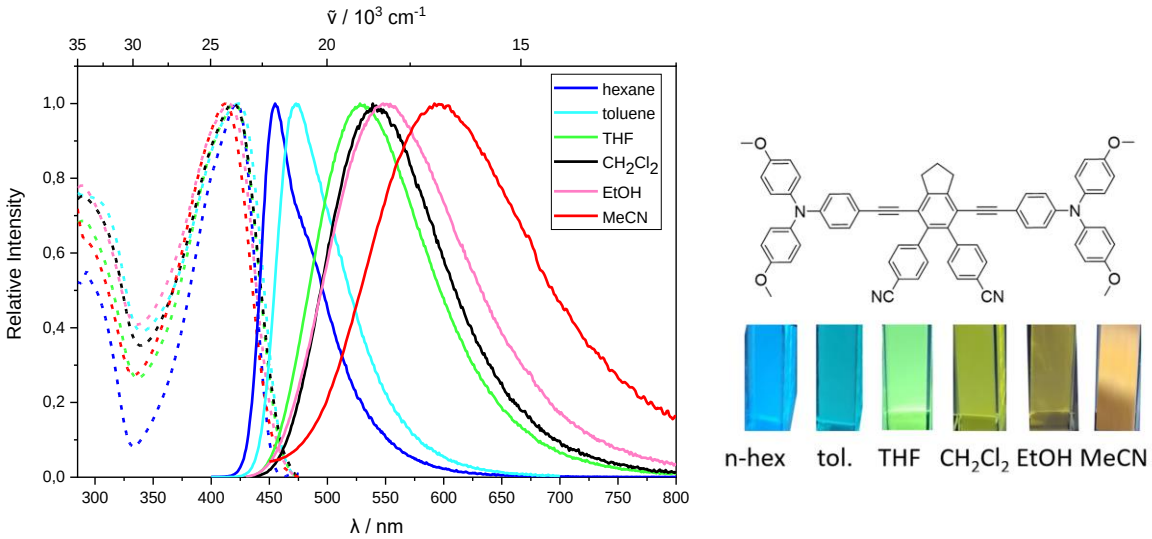

*Figure 67: Absorptions- (gestrichelt) und Emissionsspektren (durchgezogen) von **2-8** in verschiedenen Lösungsmitteln und Fotos der Emission in Küvetten mit einer Absorption von 0.1, bestrahlt bei 365 nm.*

Die Schwingungsspektren der Triarylaminfarbstoffe zeigen eine charakteristische C≡C-Streckbande in den Raman- und IR-Spektren bei ca. 2194 cm^{-1} (Abbildung 68); die Bande ist in den Raman-Spektren deutlich stärker als in den IR-Spektren.

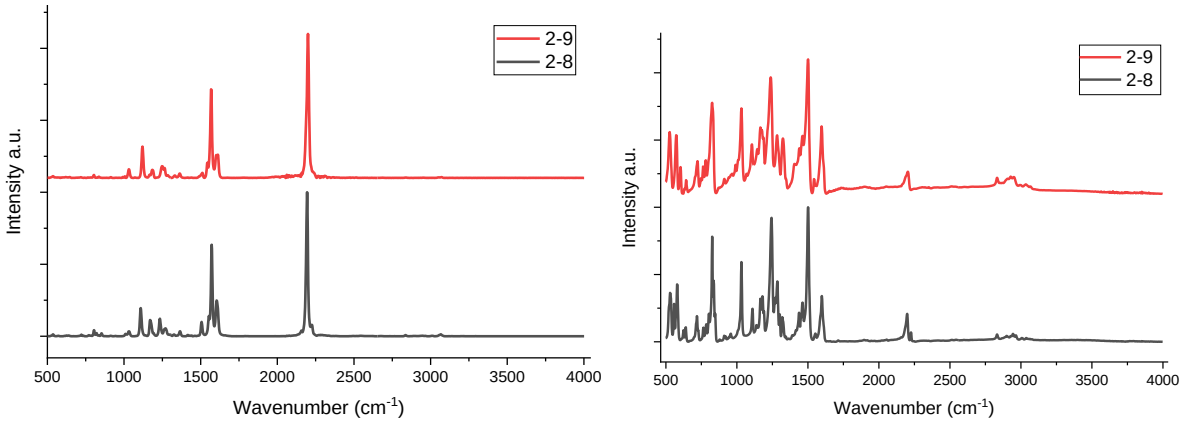

*Figure 68: Raman (links) and IR Spektren (rechts) von **2-8** und **2-9**.*

Kapitel 3

Es wurden stabförmige Bis-Triarylboran-Tetrain-Farbstoffe sowohl in neutraler als auch in tetrakationischer Form synthetisiert, die Anwendungen in der Zellbildgebung und als Sensoren für DNA, RNA oder andere Biomoleküle finden könnten. Zunächst wurde Trimethylsilyl-1,3-butadiin **3-9** über ein modifiziertes, schrittweises Cadiot-Chodkiewicz-Protokoll synthetisiert, und wurde dann basisch entschützt wurde, um **3-10** zu erhalten (Abbildung 69). In einer Pd/Cu-cokatalysierten Reaktion vom Glaser-Typ wurde 1,3-Butadin **3-10** homogekuppelt, wobei Tetrayne **3-11** entstand. Um einen wasserlöslichen Farbstoff zu erhalten, wurde **3-11** anschließend an allen vier Stickstoffatomen methyliert, um das Triflatsalz **3-12** zu erhalten.

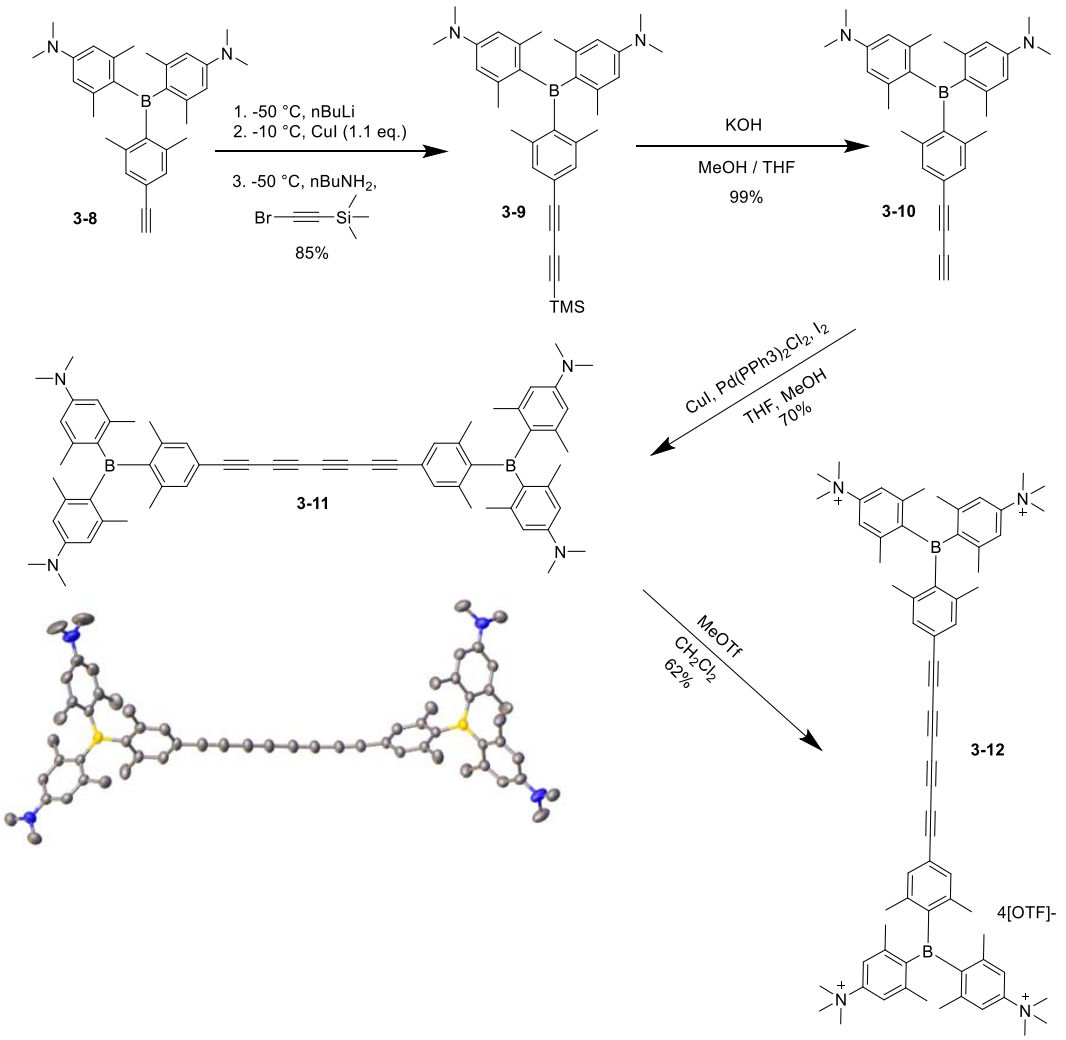

*Figure 69: Synthetische Route zu den neutralen und geladenen Tetrainen **3-11** und **3-12**.*

Die Struktur der neutralen Verbindung im festen Zustand ist leicht S-förmig gebogen. Im Kristallgitter sind die Alkinstäbe gestaffelt und werden durch die sperrigen Endkappen auf Abstand gehalten. Die Länge der Kette, gemessen zwischen den beiden Boratomen, beträgt 20,382(2) Å. Beide Tetrain-Farbstoffe absorbieren im nahen UV und im blauen Bereich des sichtbaren Spektrums und sind in Lösung schwach fluoreszierend. Die geladene Version **3-12** weist eine reduzierte Quantenausbeute auf; durch die Methylierung der Amine findet kein Ladungstransferprozess mehr statt. Es wurden IR- und Raman-Spektren von festen Proben von **3-11** und **3-12** aufgenommen, die beide charakteristische C≡C-Streckschwingungsabsorptionen bei 2125 cm^{-1} zeigen (Abbildung 70). In den Raman-Spektren sind die C≡C-Banden im Vergleich zu den IR-Spektren deutlich intensiver.

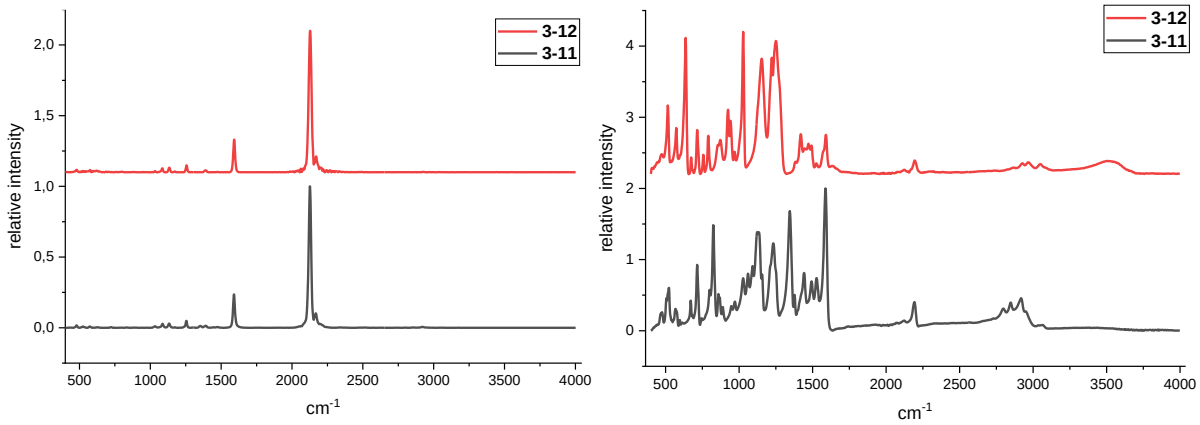

*Figure 70: Raman- (links) und IR-Spektren (rechts) von **3-11** (schwarz) und **3-12** (rot) im festen Zustand.*

Kapitel 4

In Zusammenarbeit mit Santos et al. wurde ein Protokoll für die selektive trans-Hydroborierung von 1,3-Diinen mit Pinacolboran (HBpin) entwickelt, das durch Tri-n-butylphosphin ($PnBu_3$) katalysiert wird, um (E)-1-Boryl-1,3-Enine zu erhalten, wobei ein breites Substratspektrum realisiert wurde. Die Reaktion ist regioselektiv für die Borylierung am terminalen Kohlenstoff und funktioniert schneller mit elektronenziehenden Gruppen an den Arylsubstituenten. Zuvor wurden von unseren anderen Kooperationspartnern Lin et al. DFT-Berechnungen durchgeführt, um den Mechanismus aufzuklären, was zu dem in Abbildung 71 dargestellten katalytischen Zyklus führte. Auf der Grundlage der Modellreaktion in Abbildung 71 wurde eine Reihe von In-situ-NMR-Experimenten durchgeführt, um den vorgeschlagenen Mechanismus zu unterstützen und um alternative Reaktionswege auszuschließen.

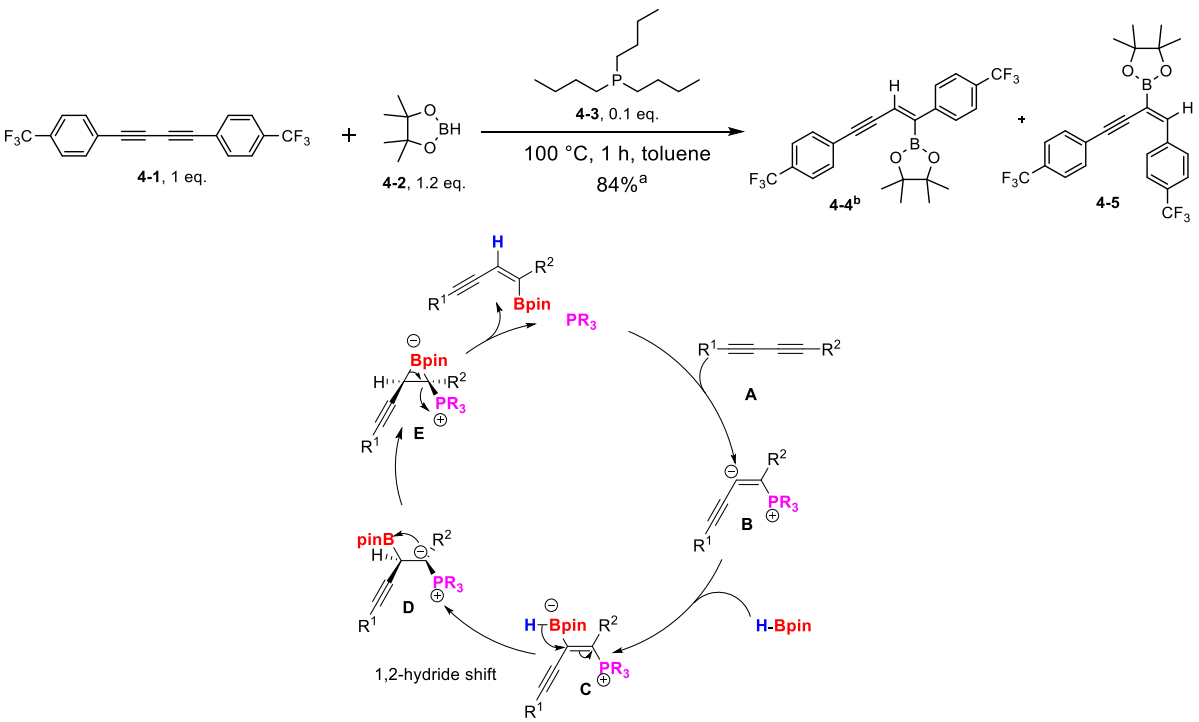

*Figure 71: Oben: Modellreaktion für weitere Untersuchungen zur phosphinkatalysierten Hydroborierungsreaktion von 1,3-Butadiinen. [a]Isolierte Ausbeute, [b]Das cis-Hydroborierungsisomer **4-5** lag in Spuren von <1% vor, das Z-Isomer von **4-4** wurde ebenfalls gebildet, mit einem E/Z-Verhältnis von 89:11 (basierend auf GC-MS-Analyse).*
Unten: Vorgeschlagener katalytischer Zyklus für die Phosphin-katalysierte 1,3-Butadin-Hydroborierung.

Wir haben experimentell bestätigt, dass die Hydroborierung von Diin **4-1** mit HBpin nicht ohne den Phosphin-Katalysator erfolgt. Wir kombinierten HBpin und $PnBu_3$ und konnten keine Addukte oder andere Reaktionen zwischen diesen beiden Komponenten beobachten. Wenn Diin **4-1** und $PnBu_3$ bei Raumtemperatur zusammengefügt werden, reagieren sie und erzeugen ein, scheinbar zwitterionisches, Addukt sowie Addukte, die mehrere Phosphine und

Diine enthalten (siehe $^{31}P\{^{1}H\}$ NMR-Spektrum in Abbildung 72 und LIFDI HRMS in Abbildung 73). Die meisten dieser Addukte enthalten mehr Diin als Phosphin. Die Hydroborierung des Diins mit HBpin findet ebenfalls mit Tributylphosphinoxid ($O{=}PnBu_3$) als Präkatalysator statt. Das Phosphinoxid wird dabei während der Reaktion zum Phosphin reduziert, das dann als Katalysator dienen kann. Das Phosphinoxid ($O{=}PnBu_3$) reagierte im Gegensatz zu $PnBu_3$ nicht mit Diin **4-1**. Bei Verwendung von Phosphinoxid anstelle von Phosphin verläuft die Reaktion langsamer. Insgesamt unterstützen die experimentellen Belege den katalytischen Zyklus in Abbildung 71.

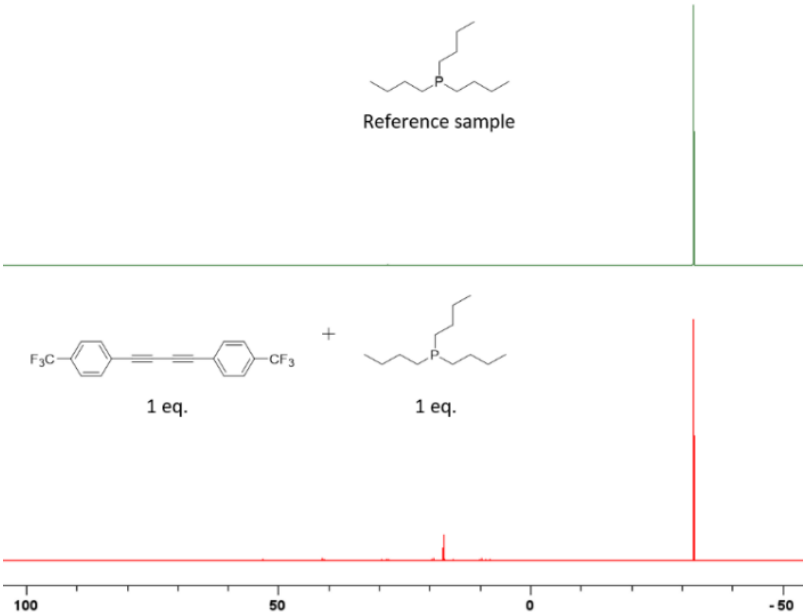

*Figure 72: $^{31}P\{^{1}H\}$ (121 MHz, Skala in ppm) NMR Spektren einer Mischung aus $PnBu_3$ (0.1 mmol) und Diin **4-1** (0.1 mmol) nach 3 Tagen bei Raumtemperatur (unten, rot) und einer $PnBu_3$-Referenzprobe (oben, grün). In dem unteren Spektrum ist eine Reihe neuer Signale zu beobachten, wobei das stärkste bei 17 ppm liegt.*

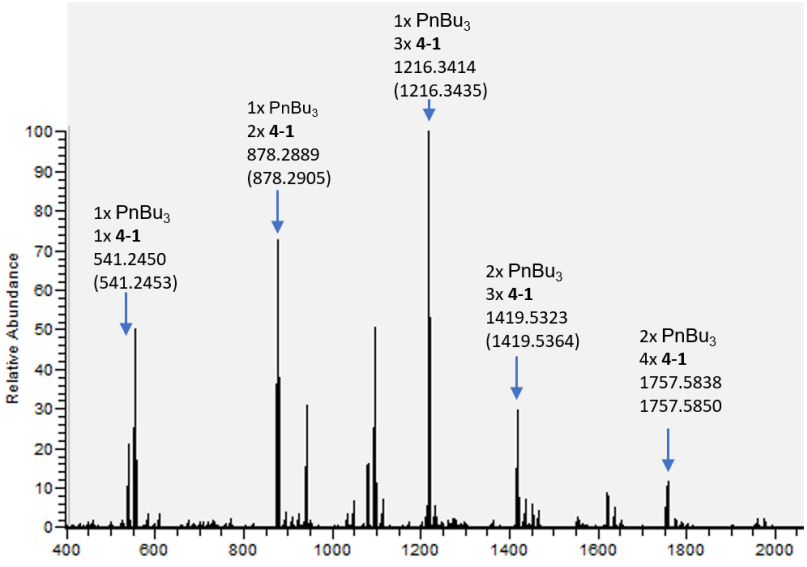

*Figure 73: LIFDI-HRMS einer 1:1-Mischung von $PnBu_3$ und Diin **4-1** nach 3 Tagen bei r.t. Das 1:1-Addukt der Substrate ist links markiert, es sind mehrere schwerere Addukte unterschiedlicher Zusammensetzung enthalten.*

Experimental

Chapter 1

Synthesis

General information:

Unless otherwise noted, all reactions were performed using standard Schlenk or glovebox (Innovative Technology Inc.) techniques under argon. Reagent grade solvents were argon saturated, dried using an Innovative Technology Inc. Pure-Solv Solvent Purification System, and further deoxygenated by using the freeze-pump-thaw method. The compounds dimethyl 4,4'-(undeca-1,3,8,10-tetrayne-1,11-diyl)dibenzoate,[15] 4,4'-(undeca-1,3,8,10-tetrayne-1,11-diyl)bis(N,N-dimethylaniline),[53] and $Pd_2(dba)_3{\cdot}CHCl_3$[134] were prepared according to the literature. All other starting materials were purchased from commercial sources and used without further purification.

Automated flash chromatography was performed using a Biotage® Isolera Four system on silica gel. Commercially available, precoated TLC plates (Polygram® Sil G/UV_{254} and Polygram® Alox N/UV_{254}) were purchased from Macherey-Nagel. The removal of solvent was performed on a rotary evaporator *in vacuo* at a maximum temperature of 50 °C.

GC-MS analyses were performed using an Agilent 7890A gas chromatograph equipped with an Agilent 5975C inert MSD with triple-axis detector operating in EI mode and an Agilent 7693A series auto sampler/injector. High resolution mass spectrometry was obtained from a Thermo Scientific Exactive Plus MS System with either an atmospheric-pressure chemical ionization (APCI) or a heated-electrospray ionization (HESI) probe.

NMR spectra were recorded at ambient temperature using Bruker DRX-300 (^{1}H, 300 MHz; ^{13}C{^{1}H}, 75 MHz), or a Bruker Avance 500 NMR (^{1}H, 500 MHz; ^{13}C{^{1}H}, 125 MHz) spectrometers. ^{1}H NMR chemical shifts are reported in ppm relative to TMS and were referenced *via* residual proton resonances of the corresponding deuterated solvent ($CDCl_3$: 7.26 ppm) whereas ^{13}C{^{1}H} NMR spectra are reported relative to TMS *via* the carbon signals of the deuterated solvent ($CDCl_3$: 77.16 ppm).

Infrared spectra were recorded on a Bruker Alpha FT-IR spectrometer as solids by using an ATR unit with a resolution of 4 cm^{-1} and are reported in cm^{-1}. Raman spectra were recorded at room temperature with a MultiRAM FT-Raman spectrometer in melting point capillaries. Elemental analyses were performed with an Elementar vario micro cube device.

1,7-Dibromo-1,6-heptadiyne

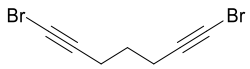

To a mixture of 1,6-heptadiyne (3,2 g, 34 mmol) and N-bromosuccinimide (14.8 g, 83 mmol) in acetone (200 mL) finely ground silver nitrate (1.15 g, 6.7 mmol) was added. After stirring for 10 h at room temperature, the slurry was filtered through a celite pad with additional acetone and the filtrate was collected. After evaporation of the volatiles, the mixture was dissolved in n-hexane and filtered through a 4 cm silica pad, while further product was eluted with n-hexane (800 mL). After carefully evaporating the solvent from the filtrate, the product was obtained as a yellow oil (8.35 g, 99%).

The procedure and NMR data are similar to those reported previously.[135]

^{1}H NMR (300 MHz, $CDCl_3$): $\delta =$ 2.32 (t, 4H), 1.72 (m, 2H); $^{13}C\{^{1}H\}$ NMR (75 MHz, $CDCl_3$): $\delta =$ 79.24, 38.93, 27.18, 18.95.

Trimethyl(p-tolylethynyl)silane

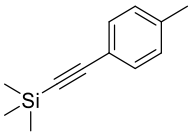

The compounds 4-iodotoluene (30 g, 139 mmol, 1 eq.), $Pd(PPh_3)_2Cl_2$ (0.96 g, 1.4 mmol, 1 mol%) and CuI (0.53 g, 2.8 mmol, 2 mol%) were placed in a Schlenk flask. Triethylamine (450 mL) and trimethylsilylacetylene (15.4 g, 157 mmol, 1.15 eq.) were added and the solution was stirred overnight at room temperature. GC/MS showed complete conversion of the starting material. The solvent was removed under reduced pressure and the precipitated solid was dissolved in n-hexane. The suspension was filtered through a celite pad and washed with n-hexane (1.75 L); the filtrate was collected. The solution was concentrated *in vacuo* to afford the product (26.0 g, 138.0 mmol, 99%) as a dark-yellow oil which was used in the following step without further purification.

The procedure is similar to those reported previously.[51]

GC-MS (EI): *m/z* calcd. 188 [M], found 188.

4-Ethylnyltoluene

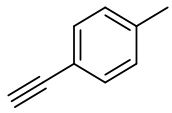

The compound 4-((trimethylsilyl)ethynyl)toluene (26 g, 138 mmol) was dissolved in dichloromethane (100 mL). A solution of KOH (16 g, 0.285 mol) in methanol (115 mL) was added and the mixture was stirred for 1 h at room temperature under air. The solution was filtered through a silica pad and the solvent was partially removed under reduced pressure. Pentane was added and the solution was and filtered through a small silica column. The clear solution was concentrated *in vacuo* to afford the product (12 g, 103 mmol, 75%) as a yellow oil.

The procedure and NMR data are similar to those reported previously.[51]

^{1}H NMR (300 MHz, $CDCl_3$): δ = 7.40 (m, 2H), 7.16 (m, 2H), 3.05 (s, 1 H), 2.37 (s, 3H); GC-MS (EI): *m/z* calcd. 116 [M], found 116.

1,11-Di-p-tolylundeca-1,3,8,10-tetrayne **1-1**

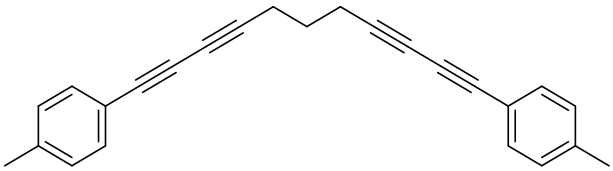

CuI (120.0 mg, 0.63 mmol, 0.05 eq.) was dissolved in n-butylamine (25 mL) and methanol (240 mL). Hydroxylammonium chloride (875 mg, 12.6 mmol, 0.9 eq.) was added and the solution was stirred for 10 min. Then, 4-ethylnyltoluene (3.5 g, 30.5 mmol, 2.2 eq.) was added and the solution was stirred for 5 min. Then 1,7-dibromohepta-1,6-diyne (3.4 g, 13.9 mmol, 1 eq.) was added by syringe and the solution was stirred for 2 h at room temperature and another 30 min at 60 °C. The solution, which already contained a precipitate, was concentrated to 200 mL and cooled in an ice bath. The precipitated solid was collected by filtration and washed with methanol, to afford **1-1** (3.0 g, 9.4 mmol, 67%) as a colorless solid.

The procedure and NMR data are similar to those reported previously.[51]

^{1}H NMR (300 MHz, $CDCl_3$): δ = 7.38 (m, 4H), 7.11 (m, 4H), 2.53 (t, *J* = 7 Hz, 4H), 2.35 (s, 6H), 1.84 (q, *J* = 7 Hz, 2H); HRMS (APCI+): *m/z* calcd. 321.1630 [M+H], found. 321.1638.

4-((Trimethylsilyl)ethynyl)benzonitrile

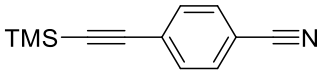

The compounds 4-iodobenzonitrile (12.9 g, 56.3 mmol, 1 eq.), $[Pd(PPh_3)_2Cl_2]$ (393 mg, 0.56 mmol, 1 mol%) and CuI (213 mg, 1.12 mol, 2 mol%) were placed in a Schlenk flask. Triethylamine (200 mL) and trimethylsilylacetylene (6.35 g, 64.7 mmol, 1.15 eq.) were added and the solution was stirred overnight at room temperature. GC/MS showed complete conversion of the 4-iodobenzonitrile starting material. The solvent was removed under reduced pressure and the residue was suspended in *n*-hexane. The suspension was filtered through a celite pad and rinsed with *n*-hexane. The filtrate was concentrated *in vacuo* to afford the product (9.0 g, 45.0 mmol, 80%) as a colorless solid, which was used in the next step.

The procedure is similar to that reported previously.[136, 137]

4-Ethynylbenzonitrile

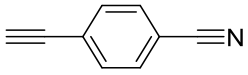

The compound 4-((trimethylsilyl)ethynyl)benzonitrile (8.66 g, 43.5 mmol) was dissolved in dichloromethane (50 mL). A solution of potassium hydroxide (12.0 g, 214 mmol) in methanol (55 mL) was added and the mixture was stirred for 2 h at room temperature under air. GC/MS showed complete conversion of the starting material. The solution was filtered through a silica pad and the solvent was removed under reduced pressure. Hexane (200 mL) and dichloromethane (200 mL) were added. The mixture was filtered through a silica pad and the solvent was removed from the filtrate under vacuum to afford a colorless solid (5.07 g, 39.9 mmol, 92%).

The procedure and NMR data are similar to that reported previously.[136, 137]

^{1}H NMR (300 MHz, $CDCl_3$): $\delta = 7.66 – 7.53$ (m, 4H), 3.30 (s, 1H); GC-MS (EI): m/z calcd. 127 [M], found 127.

*4,4'-(Undeca-1,3,8,10-tetrayne-1,11-diyl)dibenzonitrile (**1-5**)*

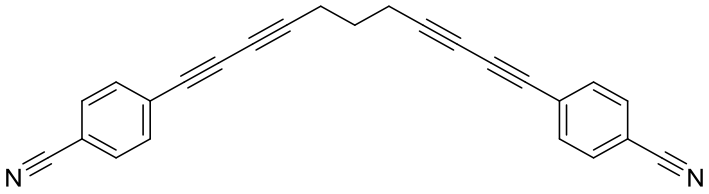

CuI (137 mg, 720 µmol, 0.06 eq.) was suspended in *n*-butylamine (22 mL) and methanol (420 mL) in a Schlenk flask. Hydroxylammonium chloride (830 mg, 12 mmol, 1.0 eq.) was added and the solution was stirred for 10 min. Then, 4-ethynylbenzonitrile (3.36 g, 23.6 mmol, 2.2 eq.) was added and the solution was stirred for 5 min before 1,7-dibromohepta-1,6-diyne (3.00 g, 12.0 mmol, 1.0 eq.) was added by syringe and the solution was stirred for an additional 2 h at room temperature. The precipitated solid was collected by filtration and dissolved in dichloromethane. The solution was filtered through a silica pad and the solvent was removed under reduced pressure from the filtrate to afford **1-5** (1.87 g, 5.46 mmol, 46%) as a colorless solid.

^{1}H NMR (300 MHz, $CDCl_3$): δ = 7.64 – 7.50 (m, 8H), 2.57 (t, 2H, J = 7 Hz), 1.88 (q, 2H, J = 7 Hz); $^{13}C\{^{1}H\}$ NMR (75 MHz, $CDCl_3$) δ = 133.1, 132.1, 127.0, 118.3, 112.3, 85.6, 78.4, 73.3, 65.8, 26.7, 18.9; Elemental analysis calcd.: C: 87.70, H: 4.12, N: 8.18 found: C: 87.33 H: 4.31, N: 8.28 HRMS (APCI+) *m/z* calcd.: 343.1235 $[M+H]^+$, found: 343.1220.

*4,4',4''-((5-(4-Cyanophenyl)-1,2,3,7,8,9-hexahydrodicyclopenta[a,g]naphthalene-4,6,10-triyl)tris(ethyne-2,1-diyl))tribenzonitrile (**1-6**)*

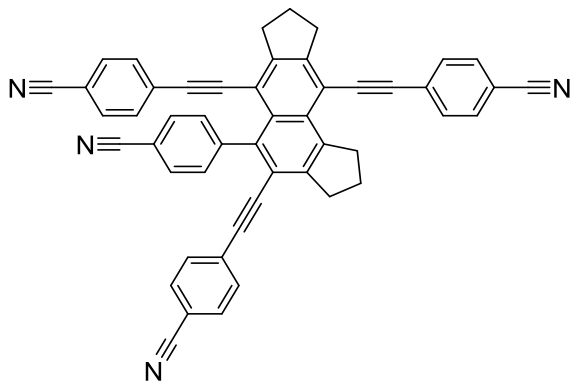

The compounds 4,4'-(undeca-1,3,8,10-tetrayne-1,11-diyl)dibenzonitrile **1-5** (136.84 mg, 0.4 mmol, 1 eq.), $Pd_2(dba)_3 \cdot CHCl_3$ (15.5 mg, 0.015 mmol, 0.0375 eq.) and triphenylphosphine (7.9 mg, 0.03 mmol, 0.075 eq.) were dissolved in 5 mL of acetonitrile and 5 mL of 1,2-dichloroethane. The mixture was stirred at 60 °C for 6 h and then filtered through a silica pad with dichloromethane (50 mL). After removal of the solvents from the filtrate, the product was washed with acetone and *n*-hexane to yield 55 mg (40%) of the yellow product.

^{1}H NMR (300 MHz, $CDCl_3$): $\delta =$ 7.73 – 7.54 (m, 12H), 7.18 – 7-10 (m, 4H), 4.03 (t, 2H, *J* = 8 Hz), 3.38 – 3.22 (m, 4H), 3.17 (t, 2H, *J* = 8 Hz), 2.37 – 2.14 (m, 4H); $^{13}C\{^1H\}$ NMR (125 MHz, $CDCl_3$) δ = 150.2, 150.1, 146.7, 144.2, 140.9, 140.0, 132.5, 132.4, 132.2, 132.1, 131.8, 131.5, 131.5, 131.2, 130.9, 129.4, 128.4, 127.8, 127.7, 119.4, 118.7, 116.6, 115.9, 112.0, 111.9, 111.8, 111.8, 102.8, 98.10, 96.19, 92.64, 91.74, 36.16, 34.97, 34.72, 33.74, 24.45, 23.67. Elemental Analysis calcd.: C: 87.69, H: 4.13, N: 8.18, found: C: 87.12, H: 4.19, N: 8.26; HRMS (ASAP$^-$) *m/z* calcd.: 684.2308 [M], found: 684.2312.

*(E)-3-Phenyl-1-(6-phenyl-4,7-bis(p-tolylethynyl)-2,3,5,6-tetrahydro-1H-inden-5-yl)prop-2-en-1-one (**1-4**)*

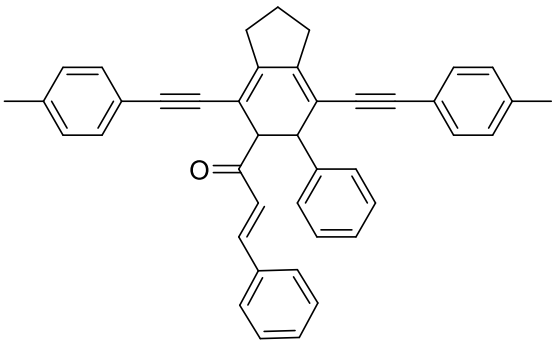

The compounds 1,11-di-*p*-tolylundeca-1,3,8,10-tetrayne **1-1** (256 mg, 799 µmol, 1 eq.), (1E, 4E)-1,5-diphenylpenta-1,4-dien-3-one (dba, 159 mg, 679 µmol, 0.85 eq.), $Pd_2(dba)_3 \cdot CHCl_3$ (41.3 mg, 40.0 µmol, 0.05 eq.) and 2-dicyclohexylphosphino-2',6'-dimethoxybiphenyl (SPhos, 32.8 mg, 80.0 µmol, 0.1 eq.) were placed in a Schlenk flask. Toluene (32 mL) was added, and the mixture was stirred at 60 °C for 6 h. The solvent was removed under reduced pressure and the crude product was purified by flash chromatography (hexane / dichloromethane, 0 – 40% dichloromethane) to afford **1-4** (412 mg, 93%) as an orange solid.

^{1}H NMR (500 MHz, $CDCl_3$): δ = 7.67 (m, 1H), 7.55 – 7.50 (m, 2H), 7.38 – 7.26 (m, 10H), 7.25 – 7.24 (m, 1H), 7.20 – 7.15 (m, 2H), 7.10 – 7.03 (m, 4H), 4.33 – 4.28 (m, 1H), 3.88 – 3.81 (m, 1H), 2.88 – 2.64 (m, 4H), 2.33 (s, 3H), 2.31 (s, 3H), 1.98 – 1.87 (m, 2H); ^{13}C{^{1}H} NMR (125 MHz, $CDCl_3$) δ = 197.0, 149.4, 145.5, 143.3, 142.6, 138.5, 138.2, 135.0, 131.4, 131.3, 130.4, 129.2, 128.9, 128.7, 128.5, 128.0, 127.1, 124.6, 120.7,120.4, 114.9, 106.1, 98.27, 97.70, 89.74, 89.20, 57.84, 45.57, 32.37, 31.98, 23.95, 21.64, 21.62; Elemental Analysis calcd.: C: 90.94, H: 6.18; found: C: 89.73, H: 6.37. HRMS (APCI+) *m/z* calcd.: 555.2688 $[M+H]^+$, found: 555.2663.

*(E)-1-(4,7-Bis((4-(dimethylamino)phenyl)ethynyl)-6-phenyl-2,3,5,6-tetrahydro-1H-inden-5-yl)-3-phenylprop-2-en-1-one (**1-8**)*

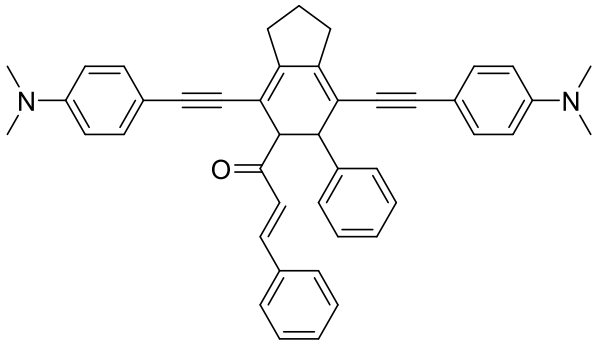

The compounds 4,4'-(undeca-1,3,8,10-tetrayne-1,11-diyl)bis(*N,N*-dimethylaniline) (**1-7**) (151 mg, 399 µmol, 1 eq.), (1E, 4E)-1,5-diphenylpenta-1,4-dien-3-one (dba, 79.5 mg, 339 µmol, 0.85 eq.), $Pd_2(dba)_3{\cdot}CHCl_3$ (20.8 mg, 20.1 µmol, 0.05 eq.) and triphenylphosphine (10.5 mg, 40.0 µmol, 0.1 eq.) were placed in a Schlenk flask. Toluene (16 mL) was added, and the mixture was stirred at 60 °C for 6 h. The solvent was removed under reduced pressure and the crude product was purified by flash chromatography (dichloromethane) to afford **1-8** (212 mg, 87%) as an orange solid.

^{1}H NMR (300 MHz, $CDCl_3$): δ = 7.68 – 7.61 (m, 1H), 7.55 – 7,49 (m, 2H), 7.38 – 7.26(m, 9H), 7.25 – 7.12 (m, 4H), 6.64 – 6.51 (m, 4H), 4.28(m, 1H), 3.81(m, 1H), 2.96 (s, 6H), 2.94 (s, 6H), 2.83 – 2.66 (m, 4H), 1.90 (m, 2H); ^{13}C{^{1}H} NMR (75 MHz, $CDCl_3$): δ= 197.3, 150.0, 149.9, 147.9, 144.1, 142.9, 142.8, 135.1, 132.6, 132.5, 130.1, 129.0, 128.8, 128.5, 128.5, 128.4, 128.0, 126.8, 124.7, 114.7, 111.8, 111.7, 110.4, 105.8, 99.2, 98.6, 88.7, 88.2, 58.0, 45.6, 40.2, 32.2, 31.9, 23.9; Elemental Analysis calcd.: C: 86.24, H: 6.58, N: 4.57; found: C: 85.55, H: 6.55, N: 4.42; HRMS ($APCI^+$) *m/z* calcd.: 613.3213 $[M+H]^+$, found: 613.3194.

*Dimethyl 4,4'-((5-cinnamoyl-6-phenyl-2,3,5,6-tetrahydro-1H-indene-4,7-diyl)bis(ethyne-2,1-diyl))dibenzoate (**1-10**)*

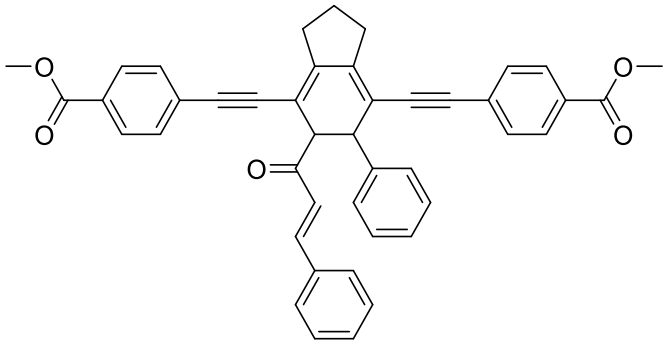

Dimethyl 4,4'-(undeca-1,3,8,10-tetrayne-1,11-diyl)dibenzoate (163 mg, 400 µmol, 1 eq.), (1E, 4E)-1,5-diphenylpenta-1,4-dien-3-one (dba, 80.0 mg, 341 µmol, 0.85 eq.), $Pd_2(dba)_3 \cdot CHCl_3$ (20.8 mg, 20.1 µmol, 0.05 eq.) and triphenylphosphine (10.5 mg, 40.0 µmol, 0.1 eq.) were placed in a Schlenk flask. Toluene (16 mL) was added, and the mixture was stirred for 6 h at 60 °C. The solvent was removed under reduced pressure and the crude product was purified by flash chromatography (70% - 100% dichloromethane in *n*-hexane) to afford **1-10** (217 mg, 84%) as a yellow solid.

^{1}H NMR (300 MHz, $CDCl_3$) δ = 7.95 – 7.88 (m, 4H), 7.71 – 7.64 (m, 1H), 7.51 (m, 2H), 7.41 (m, 2H), 7.37 – 7.27 (m, 10H), 7.22 – 7.16 (m, 1H), 4.32 (m, 1H), 3.92 – 3.87 (m, 7H), 2.88 – 2.71 (m, 4H), 2.02 – 1.90 (m, 2H); $^{13}C\{^1H\}$ NMR (75 MHz, $CDCl_3$): δ = 196.6, 166.6, 166.6, 150.8, 147.0, 143.7, 142.1, 134.7, 131.4, 131.2, 130.7, 129.6, 129.5, 129.4, 129.3, 129.0, 128.8, 128.5, 128.2, 127.9, 127.3, 124.4, 115.1, 106.5, 97.6, 97.0, 93.0, 92.6, 63.8, 57.5, 52.31, 52.25, 45.4, 32.4, 32.0, 23.8; m.p. : 175 °C; HRMS (APCI$^+$) *m/z* calcd.: 643.2484 $[M+H]^+$, found: 643.2469.

*4,4'-((5-Cinnamoyl-6-phenyl-2,3,5,6-tetrahydro-1H-indene-4,7-diyl)bis(ethyne-2,1-diyl))dibenzonitrile (**1-11**)*

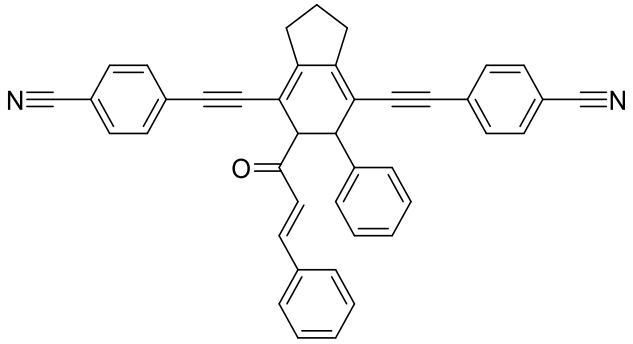

The compounds 4,4'-(undeca-1,3,8,10-tetrayne-1,11-diyl)dibenzonitrile (272 mg, 800 µmol, 1 eq.), (1E, 4E)-1,5-diphenylpenta-1,4-dien-3-one (dba, 160 mg, 680 µmol, 0.85 eq.), $Pd_2(dba)_3 \cdot CHCl_3$ (41.6 mg, 40 µmol, 0.05 eq.) and 2-dicyclohexylphosphino-2',6'-dimethoxybiphenyl (SPhos, 32.8 mg, 80 µmol, 0.1 eq.) were placed in a Schlenk flask. Toluene (16 mL) was added, and the mixture was stirred at 60 °C for 6 h. The solvent was removed under reduced pressure and the crude product was purified by flash chromatography (dichloromethane) to afford **1-11** (308 mg, 67%) as a yellow solid.

^{1}H NMR (300 MHz, $CDCl_3$): δ = 7.67 (m, 1H), 7.57 – 7.48 (m, 6H), 7.45 – 7.27 (m, 12H), 7.12 (m, 1H), 4.36 – 4.27 (m, 1H), 3.96 – 3.88 (m, 1H), 2.91 – 2.67 (m, 4H), 2.10 – 1.89 (m, 2H). ^{13}C{^{1}H} NMR (75 MHz, $CDCl_3$): δ = 196.6, 151.3, 147.6, 144.0, 141.9, 134.6, 132.1, 132.0, 131.9, 131.8, 130.9, 129.1, 128.9, 128.5, 128.3, 128.0, 127.9, 127.5, 124.3, 118.6, 118.5, 115.0, 111.5, 111.3, 106.6, 96.8, 96.2, 94.1, 93.7, 57.3, 45.5, 32.4, 32.0, 23.8; Elemental Analysis calcd.: C: 87.47, H: 4.89, N: 4.86; O: 2.77; found: C: 86.42, H: 5.31, N: 4.38; HRMS (APCI$^+$) *m/z* calcd.: 577.2208 $[M]^+$, found: 577.2271.

Ligand and solvent screening reactions

To examine selectivity for the palladium-catalyzed bisdiyne cyclization reaction, several different ligands (**L**) and solvents (**S**) were tested. The reactions were carried out in NMR scale, the yields were determined by ^{1}H NMR spectroscopy using benzyl acetate as the internal standard.

The reactions were prepared in flasks under argon with 4 mL of solvent. After the reaction, 0.5 mL was taken from the mixture, from which the solvent was evaporated. Then, 0.8 mL of $CDCl_3$ was added, and the internal standard benzyl acetate was weighed in on an analytical balance, followed by ^{1}H NMR measurement of the samples. Yields were calculated by setting the product signals in relation to the internal standard, based on integrals of suitable CH_2 or CH_3 signal of the internal standard and products. Some experiments do not add up to 100%, due to the formation of unknown side products.

Table 4: NMR yields of the palladium-catalyzed bisdiyne cyclization reaction below with varied solvents S, using PPh_3 as the ligand.

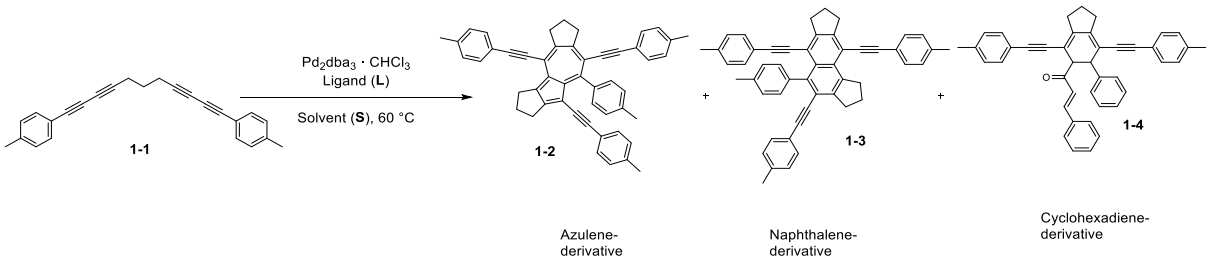

	NMR yield %			
Solvent S	**Substrate 1-1**	**Azulene 1-2**	**Naphthalene 1-3**	**Cyclohexadiene 1-4**
toluene	0	65	7	15
MeCN	0	0	48	0
1:1 MeCN / toluene	0	4	66	2
DMF	26	6	8	0
*t*BuOH	0	28	2	5
1,2-dichloroethane	0	64	3	15
1:1 1,2-dichloroethane/MeCN	0	0	58	0
MTBE (55 °C)	0	30	3	6
dimethyl ethylene glycol	27	27	3	10
THF	0	79	4	8
dioxane	0	46	3	1

Table 5: NMR yields of the palladium-catalyzed bisdiyne cyclization reaction below with varied ligands L, using toluene as the solvent.

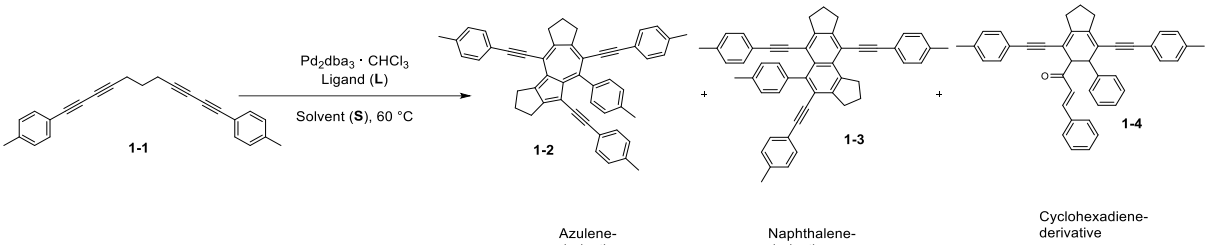

	NMR yield %			
Ligand L	**Substrate 1-1**	**Azulene 1-2**	**Naphthalene 1-3**	**Cyclohexadiene 1-4**
PPh_3	0	65	7	15
PMe_3	40	6	13	0
$PMes_3$	96	0	0	0
Xantphos	63	0	3	0
SPhos	0	2	1	15
PCy_3	0	42	12	0
Tri(2-furyl)phosphine	0	13	18	11
P(*o*-tol)$_3$	0	57	7	12
$P(OPh)_3$	85	0	0	2
Imes*BF4 + Cs_2CO_3	45	0	0	0
Ipr*Cl + Cs_2CO_3	43	0	0	10
P(*p*-tol)$_3$	36	30	3	12
dppf	60	0	0	7
1,10-Phenanthroline	100	0	0	0
2,2'-Bipyridine	98	0	0	0
dppm	92	0	1	0
Xphos	78	0	0	13

Unsuccessful attempts

The protocol used for the bisdiyne-olefin cyclizations (Figure 6) was tested for olefins other than dibenzylideneacetone, but the [2+2+2] cross-cyclization did not work for any of them.

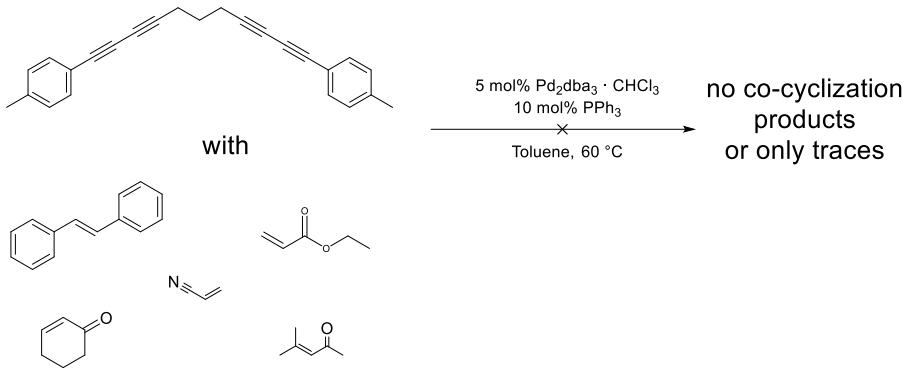

Attempts to react bisdiynes with dimethyl-acetylenedicarboxylate gave hexamethyl mellitate or failed for other acetylene derivatives:

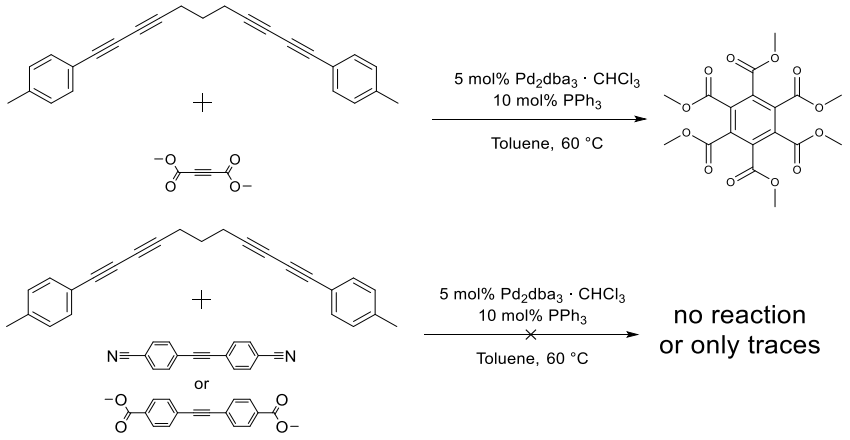

Computational details

DFT calculations were carried out with the Gaussian09 package.[138] The geometries of the different structures were optimized at the DFT level using the B3LYP[139, 140] hybrid functional with a mixed basis set (BS1) of SDD[141, 142] for Pd and 6-31G(d,p) for the other atoms in toluene solvent (using the SMD[143] solvent model). Frequency analysis was carried out at the same level to verify the stationary points as an intermediate or transition state and to obtain the thermodynamic energy corrections. To obtain more accurate energy information, single-point energy calculations were performed at the B3LYP-D3(BJ) level of theory using a larger basis set (BS2) of LANL08(f)[144] for Pd and 6-311++G(d,p) for the other atoms. All of the three-dimensional molecular diagrams of the molecules were generated with CYLView.[145]

Table 6: Calculated energies in toluene (B3LYP-D3(BJ), Hartrees)

	E	G	IF
1-4	-1696,026469	-1695,476907	
dba	-731,428039	-731,214892	
A	-1164,232478	-1164,006882	
B	-2128,768185	-2128,214268	
TS_{BC}	-2128,728369	-2128,175772	-158,7
C	-2128,802856	-2128,249043	
TS_{CA}	-2860,193464	-2859,399353	-362,44
D	-2860,235963	-2859,438696	
TS_{DE}	-2860,205703	-2859,410448	-353,05
E	-2860,250459	-2859,453975	
TS_{EA}	-2860,23947	-2859,444447	-237,45
A + **1-4**	-2860,298033	-2859,502499	

Single-crystal X-ray diffraction

General information

Crystals suitable for single-crystal X-ray diffraction were selected, coated in perfluoropolyether oil, and mounted on MiTeGen sample holders. Diffraction data were collected on a Bruker X8-APEX II diffractometer with a CCD area detector and multi-layer mirror (**1-4**, **1-8**, **1-10**) or graphite (**1-5**) monochromated Mo-Kα radiation. The diffractometer was equipped with an open flow N_2 Cryoflex II (Bruker) device and data was collected at 100 K. The structures were solved using intrinsic phasing method (ShellXT)[146] refined with the (ShellXL) program[147] and expanded using Fourier techniques. All non-hydrogen atoms were refined anisotropically. Hydrogen atoms were included in structure factor calculations. All hydrogen atoms were assigned to idealized geometric positions and omitted for clarity.

Table 7: Single-crystal X-ray diffraction data and structure refinements.

Data	**1-4**	**1-5**	**1-8**	**1-10**
Empirical formula	$C_{45}H_{37}O$	$C_{25}H_{14}N_2$	$C_{58}H_{56}N_2O$	$C_{44}H_{34}O_5$
Formula weight ($g \cdot mol^{-1}$)	593.74	342.38	797.04	642.71
Temperature (K)	100(2)	100(2)	100(2)	100(2)
Radiation (Å)	Mo-Kα 0.71073	Mo-Kα 0.71073	Mo-Kα 0.71073	Mo-Kα 0.71073
Crystal system	Monoclinic	Monoclinic	Monoclinic	Monoclinic
Space group	$P2_1/c$	$P2/c$	$P2_1/c$	$P2_1/c$
Unit cell dimensions				
a (Å)	14.871(6)	9.162(3)	13.209(3)	11.876(6)
b (Å)	9.377(2)	5.4480(18)	17.676(5)	12.301(4)
c (Å)	23.728(7)	18.942(6)	19.903(6)	22.655(10)
α (°)	90	90	90	90
β (°)	96.817(12)	103.896(15)	106.110(9)	91.29(2)
γ (°)	90	90	90	90
Volume ($Å^3$)	3285.3(18)	917.8(5)	4465(2)	3309(2)
Z	4	2	4	4
Absorption coefficient (mm^{-1})	0.070	0.073	0.069	0.083
F(000)	1260	356	1704	1352
Theta range for collection	2.573 to 25.679°	2.215 to 26.351°	2.022 to 27.877°	1.715 to 28.699°
Reflections collected	53852	1889	122743	44101
Independent reflections	6224	1889	10642	8547
Minimum/maximum transmission	0.6744/0.7455	0.651616/0.745372	0.6801/0.7457	0.6483/0.7463
Refinement method	Full-matrix least-squares on F^2	Full-matrix least-squares on F^2	Full-matrix least-squares on F^2	Full-matrix least-squares on F^2
Data / parameters / restraints	6224 / 481 / 352	1889 / 124 / 0	10642 / 716 / 803	8547 / 499 / 397
Goodness-of-fit on F^2	1.051	1.057	1.083	1.026
Final R indices [I>=2σ (I)]	R_1 = 0.0590, wR^2 = 0.1295	R_1 = 0.0482, wR^2 = 0.1067	R_1 = 0.0831, wR^2 = 0.2418	R_1 = 0.0526, wR^2 = 0.1314
R indices (all data)	R_1 = 0.1090, wR^2 = 0.1553	R_1 = 0.0735, wR^2 = 0.1202	R_1 = 0.1102, wR^2 = 0.2706	R_1 = 0.0727, wR^2 = 0.1454
Maximum/minimum residual electron density ($e \cdot Å^{-3}$)	0.375 / –0.236	0.209 / –0.221	0.695 / –0.570	0.406 / –0.250

*Crystal Structure of **1-5**:*

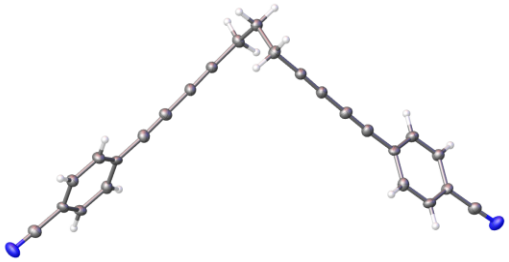

The crystal was a pseudo-merohedral twin with domains rotated by 179.7 ° around real axis [1.000 0.007 -0.460]. The BASF parameter was refined to 45%.

Photophysical characterization

General information

All measurements were performed in standard quartz cuvettes (1 cm x 1 cm cross-section). UV-visible absorption spectra were recorded using an Agilent 8453 diode array UV-visible spectrophotometer. Emission spectra were recorded using an Edinburgh Instruments FLSP920 spectrometer equipped with a double monochromator for both excitation and emission, operating in right-angle geometry mode, and all spectra were fully corrected for the spectral response of the instrument. All solutions used in photophysical measurements had concentrations lower than $5 \cdot 10^{-6}$ M to minimize inner filter effects during fluorescence measurements.

Fluorescence quantum yield measurements. The fluorescence quantum yields were measured using a calibrated integrating sphere (inner diameter: 150 mm) from Edinburgh Instruments combined with the FLSP920 spectrometer described above. For solution-state measurements, the longest-wavelength absorption maximum of the compound in the respective solvent was chosen as the excitation wavelength, unless stated otherwise.

Lifetime measurements. Fluorescence lifetimes were recorded using the time-correlated single-photon counting (TCSPC) method using an Edinburgh Instruments FLS980 spectrometer equipped with a high-speed photomultiplier tube positioned after a single emission monochromator. Measurements were made in right-angle geometry mode, and the emission was collected through a polarizer set to the magic angle. The full-width-at-half-maximum (FWHM) of the pulse from the diode laser was ca. 75-90 ps with an instrument response function (IRF) of ca. 230 ps FWHM. The IRFs were measured from the scatter of an aqueous suspension of Ludox at the excitation wavelength. Decays were recorded to 10000 counts in the peak channel with a record length of 8192 channels. The band pass of the emission monochromator and a variable neutral density filter on the excitation side were adjusted to give a signal count rate of <60 kHz. Iterative reconvolution of the IRF with one decay function and non-linear least-squares analysis were used to analyze the data. The quality of all decay fits was judged to be satisfactory, based on the calculated values of the reduced χ^2 and Durbin-Watson parameters and visual inspection of the weighted residuals.

Due to technical limitations of our spectrometer set up (temporal resolution/ detector response time), only lifetimes >1 ns can be accurately determined, the found values <1 ns were still given.

Spectra of 1,3-cyclohexadiene derivatives **1-4**, **1-8**, **1-10** and **1-11** were obtained in toluene, but they seem to be unstable when irradiated in dilute solutions.

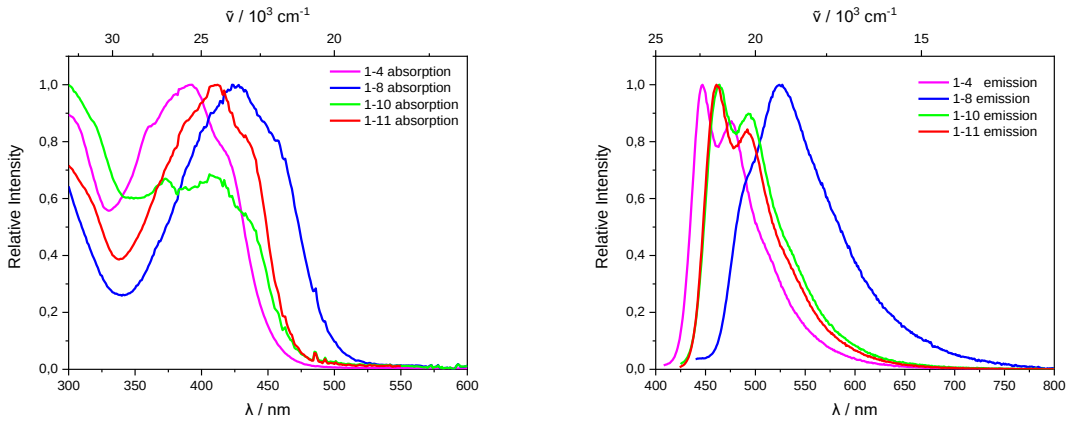

*Absorption and emission spectra of **1-4**, **1-8**, **1-10** and **1-11** in toluene.*

We compared the absorption and emission spectra of compound **1-11** in both toluene and CH_2Cl_2; the compound shows little solvatochromism.

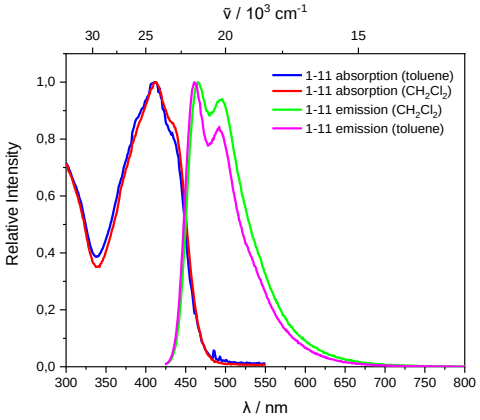

*Absorption and emission spectra of **1-11** in toluene and dichloromethane.*

We further measured the absorption spectrum of compound **1-11** before and after all photophysical measurements. The absorption spectrum changes significantly, indicating decomposition of the sample during the spectroscopic experiments:

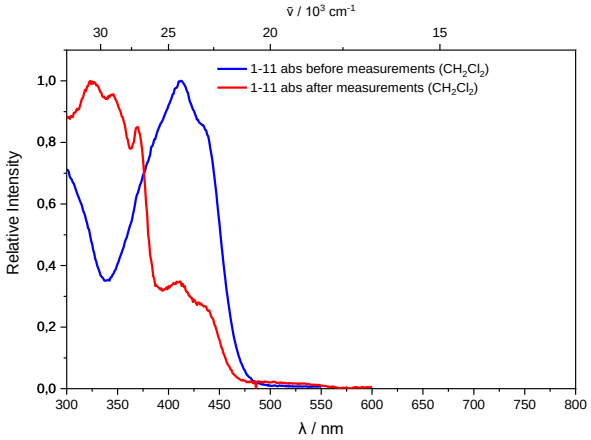

*Absorption and emission spectra of **1-11** in in dichloromethane before and after the full photophysical characterization.*

*Photophysical data for compounds **1-4**, **1-8**, **1-10** and **1-11** in toluene as well as **1-11** in CH_2Cl_2.*

#	Solvent	λ_{max} abs (nm)	λ_{max} em (nm)	Stokes shift (cm^{-1})	Φ	τ (ns)	τ_0 (ns)	$K_{nr}/10^7 s^{-1}$	$K_r/10^7 s^{-1}$
1-8	toluene	426 457	492 525	1556	0.07	0.93	13.3	100.0	7.5
1-11	toluene	410 440	460 491	988	0.60	0.91	1.5	44.0	65.9
1-11	CH_2Cl_2	410 440	466 495	1268	/	/			
1-10	toluene	373 410 434	464 495	1489	0.75	0.88	1.2	28.4	85.2
1-4	toluene	393 420	448 475	1488	0.08	1.51	18.9	60.9	5.3

Chapter 2

Synthesis

General information:

Unless otherwise noted, all reactions were performed using standard Schlenk or glovebox (Innovative Technology Inc.) techniques under argon. Reagent grade solvents were argon saturated, dried using an Innovative Technology Inc. Pure-Solv Solvent Purification System, and further deoxygenated by using the freeze-pump-thaw method. The compounds 1,11-bis(*p*-tolyl)undeca-1,3,8,10-tetrayne[51], 4,4'-(undeca-1,3,8,10-tetrayne-1,11-diyl)bis(N,N-dimethylaniline)[53] were prepared according to the literature. All other starting materials were purchased from commercial sources and used without further purification.

Automated flash chromatography was performed using a Biotage® Isolera Four system on silica gel or NH-silica. Commercially available, precoated TLC plates (Polygram® Sil G/UV_{254} and Polygram® Alox N/UV_{254}) were purchased from Macherey-Nagel. The removal of solvent was performed on a rotary evaporator *in vacuo* at a maximum temperature of 45 °C.

GC-MS analyses were performed using an Agilent 7890A gas chromatograph equipped with an Agilent 5975C inert MSD with triple-axis detector operating in EI mode and an Agilent 7693A series auto sampler/injector. High resolution mass spectrometry was obtained from a Thermo Scientific Exactive Plus MS System with either an atmospheric-pressure chemical ionization (APCI) or a heated-electrospray ionization (HESI) probe.

NMR spectra were recorded at ambient temperature using Bruker DRX-300 (^{1}H, 300 MHz; ^{13}C{^{1}H}, 75 MHz). ^{1}H NMR chemical shifts are reported relative to TMS and were referenced *via* residual proton resonances of the corresponding deuterated solvent, whereas ^{13}C{^{1}H} NMR spectra are reported relative to TMS *via* the carbon signals of the deuterated solvent.

Elemental analyses were performed with an Elementar vario micro cube device. Infrared spectra were recorded on a Bruker Alpha FT-IR spectrometer as solids by using an ATR unit with a resolution of 4 cm^{-1} and are reported in cm^{-1}. Raman spectra were recorded at room temperature with a MultiRAM FT-Raman spectrometer in melting point capillaries. Cyclic voltammetry measurements were performed at 100 mV/s in THF/ 0.1M [n-Bu_4N][PF_6] with a Metrohm Autolab PGSTAT30 potentiostat-galvanostat. Working electrode: Glassy carbon sealed in glass (external diameter ø 6 mm; internal diameter ø 3 mm; active surface area:

7.07 mm_2). Counter electrode: Pt-wire (ø 0.5 mm; length: 5 cm) Reference electrode: Ag/Ag+ (Ag-wire in 0.01 M AgNO3 / 0.1M $[nBu_4N][PF_6]$ / THF).

[(TMEDA)Ni(o-tolyl)Cl]

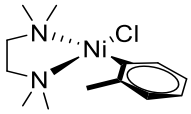

Preparation solution of $Al(OEt)Me_2$

The compounds 2-chlorotoluene (10 mL), a 2M $AlMe_3$-solution in toluene (10.5 mL, 21 mmol) and diethyl ether (2.2 mL, 21 mmol) were placed in a Schlenk flask. The mixture was cooled to 0 °C, and anhydrous ethanol (1.22 mL, 10.5 mmol) was added dropwise over 1 h. After bubbling ceased, the reaction was allowed to warm to room temperature.

[(TMEDA)Ni(o-tolyl)Cl]

A mixture of $Ni(acac)_2$ (2.58 mg, 10.0 mmol), TMEDA (6.0 mL, 40.2 mmol) and 2-chlorotoluene was cooled to 0 °C. A solution of $Al(OEt)Me_2$ (2.14 g, 21 mmol) in 2-chlorotoluene (10 mL) was added to the reaction mixture by cannula. The mixture turned green and was kept at 0 °C until bubbling ceased, before it was stirred for 2 h and allowed to warm to room temperature. Then the reaction mixture was heated to 60 °C and stirred for 1 h. The oil bath was turned off, for the reaction to slowly cool overnight. The orange-red needles were washed and decanted off with n-hexane (5 x 25 mL). The product was collected by filtration, rinsed with n-hexane (3 x 10 mL) and dried under vacuum to yield an orange-red solid (1.9 g, 63%).

The procedure and NMR data are similar to those reported previously.[55]

^{1}H NMR (300 MHz, CD_2Cl_2): δ [ppm] = 7.38 (m, 1H), 6.75–6.54 (m, 3H), 3.43 (s, 3H), 2.77–2.10 (m, 12H), 1.83 (m, 2H); ^{13}C NMR (75 MHz, CD_2Cl_2): δ [ppm] = 146.06, 143.50, 135.47, 126.43, 122.35, 122.00, 61.50, 57.11, 54.52, 47.91, 25.86.

4,4´-(ethyne-1,2-diyl) benzonitrile

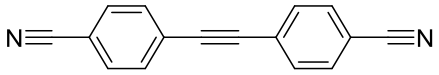

The compounds 4-iodobenzonitrile (3.43 g, 2 equiv., 15 mmol), trimethylsilylacetylene (736 mg, 7.5 mmol, 1 eq.), [$PdCl_2(PPh_3)_2$] (105 mg, 1 mol%), copper(I) iodide (90 mg, 3 mol%), 1,8-diazabicyclo[5.4.0]undec-7-ene (15 mL, 6.6 eq.) and degassed water (0.1 mL) were dissolved in triethylamine (30 mL). The reaction mixture was stirred for 2 h at room temperature, then some of the solvent was removed. After adding 30 mL of water, the mixture was filtered through a glass frit. The product was recrystallized from EtOAc (2.06 g, 7.0 mmol, 93%).

The procedure and NMR data are similar to those reported previously.[148, 149 150]

^{1}H NMR (300 MHz, $CDCl_3$): δ [ppm] = 7.69-7.7.61 (m, 8H); $^{13}C\{^1H\}$ NMR (75 MHz, $CDCl_3$): δ [ppm] = 132.29, 132.19, 127.08, 118.26, 112.44, 91.56; HRMS (ASAP+): m/z calculated: 229.0760 [M+H], m/z found: 229.0754

dimethyl 4,4'-(ethyne-1,2-diyl)dibenzoate

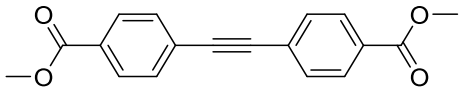

The compounds methyl 4-iodobenzoate (3.93 g, 2 equiv., 15 mmol), trimethylsilylacetylene (736 mg, 7.5 mmol, 1 eq.), [$PdCl_2(PPh_3)_2$] (105 mg, 1 mol%), copper(I) iodide (90 mg, 3mol%), 1,8-diazabicyclo[5.4.0]undec-7-ene (15 mL, 6.6 eq.) and degassed water (0.1 mL) were dissolved in triethylamine (30 mL). The reaction mixture was stirred for 2 h at room temperature, then some of the solvent was removed. After adding of 30 mL of water, the mixture was poured on a glass frit. The product was recrystallized from EtOAc (1.3 g, 33 mmol, 76%).

The procedure and NMR data are similar to those reported previously. [148, 149 150]

^{1}H NMR (300 MHz, $CDCl_3$): δ [ppm] = 8.1-7.95 (m, 4H), 7.6-7.5 (m, 4H), 3.93 (s, 6H); $^{13}C\{^1H\}$ NMR (75 MHz, $CDCl_3$): δ [ppm] = 166.59, 131.78, 130.09, 129.72, 127.49, 91.50, 52.43; HRMS (ASAP+): m/z calculated: 295.0965 [M+H], m/z found: 295.0954.

1,2-di(pyridine-4-yl)ethyne

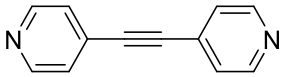

The compounds 4-iodopyridine (2.0 g, 9.8 mmol), CuI (92.9 mg, 0.5 mmol) and $Pd(PPh_3)_2Cl_2$ (205.4 mg, 0.3 mmol) were dissolved in THF (60 mL) and NEt_3 (20 mL). Then degassed trimethylsilylacetylene (0.7 mL, 4.9 mmol) was added and the reaction mixture was stirred at 70 °C for 3 h. After the mixture cooled to room temperature, 8 mL of 1 M nBu_4NF solution in THF was added. The reaction was stirred 1.5 h at RT and then poured into EtOAc and water. The organic layer was washed with water (3 x 100 mL) and dried over $MgSO_4$. The brown substance, that appeared during the extraction, was insoluble in either EtOAc or water and was discarded, as it is not the product. The solvent was removed under reduced pressure. To the crude product, dissolved in a small amount of EtOAc, n-hexane was added to precipitate an impurity. After filtration and removal of the solvent from the filtrate, the product was dissolved in a small amount of acetone and crystallized in the freezer to give colorless crystals (550 mg, 62%).

The procedure and NMR data are similar to those reported previously.[151]

^1H NMR (300 MHz, $CDCl_3$): δ [ppm] = 8.68-8.62 (m, 4H), 7.43-7.39 (m, 4H); $^{13}C\{^1H\}$ NMR (75 MHz, $CDCl_3$): δ [ppm] = 150.0, 130.5, 125.8, 90.8; HRMS (ASAP+): m/z calculated: 181.0760 [M+H], m/z found: 181.0756; R_f (100% EtOAc) = 0.2

4,4'-(ethyne-1,2-diyl)bis(N,N-dimethylaniline)

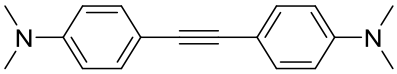

The compound 4-iododimethylaniline (6.1 g, 24.7 mmol) was dissolved in triethylamine (60 mL) and cooled to 0 °C. The catalysts $Pd(PPh_3)_2Cl_2$ (420 mg, 0.6 mmol) and CuI (155 mg, 0.82 mmol) were added. Then 4-ethynyl-N,N-dimethylaniline (3.0 g, 20.7 mmol) was added to the reaction mixture. The mixture was stirred for 8 h at 0 °C and another 5 h at room temperature. The end of the reaction was confirmed by TLC. The solvent was removed under reduced pressure. The crude product was suspended in MeOH and heated, then the mixture was

filtered through a glass frit. The product was further washed with MeOH and n-hexane on the frit, to obtain an amber solid (5.0 g, 92%).

The procedure and NMR data are similar to those reported previously. [152]

^{1}H NMR (300 MHz, $CDCl_3$): δ [ppm] = 7.4-7.37 (m, 4H), 6.67-6.64 (m, 4H), 2.98 (s, 12H); ^{13}C NMR (300 MHz, $CDCl_3$): δ [ppm] = 149.71, 133.64, 132.39, 111.96, 111.17, 88.09, 40.31; HRMS: (ASAP+): m/z calculated [M+H]: 265.1699; m/z found: 265.1692; R_f (cyclohexane: EtOAc 7:1) = 0.3.

4-methoxy-N-(4-methoxyphenyl)-N-phenylaniline

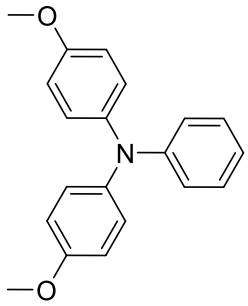

The compounds $Pd(OAc)_2$ (130 mg, 0.58 mmol) and XPhos (440 mg, 0.92 mmol) were dissolved in toluene (2 mL) and stirred for 30 min. This catalyst solution was added to a mixture of 4-bromoanisole (18.5 g, 100 mmol), aniline (3.88 g, 41 mmol), and NaOtBu (11 g, 114.5 mmol) in toluene (70 mL). The reaction mixture was stirred at 104 °C for 21 h. After cooling the reaction to room temperature, saturated NH_4Cl solution (20 mL) and water (150 mL) were added. The aqueous phase was washed with EtOAc (2 x 20 mL). The combined organic layers were dried over $MgSO_4$ and the solvent was removed *in vacuo*. The brown, oily substance was dissolved in n-hexane and cooled with liquid nitrogen to encourage precipitation. The residue was washed 3 times with n-hexane and the crude product was dried *in vacuo*. The product was obtained as an off-white solid (11.36 g, 90%).

The procedure and NMR data are similar to those reported previously.[153]

^{1}H NMR (300 MHz, $CDCl_3$): δ [ppm] = 7.22-7.13 (m, 2H), 7.12-7.00 (m, 4H), 6.98-6.89 (m, 2H), 6.88-6.78 (m, 5H), 3.80 (s, 6H); $^{13}C\{^{1}H\}$ NMR (75 MHz, $CDCl_3$): δ [ppm] = 155.8, 148.9, 141.3,

129.1, 126.5, 121.1, 120.7, 114.8, 55.6; GC-MS (EI): m/z calculated: 305.1, m/z found: 305.2; R_f (cyclohexane:EtOAc, 15:1) = 0.3.

4-Iodo-*N,N*-bis(4-methoxyphenyl)aniline

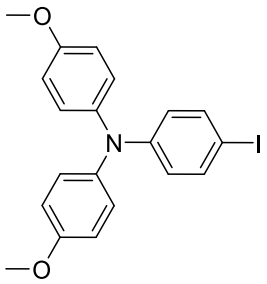

The compound N-Iodosuccinimide (8.2 g, 36.4 mmol) was added to a solution of 4-methoxy-N-(4-methoxy-phenyl)-N-phenylaniline (11.1 g, 36.4 mmol) in $CHCl_3$ (60 mL) and acetic acid (60 mL). The solution was stirred for 3 h at room temperature in the dark. Then diethyl ether (150 mL) and water (150 mL) were added to the mixture. The organic layer was separated and washed with water and saturated aqueous $NaHCO_3$ and dried over $MgSO_4$. The solvent was evaporated under reduced pressure and the crude product was obtained as a brown oil. The crude product was thoroughly washed with n-hexane to obtain the product as a light grey solid (11.8 g, 75%).

The procedure and NMR data are similar to those reported previously.[153]

^{1}H NMR (300 MHz, $CDCl_3$): δ [ppm] = 7.43-7.38 (m, 2H), 7.06-7.00 (m, 4H), 6.86-6.79 (m, 4H), 6.70-6.64 (m, 2H), 3.79 (s, 6H); GC-MS (EI): m/z calculated: 431.0, m/z found: 431.1; HRMS (APCI+): m/z calculated: 432.0460 [M+H], m/z found: 432.0451; R_f (cyclohexane:EtOAc 6:1) = 0.6.

4-methoxy-N-(4-methoxyphenyl)-N-(4-((trimethylsilyl)-ethynyl)phenyl)aniline

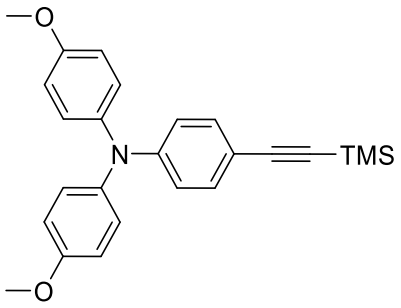

The compounds 4-iodo-*N,N*-bis(4-methoxyphenyl)aniline (7.00 g, 16.2 mmol), $Pd(PPh_3)_2Cl_2$ (456 mg, 0.65 mmol), and CuI (61.8 mg, 0.32 mmol) were put into a Schlenk flask. A degassed mixture of triethylamine (50 mL), THF (40 mL), and trimethylsilylacetylene (3.40 mL, 24.4 mmol) were added and the reaction mixture was stirred for 1 h. The solvent was removed under reduced pressure, then Et_2O (100 mL) and water (100 mL) were added. The aqueous layer was washed with Et_2O (3 x 100 mL), and the organic fractions were combined, washed with brine (100 mL) and then dried over Na_2SO_4. The solvent was removed under reduced pressure, then the residue was purified on a silica plug eluting with n-hexane/CH_2Cl_2 (2:1, 360 mL). The product was obtained as an amber oil, which was used directly in the next step without quantifying the yield.

The procedure and NMR data are similar to those reported previously. [153, 154]

^{1}H NMR (300 MHz, CD_2Cl_2): δ [ppm] = 7.23-7.18 (m, 2H), 7.08-7.02 (m, 4H), 6.88-6.82 (m, 4H), 6.78-6.72 (m, 2H), 3.78 (s, 6H), 0.22 (s, 9H); $^{13}C\{^1H\}$ NMR (75 MHz, CD_2Cl_2): δ [ppm] = 157.0, 149.5, 140.4, 133.0, 127.7, 118.9, 115.2, 113.8, 106.1, 92.5, 55.8, 0.15; HRMS (ASAP+): m/z calculated: 402.1889 [M+H], m/z found: 402.1877; R_f (cyclohexane:EtOAc 6:1) = 0.8

4-ethynyl-*N*,*N*-bis(4-methoxyphenyl)aniline

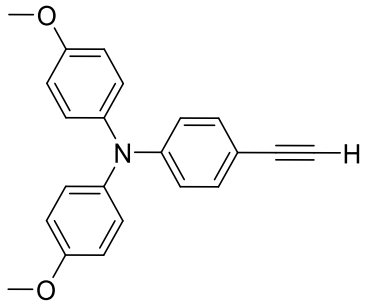

The compound 4-methoxy-*N*-(4-methoxyphenyl)-*N*-(4-((trimethylsilyl)-ethynyl)phenyl)aniline (6.5 g, 16.2 mmol) was dissolved in chloroform (40 mL). Then MeOH (100 mL) and KOH (1.8 g, 32.4 mmol), dissolved in methanol (10 mL), were added. After 1 h of stirring at room temperature, the mixture was poured into chloroform and water. The organic layer was washed with brine (100 mL) and the aqueous layer was extracted with chloroform (3 x 100 mL). The combined organic layers were dried over $MgSO_4$, and the solvent was removed under reduced pressure. The crude product was purified on a silica plug, eluting with n-hexane/CH_2Cl_2 (2:1, 450 mL). The solvent was removed under reduced pressure. The substance was recrystallized from n-hexane (25 mL) and then cooled in liquid nitrogen to encourage precipitation. The precipitate was collected by filtration, washed with n-hexane (3 x 10 mL) to obtain the product as a yellow solid (4.40 g, 82%).

The procedure and NMR data are similar to those reported previously.[154]

^{1}H NMR (300 MHz, $CDCl_3$): δ [ppm] = 7.29-7.24 (m, 2H), 7.08-7.03 (m, 4H), 6.86-6.78 (m, 6H), 3.80 (s, 6H) 2.99 (s, 1H); $^{13}C\{^1H\}$ NMR (75 MHz, $CDCl_3$): δ [ppm] = 156.5, 149.3, 140.2, 133.1, 127.3, 119.0, 115.0, 112.7, 84.5, 75.7, 55.6; GC-MS: m/z calculated: 329.1, m/z found: 329.1; HRMS (ASAP+): m/z calculated: 330.1481 [M+H], m/z found: 330.1484; R_f (cyclohexane:EtOAc 6:1) = 0.4.

4,4'-(undeca-1,3,8,10-tetrayne-1,11-diyl)bis(N,N-bis(4-methoxyphenyl)aniline)

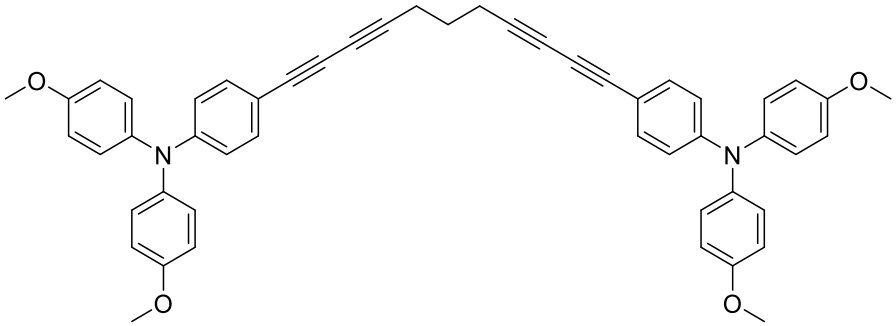

The compounds 4-ethynyl-*N,N*-bis(4-methoxyphenyl)aniline (2.0 g, 6.2 mmol), CuI (32.0 mg, 0.17 mmol) and $NH_2OH{\cdot}HCl$ (100 mg) were placed in a Schlenk flask and then degassed. Then degassed n-$BuNH_2$ (20 mL) and degassed MeOH (80 mL) were added. The reaction mixture was cooled to 0 °C and 1,7-dibromohepta-1,6-diyne (768 mg, 3.1 mmol) was added. The mixture was stirred for 3 h. Because HRMS showed that there was substrate left in the mixture, more 1,7-dibromohepta-1,6-diyne (60 mg, 0.24 mmol) was added and the mixture was stirred for 1 h at room temperature. The precipitated, rubbery solid was taken out of the flask and dissolved in a small amount of EtOAc in the ultrasonic bath, then an excess of MeOH was added and the mixture was cooled in liquid nitrogen to precipitate the product. After filtering of the solution at 0 °C and drying *in vacuo*, the product was obtained as an amber solid. (1.73 g, 75%).

^{1}H NMR (300 MHz, $CDCl_3$): δ [ppm] = 7.28-7.21 (m, 4H), 7.11-7.00 (m, 8H), 6.90-6.80 (m, 8H), 6.80-6.71 (m, 4H), 3.80 (s, 12H), 2.51 (t, 4H), 1.82 (q, 2H); $^{13}C\{^1H\}$ NMR (75 MHz, $CDCl_3$): δ [ppm] = 156.7, 149.5, 140.0, 133.6, 127.5, 118.7, 115.0, 112.1, 82.6, 76.2, 72.9, 66.5, 55.6, 27.3, 19.0; HRMS (APCI+): m/z calculated: 747.3223 [M+H], m/z found: 747.3210; Elemental Analysis: calculated: C: 82.01, H: 5.67, N: 3.75 found: C: 80.02, H: 5.67, N: 3.67; R_f (cyclohexane:EtOAc 6:1) = 0.3; m.p. : 84 °C.

4,4'-(4,7-bis(p-tolylethynyl)-2,3-dihydro-1H-indene-5,6-diyl)dibenzonitrile ***2-4***

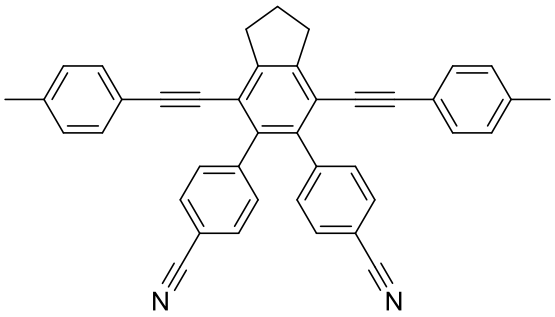

The compounds 1,11-di-*p*-tolylundeca-1,3,8,10-tetrayne (128 mg, 0.4 mmol, 1.0 eq.), 4,4´-(ethyne-1,2-diyl)benzonitrile (102.9 mg, 0.45 mmol, 1.1 eq.), [(TMEDA)Ni(*o*-tolyl)Cl] (10 mol%, 12 mg, 0.04 mmol, 0.1 eq.), triphenylphosphine (20 mol%, 20.8 mg, 0.08 mmol, 0.2 eq.), and K_3PO_4 (168 mg, 2 eq.) were dissolved in toluene (12 mL) and heated to 100 °C for 5 h. Then, the solvent was removed *in vacuo*. The crude product was purified by flash chromatography on silica (n-hexane/CH_2Cl_2) to afford the product as a white solid (45 mg, 0.08 mmol, 20%).

^{1}H NMR (300 MHz, $CDCl_3$): δ [ppm] = 7.57-7.50 (m, 4H), 7.30-7.28 (m, 2H), 7.27-7.25 (m, 2H), 7.14 - 7.02 (m, 8H), 3.25 (t, 4H), 2.35 (s, 6H), 2.27 (q, 2H); $^{13}C\{^1H\}$ NMR (75 MHz, $CDCl_3$): δ [ppm] = 147.20, 144.50, 139.15, 131.82, 131.44, 131.30, 129.33, 119.76, 119.52, 118.95, 110.90, 98.49, 86.38, 33.89, 24.19, 21.68; Elemental Analysis: calculated: C: 89.75, H: 5.14, N: 5.11, found: C: 89.51, H: 5.28, N: 4.85; HRMS (APCI-): m/z calculated: 548.2252 [M]; m/z found: 548.2265.

4,4'-(4,7-bis((4-(dimethylamino)phenyl)ethynyl)-2,3-dihydro-1H-indene-5,6-diyl)dibenzonitrile

2-5

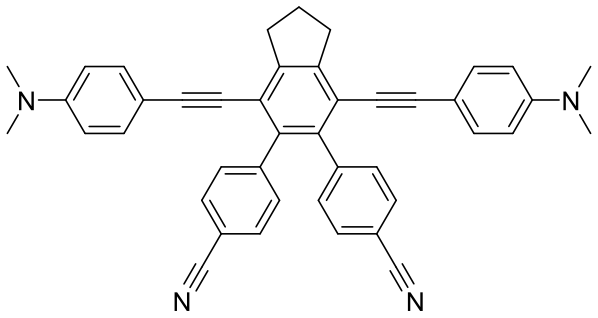

The compounds 4,4´-(undeca-1,3,8,10-tetrayne-1,11-diyl)bis(N,N-dimethylaniline) (310 mg, 0.82 mmol, 1eq.), 4,4´-(ethyne-1,2-diyl)benzonitrile (187 mg, 0.82 mmol, 1 eq.), [(TMEDA)Ni(*o*-tolyl)Cl] (24 mg, 0.082 mmol, 0.1 eq. 10 mol%), triphenylphosphine (43 mg, 0.164 mmol, 0.2 eq. 20 mol%), and K_3PO_4 (348 mg, 1,64 mmol, 2 eq.) were dissolved in toluene (20 mL). The reaction mixture was stirred for 5 h at 100 °C. The reaction mixture was then filtered through a glass frit and washed with toluene, water, n-hexane, and cold acetone. The solvents were removed *in vacuo* to afford the product as a yellow solid (370 mg, 0.61 mmol, 74%).

^{1}H NMR (300 MHz, $CDCl_3$): δ [ppm] = 7.54-7.51 (m, 4H), 7.30-7.26 (m, 2H), 7.26-7.24 (m, 1H), 7.03-7.00 (m, 4H), 6.61-6.58 (m, 4H), 3.23 (t, 4H), 2.97 (s, 12H), 2.26-2.21 (m, 2H); ^{13}C NMR {^{1}H} (75 MHz, $CDCl_3$): δ [ppm] = 146.30, 144.81, 138.56, 132.45, 131.83, 131.22, 119.32, 118.98, 111.91, 110.46, 99.45, 85.48, 40.30, 33.78, 24.05; Elemental Analysis: calculated: C: 85.12, H: 5.65, N: 9.23 found: C: 85.07, H: 5.81, N: 9.17; HRMS (ASAP+): m/z calculated [M+H]: 607.2856; m/z found: 607.2843.

Dimethyl 4,4'-(4,7-bis((4-(dimethylamino)phenyl)ethynyl)-2,3-dihydro-1H-indene-5,6-diyl)dibenzoate ***2-6***

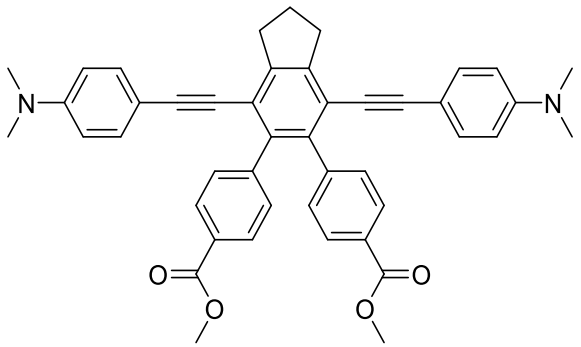

The compounds 4,4'-(undeca-1,3,8,10-tetrayne-1,11-diyl)bis(N,N-dimethylaniline) (64 mg, 0.18 mmol, 1.00 eq.), dimethyl 4,4'-(ethyne-1,2-diyl)dibenzoate (60 mg, 0.22 µmol, 1.2 eq.), [(TMEDA)Ni(o-tolyl)Cl] (5 mg, 16.6 µmol, 0.1 eq.), triphenylphosphine (8.8 mg, 33.6 µmol, 0.2 eq.), and K_3PO_4 (71.4 mg, 372 µmol, 2.0 eq.) were dissolved in toluene (8 mL). The reaction mixture was heated to 100 °C and stirred for 5 h. The reaction mixture was then concentrated *in vacuo* and the crude product was purified by a flash chromatography on NH-silica (n-hexane/ CH_2Cl_2 with 1% NEt_3). The solvents were removed *in vacuo*, and the product was washed with cold acetone, methanol, and n-hexane (61 mg, 51%).

^{1}H NMR (300 MHz, $CDCl_3$): δ [ppm] = 7.88-7.82 (m, 4H) 7.27-7.21 (m, 4H, *contains $CDCl_3$ signal*), 7.06-7.01 (m, 4H), 6.69-6.53 (m, 4H), 3.89 (s, 6H), 3.22 (t, 4H), 2.94 (s, 12H), 2.23 (t, 2H); ^{13}C{^{1}H} NMR (75 MHz, $CDCl_3$): δ [ppm] = 167.32, 145.88, 145.11, 139.77, 131.79, 129.73, 128.19, 119.44, 111.98, 52.1, 40.41, 33.94, 24.22; Elemental Analysis: calculated: C: 80.3, H: 6.00, N: 4.16 found: C: 79.21, H: 6.18, N: 3.13; HRMS (APCI+): m/z calculated: 673.3042 [M+H], m/z found 673.3043.

4,4'-((5,6-di(pyridin-4-yl)-2,3-dihydro-1H-indene-4,7-diyl)bis(ethyne-2,1-diyl))bis(N,N-dimethylaniline) **2-7**

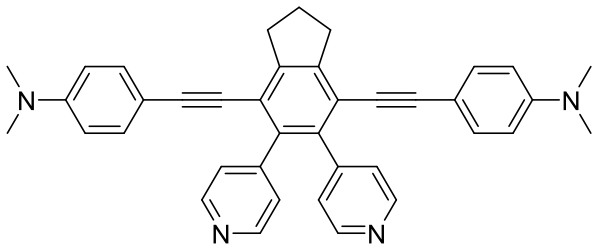

The compounds 1,2-di(pyridine-4-yl)ethyne (147.8 mg, 0.82 mmol), 4,4'-(undeca-1,3,8,10-tetrayne-1,11-diyl)bis(N,N-dimethylaniline) (310.4 mg, 0.82 mmol), [(TMEDA)Ni(o-tolyl)Cl] (24 mg, 0.08 mmol), triphenylphosphine (43 mg, 0.16 mmol), and K_3PO_4 (348 mg, 1.64 mmol) were dissolved in degassed toluene (10 mL). The reaction mixture was stirred in a microwave reactor at 100 °C for 2 h. The precipitated product was collected by filtration and washed with toluene, water, n-hexane, acetone and THF. The product was dissolved in chloroform to separate it from an impurity. The solvent was removed *in vacuo* and the product was obtained as a solid (232 mg, 51%).

^{1}H NMR (300 MHz, $CDCl_3$): δ [ppm] = 8.54-8.42 (m, 4 H), 7.23-7.14 (m, 4 H), 7.07-6.96 (m, 4 H), 6.62-6.50 (m, 4 H), 3.22 (m, 4 H), 2.69 (s, 12 H), 2.24 (m, 2 H); $^{13}C\{^1H\}$ NMR (75 MHz, $CDCl_3$) δ [ppm] = 150.38, 149.00, 146.38, 137.66, 132.64, 126.15, 119.27, 111.87, 109.67, 99.69, 85.48, 40.29, 33.92, 24.19; HRMS (APCI+): m/z calculated: 559.2856 [M+H], m/z found: 559.2845; Elemental Analysis: calculated: C: 83.84, H: 6.13, N: 10.03 found: C: 82.94, H: 6.09, N: 9.94; R_f (MeOH:EtOAc 1:16) = 0.2.

4,4'-(4,7-bis((4-(bis(4-methoxyphenyl)amino)phenyl)ethynyl)-2,3-dihydro-1H-indene-5,6-diyl)dibenzonitrile **2-8**

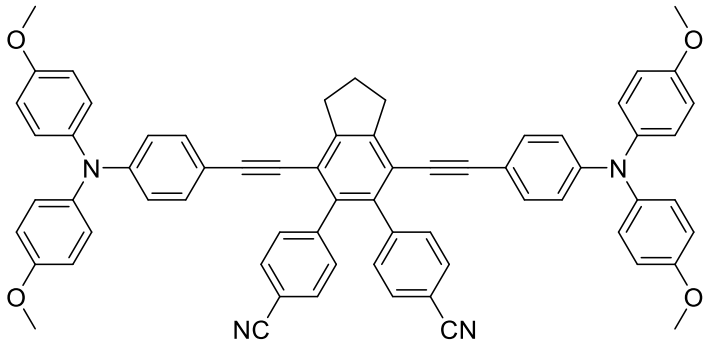

The compounds 4,4'-(undeca-1,3,8,10-tetrayne-1,11-diyl)bis(N,N-bis(4-methoxyphenyl)aniline) (612.5 mg, 0.82 mmol), 4,4'-(ethyne-1,2-diyl)dibenzonitrile (205.9 mg, 0.90 mmol), [(TMEDA)Ni(o-tolyl)Cl] (24 mg, 0.08 mmol), triphenylphosphine (43 mg, 0.16 mmol), and K_3PO_4 (348 mg, 1.64 mmol) were dissolved in degassed toluene (10 mL). The reaction mixture was stirred in a microwave reactor at 100 °C for 2 h. The precipitated solid was collected by filtration and then washed with n-hexane and methanol, then dissolved in dichloromethane and filtered through a silica plug. The solvent was removed under reduced pressure, then acetone was added to precipitate the product. The product, an orange solid (183 mg, 23%), was then dried *in vacuo*.

^{1}H NMR (500 MHz, C_2DCl_2): δ [ppm] = 7.53-7.43 (m, 4H), 7.26-7.22 (m, 4H), 7.15-6.70 (m, 24H), 3.80 (s, 12H), 3.20 (m, 4H), 2.23 (m, 2H); $^{13}C\{^1H\}$ NMR (125 MHz, C_2DCl_2): δ [ppm] = 146.7, 144.7, 138.8, 132.2, 131.9, 131.4, 127.3, 119.5, 119.0, 115.0, 110.7, 55.6, 33.9, 31.1, 24.1; HRMS (APCI+): m/z calculated: 975.3910 [M+H], m/z found: 975.3892; R_f (cyclohexane:EtOAc 3:1) = 0.5; Elemental Analysis: calculated: C: 82.52, H: 5.17, N: 5.75 found: C: 81.55, H: 5.34, N: 5.83.

4,4'-((5,6-di(pyridin-4-yl)-2,3-dihydro-1H-indene-4,7-diyl)bis(ethyne-2,1-diyl))bis(N,N-bis(4-methoxyphenyl)aniline) **2-9**

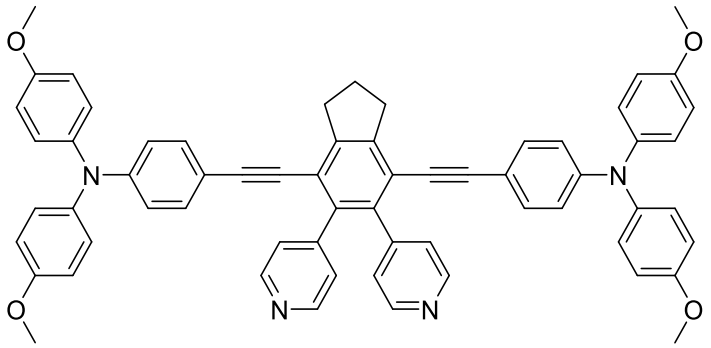

The compounds 1,2-di(pyridine-4-yl)ethyne (147.8 mg, 0.82 mmol), 4,4'-(undeca-1,3,8,10-tetrayne-1,11-diyl)bis(N,N-bis(4-methoxyphenyl)aniline) (612.5 mg, 0.82 mmol), [(TMEDA)Ni(o-tolyl)Cl] (24 mg, 0.08 mmol), triphenylphosphine (43 mg, 0.16 mmol) and K_3PO_4 (348 mg, 1.64 mmol) were dissolved in degassed toluene (10 mL). The reaction mixture was stirred in a microwave reactor at 100 °C for 2 h. The crude product was purified by flash chromatography on silica (EtOAc). The product was then washed by adding methanol to a concentrated EtOAc solution of the product. Then, the product was precipitated from a CH_2Cl_2 solution by adding n-hexane to give a yellow solid (201 mg, 26%).

^{1}H NMR (300 MHz, CD_2Cl_2): δ [ppm] = 8.43-8.39 (m, 4H), 7.14-7.07 (m, 4H), 7.06-6.98 (m, 8H), 6.96-6.89 (m, 4H), 6.88-6.79 (m, 8H), 6.76-6.66 (m, 4H), 3.77 (s, 12H), 3.19 (t, 4H), 2.22 (q, 2H); ^{13}C{^{1}H} NMR (75 MHz, CD_2Cl_2): δ [ppm] = 157.05, 149.57, 149.38, 147.87, 146.88, 140.21, 138.32, 132.42, 127.83, 127.68, 126.18, 119.41, 118.90, 115.16, 99.09, 86.23, 55.83, 34.114, 24.44; HRMS (APCI+): m/z calculated: 927.3905 [M+H], m/z found: 927.3885; Elemental Analysis: calculated: C: 81.62, H: 5.44, N: 6.04 found: C: 81.31, H: 5.39, N: 6.06; R_f (100% EtOAc) = 0.2.

4,4'-(4,7-bis((4-(bis(4-methoxyphenyl)amino)phenyl)ethynyl)-2,3-dihydro-1H-indene-5,6-diyl)bis(1-methylpyridin-1-ium) ditriflate **2-10**

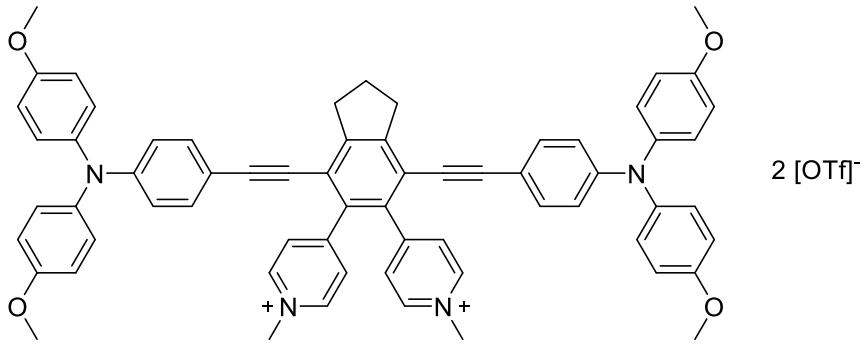

In a soda-lime glass vial, compound **2-9** (18.5 mg, 0.02 mmol) was dissolved in CH_2Cl_2 (3 mL) and MeOTf (11 uL, 16.4 mg, 0.1 mmol) was added. The mixture was stirred for 3 h in the dark. After addition of cyclohexane, the precipitate was collected and washed with pentane to obtain the product as a red solid (18 mg, 70%).

^{1}H NMR (300 MHz, CD_2Cl_2): δ [ppm] = 8.64-8.57 (m, 4H), 7.91-7.85 (m, 4H), 7.09-7.00 (m, 12H), 6.89-6.82 (m, 4H), 4.33 (s, 6H), 3.78 (s, 12 H), 3.25 (t, 4H), 2.27 (q, 2H); ^{13}C{^{1}H} NMR (75 MHz, CD_2Cl_2) δ [ppm] = 157.33, 155.88, 150.35, 145.42, 139.85, 134.33, 132.65, 130.96, 127.93, 119.78, 118.45, 115.25, 101.69, 84.32, 55.85, 48.96, 34.41, 24.16; HRMS (ESI+): m/z calculated: 478.2145 (M), m/z found: 478.2138; (ESI-): m/z calculated: 148.9515 (OTf^-), m/z found: 148.9513; Elemental Analysis: calculated: C: 64.11, H: 4.50, N: 4.46, , S: 5.11; Found: C: 63.20, H: 4.63, N: 4.36, S: 4.32.

5-(7-(p-tolyl)hepta-4,6-diyn-1-yl)-4,6,7-tris(p-tolylethynyl)-2,3-dihydro-1H-indene **2-2**

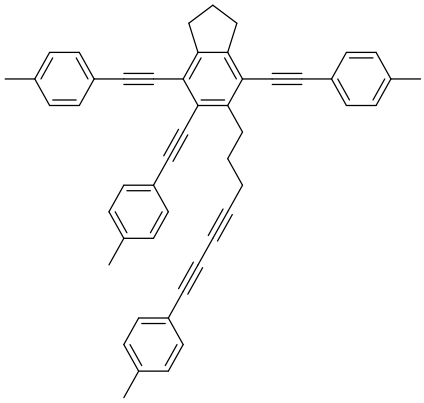

The compounds 1,11-di-p-tolylundeca-1,3,8,10-tetrayne (64 mg, 200 µmol, 1.00 eq.), [(TMEDA)Ni(*o*-tolyl)Cl] (6 mg, 19.9 µmol, 0.1 eq.), triphenylphosphine (10.4 mg, 40.0 µmol, 0.2 eq.), and K_3PO_4 (84.0 mg, 400 µmol, 2.0 eq.) were dissolved in toluene (8 mL). The reaction mixture was heated to 100 °C and stirred for 5 hours, the reaction progress was monitored by TLC. Complete consumption of the substrate was not achieved; however, the reaction was terminated. The solvent was removed *in vacuo*. After flash chromatography on silica, the product was isolated as a pale beige solid (24 mg, 18%).

The product still contained minor impurities, but as the NMR and HRMS spectra were according to what we obtained earlier for the compound, it was not further purified.[53]

HRMS (APCI+): *m/z* calcd. for $C_{50}H_{40}$ 641,3203 [M+H], found 641.3185; ^{1}H NMR (500 MHz, $CDCl_3$): δ = 7.50 (m, 2H), 7.47 (m, 4H), 7.17-7.12 (m, 6H), 7.10 (d, 2H), 3.33 (m, 2H), 3.12 (q, 4H), 2.55 (t, 2H), 2.38 (s, 3H), 2.35 (s, 3H), 2.33 (s, 6H), 2.15 (q, 2H), 2.06 (q, 2H); TLC: R_f = 0.7 (n-hexane / dichloromethane = 1:2, [UV]).

Test reactions and unsuccessful attempts:

When the reaction was conducted without the Ni-precatalyst, no reaction was observed:

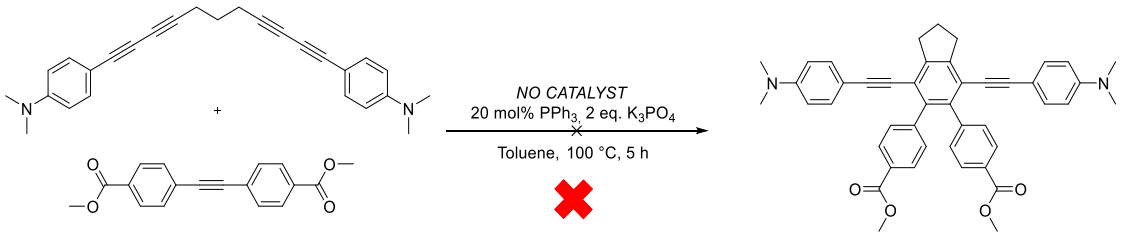

A test reaction, using a cobalt precatalyst with common conditions for alkyne trimerization[57], instead of nickel, did not give the desired product. In this case, the bisdiyne was still present in the reaction mixture, while all the diphenylacetylene was consumed. In the HRMS, traces of the product were found, along with dimers and trimers of the bisdiyne starting material. Trimerization products of the diphenylacetylene substrate could not be identified in the mixture:

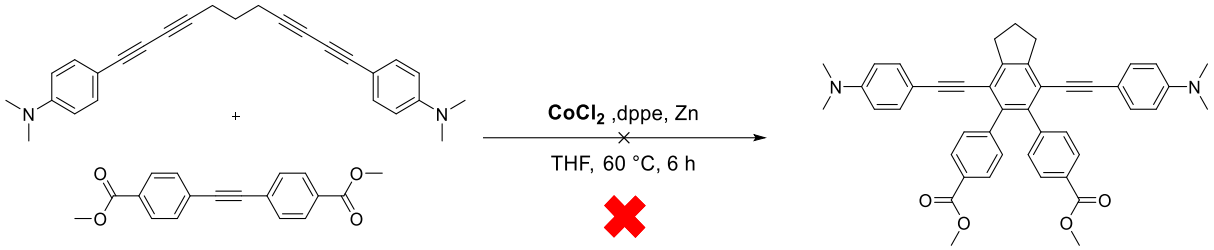

Attempts on Ni-catalyzed 2+2+2 cyclization with some olefins and with DMAD failed:

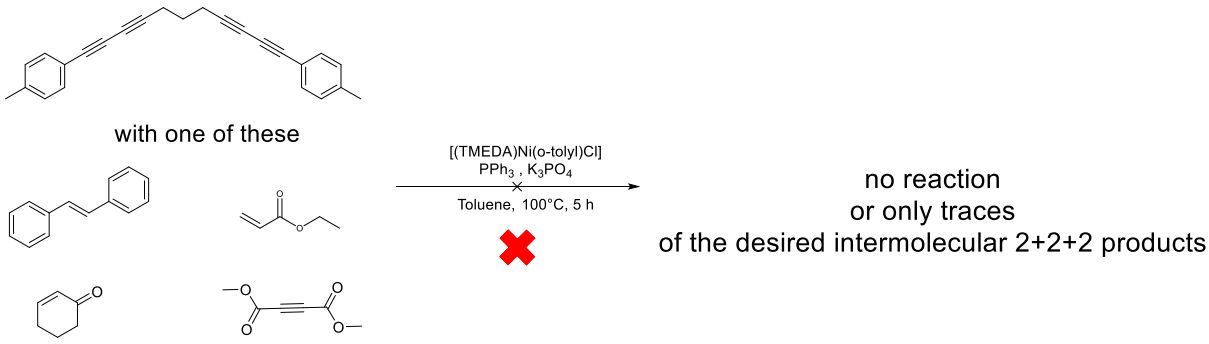

It was further tested, if the previously used reaction conditions would be able to cyclizate a bisdiyne with terephthalonitrile, to form one or two pyridine rings. The reaction did not work, only bisdiyne-dimer was found in this case:

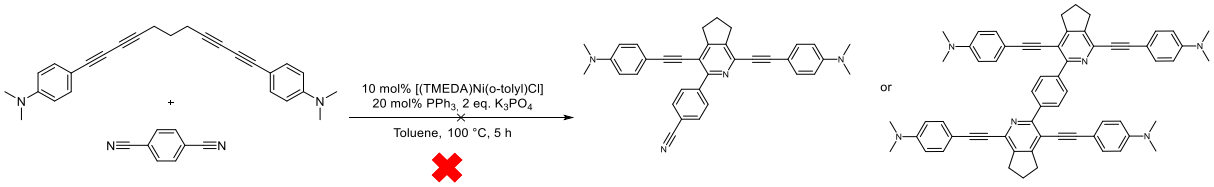

Single-crystal X-ray diffraction

General information

Crystals suitable for single-crystal X-ray diffraction were selected, coated in perfluoropolyether oil, and mounted on MiTeGen sample holders. Diffraction data were collected on a Bruker X8-APEX II diffractometer with a CCD area detector and multi-layer mirror (**2-4**) or a graphite (**2-5**) monochromated Mo-Kα radiation. The diffractometers were equipped with an open flow N_2 Cryoflex II (Bruker) device and data was collected at 100 K.

Diffraction data of **2-6**, **2-8** and **2-9** were collected on a Rigaku Oxford Diffraction XTALAB Synergy diffractometer with a semiconductor HPA-detector (HyPix-6000) and multi-layer mirror monochromated Cu-K_α or Mo-Kα (**2-9**) radiation. The crystals were cooled using an Oxford Cryostreams 800 low-temperature device. Data was collected at 100 K. The images were processed and corrected for Lorentz-polarization effects and absorption (empirical scaling) as implemented in the CrysAlis^{Pro} software.

The structures were solved using intrinsic phasing method (SHELXT)[146] refined with the SHELXL program[147] and the SHELXLE graphical user interface[155] and expanded using Fourier techniques. All non-hydrogen atoms were refined anisotropically. Hydrogen atoms were included in structure factor calculations. All hydrogen atoms were assigned to idealized geometric positions and omitted for clarity.

Single-crystal X-ray diffraction data and structure refinements.

Data	**2-4**	**2-5**	**2-6**	**2-8**	**2-9**
Empirical formula	$C_{41}H_{28}N_2$	$C_{45}H_{35}Cl_6N_4$	$C_{45}H_{40}N_2O_4$	$C_{67}H_{50}N_4O_4$	$C_{63}H_{50}N_4O_4$
Formula weight	548.65	844.47	672.79	975.11	927.07
Temperature/K	100.15	100.15	100.01(13)	100(2)	100(2)
Crystal system	triclinic	monoclinic	triclinic	orthorhombic	triclinic
Space group	P-1	$P2_1/c$	P-1	Pbcn	P-1
a/Å	11.011(7)	18.389(11)	9.41062(13)	51.3057(5)	10.8413(4)
b/Å	12.107(8)	11.504(4)	12.8526(2)	10.37368(14)	11.4653(4)
c/Å	12.166(7)	19.655(9)	30.2831(4)	9.74971(12)	20.5288(9)
α/°	76.511(11)	90	91.3349(13)	90	88.583(3)
β/°	81.280(13)	99.510(12)	95.2146(11)	90	76.648(4)
γ/°	71.072(14)	90	99.2858(13)	90	79.855(3)
Volume/Å^3	1486.7(16)	4101(3)	3597.12(10)	5189.08(11)	2443.58(17)
Z	2	4	4	4	2
ρ_{calc}g/cm^3	1.226	1.368	1.242	1.248	1.260
μ/mm^{-1}	0.071	0.457	0.561	0.614	0.079
F(000)	576.0	1740.0	1424.0	2048.0	976.0
Crystal size/mm^3	0.59 × 0.26 × 0.224	0.379 × 0.31 × 0.22	0.181 × 0.034 × 0.028	0.247 × 0.115 × 0.048	0.254 × 0.076 × 0.032
Radiation	MoKα (λ = 0.71073)	MoKα (λ = 0.71073)	Cu Kα (λ = 1.54184)	CuKα (λ = 1.54184)	MoKα (λ = 0.71073)
2Θ range for data collection/°	3.454 to 52.748	2.246 to 58.262	5.866 to 155.18	6.892 to 149.002	3.922 to 52.744
Index ranges	-13 ≤ h ≤ 13, -15 ≤ k ≤ 15, -15 ≤ l ≤ 15	-25 ≤ h ≤ 25, -15 ≤ k ≤ 15, -26 ≤ l ≤ 26	-11 ≤ h ≤ 11, -16 ≤ k ≤ 16, -38 ≤ l ≤ 33	-61 ≤ h ≤ 64, -7 ≤ k ≤ 12, -11 ≤ l ≤ 12	-13 ≤ h ≤ 13, -13 ≤ k ≤ 14, -25 ≤ l ≤ 25
Reflections collected	64013	51208	75873	28683	40046
Independent reflections	6073 [R_{int} = 0.0447, R_σ = 0.0198]	11046 [R_{int} = 0.0480, R_σ = 0.0432]	15056 [R_{int} = 0.0518, R_σ = 0.0394]	5302 [R_{int} = 0.0316, R_σ = 0.0260]	9998 [R_{int} = 0.0822, R_σ = 0.0749]
Data/restraints/ parameters	6073/0/390	11046/10/520	15056/96/1141	5302/16/351	9998/0/644
Goodness-of-fit on F^2	1.086	1.027	1.036	1.034	1.016
Final R indexes [I>=2σ (I)]	R_1 = 0.0412, wR_2 = 0.1171	R_1 = 0.0490, wR_2 = 0.1154	R_1 = 0.0465, wR_2 = 0.1239	R_1 = 0.0378, wR_2 = 0.0937	R_1 = 0.0619, wR_2 = 0.1176
Final R indexes [all data]	R_1 = 0.0504, wR_2 = 0.1344	R_1 = 0.0797, wR_2 = 0.1303	R_1 = 0.0611, wR_2 = 0.1343	R_1 = 0.0421, wR_2 = 0.0964	R_1 = 0.1084, wR_2 = 0.1324
Largest diff. peak/hole / e Å^{-3}	0.97/-0.47	0.78/-0.76	0.22/-0.31	0.23/-0.21	0.21/-0.21

Photophysical characterization

General information

All measurements were performed in standard quartz cuvettes (1 cm x 1 cm cross-section). UV-visible absorption spectra were recorded using an Agilent 8453 diode array UV-visible spectrophotometer. Emission spectra were recorded using an Edinburgh Instruments FLSP920 spectrometer equipped with a double monochromator for both excitation and emission, operating in right-angle geometry mode, and all spectra were fully corrected for the spectral response of the instrument. All solutions used in photophysical measurements had concentrations lower than $5 \cdot 10^{-6}$ M to minimize inner filter effects during fluorescence measurements.

Fluorescence quantum yield measurements. The fluorescence quantum yields were measured using a calibrated integrating sphere (inner diameter: 150 mm) from Edinburgh Instruments combined with the FLSP920 spectrometer described above. For solution-state measurements, the longest-wavelength absorption maximum of the compound in the respective solvent was chosen as the excitation wavelength, unless stated otherwise.

Lifetime measurements. Fluorescence lifetimes were recorded using the time-correlated single-photon counting (TCSPC) method using an Edinburgh Instruments FLS980 spectrometer equipped with a high-speed photomultiplier tube positioned after a single emission monochromator. Measurements were made in right-angle geometry mode, and the emission was collected through a polarizer set to the magic angle. The full-width-at-half-maximum (FWHM) of the pulse from the diode laser was ca. 75-90 ps with an instrument response function (IRF) of ca. 230 ps FWHM. The IRFs were measured from the scatter of an aqueous suspension of Ludox at the excitation wavelength. Decays were recorded to 10000 counts in the peak channel with a record length of 8192 channels. The band pass of the emission monochromator and a variable neutral density filter on the excitation side were adjusted to give a signal count rate of <60 kHz. Iterative reconvolution of the IRF with one decay function and non-linear least-squares analysis were used to analyze the data. The quality of all decay fits was judged to be satisfactory, based on the calculated values of the reduced χ^2 and Durbin-Watson parameters and visual inspection of the weighted residuals. All compounds except **2-10** were transferred into EtOH and MeCN solutions by first dissolving them in a few µL of THF

and then transferring them into respective solvent-filled cuvettes, as they were only poorly soluble in these strongly polar solvents.

Due to technical limitations of our spectrometer set up (temporal resolution/ detector response time), only lifetimes >1 ns can be accurately determined, the found values <1 ns were still given.

We further investigated the photophysical properties of the bis-triarylamine bisdiyne substrate, which shows strong solvatochromic fluorescence in the visible spectrum with quantum yields of up to Φ=0.72 in THF with a molar extinction coefficient of 79000 mol^{-1} cm^{-1}.

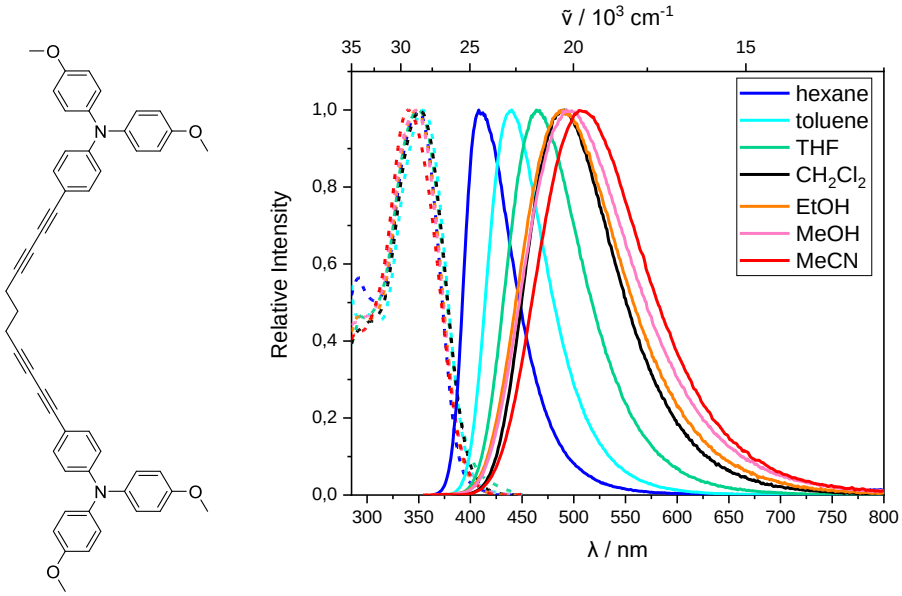

Figure 74: Structural formula of the bis-triarylamine bisdiyne substrate and absorption (dashed) and emission (solid) spectra in seven solvents.

Table 8: Photophysical data for the bis-triarylamine bisdiyne substrate above.

Solvent	λ_{max} abs (nm)	λ_{max} em (nm)	Stokes shift (cm^{-1})	Φ	τ (ns)	τ_0 (ns)	$K_{nr}/10^7 s^{-1}$	$K_r/10^7 s^{-1}$
hexane	349	409	4203	0.31	1.28	4.1	53.9	24.2
toluene	353	440	5601	0.62	2.96	4.8	12.8	20.9
THF	349	465	7148	0.72	4.78	6.6	5.9	15.1
CH_2Cl_2	351	489	8040	0.68	6.02	8.9	5.3	11.3
EtOH	347	490	8410	0.30	2.36	7.9	29.7	12.7
MeOH	346	496	8740	0.10	1.23	12.3	73.2	8.1
MeCN	340	508	9727	0.40	3.89	9.7	15.4	10.3

Chapter 3

Synthesis

General information:

Unless otherwise noted, all reactions were performed using standard Schlenk or glovebox (Innovative Technology Inc.) techniques under argon. Reagent grade solvents were argon saturated, dried using an Innovative Technology Inc. Pure-Solv Solvent Purification System, and further deoxygenated by using the freeze-pump-thaw method. All starting materials were purchased from commercial sources and used without further purification.

Automated flash chromatography was performed using a Biotage® Isolera Four system on silica gel or NH-silica. Commercially available, precoated TLC plates (Polygram® Sil G/UV_{254} and Polygram® Alox N/UV_{254}) were purchased from Macherey-Nagel. The removal of solvent was performed on a rotary evaporator *in vacuo* at a maximum temperature of 45 °C.

GC-MS analyses were performed using an Agilent 7890A gas chromatograph equipped with an Agilent 5975C inert MSD with triple-axis detector operating in EI mode and an Agilent 7693A series auto sampler/injector. High resolution mass spectrometry was obtained using a Thermo Scientific Exactive Plus MS System with either an atmospheric-pressure chemical ionization (APCI) or a heated-electrospray ionization (HESI) probe.

NMR spectra were recorded at ambient temperature on a Bruker DRX-300 (^{1}H, 300 MHz; ^{13}C{^{1}H}, 75 MHz; ^{11}B{^{1}H}, 96 MHz), Bruker Avance 500 NMR (^{1}H, 500 MHz; ^{13}C{^{1}H}, 125 MHz) or on Bruker Avance Neo I 600 (^{1}H: 600 MHz, ^{11}B: 192 MHz, ^{13}C: 150 MHz) spectrometers. NMR chemical shifts for ^{1}H and ^{13}C are reported relative to TMS and were referenced *via* carbon signals or residual proton resonances of the corresponding deuterated solvent. The ^{11}B{^{1}H} NMR spectra are reported relative to the external standard $BF_3 \cdot Et_2O$.

Elemental analyses were performed with an Elementar vario micro cube device. Infrared spectra were recorded on a Bruker Alpha FT-IR spectrometer as solids by using an ATR unit with a resolution of 4 cm^{-1} and are reported in cm^{-1}. Raman spectra were recorded as solids at room temperature with a MultiRAM FT-Raman spectrometer in melting point capillaries.

4-Bromo-N,N,3,5-tetramethylaniline **3-2**

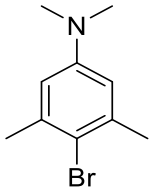

N,N,3,5-tetramethylaniline (25.5 g, 171 mmol) was dissolved in MeCN (600 mL) and cooled to 0 °C. NBS (30.44 g, 171 mmol) was slowly added. After stirring at 0 °C for 2 h, the solution was warmed to room temperature. To the solution, water (150 mL) was added, and the aqueous phase was extracted with hexane (3 x 80 mL). The organic phases were combined and dried over $MgSO_4$. The reaction mixture was filtered, and the solvent was removed under reduced pressure.

The procedure and NMR data are similar to those reported previously.[156, 157]

Yield: 33.0 g (145 mmol, 85%) of a yellow liquid.
^{1}H NMR (300 MHz, $CDCl_3$): δ [ppm] = 6.50 (m, 2H), 2.92 (s, 6H), 2.40 (m, 6H).

4,4'-(Fluoroboranediyl)-bis-(N,N,3,5-tetramethylaniline) **3-3**

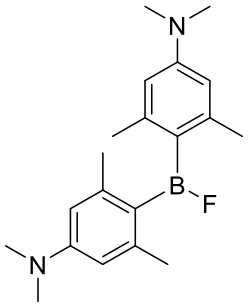

Compound 4-bromo-N,N,3,5-tetramethylaniline **3-2** (33.0 g, 145 mmol) was reacted with Mg (4.12 g, 170 mmol) in THF (180 mL) under reflux for 5 h. After cooling to room temperature, the reaction mixture was filtered, and the filtrate was slowly added to a solution of $BF_3{\cdot}Et_2O$ (8.6 mL, 68 mmol) in THF (50 mL) at 0 °C with the exclusion of light. The reaction mixture was stirred for 2 h at 0 °C and then overnight at room temperature, also under exclusion of light. The solvent was removed under reduced pressure and the residue was extracted with hexane (2 x 150 mL) under an argon atmosphere. The hexane fractions were combined, and the solvent was removed under reduced pressure. The product was stored under argon.

The procedure and NMR data are similar to those reported previously.[158, 159]

Yield: 12.3 g (37.7 mmol, 53%) of a yellow powder.
^{1}H NMR (300 MHz, C_6D_6): δ [ppm] = 6.37 (m, 4H), 2.53 (s, 12H), 2.50 (m, 12H).

2,5-Dibromo-1,3-dimethylbenzene **3-5**

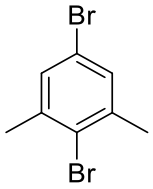

B_2pin_2 (15.0 g, 59.0 mmol), $[Ir(COD)(OMe)]_2$ (180 mg, 272 mmol) and 4,4'-di-^{t}butyl-2,2'-dipyridyl (dtbpy) (149 mg, 547 mmol) were dissolved in dry and degassed hexane (80 mL). The solution was stirred at room temperature for 2 h. Then, 2-bromo-1,3-dimethylbenzene (10.1 g, 54.6 mmol) was added and the mixture was stirred at 60 °C for 16 h. After cooling to r.t., the solvent was removed under reduced pressure. The crude intermediate was dissolved in MeOH (300 mL) and $CuBr_2$ (36.6 g, 164 mmol) in water (300 mL) was added. The mixture was stirred at 90 °C for 4 days. Then, the mixture was cooled to 0 °C, and the precipitate was collected by filtration and then extracted with hexane (3 x 100 mL). The combined organic fractions were filtered through a short silica plug and the solvent was removed under reduced pressure.

The procedure and NMR data are similar to those reported previously.[110, 160]

Yield: 12.2 g (46.2mmol, 85%) of a colorless liquid.
^{1}H NMR (300 MHz, $CDCl_3$): δ [ppm] = 7.21 (s, 2H), 2.38 (s, 6H).

(4-Bromo-3,5-dimethylphenyl)ethynyl)trimethylsilane **3-6**

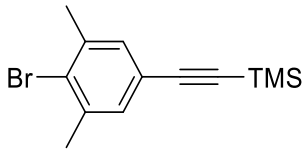

The compounds $Pd(PPh_3)_2Cl_2$ (617 mg, 877 µmol) and CuI (472 mg, 2.48 mmol) were dissolved in dry, degassed NEt_3 (350 mL). Trimethylsilylacetylene (5.09 g, 51.9 mmol) and **3-5** (12.2 g, 46.2 mmol) were added and the mixture was stirred at 80 °C overnight. Afterwards the solvent was removed under reduced pressure. The residue was suspended in hexane (450 mL) and passed through a silica plug. The solvent was removed under reduced pressure. The crude

product contained a small amount of the homo-coupled dimer of trimethylsilylacetylene, which was removed by bulb-to-bulb distillation.

The procedure and NMR data are similar to those reported previously.[110, 161]

Yield: 11.0 g (39.1 mmol, 85%) of a brown liquid.
^{1}H NMR (300 MHz, $CDCl_3$): δ [ppm] = 7.18 (m, 2H), 2.37 (m, 6H), 2.42 (s, 9H).

4,4'-((2,6-dimethyl-4-((trimethylsilyl)ethynyl)phenyl)boranediyl)bis(N,N,3,5-tetramethylaniline) **3-7**

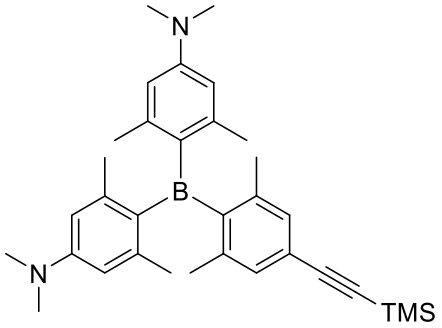

Compound **3-6** (2.67 g, 9.49 mmol) was dissolved in dry and degassed hexane (60 mL) and cooled to -70 °C. Then ^{t}BuLi (18.7 mmol, 2.1 eq, 11 mL, 1.7 M in hexane) was added *via* syringe. The solution was stirred for 30 min. Then, the cooling bath was removed, and the solution was stirred for 18 h at r.t. The mixture was cooled to -78 °C, and a solution of the fluoroborane **3-3** (2.40 g, 7.36 mmol) in THF (60 mL) was added *via* cannula. The resulting solution was stirred for additional 18 h at room temperature. Water and brine were added, and the product was extracted with dichloromethane. The combined organic phases were dried over $MgSO_4$, and the solvent was removed under reduced pressure. The crude product was directly used in the deprotection step.

4,4'-((4-ethynyl-2,6-dimethylphenyl)boranediyl)bis(N,N,3,5-tetramethylaniline) **3-8**

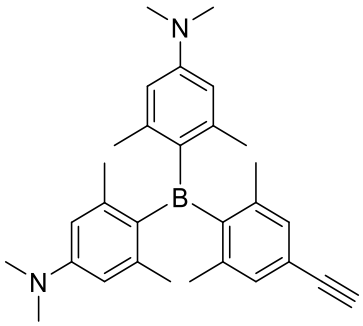

Crude **3-7** (~3.8 g) was dissolved in THF (180 mL), and MeOH (180 mL) was added, followed by powdered KOH (2.5 g, 45 mmol). The solution was stirred overnight at r. t. The solvent was

removed under reduced pressure. The residue was dissolved in dichloromethane (50 mL) and then washed with water (5 x 50 mL). The organic layer was dried over $MgSO_4$, and the solvent was removed under reduced pressure. The residue was suspended in MeOH, filtered and the resulting precipitate was dried on a glass frit to obtain the product.

The procedure and NMR data are similar to those reported previously.[110]

Yield (based on **3-3** over two steps): 2.18 g (5 mmol, 68%) of a bright yellow solid.
^{1}H NMR (300 MHz, $CDCl_3$): δ [ppm] = 7.04 (s, 2H), 6.29 (s, 4H), 3.02 (s, 1H), 2.96 (s, 12H), 2.01 (s, 12H), 1.91 (s, 6H).
$^{13}C\{^1H\}$ (75 MHz, $CDCl_3$) δ [ppm] = 151.3219, 143.26, 142.74, 140.32, 130.81, 121.29, 111.63, 84.73, 40.10, 24.17, 23.80, 22.80.
$^{11}B\{^1H\}$ (96 MHz, $CDCl_3$) δ [ppm] = 73.5.
HRMS (APCI+): m/z calculated: 437.3128 [M+H], m/z found: 437.3116.

(bromoethynyl)trimethylsilane

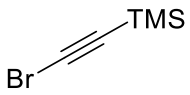

Trimethylsilylacetylene (1.96 g, 20 mmol) was dissolved in acetone (40 mL) and $AgNO_3$ (340 mg, 2.00 mmol) and NBS (4.27 g, 24 mmol) were added. The solution was stirred for 4 h at r. t., after which a white solid precipitated. The solution was filtered through a silica plug and the solvent was removed under reduced pressure from the filtrate. The residue was dissolved in pentane and filtered again. The product was obtained after removing the solvent under reduced pressure from the filtrate. It is critical, to remove the solvent gently because of the low boiling point of the product.

The procedure and NMR data are similar to those reported previously.[162]

Yield: 2.8 g (16.2 mmol, 81%) of an off-white liquid.
^{1}H NMR (300 MHz, $CDCl_3$): δ [ppm] = 0.19 (s, 9H)
GC-MS (EI): *m/z* calcd.: 176 [M], found 176.

4,4'-((2,6-dimethyl-4-((trimethylsilyl)buta-1,3-diyn-1-yl)phenyl)boranediyl)bis(N,N,3,5-tetramethylaniline) **3-9**

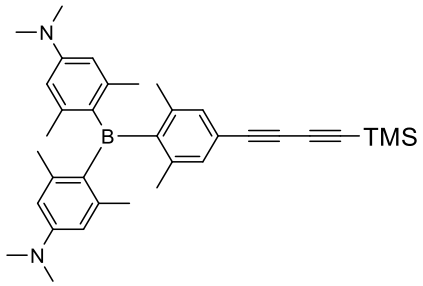

In a Schlenk flask, **3-8** (1.04 g, 2.39 mmol, 1 eq.) was dissolved in 15 mL THF and cooled to – 45 °C in a m-xylene dry ice bath. Then nBuLi (1.05 mL, 2.63 mmol, 1.1 eq, 2.5 M in hexane) was added dropwise. After 30 min CuI (501 mg, 2.62 mmol, 1.1 eq.) was added and stirred for 30 min at -45 °C. The reaction mixture was warmed up to -10 °C in an acetone/ice bath. The mixture was again cooled to -45 °C and 7.2 mL $nBuNH_2$ was added, followed by (bromoethynyl)trimethylsilane (673 mg, 3.80 mmol, 1.6 eq.). After 10 min the cooling was removed, and the mixture was stirred at r. t. for 1 h. The solvent was removed under reduced pressure and the mixture was filtered through a 5 cm silica plug CH_2Cl_2/hexane (1:9). After removal of the solvent under reduced pressure, the compound was isolated as an yellow solid. The crude product can be purified by flash chromatography (silica gel, cyclohexane/EtOAc 5%).

Yield: 1.08 g, 2.03 mmol, 85%
Rf: (12.5% EtOAc in cyclohexane): 0.5
^{1}H NMR (300 MHz, $CDCl_3$,) δ [ppm] = 7.03 (s, 2H), 6.29 (s, 4H), 2.96 (s, 12H), 2.01 (m, 12H), 1.90 (s, 6H), 0.23 (s, 6H)
$^{13}C\{^{1}H\}$ NMR (75 MHz, $CDCl_3$) δ [ppm] = 151.35, 143.32, 142.73, 140.39, 135.55, 131.26, 120.48, 111.65, 90.16, 88.41, 78.16, 73.77, 40.09, 24.18, 23.81, 22.80, -0.17.
$^{11}B\{^{1}H\}$ (192 MHz, $CDCl_3$) δ [ppm] = 71.9.
Elem. anal. calcd. (%) for $C_{35}H_{45}BN_2Si$: C, 78.92; H, 8.52; N, 5.26 found: C, 78.18; H, 8.76; N: 4.86.
HRMS (APCI+): m/z calculated: 533.3518 [M+H], m/z found: 533.3514.

4,4'-((4-(buta-1,3-diyn-1-yl)-2,6-dimethylphenyl)boranediyl)bis(N,N,3,5-tetramethylaniline) **3-10**

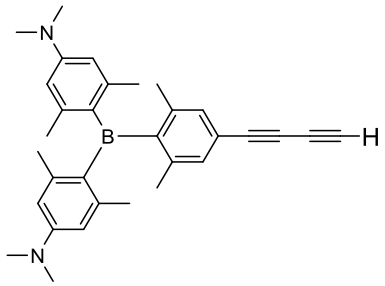

A mixture of **3-9** (1.69 g, 3.17 mmol) and KOH (890 mg, 15.85 mmol, 5 eq.) in 100 mL of THF and 100 mL of MeOH were stirred for 2 h at room temperature. After removal of most of the solvent, 200 mL of water and 200 mL of CH_2Cl_2 were added. The organic layer was separated and washed 2 times with water. After addition of ca. 5 mL of acetone, the volatiles were removed *in vacuo* to obtain a yellow solid, while maintaining the temperature below 40 °C.

The product is quite unstable and was stored in a freezer or, used in further reactions immediately.

Yield: 1.454 mg, 3.16 mmol, 99%
^{1}H NMR (300 MHz, $CDCl_3$): δ [ppm] = 7.06 (m, 2H), 6.29 (m, 4H), 2.96 (s, 12H), 2.45 (S, 1H), 2.04-1.88 (m, 18 H).
$^{13}C\{^1H\}$ NMR (75 MHz, $CDCl_3$): δ [ppm] = 151.36, 143.35, 142.72, 140.44, 131.34,120.07, 111.64, 73.03, 70.95, 68.64, 68.12, 40.09, 25.76, 24.19, 23.80, 22.79.
$^{11}B\{^1H\}$ (96 MHz, $CDCl_3$) δ [ppm] = *signal too weak to observe.*
Elem. anal. calcd. (%) for $C_{32}H_{37}BN_2$: C, 83.47; H, 8.10; N, 6.08 Found: C, 82.07; H, 8.61; N 5.72.
HRMS (APCI+): m/z calculated: 461.3113 [M+H], m/z found: 461.3123.

4,4',4'',4'''-((octa-1,3,5,7-tetrayne-1,8-diylbis(2,6-dimethyl-4,1-phenylene))bis(boranetriyl))tetrakis(N,N,3,5-tetramethylaniline) **3-11**

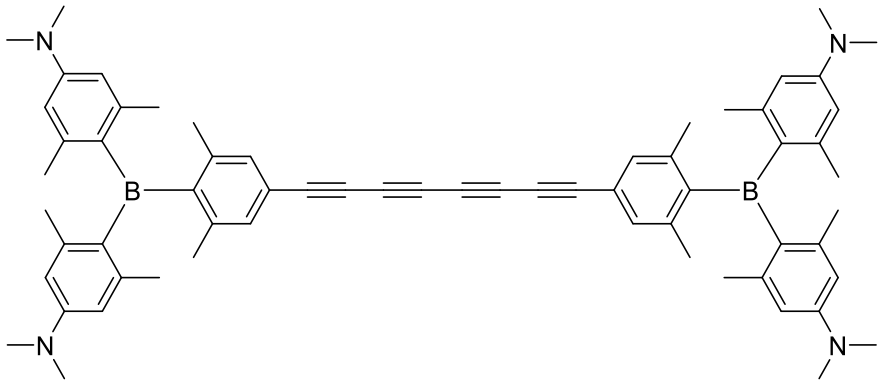

A mixture of **3-10** (1.45 g, 3.16 mmol, 1 eq.), iodine (401 mg, 1.58 mmol, 1 eq.), $Pd(PPh_3)_2Cl_2$ (44.4 mg, 0.063 mmol, 0.02 eq.) and CuI (30.1 mg, 0.158 mmol, 0.05 eq.) in 150 mL of THF

and 50 mL of MeOH was stirred at r. t. for 1 d. The solvent was removed under reduced pressure, then the mixture was filtrated through a silica plug with Et_2O to give a yellow crude product. The mixture was then flash-chromatographed on silica (4-10% EtOAc + 3% NEt_3 in cyclohexane).

Yield: 1.01 g, 1.10 mmol, 70%.
^{1}H NMR (500 MHz, CD_2Cl_2): δ [ppm] = 7.09 (m, 4H), 6.30 (m, 8H), 2.94 (s, 24H), 2.01-1.85 (m, 36H).
$^{13}C\{^1H\}$ NMR (125 MHz, CD_2Cl_2): δ [ppm] = 153.44, 151.83, 143.53, 142.92, 140.9202, 135.45, 131.93, 119.58, 111.84, 79.47, 73.96, 67.20, 64.26, 40.09, 24.09, 23.79, 22.74.
$^{11}B\{^1H\}$ NMR (192 MHz, $CDCl_3$) δ [ppm] = 71.2 ppm.
Elem. anal. calcd. (%) for $C_{64}H_{72}B_2N_4$: C, 83.65; H, 7.90; N, 6.10 found: C, 83.13; H, 8.63; N 5.60.
HRMS (APCI+): m/z calculated: 919.5971 [M+H], m/z found: 919.6020.

4,4',4'',4'''-((octa-1,3,5,7-tetrayne-1,8-diylbis(2,6-dimethyl-4,1-phenylene))bis(boranetriyl))tetrakis(N,N,N,3,5-pentamethylbenzenaminium)tetratriflate **3-12**

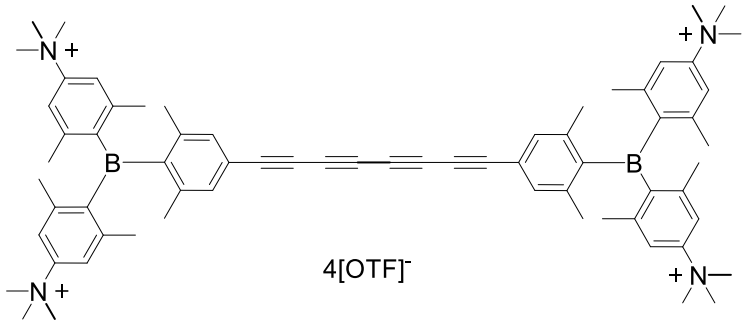

In a soda-lime glass vial, tetrayne **3-11** (32 mg, 0.035 mmol, 1 eq.) was dissolved in 5 mL of CH_2Cl_2 and MeOTf (68.8 mg, 0.42 mmol, 12 eq.) was added slowly. The mixture was stirred overnight at r. t. in the absence of light. The solid product was collected by filtration on a glass frit and was then washed with Et_2O in an ultrasonic bath.

Yield: 34 mg, 0.021 mmol, 62%.
^{1}H NMR (300 MHz, MeOD) δ [ppm] = 7.75 (m, 8H), 7.25 (m, 4H), 3.65 (S, 36H), 2.30-1.87 (m, 36H).
$^{13}C\{^1H\}$ NMR (75 MHz, MeOD): δ [ppm] = 149.91, 148.90, 148.67, 144.89, 144.74, 142.47, 133.49, 123.91, 123.65, 120.31, 119.68, 78.92, 75.41, 67.83, 64.50, 57.46, 23.47, 23.04.
$^{11}B\{^1H\}$ NMR (96 MHz, MeOD) δ [ppm] = *signal too weak to observe.*
Elem. anal. calcd. (%) for $C_{72}H_{84}B_2F_{12}N_4O_{12}S_4$: C, 54.90; H, 5.37; N, 3.56; S, 8.14. Found: C, 54.70; H, 5.89; N, 3.26; S, 8.23.
HRMS of the cation (ESI+): m/z calculated: 244.6715 (M), m/z found: 244.6715.
HRMS of the anion (ESI-): m/z calculated: 148.9515 (M), m/z found: 148.9515.

Single-crystal X-ray diffraction

Data was collected from a shock-cooled single crystal at 173 K on a XtaLAB Synergy, Dualflex, HyPix four-circle diffractometer with a micro-focus sealed X-ray tube using mirror as monochromator and a HyPix detector. The diffractometer was equipped with a low temperature device and Cu-K_α radiation (λ = 1.54184 Å) was used. All data were integrated with Crysalis pro and a Gaussian absorption correction using SCALE3 ABSPACK was applied. The structure were solved by direct methods using SHELXT and refined by full-matrix least-squares methods against F^2 by SHELXL-2014/7.[146] All non-hydrogen atoms were refined with anisotropic displacement parameters. The hydrogen atoms were refined isotopically on calculated positions using a riding model with their U_{iso} values constrained to 1.5 times the U_{eq} of their pivot atoms for terminal sp^3 carbon atoms and 1.2 times for all other carbon atoms. The CIF file was generated using FinalCif.

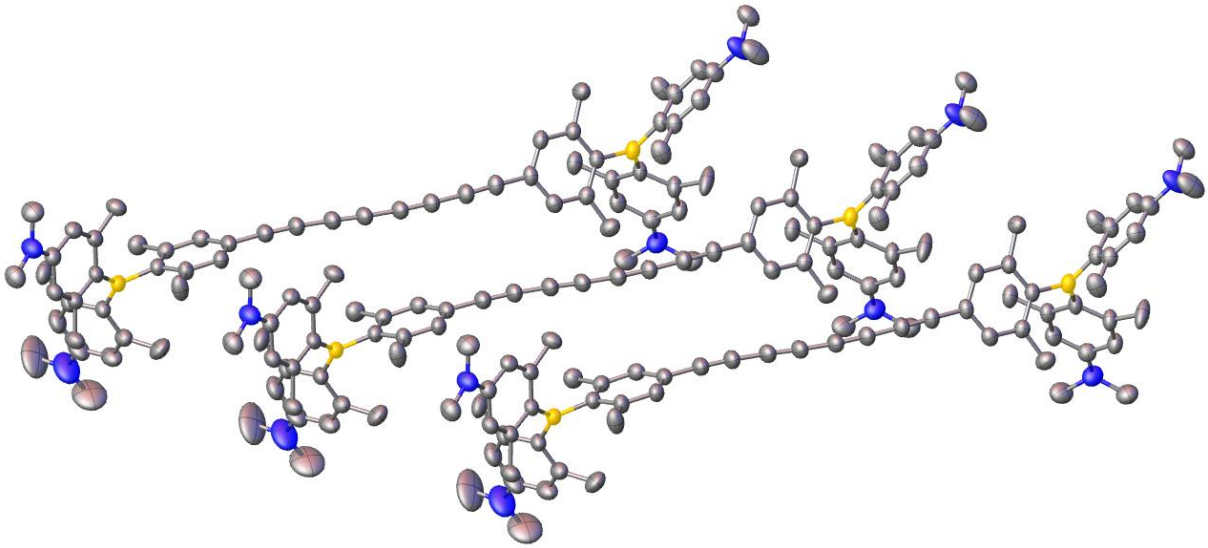

*Figure 75: Excerpt of the solid-state structure of **3-11**, depicting the staggered arrangement of the rods, view along 111.*

Crystal data for 3-11

Empirical formula	$C_{64}H_{72}B_2N_4$ + Acetone
Formula weight	918.87
Temperature [K]	173.00(10)
Crystal system	monoclinic
Space group (number)	$P2_1/n$ (14)
a [Å]	23.3558(2)
b [Å]	8.39130(10)
c [Å]	30.5505(3)
α [°]	90
β [°]	90.5770(10)
γ [°]	90
Volume [Å^3]	5987.14(11)
Z	4.00
ρ_{calc} [gcm^{-3}]	1.019
μ [mm^{-1}]	0.439
F(000)	1976
Crystal size [mm^3]	0.272 × 0.170 × 0.123
Crystal colour	orange
Crystal shape	block
Radiation	Cu K_α (λ = 1.54184 Å)
2Θ range [°]	3.78 to 160.28 (0.78 Å)
Index ranges	-29 ≤ h ≤ 26 -10 ≤ k ≤ 10 -39 ≤ l ≤ 38
Reflections collected	56261
Independent reflections	12849 R_{int} = 0.0322 R_{sigma} = 0.0303
Completeness to Θ = 74.3338°	99.8%
Data / Restraints / Parameters	12849/0/651
Goodness-of-fit on F^2	1.055
Final *R* indexes [$I \geq 2\sigma(I)$]	R_1 = 0.0455 wR_2 = 0.1257
Final *R* indexes [all data]	R_1 = 0.0574 wR_2 = 0.1340
Largest peak/hole [eÅ^{-3}]	0.24/-0.21

Photophysical characterization

General information

All measurements were performed in standard quartz cuvettes (1 cm x 1 cm cross-section). UV-visible absorption spectra were recorded using an Agilent 8453 diode array UV-visible spectrophotometer. Emission spectra were recorded using an Edinburgh Instruments FLSP920 spectrometer equipped with a double monochromator for both excitation and emission, operating in right-angle geometry mode, and all spectra were fully corrected for the spectral response of the instrument. All solutions used in photophysical measurements had concentrations lower than $5 \cdot 10^{-6}$ M to minimize inner filter effects during fluorescence measurements.

Fluorescence quantum yield measurements. The fluorescence quantum yields were measured using a calibrated integrating sphere (inner diameter: 150 mm) from Edinburgh Instruments combined with the FLSP920 spectrometer described above. For solution-state measurements, the longest-wavelength absorption maximum of the compound in the respective solvent was chosen as the excitation wavelength, unless stated otherwise.

Lifetime measurements. Fluorescence lifetimes were recorded using the time-correlated single-photon counting (TCSPC) method using an Edinburgh Instruments FLS980 spectrometer equipped with a high-speed photomultiplier tube positioned after a single emission monochromator. Measurements were made in right-angle geometry mode, and the emission was collected through a polarizer set to the magic angle. The full-width-at-half-maximum (FWHM) of the pulse from the diode laser was ca. 75-90 ps with an instrument response function (IRF) of ca. 230 ps FWHM. The IRFs were measured from the scatter of an aqueous suspension of Ludox at the excitation wavelength. Decays were recorded to 10000 counts in the peak channel with a record length of 8192 channels. The band pass of the emission monochromator and a variable neutral density filter on the excitation side were adjusted to give a signal count rate of <60 kHz. Iterative reconvolution of the IRF with one decay function and non-linear least-squares analysis were used to analyze the data. The quality of all decay fits was judged to be satisfactory, based on the calculated values of the reduced χ^2 and Durbin-Watson parameters and visual inspection of the weighted residuals.

Due to technical limitations of our spectrometer set up (temporal resolution/ detector response time), only lifetimes >1 ns can be accurately determined, the found values <1 ns were still given.

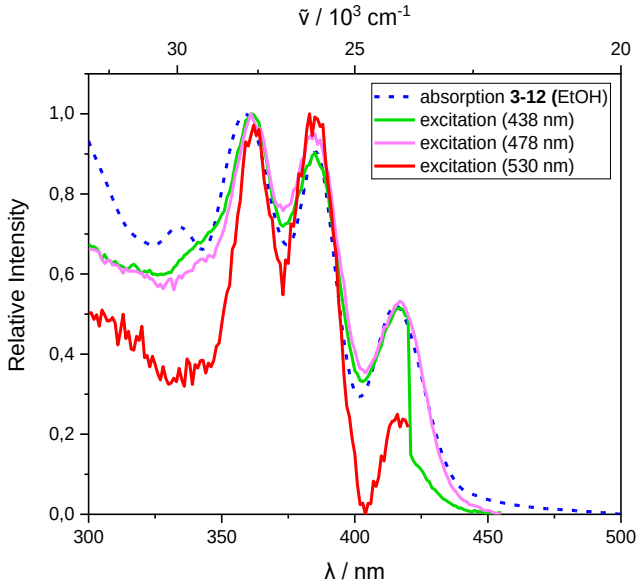

*Figure 76: Absorption and excitation spectra of **3-12** in ethanol solution.*

Chapter 4

General information:

The compounds 1,1'-(1,3-Butadiyne-1,4-diyl)bis[4-(trifluoromethyl)benzene] (**4-1**) was prepared according to the literature.[83] Pinacolborane (HBpin) and tributyl phosphine oxide ($O=PnBu_3$) were purchased from Sigma Aldrich and $PnBu_3$ from abcr, and were used without further purification, their purity was confirmed via NMR (see substrate spectra). Toluene-d_8 was purchased from Sigma Aldrich, dried by storage over molecular sieves for several days, and then degassed under vacuum in an ultrasonic bath. All reactions were conducted, and all NMR spectra were recorded in 0.5 mL of toluene-d_8 under an argon atmosphere. NMR spectra were recorded on a Bruker Avance 500 MHz (^{1}H: 500 MHz, ^{13}C: 125 MHz, ^{11}B: 160 MHz, ^{31}P: 202 MHz, ^{19}F: 470 MHz), Bruker Avance 300 MHz (^{1}H: 300 MHz, ^{11}B: 96 MHz, ^{13}C: 75 MHz, ^{31}P: 121 MHz) or on a Bruker Avance Neo I 600 (^{1}H: 600 MHz, ^{11}B: 192 MHz, ^{19}F: 564 MHz, ^{13}C: 150 MHz, ^{31}P: 242 MHz). All ^{1}H- and ^{13}C{^{1}H} NMR spectra are reported relative to TMS, using the residual signals of toluene-d_8. The ^{19}F{^{1}H} NMR spectra are reported relative to the external standard $CFCl_3$. The ^{31}P{^{1}H} NMR spectra are reported relative to the external standard H_3PO_4. The ^{11}B{^{1}H} NMR spectra are reported relative to the external standard $BF_3{\cdot}Et_2O$. All scales of the depicted NMR spectra are given in *ppm*. High resolution mass spectrometry (HRMS) was performed using a Thermo Fischer Scientific Exactive Plus Orbitrap system with a LIFDI (Liquid Injection Field Desorption Ionization) or APCI (Atmospheric Pressure Chemical Ionization) probe. GC-MS analyses were performed on an Agilent Technologies GC-MS system (GC 7890A, EI-MS 5975C). UV/Vis absorption spectra were recorded in n-hexane in standard quartz cuvettes (1 cm x 1 cm cross-section) using an Agilent 8453 diode array UV-visible spectrophotometer.

Additional spectra

Hydroboration control experiment

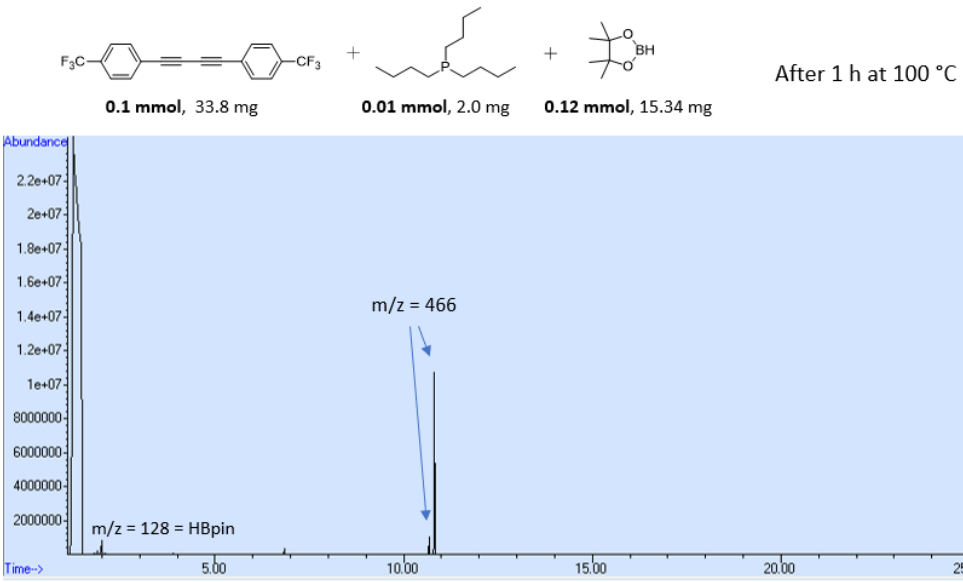

*Figure 77: GC-MS of the control experiment of the $PnBu_3$-catalyzed hydroboration of diyne **4-1** with HBpin. After 1 h at 100 °C. Two peaks matched the mass of the desired E and Z products (m/z = 466). Substrate **4-1** was consumed completely.*

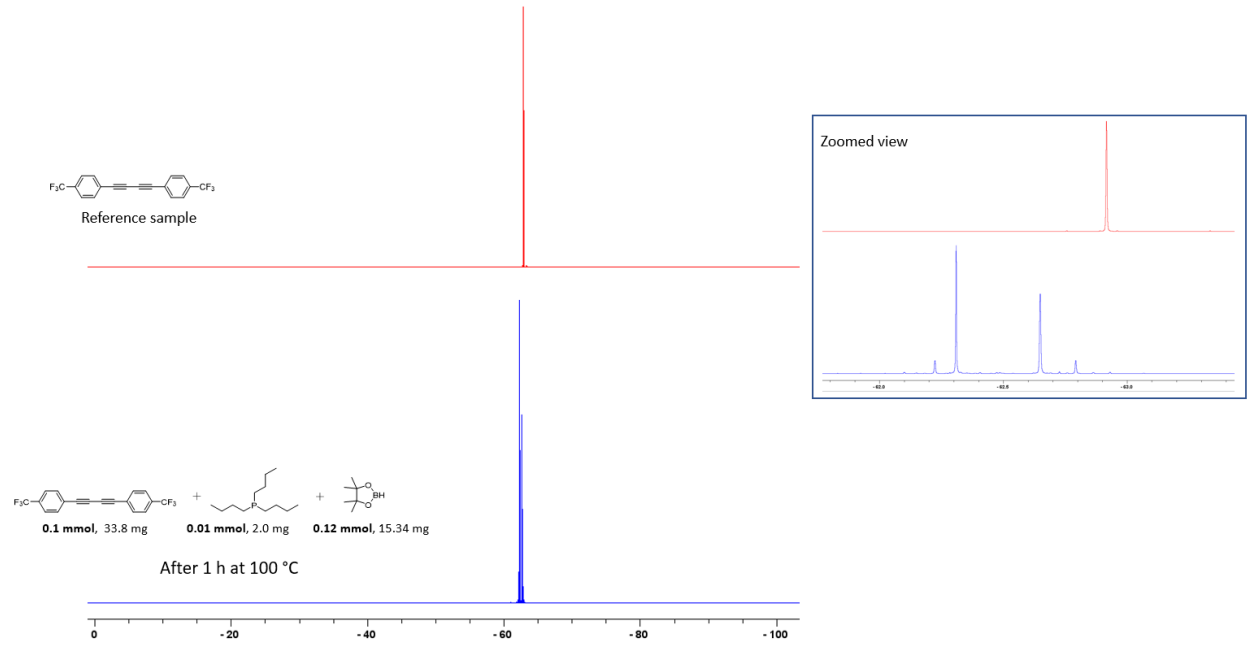

*Figure 78: $^{19}F\{^1H\}$ (470 MHz blue, 564 MHz red) NMR spectra of the control experiment of the $PnBu_3$-catalyzed hydroboration of diyne **4-1** with HBpin. After 1 h at 100 °C, the substrate signal disappeared and two new signals, belonging to the hydroboration product, appeared (see zoomed view).*

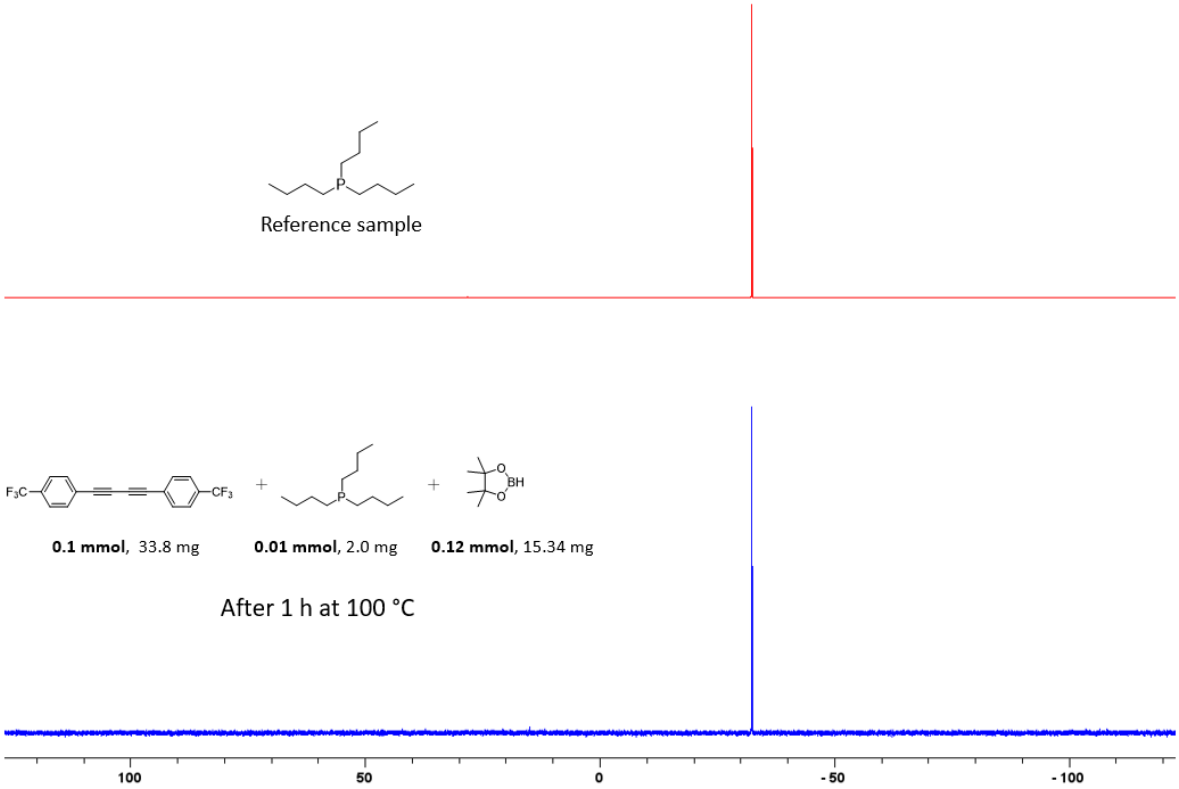

*Figure 79: $^{31}P\{^{1}H\}$ (121 MHz) NMR spectra of the control experiment of the $PnBu_3$-catalyzed hydroboration of diyne **4-1** with HBpin. The phosphine catalyst is unchanged after the reaction is complete.*

HBpin stability control

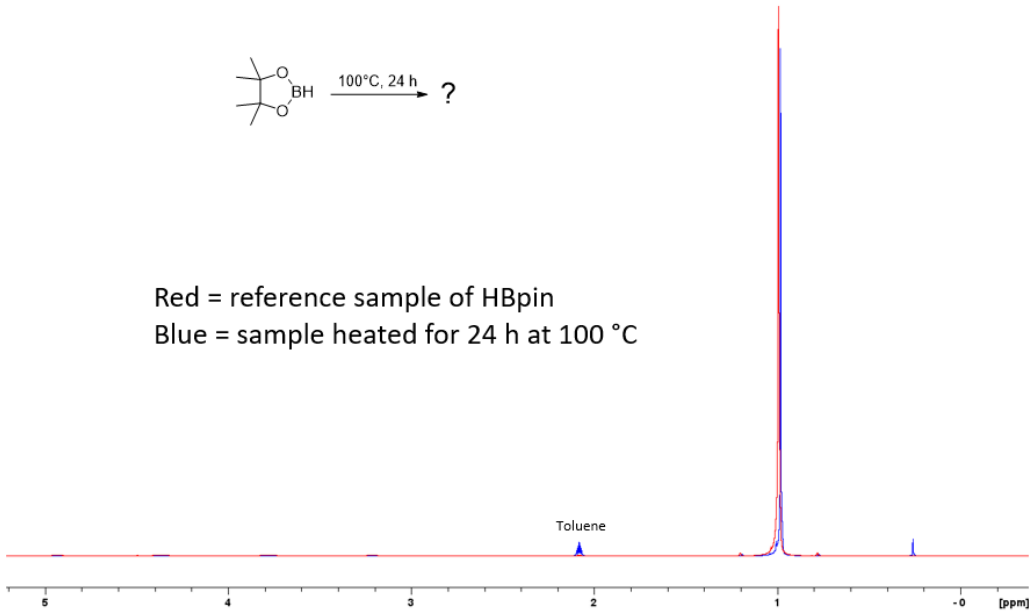

Figure 80: ^{1}H (300 MHz) NMR spectra of HBpin (0.1 mmol, 12.8 mg) after 24 h at 100 °C (blue) and HBpin reference sample (red). The signal is unchanged.

Diyne with HBpin without catalyst

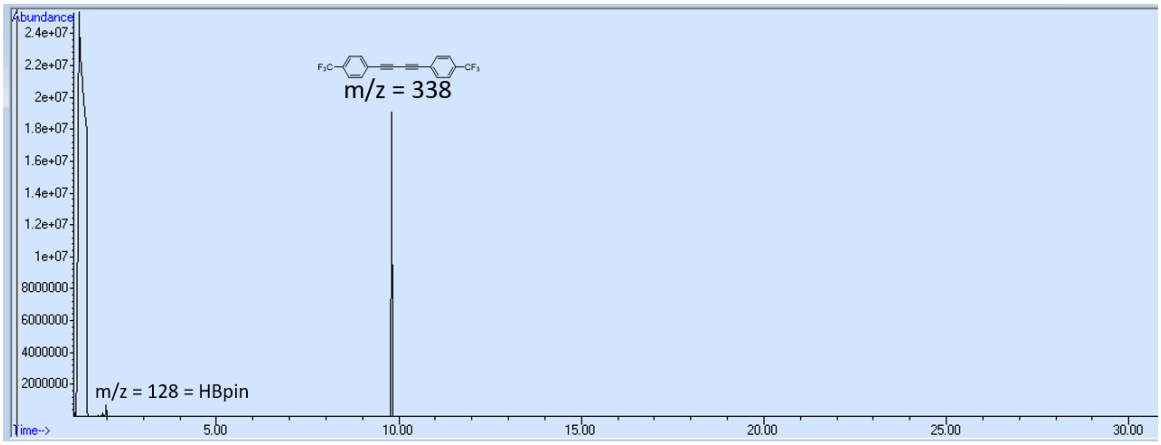

*Figure 81: GC-MS after heating a mixture of diyne **4-1** (0.1 mmol, 33.8 mg) and HBpin (0.1 mmol, 12.8 mg) at 100 °C for 24 h.*

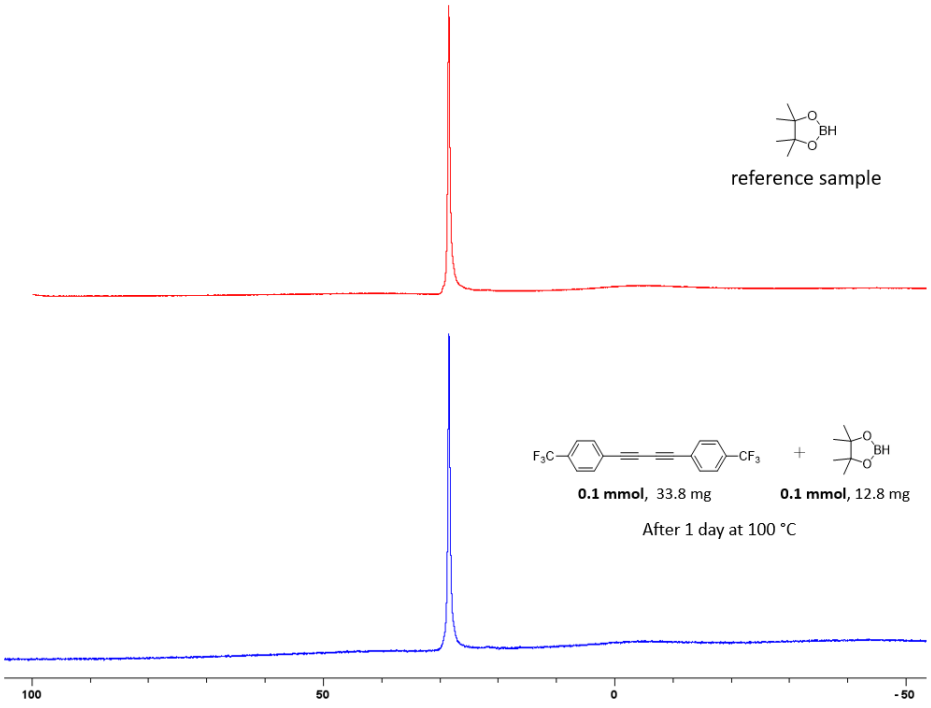

*Figure 82: $^{11}B\{^1H\}$ (96 MHz) NMR spectrum after heating a mixture of diyne **4-1** (0.1 mmol) and HBpin (0.1 mmol) at 100 °C for 1 d (blue) and reference spectrum of HBpin (red).*

HBpin with phosphine

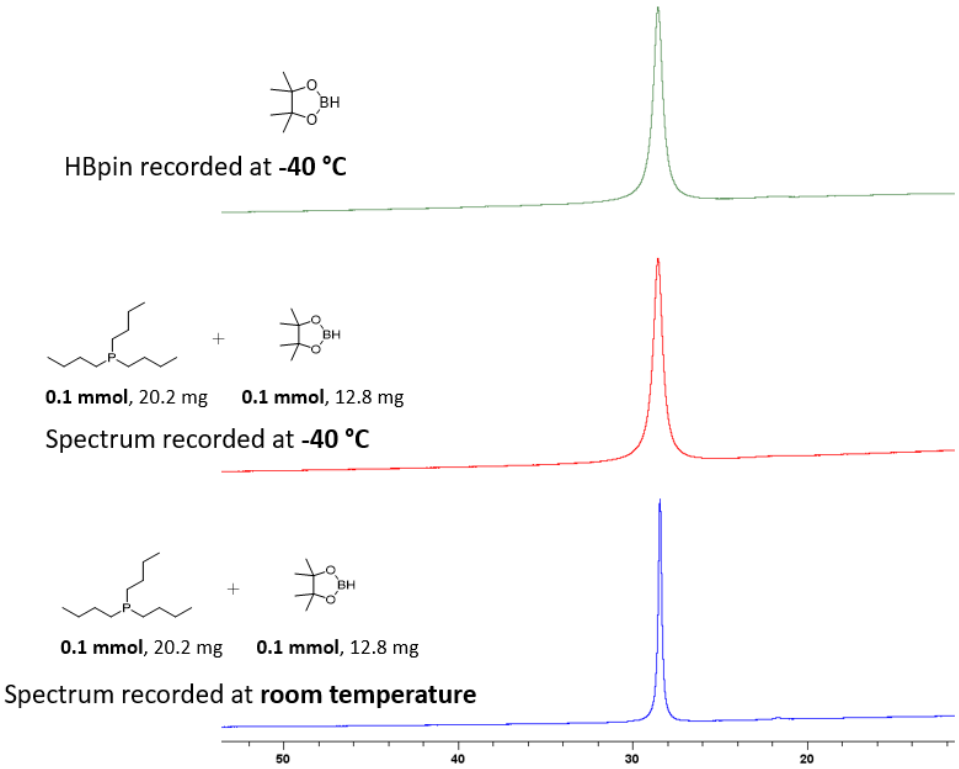

Figure 83: $^{11}B\{^1H\}$ (160 MHz) NMR spectra of a mixture of $PnBu_3$ and HBpin, after 1 d at room temperature, recorded at room temperature (blue) and at -40 °C (red) and a reference spectrum of HBpin (-40 °C, green).

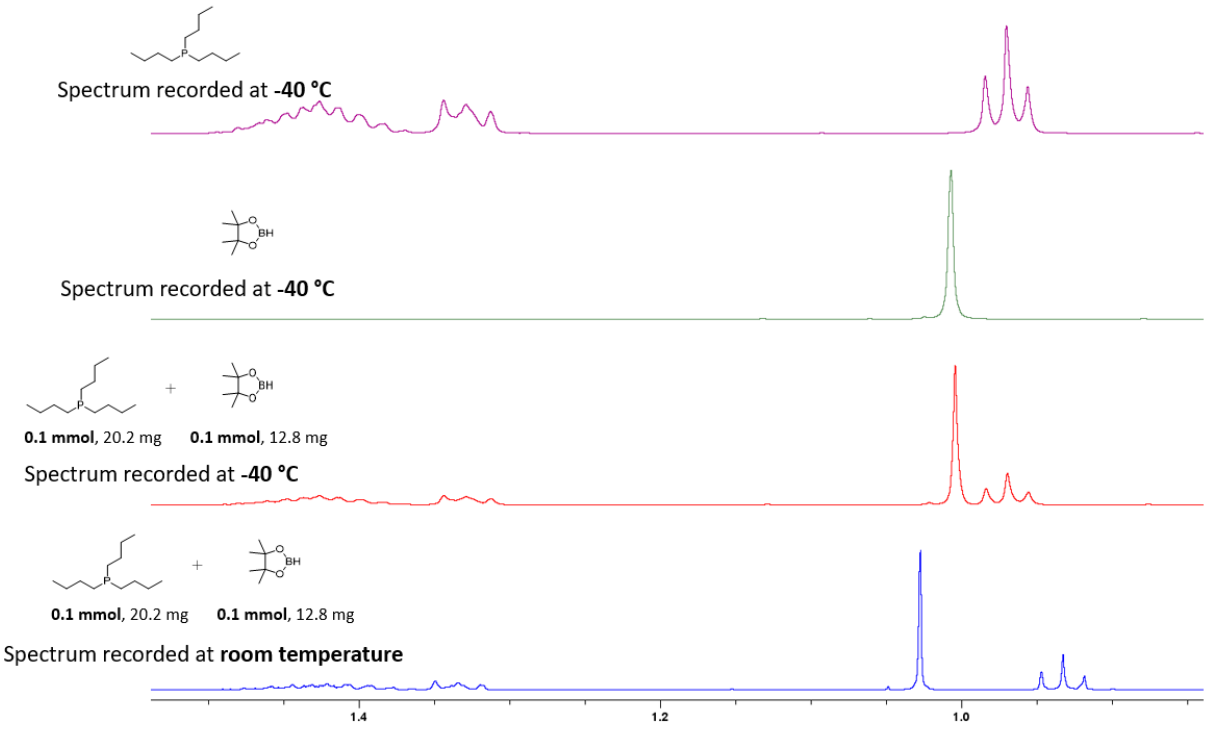

Figure 84: ^1H (500 MHz) NMR spectra of a mixture of $PnBu_3$ and HBpin, after 1 d at room temperature, recorded at room temperature (blue) and at -40 °C (red) and reference spectra of HBpin (-40 °C, green) and $PnBu_3$ (-40 °C, purple).

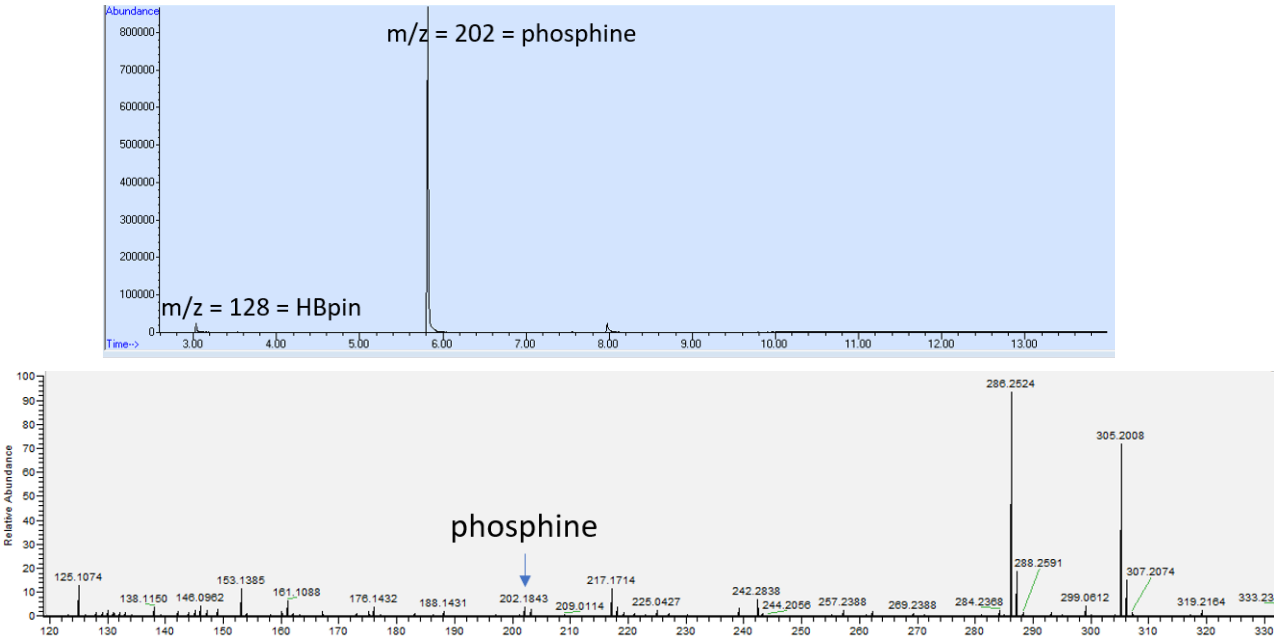

Figure 85: GC-MS (above) and LIFDI-HRMS (below) of a 1:1 mixture of $PnBu_3$ and HBpin after 1 d at room temperature. No adduct was detected. In the LIFDI, HBpin could not be detected and signals that likely stem from previous measurements are present.

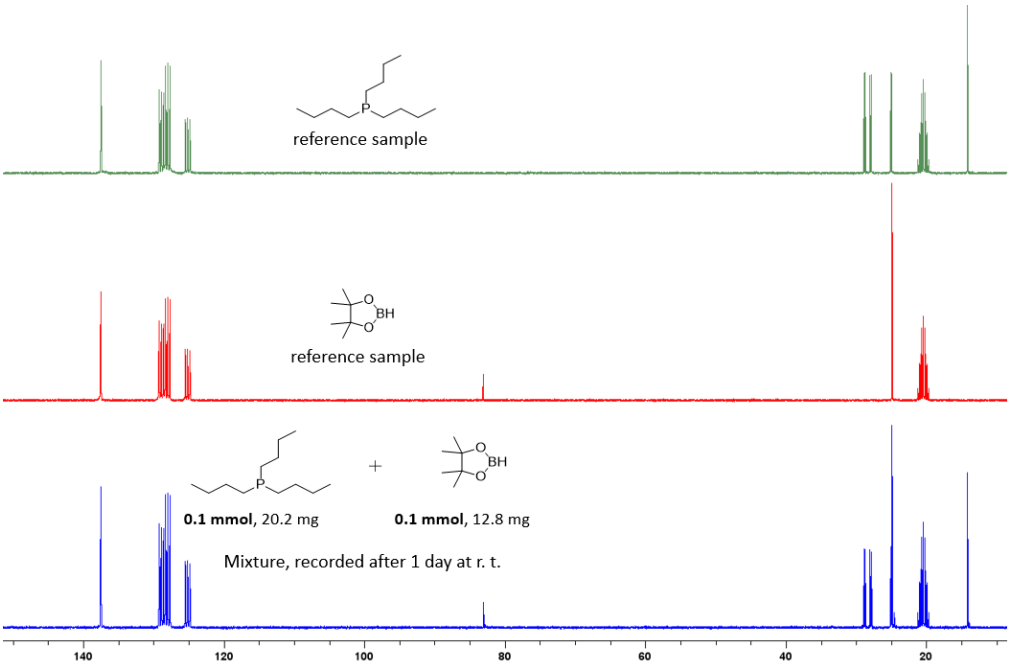

Figure 86: $^{13}C\{^1H\}$ (75 MHz) NMR sprectrum of a 1:1 mixture of $PnBu_3$ and HBpin compared to reference spectra of the components.

Diyne with Phosphine

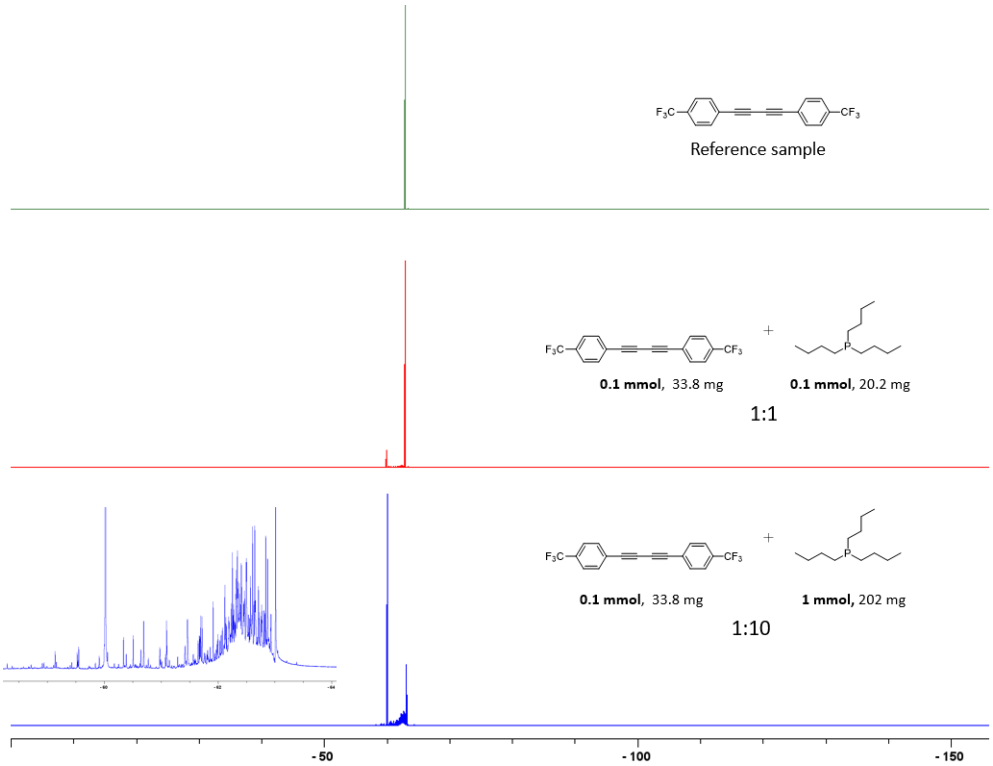

*Figure 87: $^{19}F\{^1H\}$ NMR spectra of a mixture of $PnBu_3$ and diyne **4-1**, after 3 d at room temperature in 1:1 ratio (red, middle spectrum) and in a 10:1 ratio (blue, bottom spectrum, 564 MHz) and a diyne **4-1** reference sample (green, top spectrum, 470 MHz).*

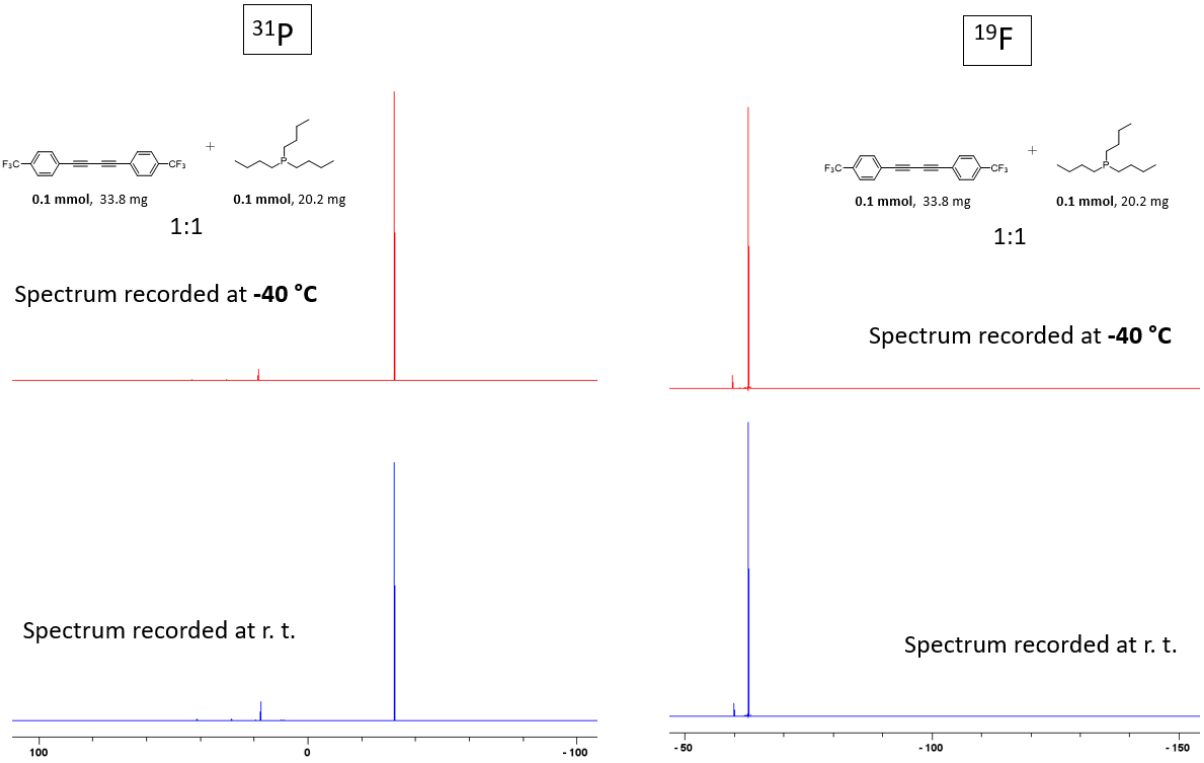

*Figure 88: Comparison of $^{31}P\{^1H\}$(220 MHz)(left) and $^{19}F\{^1H\}$(470 MHz)- (right) NMR spectra of a 1:1 mixture of diyne **4-1** and $PnBu_3$ after 3 d at room temperature. The bottom spectra were recorded at room temperature, the ones on top at -40 °C. There is no change at the lower temperature.*

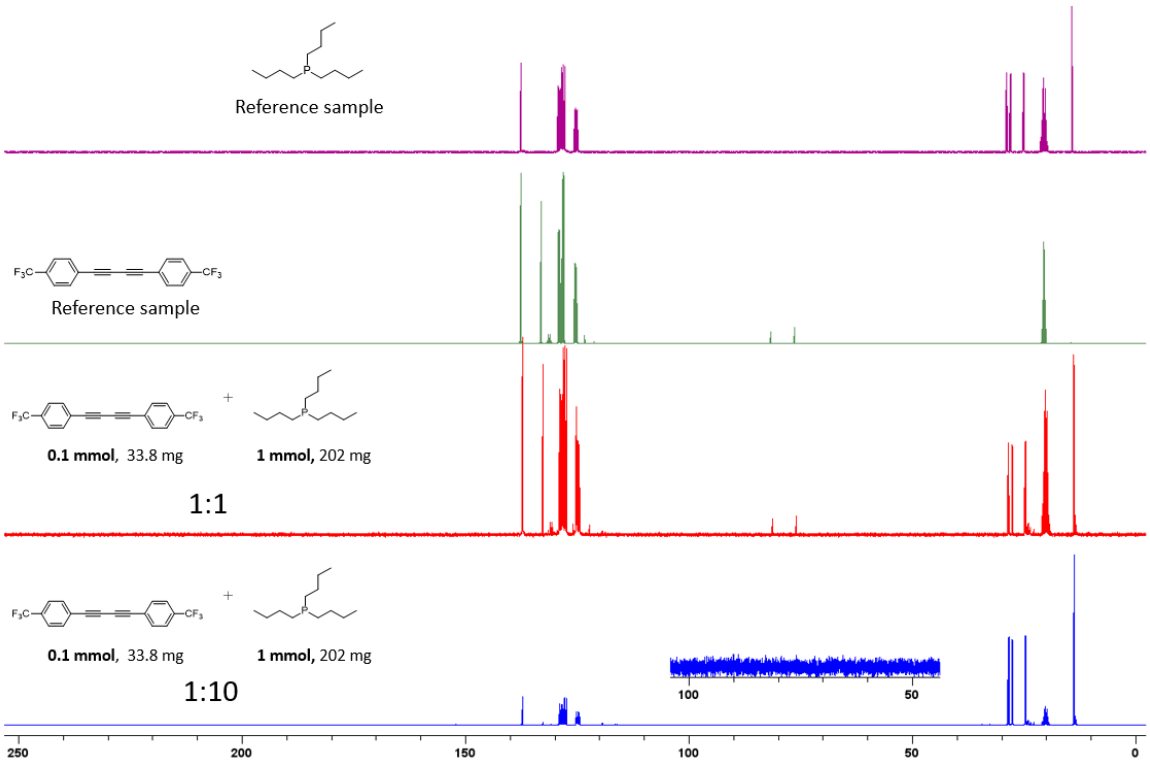

*Figure 89: $^{13}C\{^1H\}$ (75 MHz) NMR spectra of a mixture of $PnBu_3$ and diyne **4-1**, after 3 d at room temperature in 1:1 ratio (red), in a 10:1 ratio (blue), a diyne **4-1** reference sample (green), and a $PnBu_3$ reference sample (purple).*

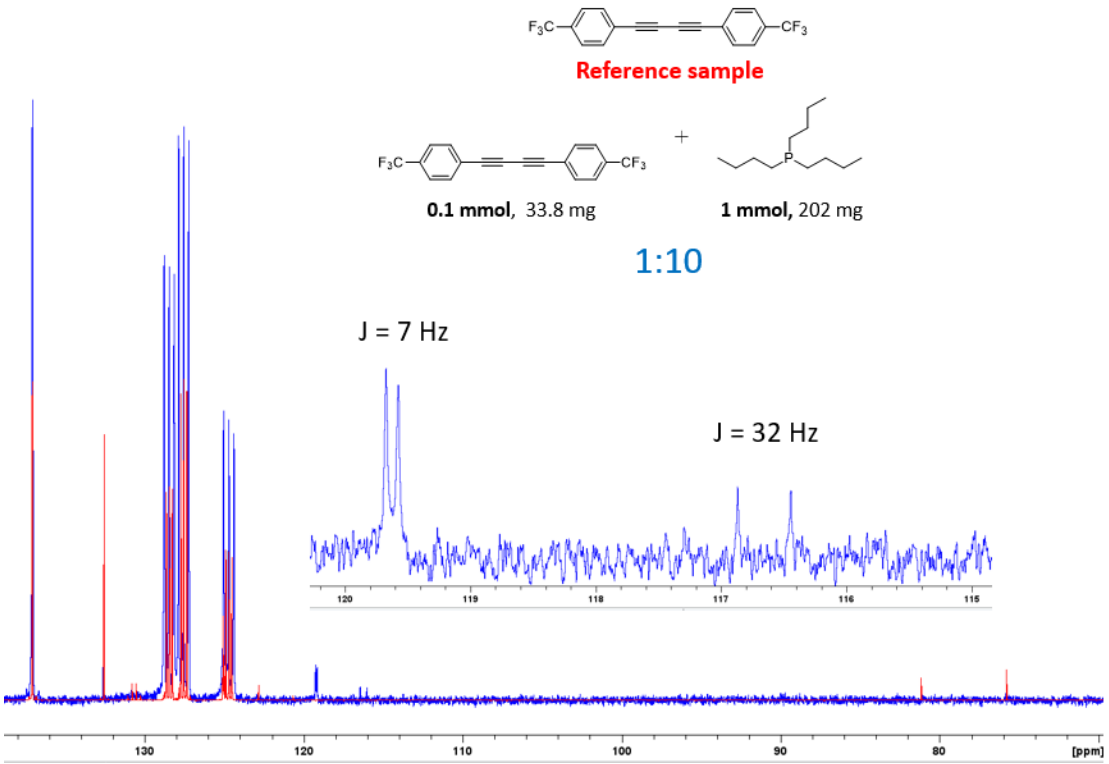

*Figure 90: $^{13}C\{^1H\}$ NMR spectrum (75 MHz, enlarged) of a mixture of $PnBu_3$ and diyne **4-1**, after 3 d at room temperature in a 10:1 ratio (blue) compared to a reference spectrum of diyne **4-1** (red). The new signals in the olefinic region are further enlarged.*

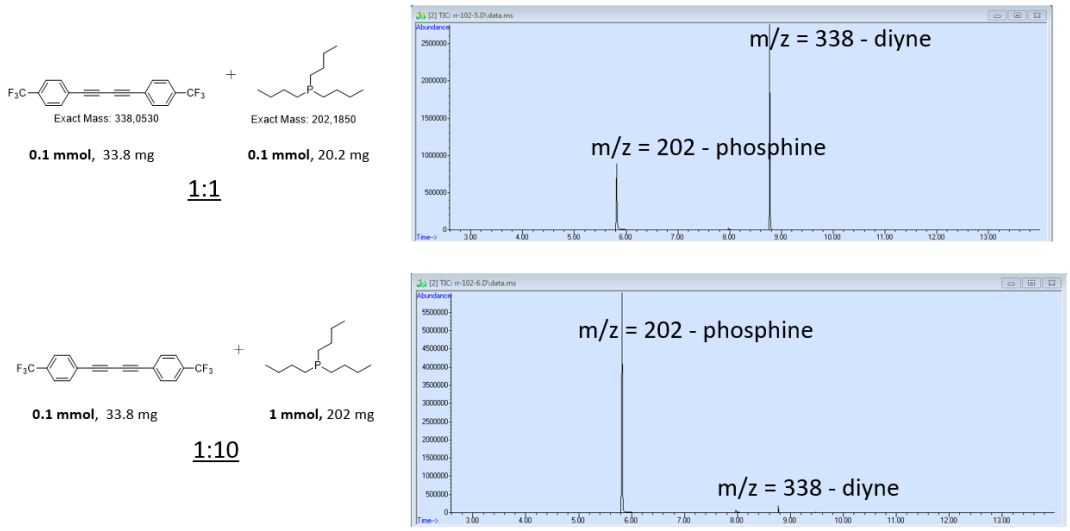

*Figure 91: GC-MS of mixtures of diyne **4-1** and $PnBu_3$ after 3 d at room temperature in ratios of 1:1 (top) and 1:10 (bottom). At the 1:10 ratio, the diyne is consumed almost completely. The resulting, likely zwitterionic, products could not be detected with this method.*

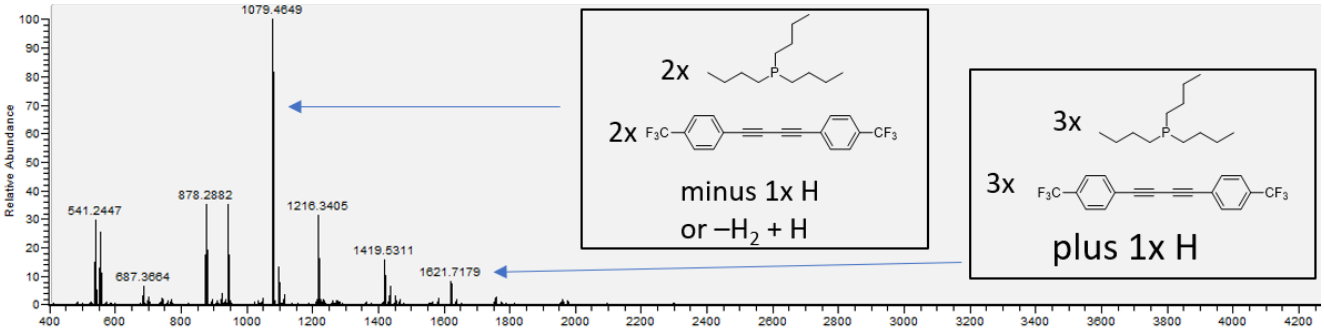

*Figure 92: LIFDI-HRMS of a 10:1 mixture of $PnBu_3$ and diyne **4-1** after 3 d at room temperature. Only the possible adducts that did not appear in the 1:1 mixture in Figure 46 are marked.*

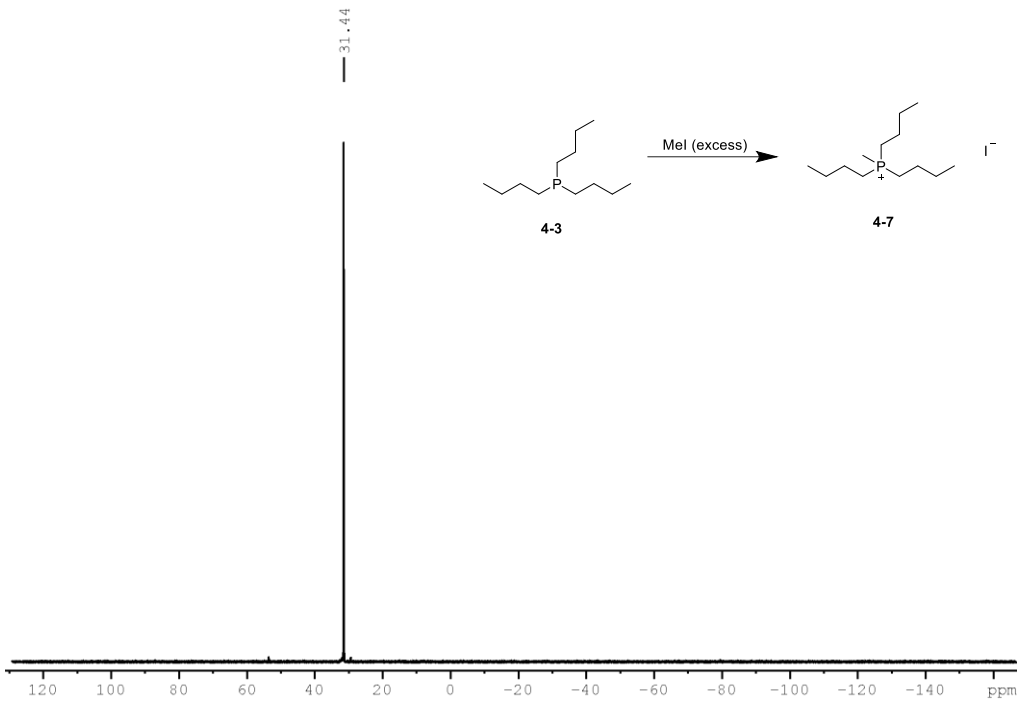

Figure 93: ^{31}P {^{1}H} (121 MHz) NMR spectrum after the methylation of $PnBu_3$ with methyl iodide, yielding methy(tributylphosphonium) iodide, which was used as a reference.

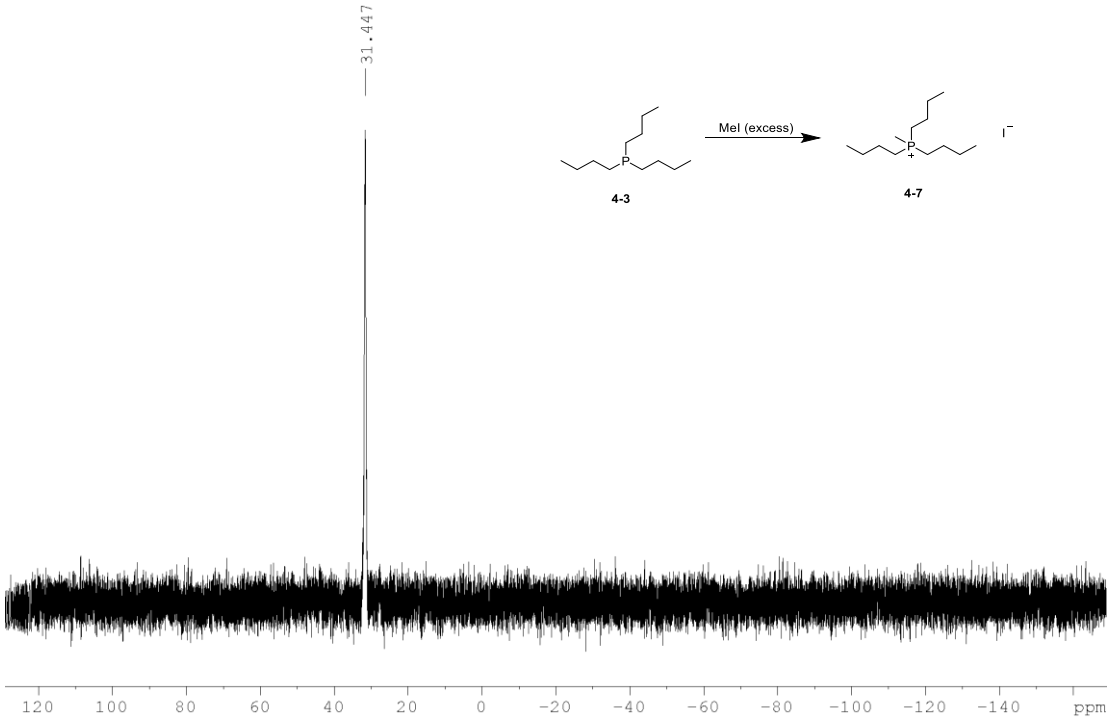

Figure 94: ^{31}P (121 MHz) NMR spectrum (intensity enhanced) after the methylation of $PnBu_3$ with methyl iodide, yielding methy(tributylphosphonium) iodide, which was used as a reference.

Diyne with HBpin using O=PnBu$_3$ as the catalyst

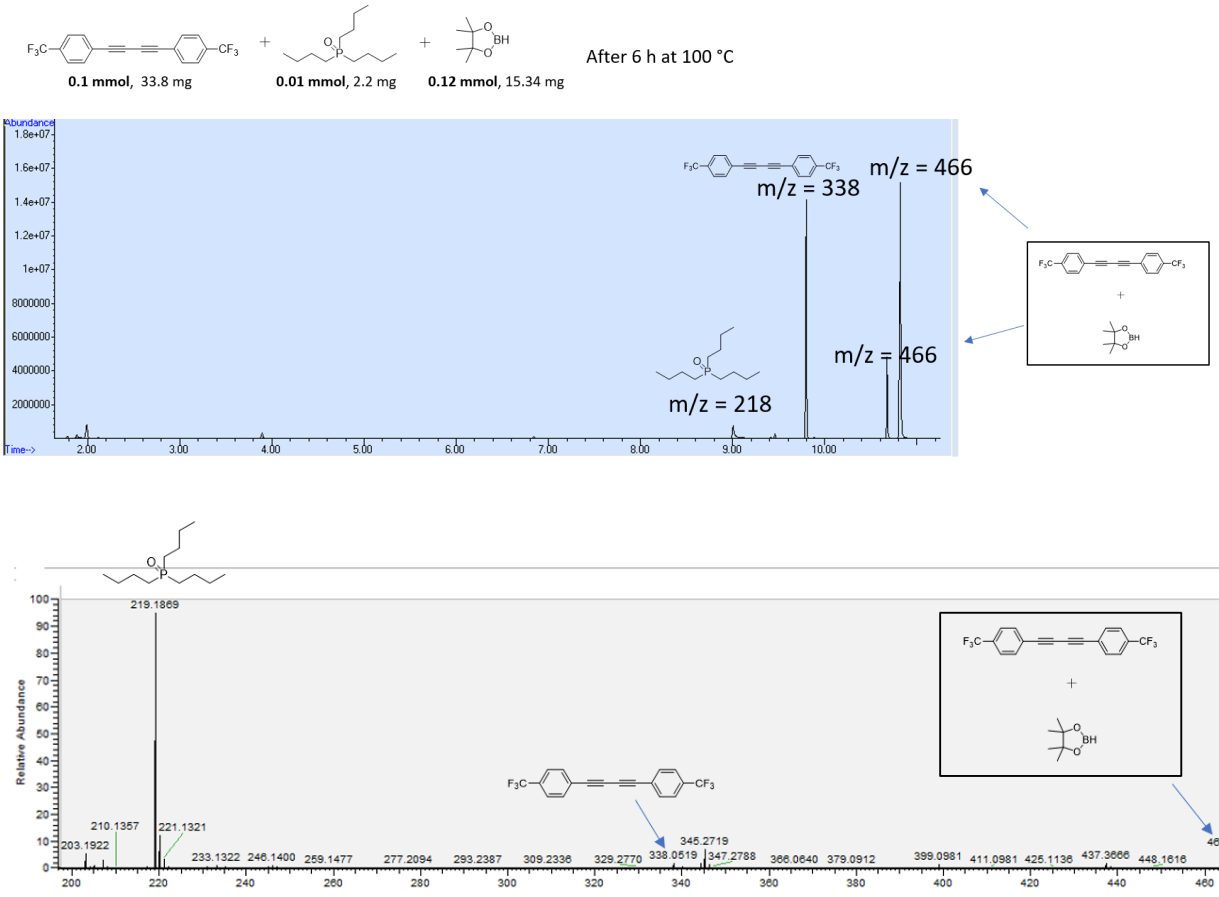

*Figure 95: GC-MS (above) and HRMS (below, APCI+) of a 1 : 0.1 : 1.2 mixture of diyne **4-1**, O=P(nBu)$_3$ and HBpin after 6 h at 100 °C . Hydroboration product signal (m/z= 466) is present, but the reaction is incomplete.*

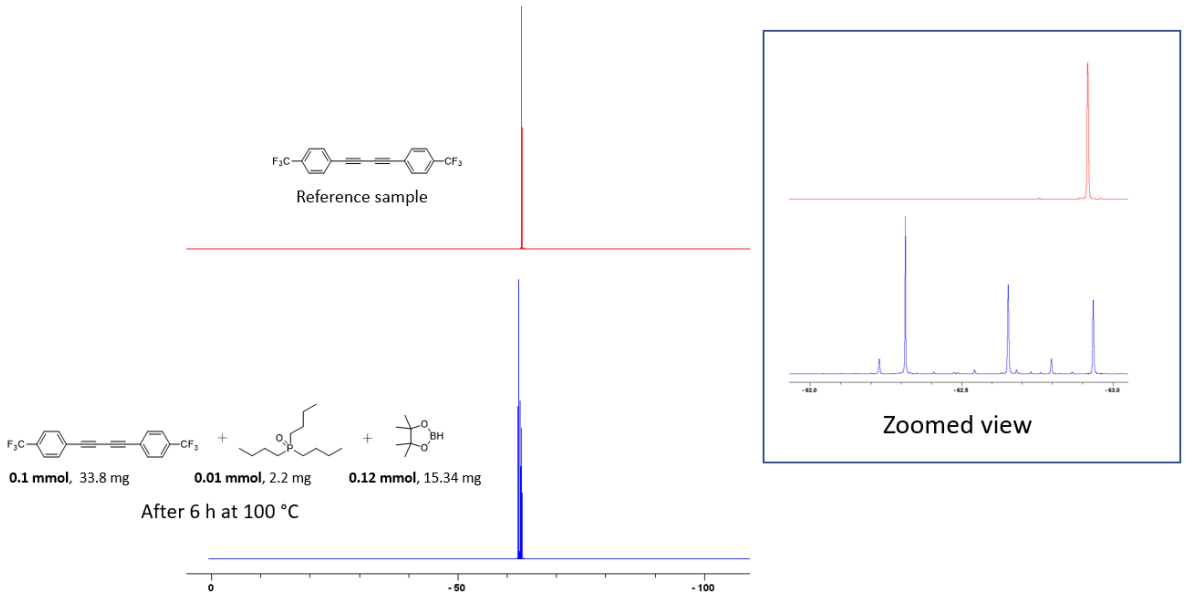

*Figure 96: $^{19}F\{^1H\}$ (470 MHz blue, 564 MHz red) NMR spectrum of a mixture of diyne **4-1** + HBpin, with O=PnBu$_3$ as the catalyst after 6 h at 100 °C, in comparison with a reference spectrum of diyne **4-1**.*

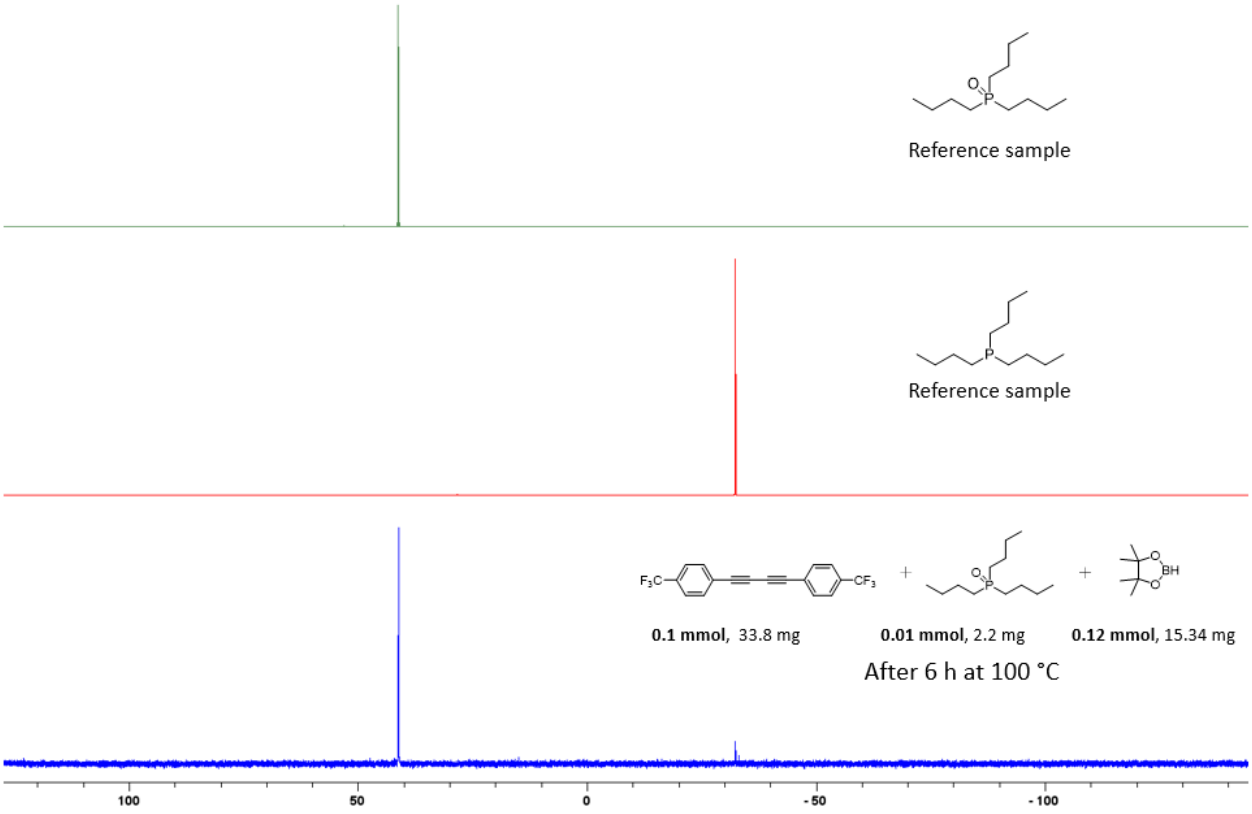

*Figure 97: $^{31}P\{^{1}H\}$ (121 MHz) NMR spectra of a mixture of diyne **4-1**, HBpin and O=PnBu$_3$ as the catalyst after 6 h at 100 °C. (blue) and PnBu$_3$ (red) and O=PnBu$_3$ (green) reference samples. A peak corresponding to PnBu$_3$, which is formed during the reaction, is observed in the bottom spectrum of the reaction mixture.*

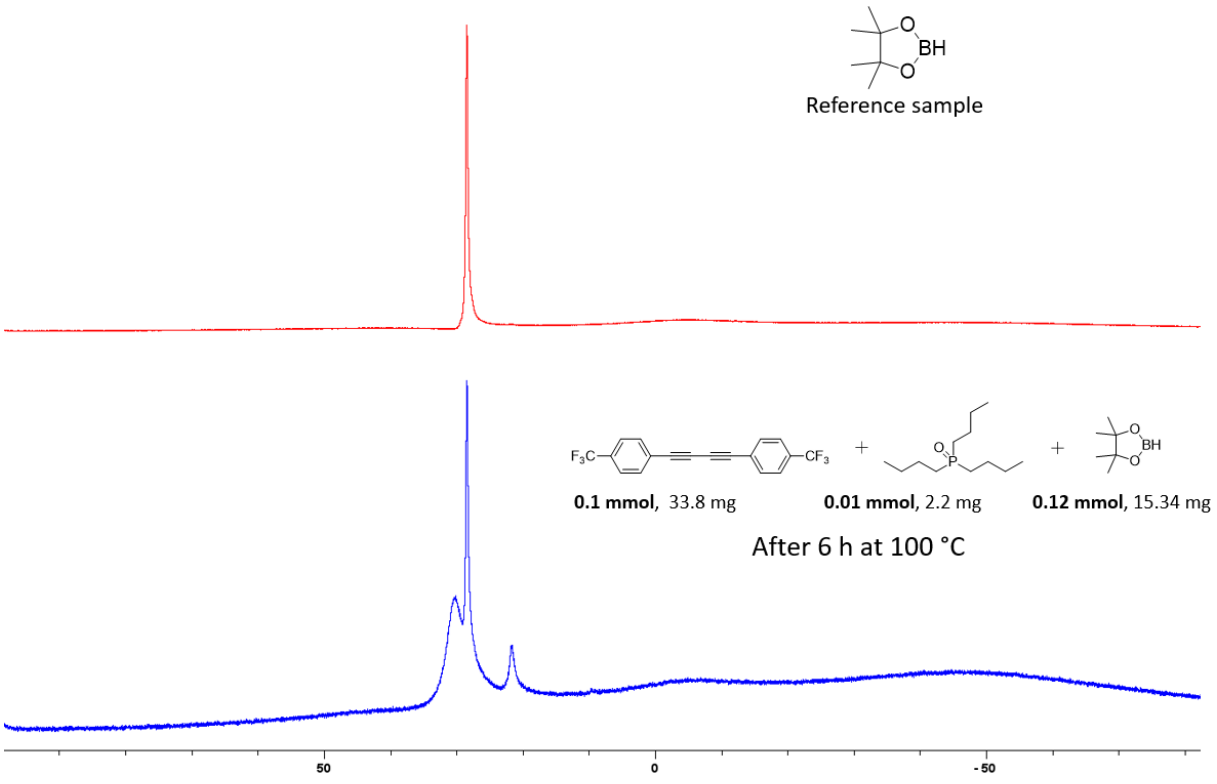

*Figure 98: $^{11}B\{^{1}H\}$ (121 MHz) NMR spectrum of a mixture of diyne **4-1**, HBpin and O=PnBu$_3$ as the catalyst after 6 h at 100 °C. (blue), and an HBpin reference spectrum(red).*

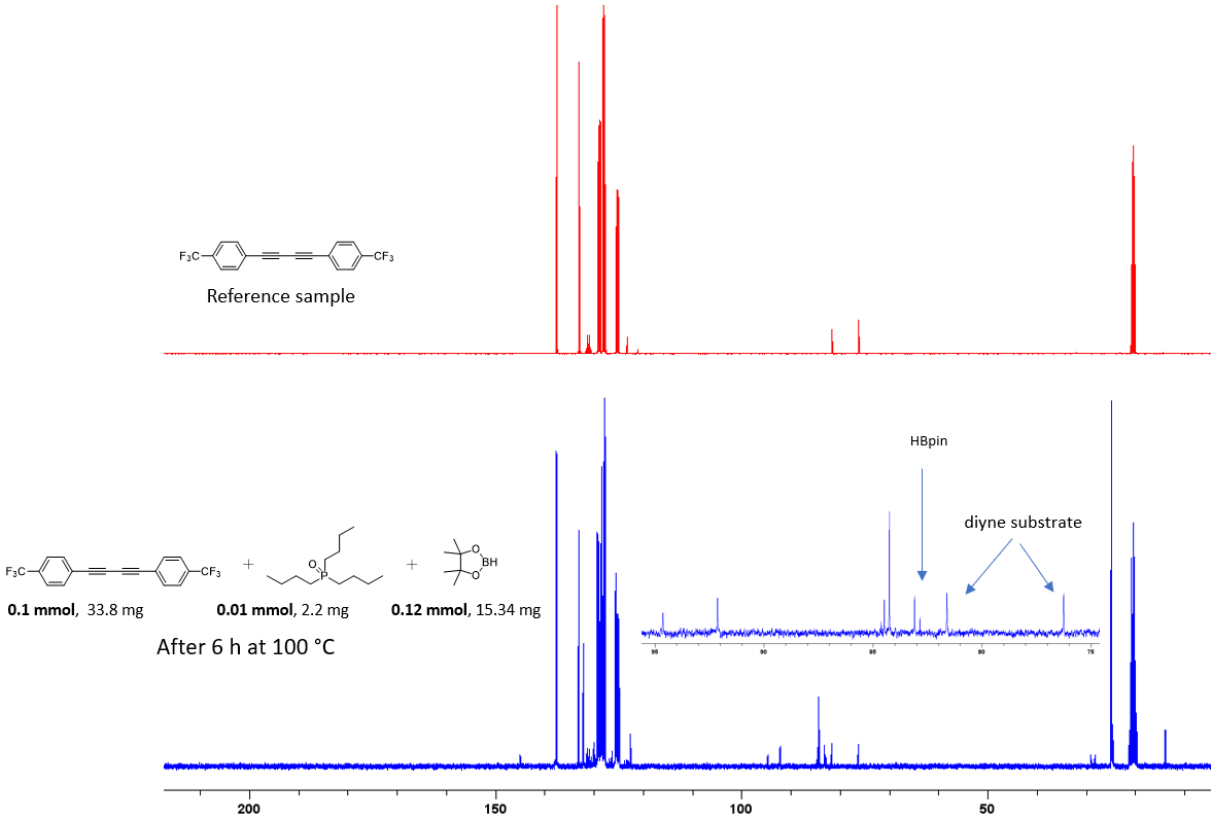

*Figure 99: $^{13}C\{^{1}H\}$ (75 MHz) NMR spectra of a mixture of diyne **4-1**, HBpin and O=PnBu$_3$ as the catalyst after 6 h at 100 °C. (blue), and of a diyne **4-1** (red) reference sample.*

HBpin with O=PnBu$_3$

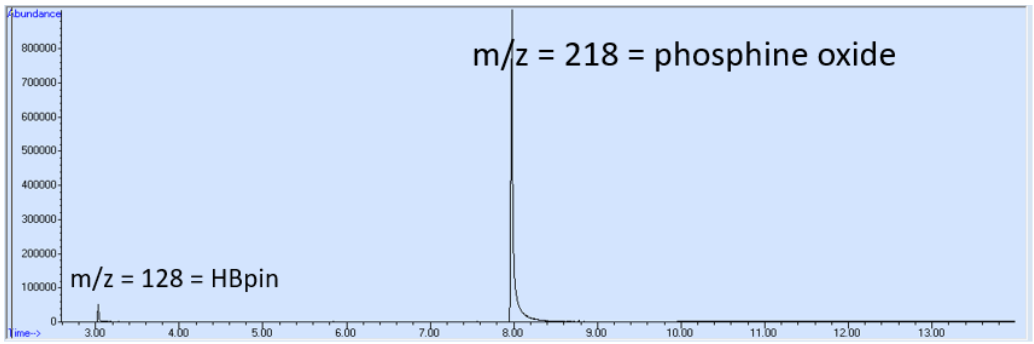

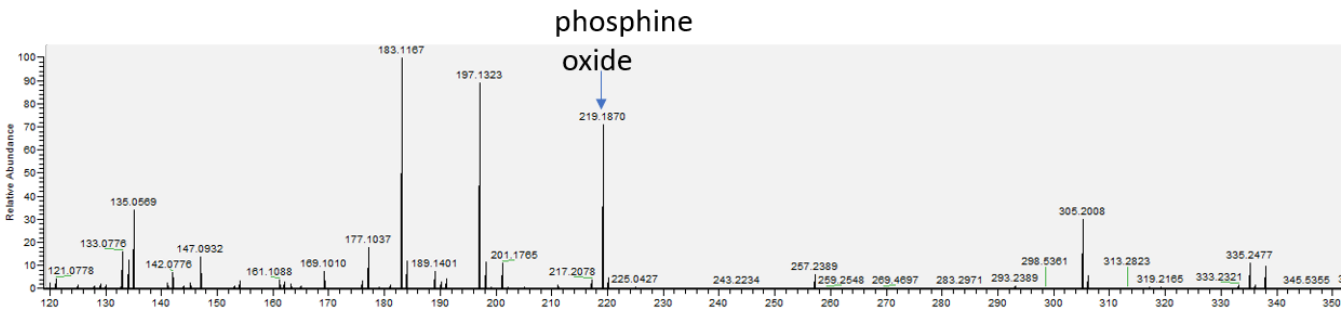

Figure 100: GC-MS (above) and ESI+ HRMS (below) of a mixture of O=PnBu$_3$ and HBpin, after 1 d at room temperature. No adduct was detected here.

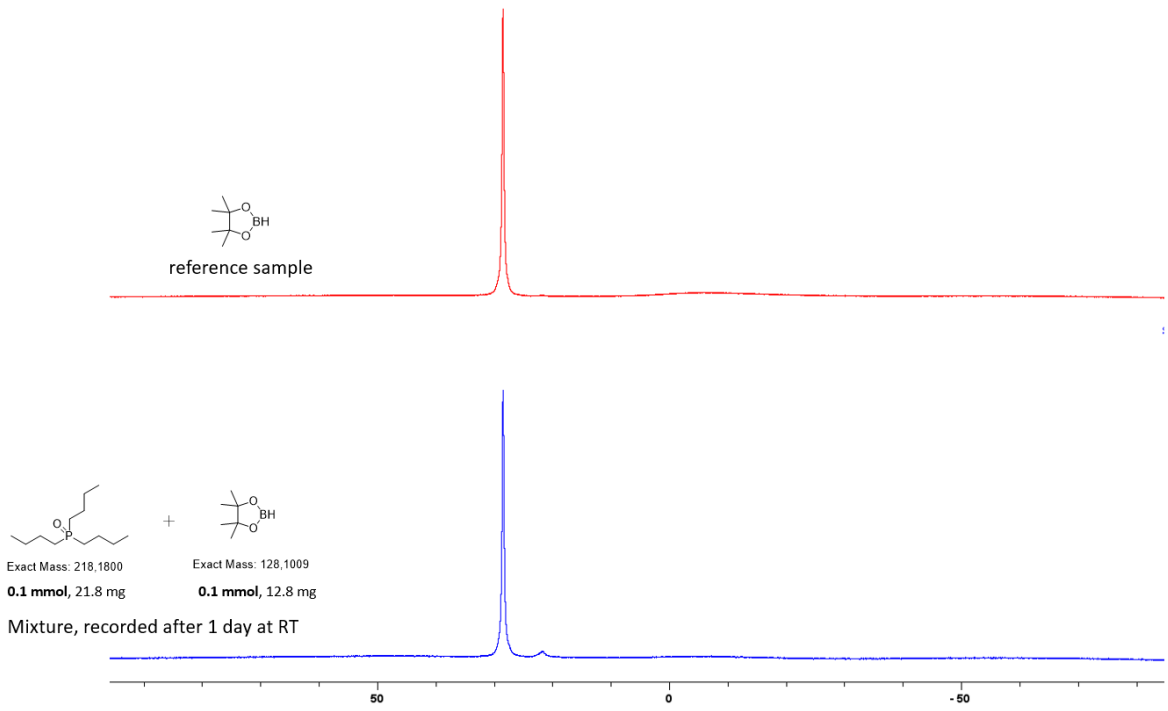

Figure 101: $^{11}B\{^1H\}$ (96 MHz) NMR spectra of a mixture of O=PnBu$_3$ (0.1 mmol) and HBpin (0.1 mmol), after 1 d at room temperature (blue) and an HBpin reference (red).

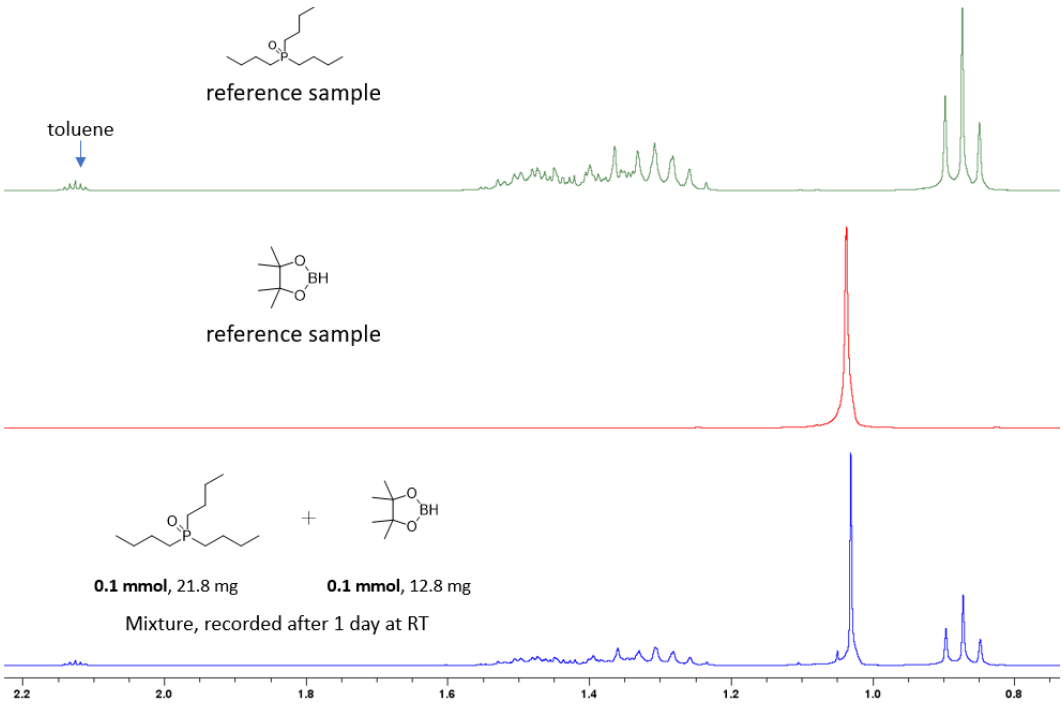

Figure 102: ^1H (300 MHz) NMR spectra of a mixture of O=PnBu$_3$ (0.1 mmol) and HBpin (0.1 mmol) after 1 d at room temperature (blue), and of a HBpin (red) and O=PnBu$_3$ reference sample (green).

Diyne with O=PnBu$_3$

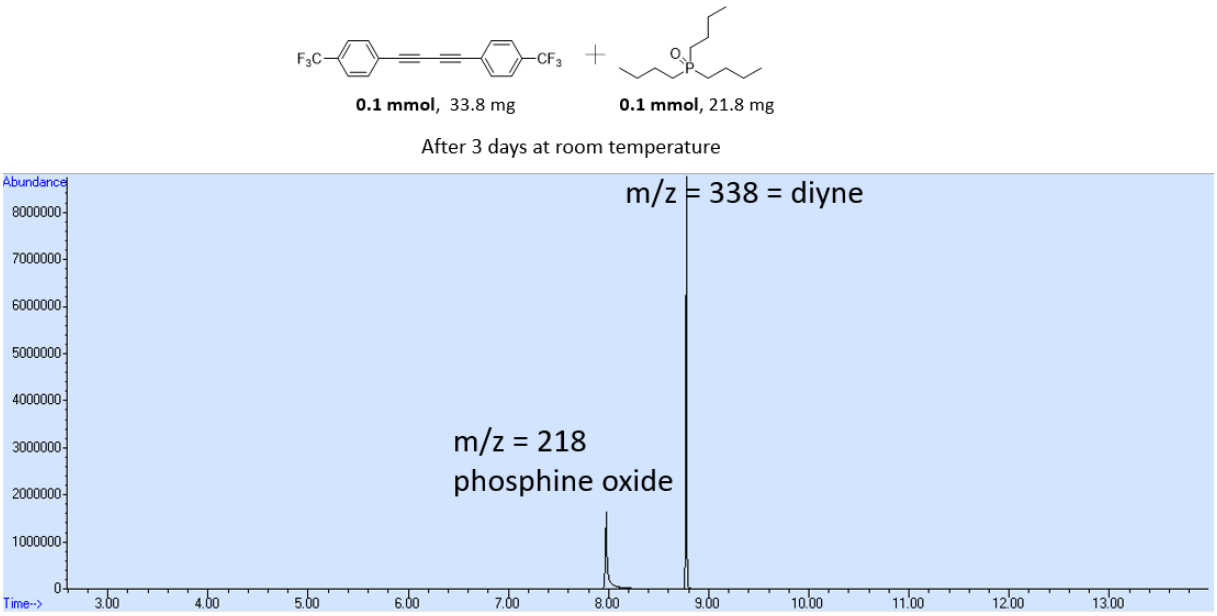

*Figure 103: GC-MS of a mixture of diyne **4-1** and O=PnBu$_3$ (0.1 mmol) after 3 d at room temperature. Only the starting material was detected in the mixture. The mixture did not turn dark-red, as the mixture of PnBu$_3$ and diyne **4-1** did.*

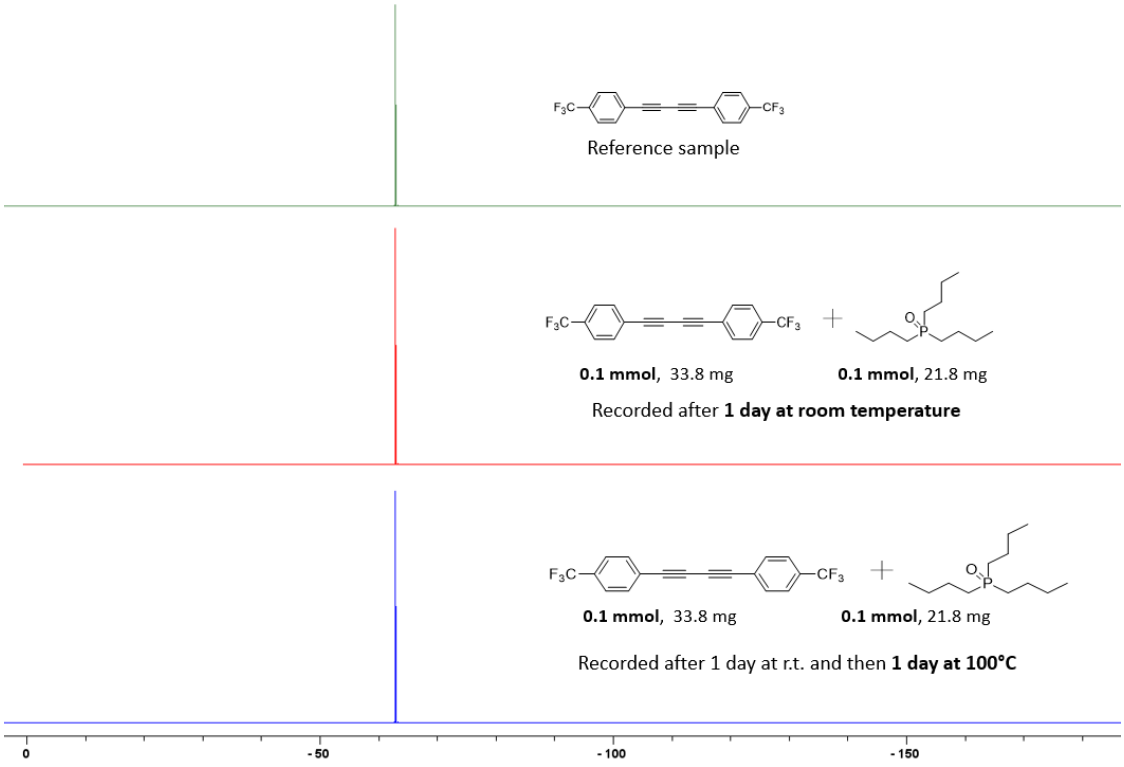

*Figure 104: $^{19}F\{^1H\}$ (470 MHz red & blue, 564 MHz green) NMR spectra of mixtures of O=PnBu$_3$ (0.1 mmol) and diyne **4-1** (0.1 mmol). No change was observed even after heating the sample.*

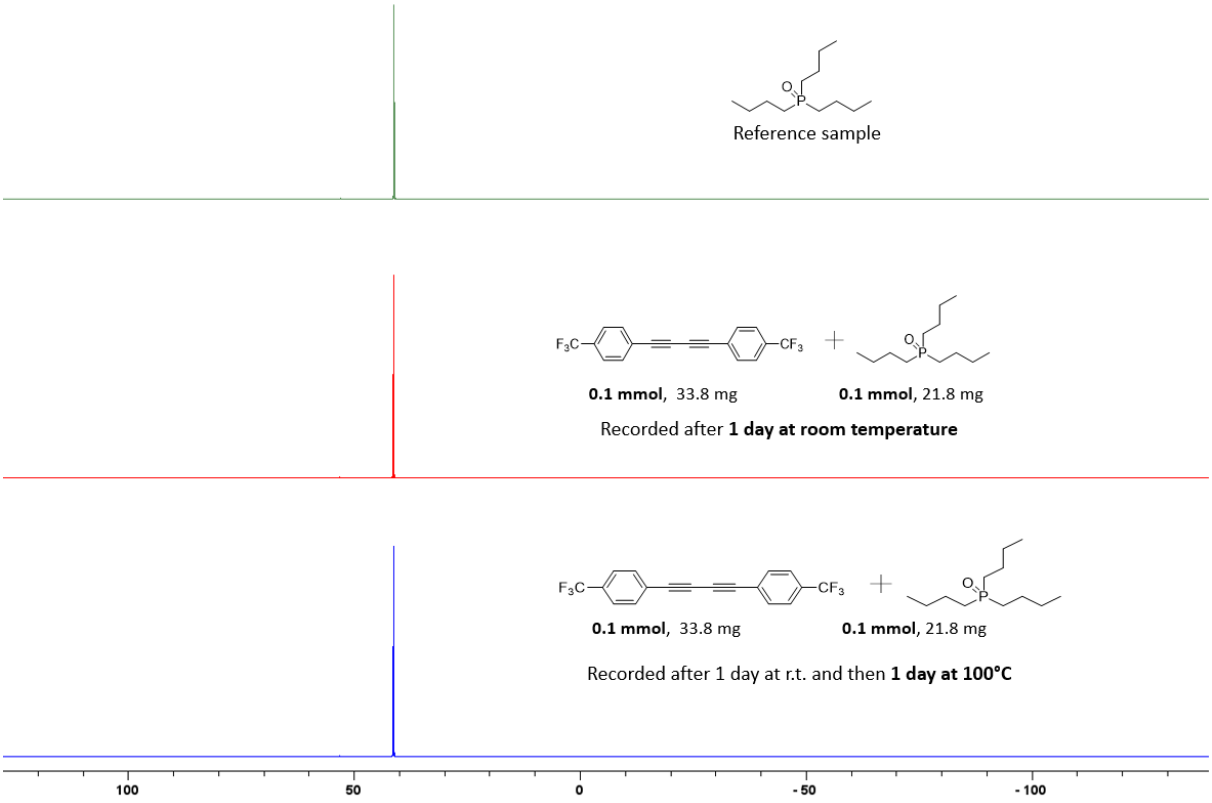

*Figure 105: $^{31}P\{^{1}H\}$ (121 MHz) NMR spectra of a mixture of O=PnBu$_3$ (0.1 mmol) and diyne **4-1** (0.1 mmol). No change was observed even after heating the sample.*

Substrate Spectra

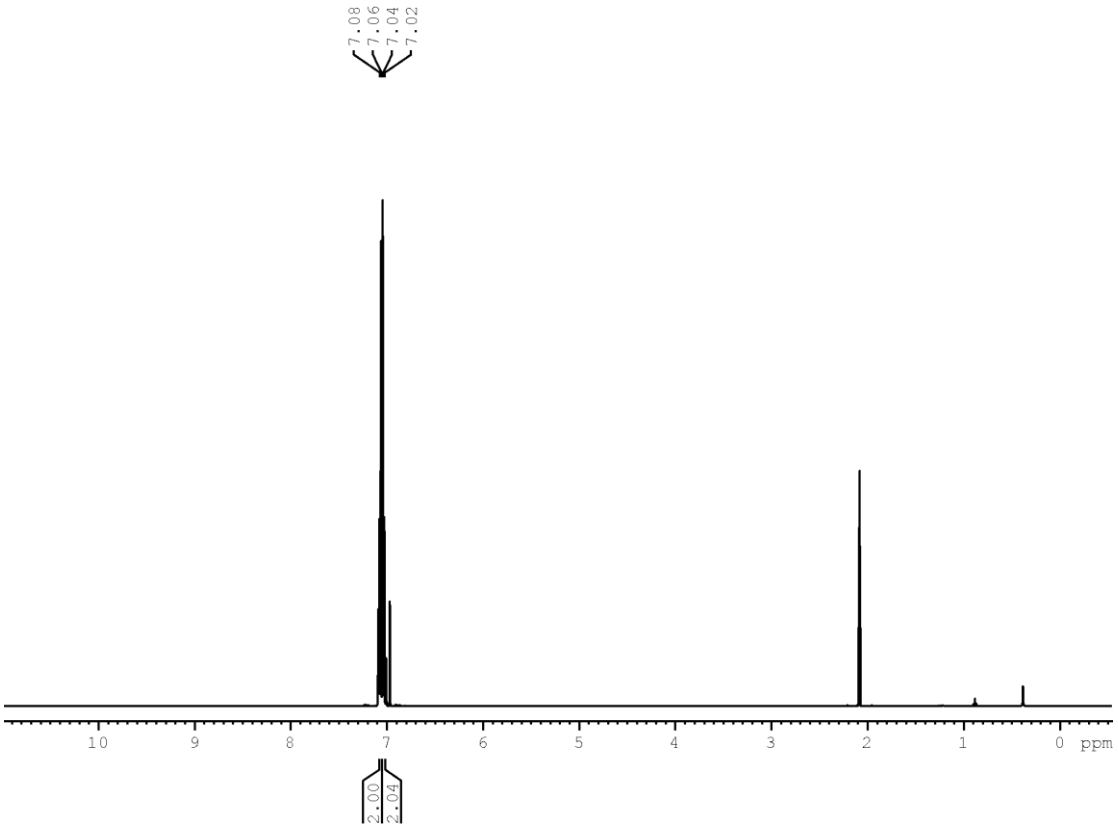

*Figure 106: ^{1}H (500 MHz) NMR spectrum of **4-1** in toluene-d_8.*

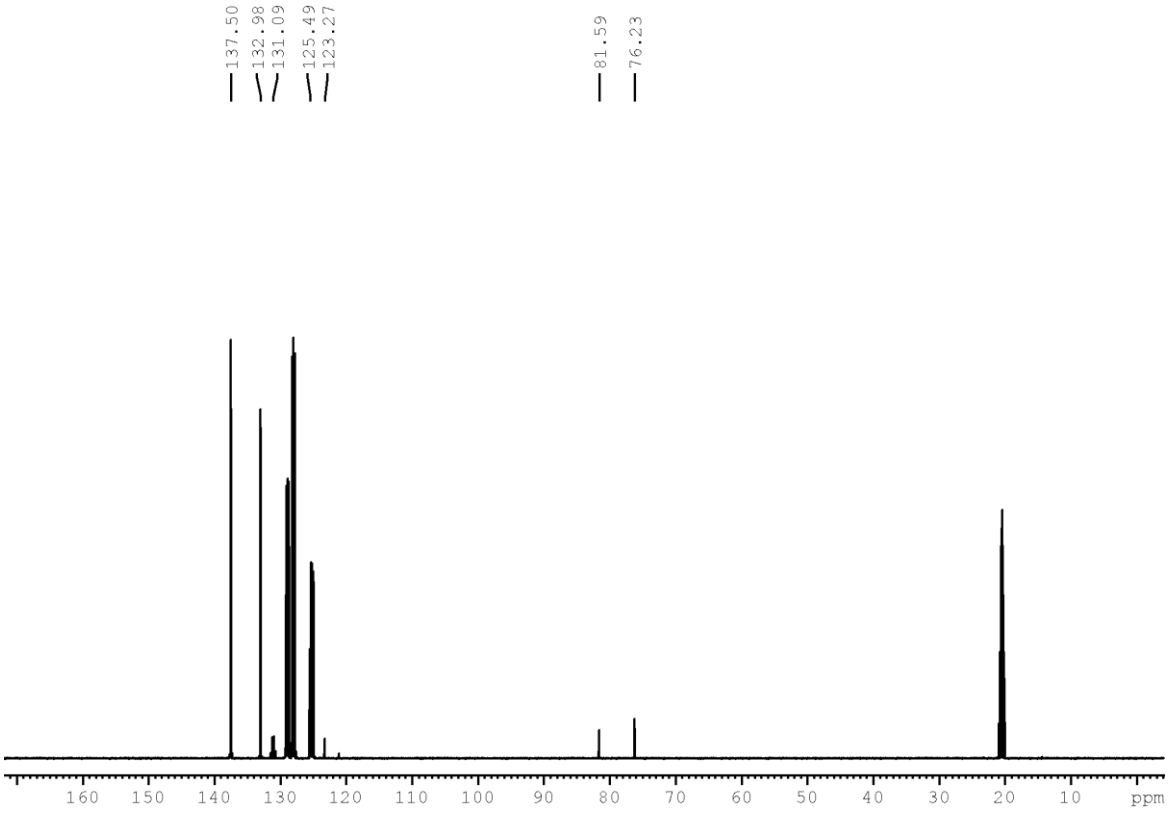

*Figure 107: $^{13}C\{^{1}H\}$ (75 MHz) NMR spectrum of **4-1** in toluene-d_8.*

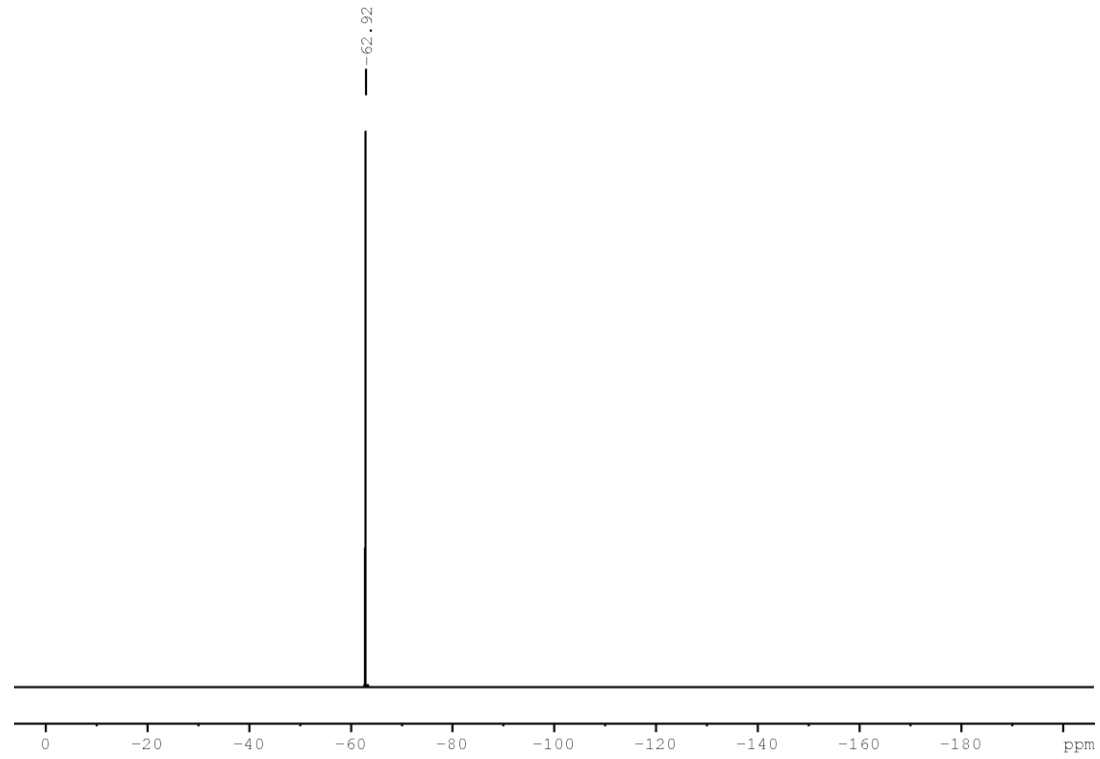

*Figure 108: ^{19}F {^{1}H} (470 MHz) NMR spectrum of **4-1** in toluene-d_8.*

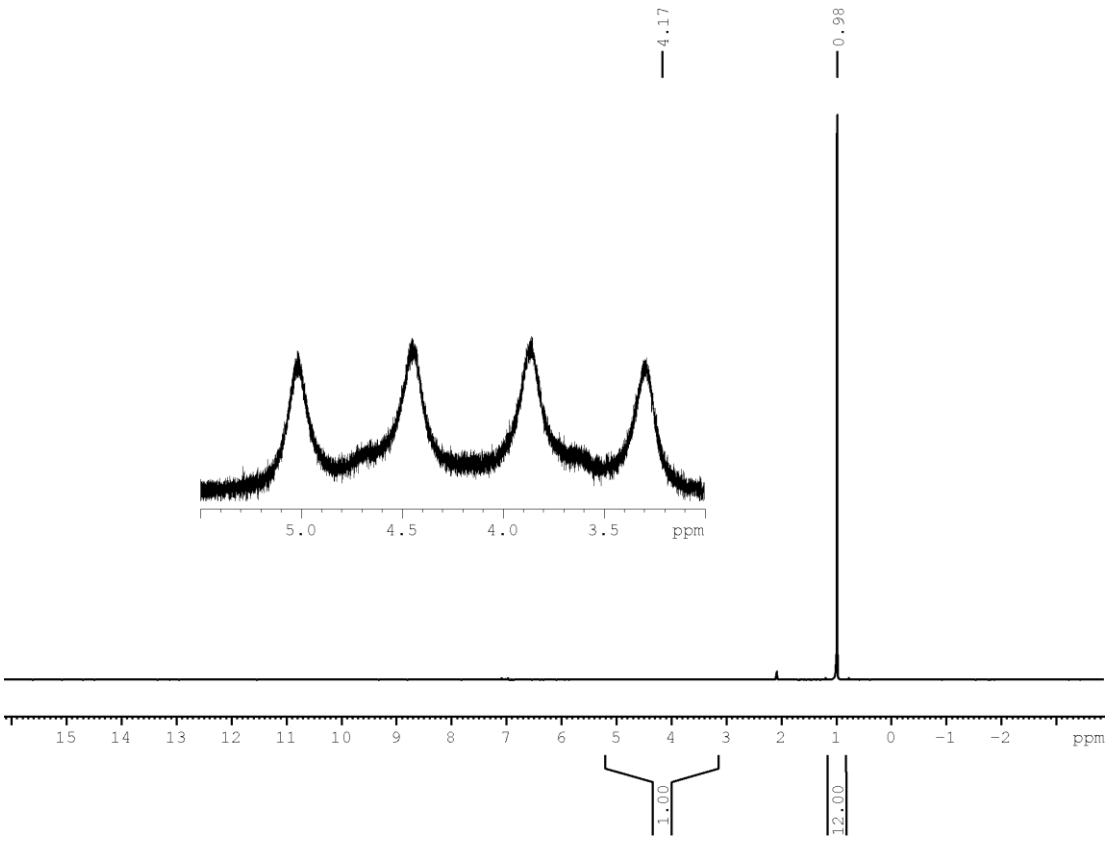

*Figure 109: ^{1}H (300 MHz) NMR spectrum of **4-2** in toluene-d_8.*

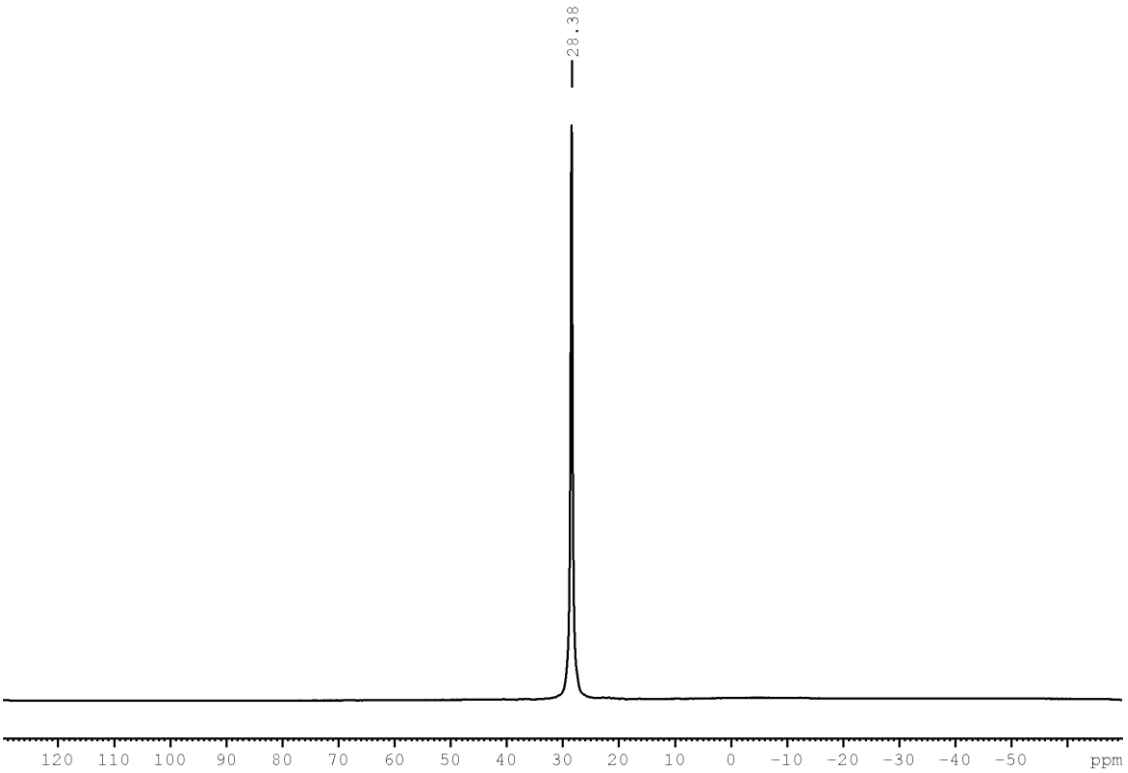

*Figure 110: $^{11}B\{^1H\}$ (96 MHz) NMR spectrum of **4-2** in toluene-d_8.*

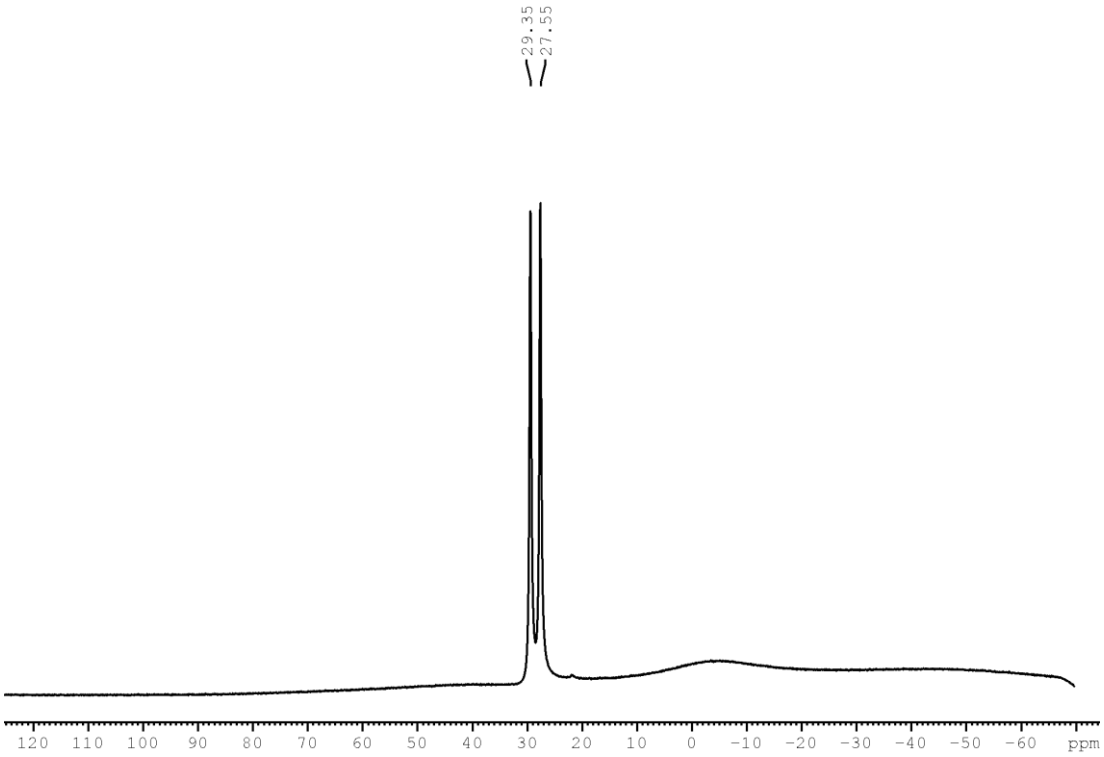

*Figure 111: ^{11}B (96 MHz) NMR spectrum of **4-2** in toluene-d_8.*

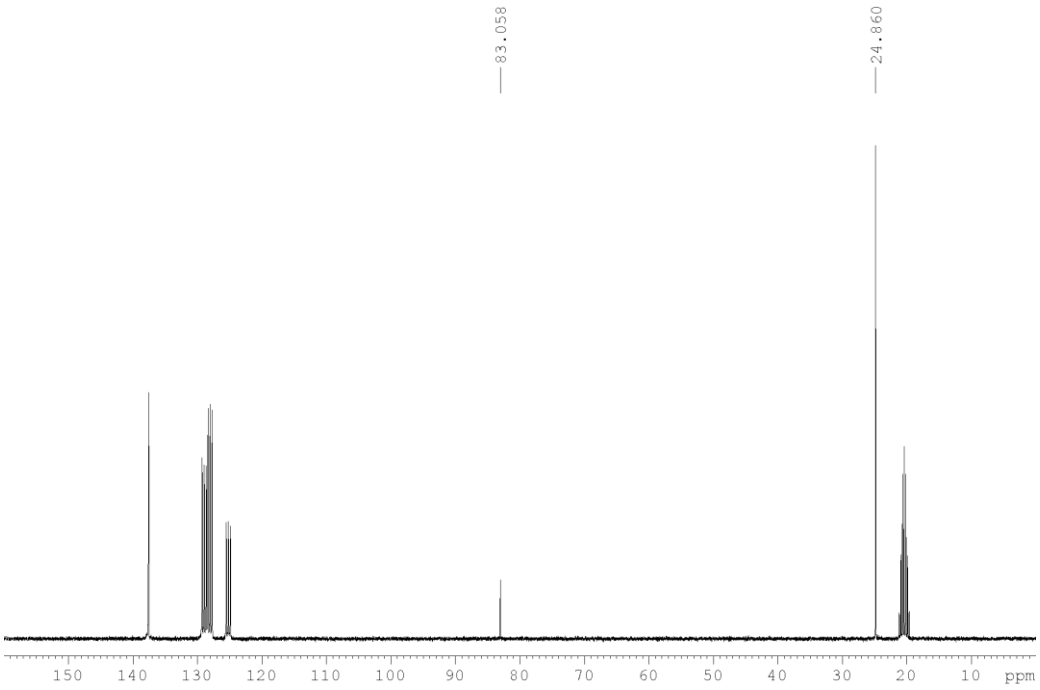

*Figure 112: $^{13}C\{^{1}H\}$ (75 MHz) NMR spectrum of **4-2** in toluene-d_8.*

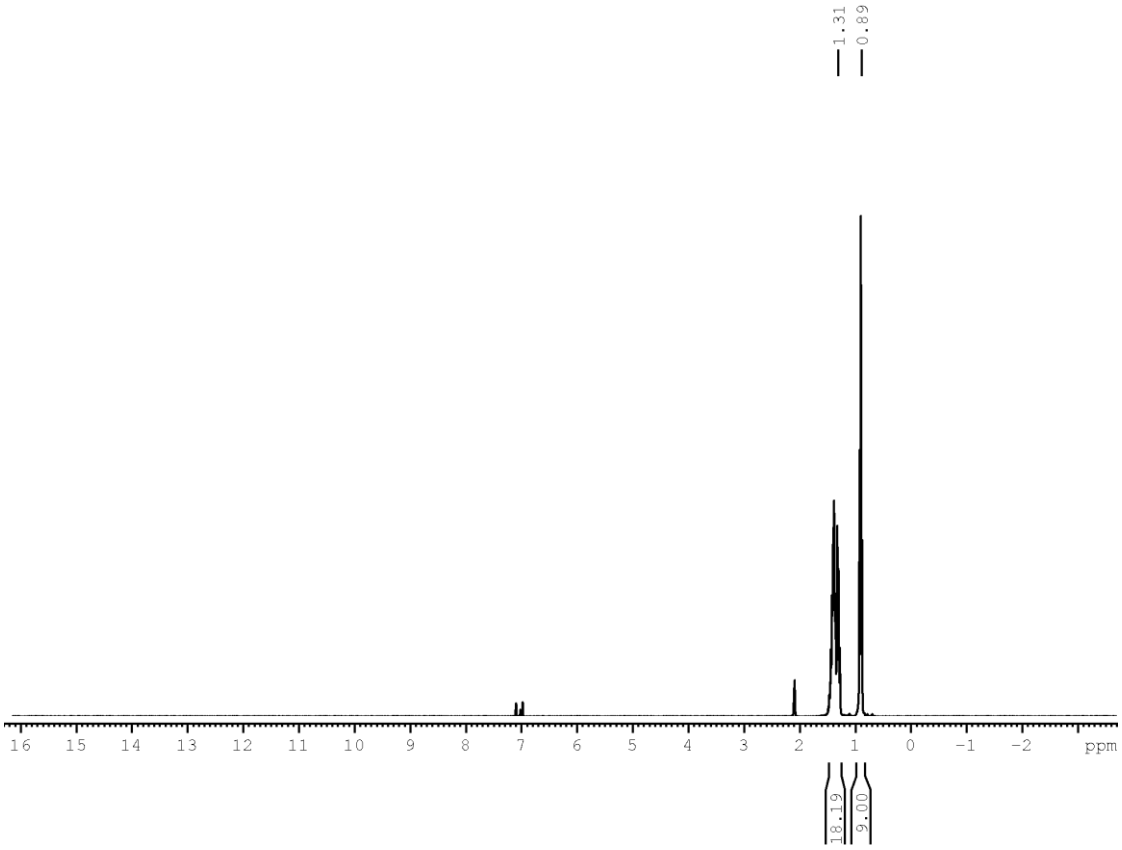

*Figure 113: ^{1}H (300 MHz) NMR spectrum of **4-3** in toluene-d_8.*

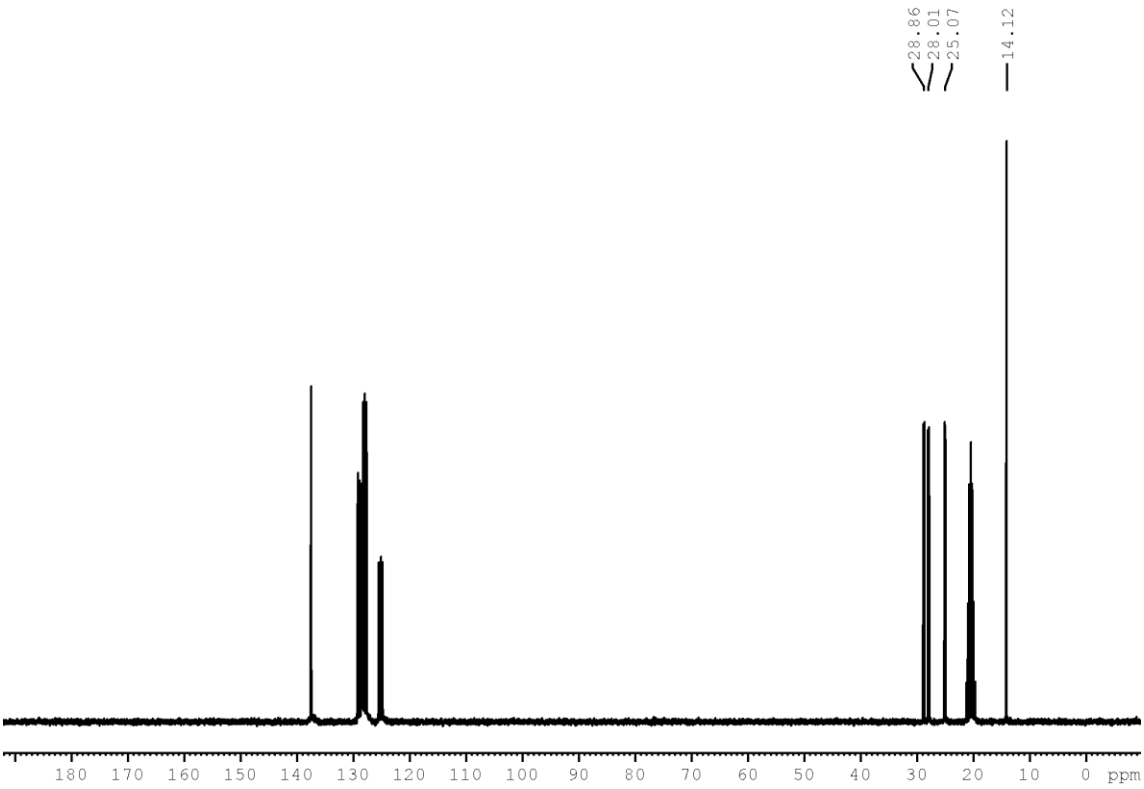

*Figure 114: $^{13}C\{^{1}H\}$ (125 MHz) NMR spectrum of **4-3** in toluene-d_8.*

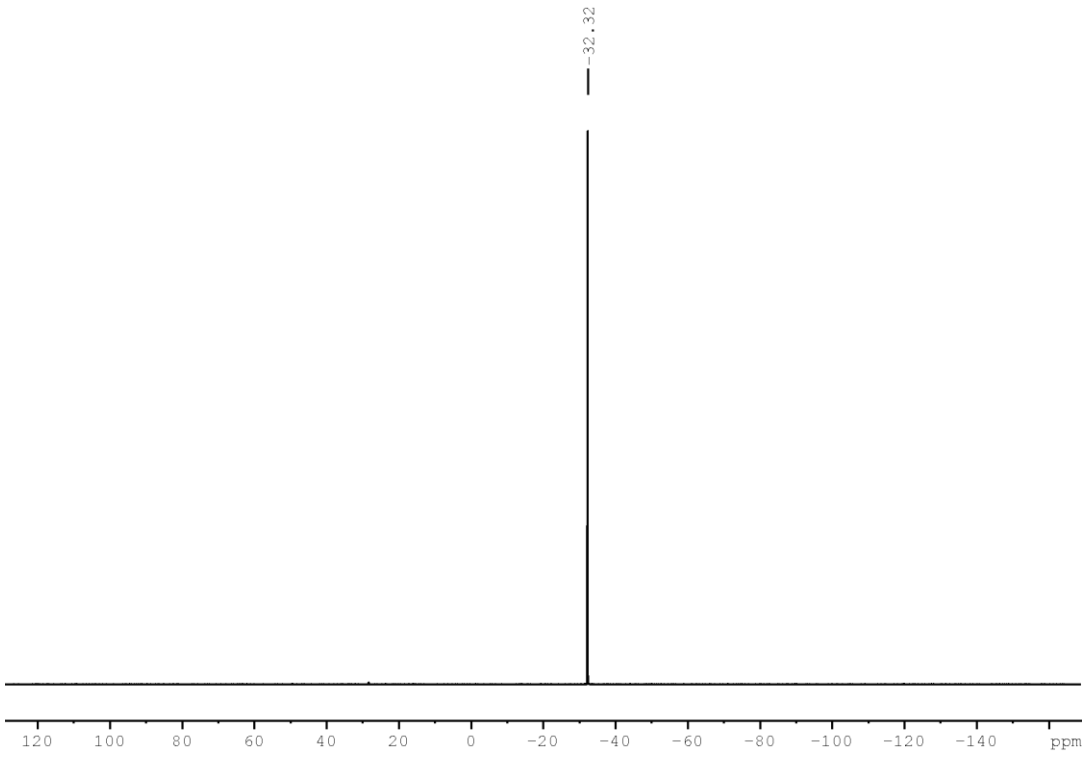

*Figure 115: $^{31}P\ \{^{1}H\}$ (121 MHz) NMR spectrum of **4-3** in toluene-d_8.*

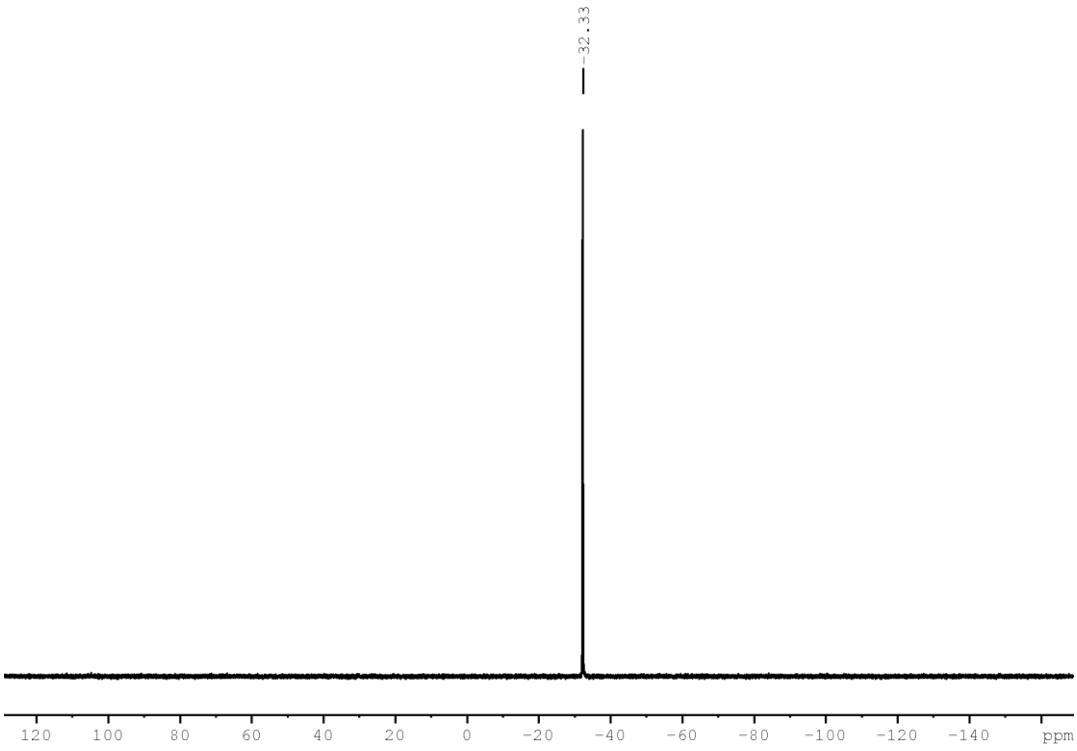

*Figure 116: ^{31}P (121 MHz) NMR spectrum of **4-3** in toluene-d_8.*

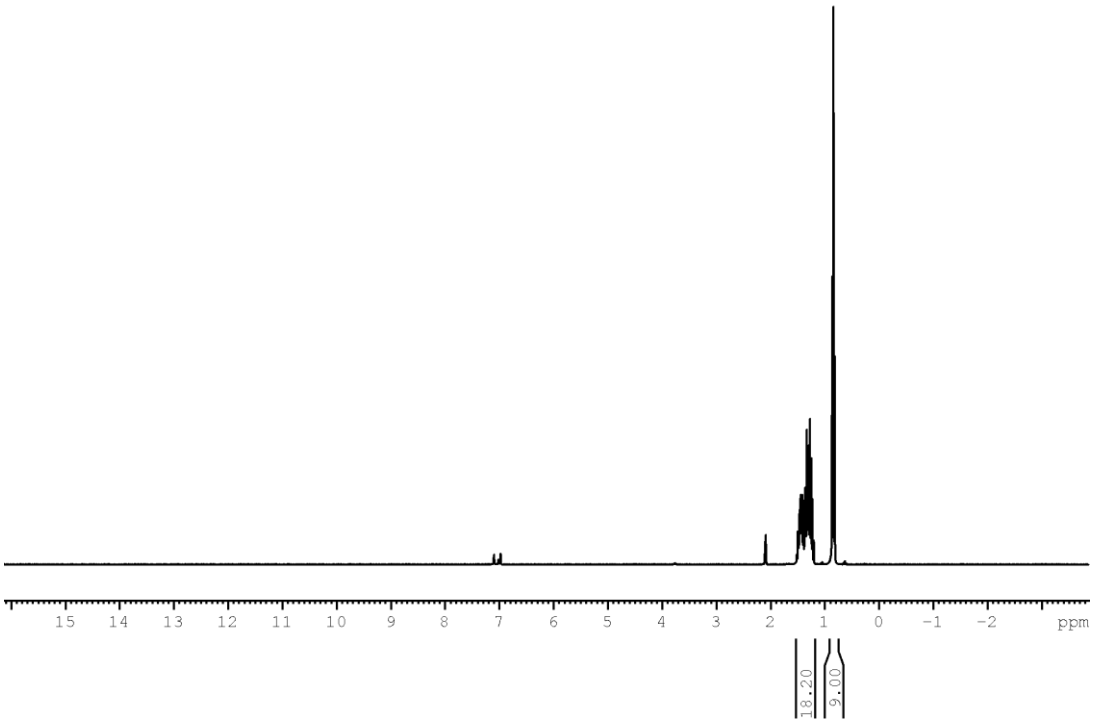

Figure 117: ^{1}H (300 MHz) NMR spectrum of $O{=}PnBu_3$ in toluene-d_8.

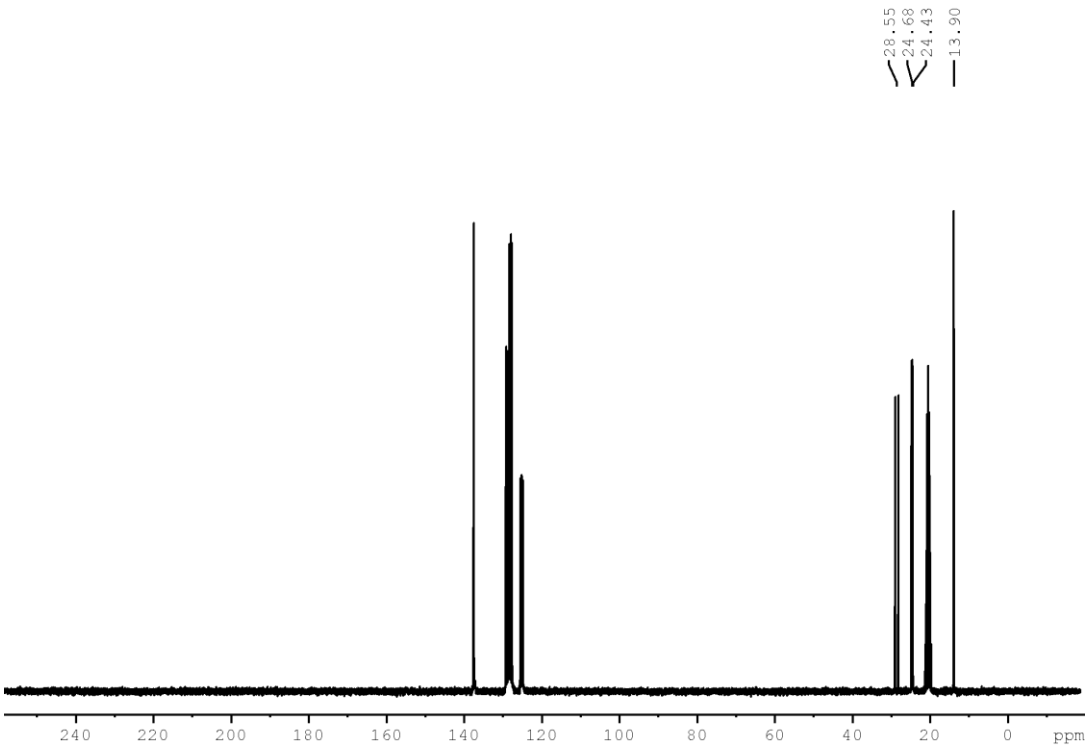

Figure 118: $^{13}C\{^1H\}$ (125 MHz) NMR spectrum of O=PnBu$_3$ in toluene-d$_8$.

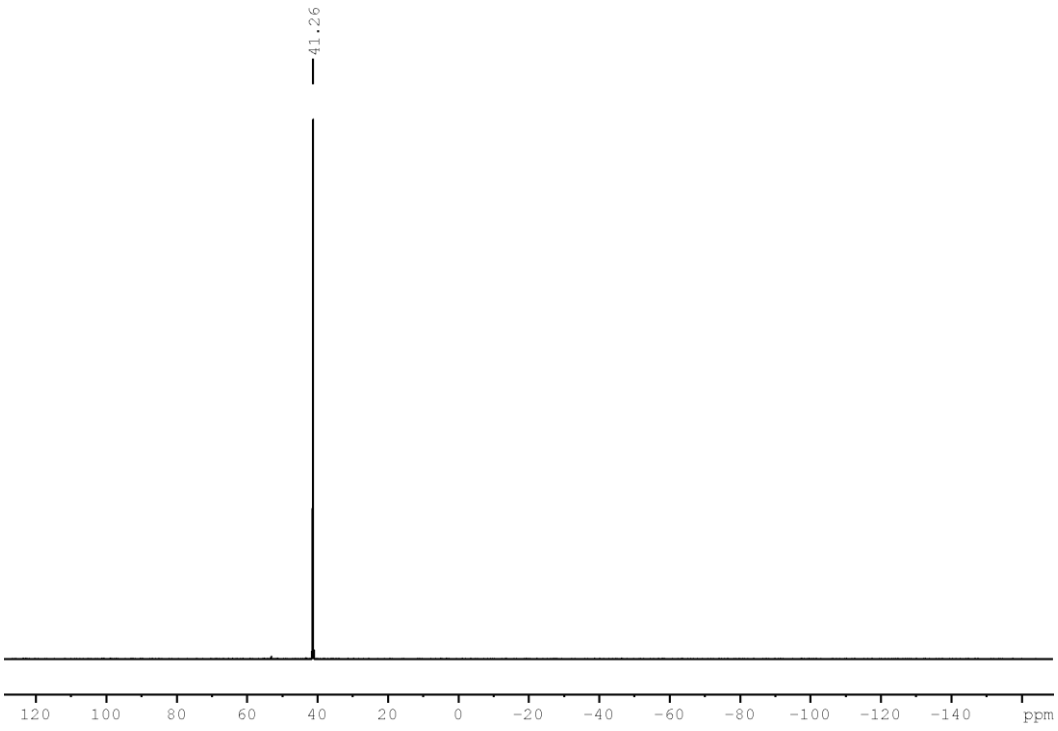

Figure 119: $^{31}P\ \{^1H\}$ (121 MHz) NMR spectrum of O=PnBu$_3$ in toluene-d$_8$.

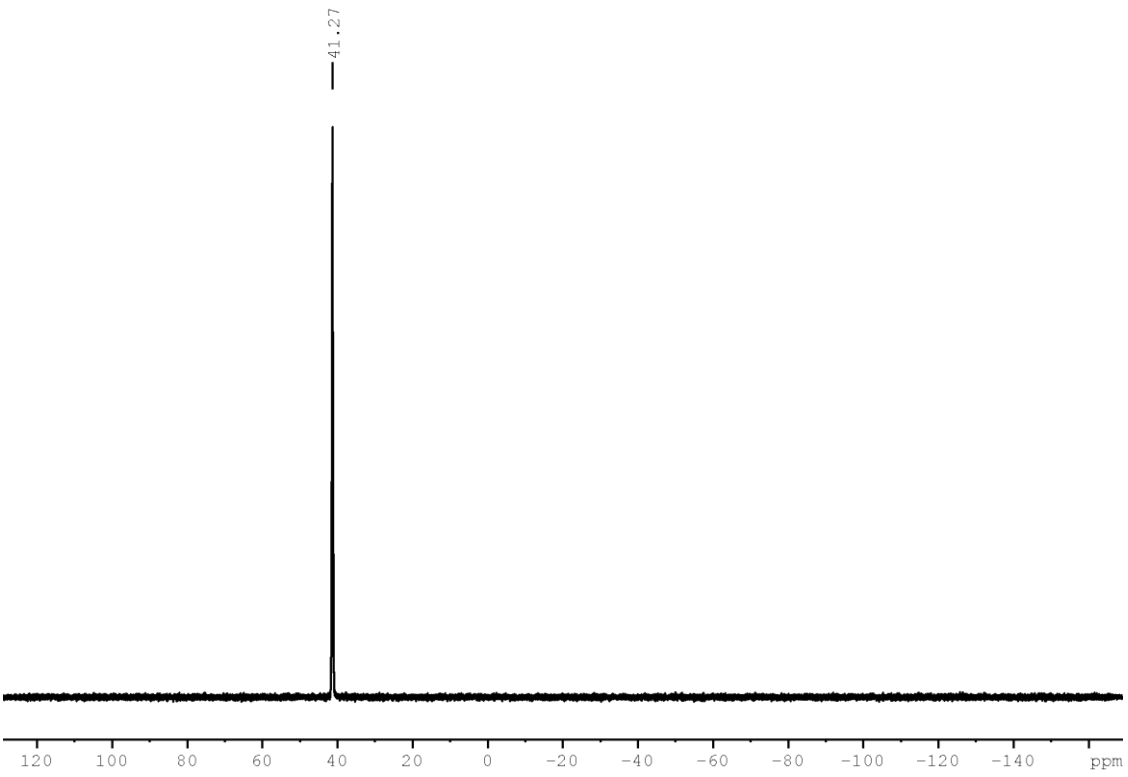

Figure 120: ^{31}P (121 MHz) NMR spectrum of O=PnBu$_3$ in toluene-d$_8$.

Appendix

NMR spectra

Chapter 1

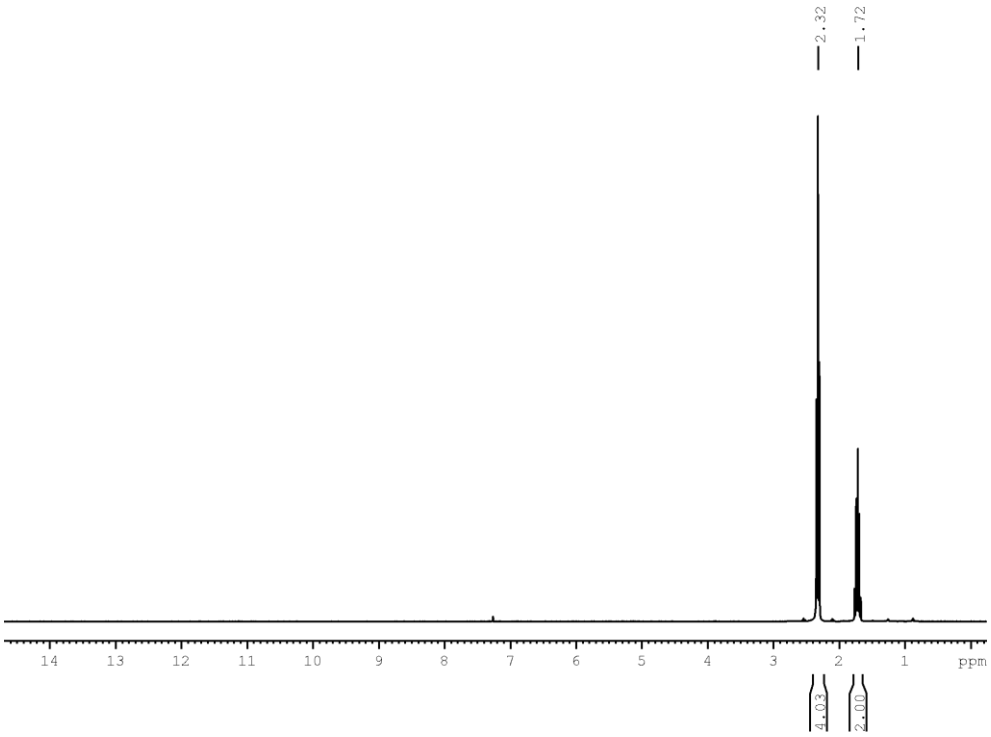

^{1}H NMR spectrum (300 MHz, $CDCl_3$) of 1,7-dibromo-1,6-heptadiyne

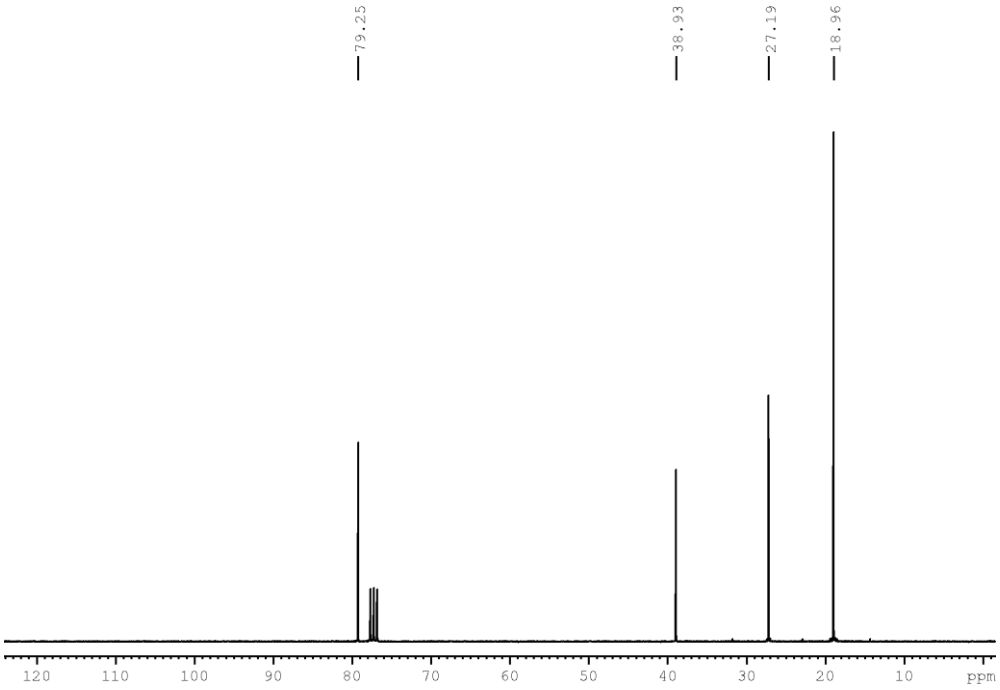

$^{13}C\{^{1}H\}$ NMR spectrum (75 MHz, $CDCl_3$) of 1,7-dibromo-1,6-heptadiyne

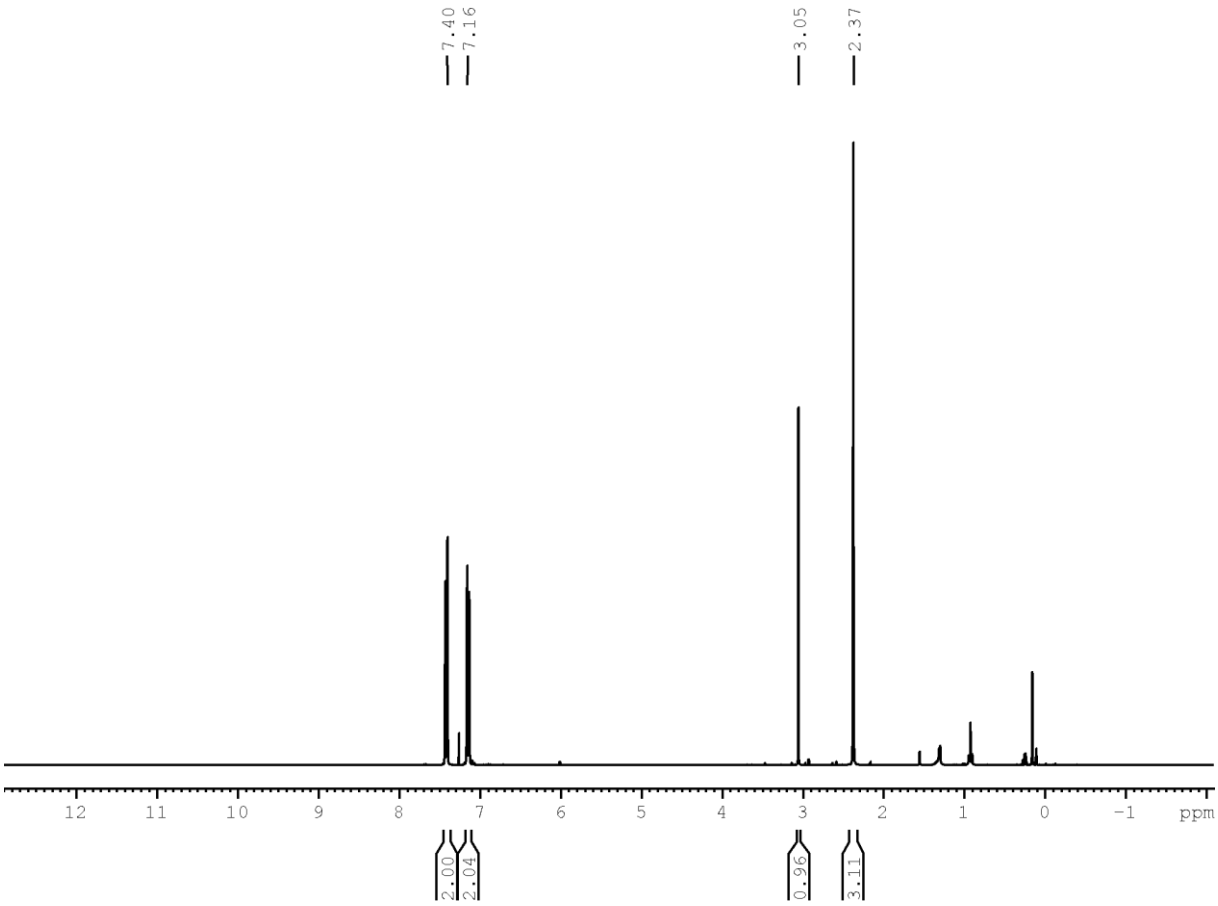

^{1}H NMR spectrum (300 MHz, $CDCl_3$) of 4-ethylnyltoluene. The spectrum contains residual water and solvent signals.

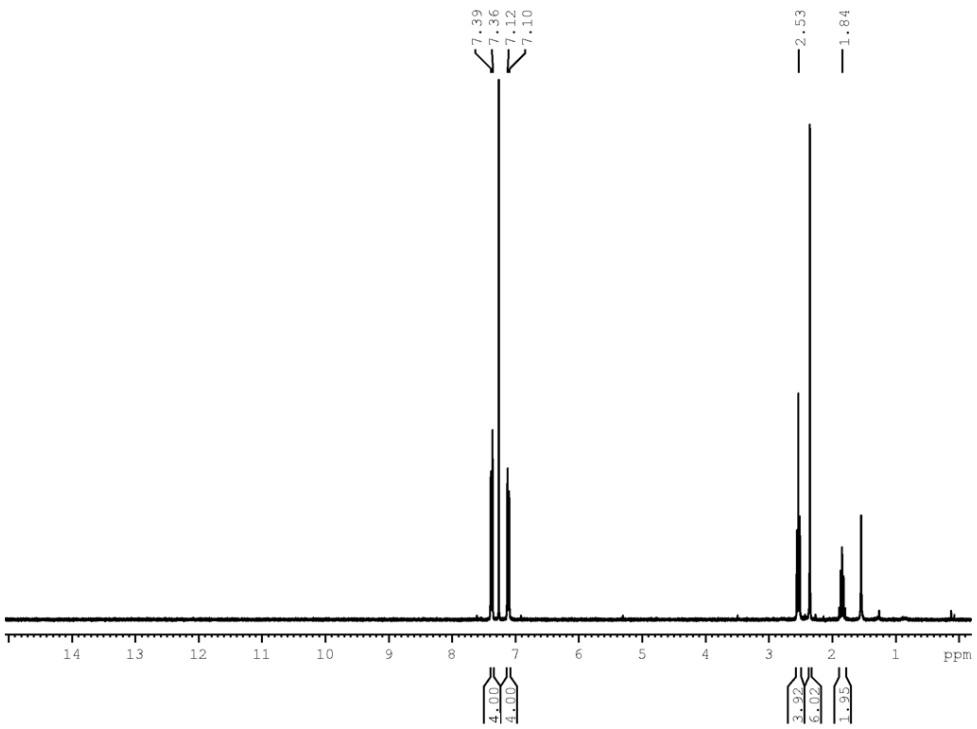

^{1}H NMR spectrum (300 MHz, $CDCl_3$) of **1-1**. The spectrum contains residual water and solvent signals.

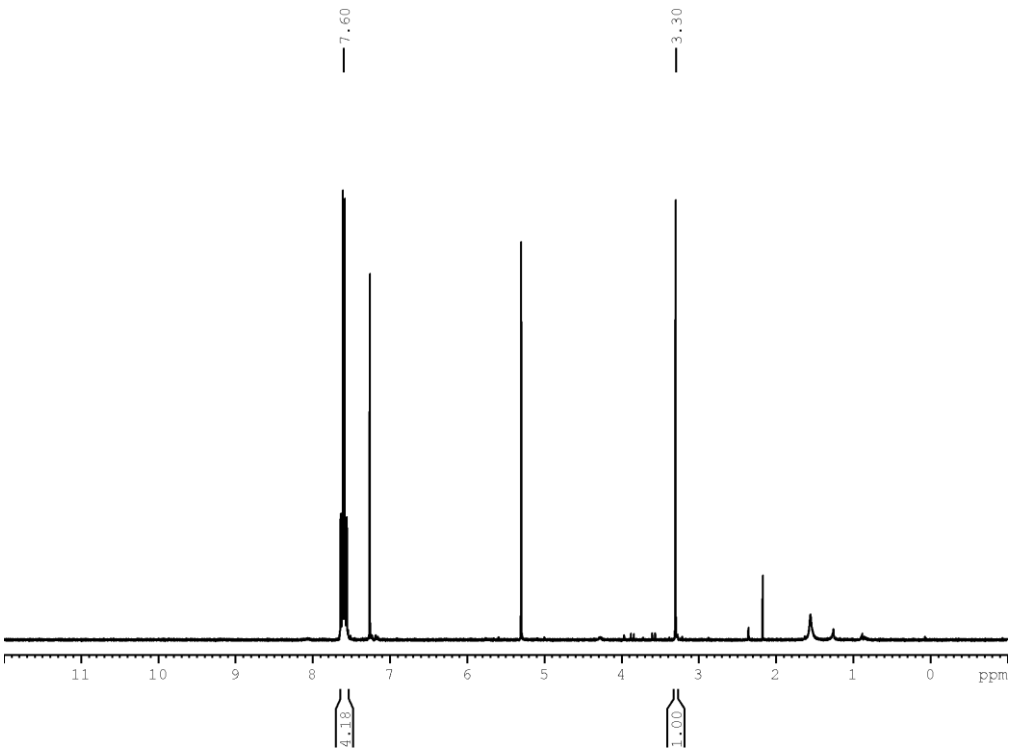

^{1}H NMR spectrum (300 MHz, $CDCl_3$) of 4-Ethynylbenzonitrile. The spectrum contains residual water and solvent signals.

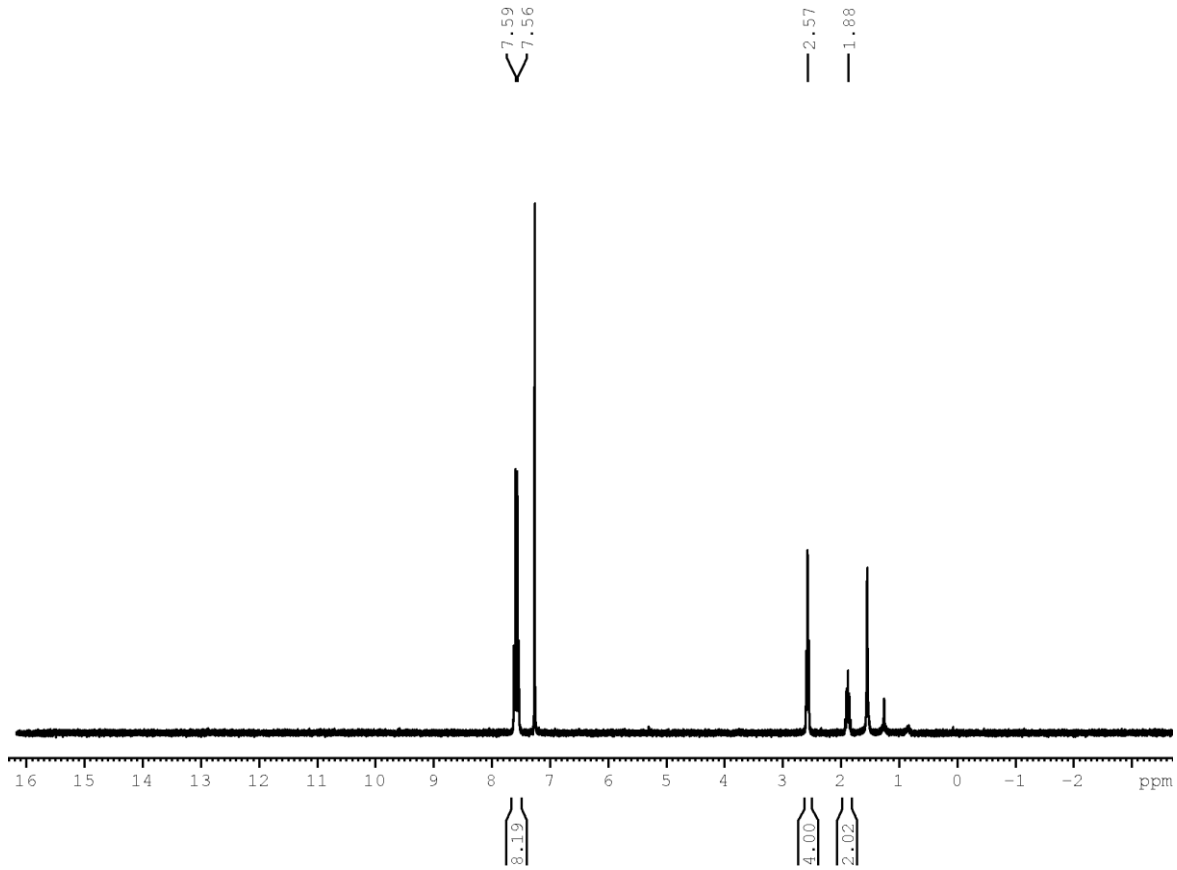

^{1}H NMR spectrum (300 MHz, $CDCl_3$) of **1-5.** The spectrum contains residual water and solvent signals.

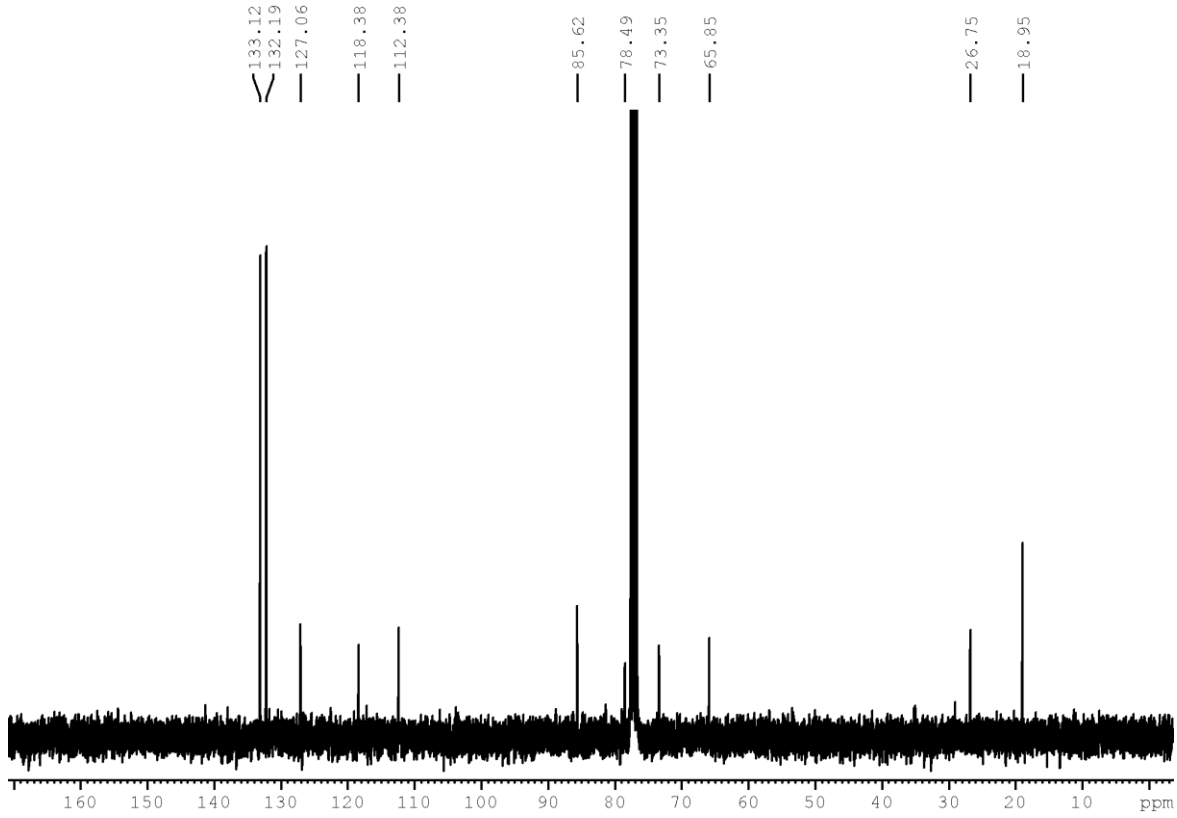

$^{13}C\{^{1}H\}$ NMR spectrum (75 MHz, $CDCl_3$) of **1-5.**

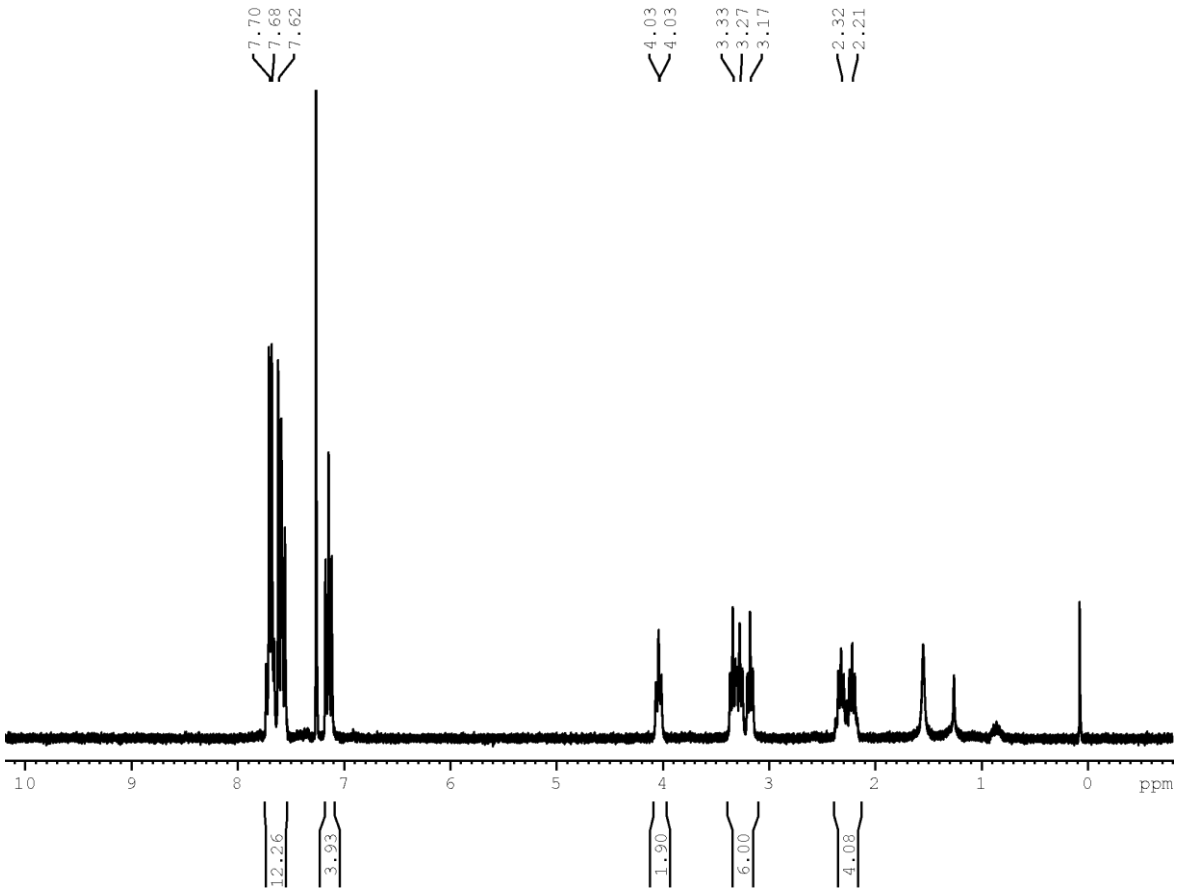

^{1}H NMR spectrum (300 MHz, $CDCl_3$) of **1-6**. The spectrum contains residual water and solvent signals.

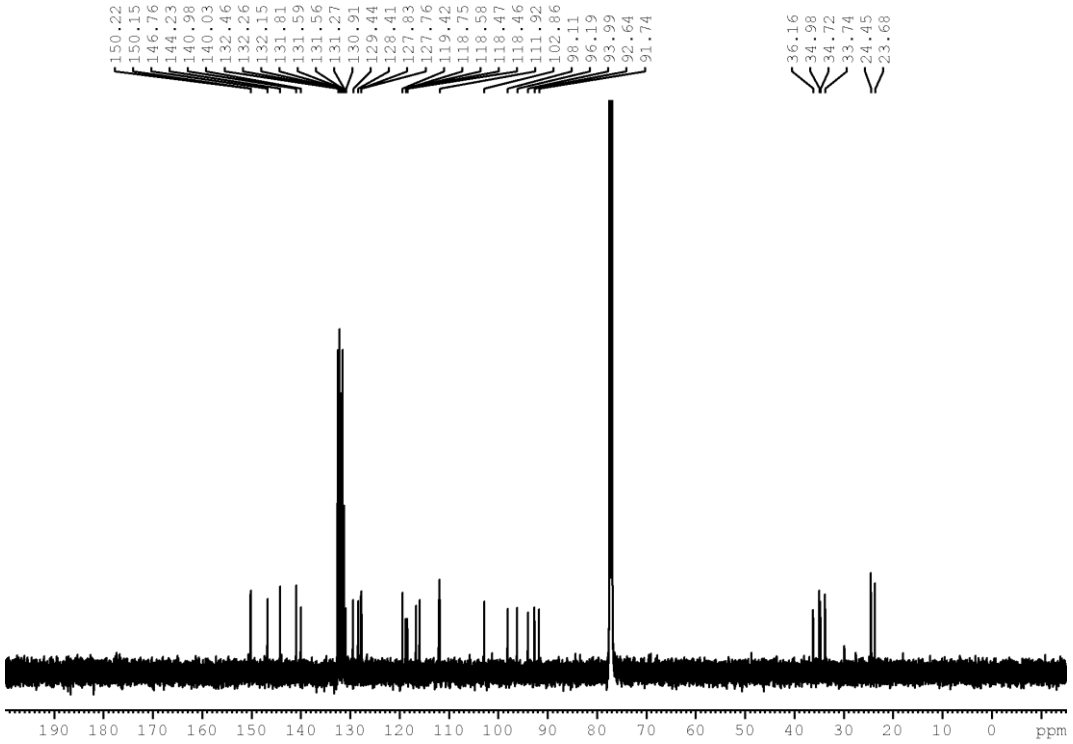

^{13}C{^{1}H} NMR spectrum (125 MHz, $CDCl_3$) of **1-6**. The signal to noise ratio is low due to poor solubility of the compound.

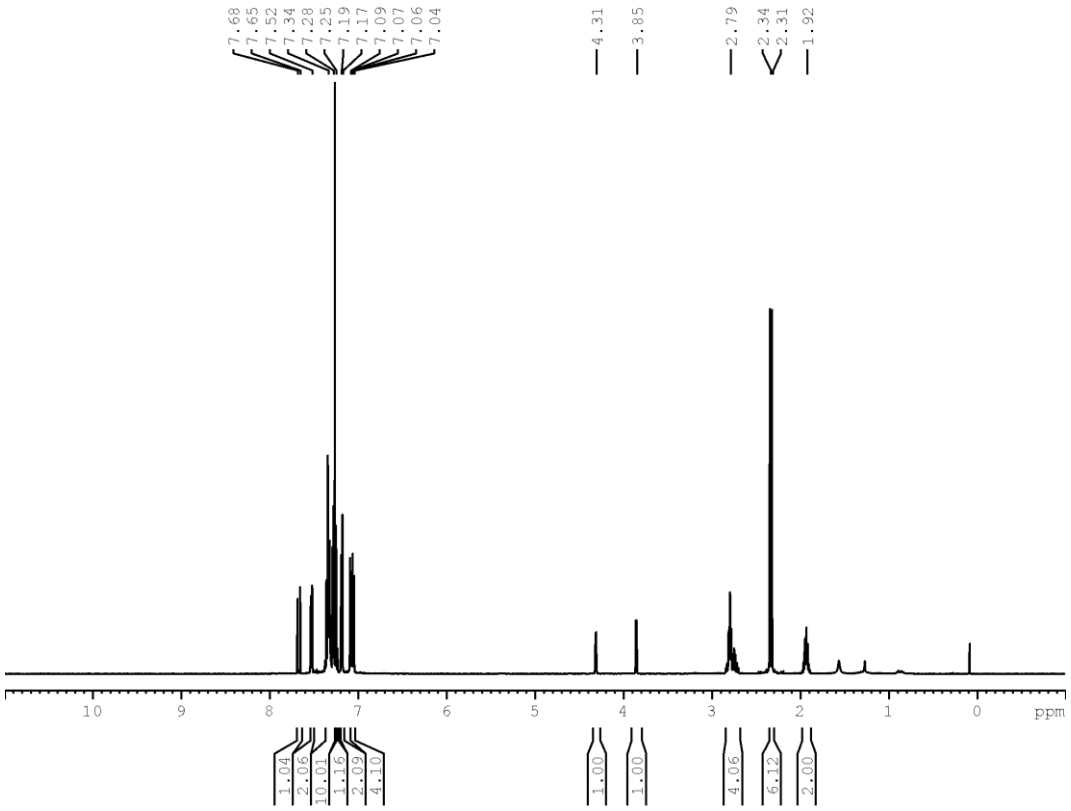

^{1}H NMR spectrum (500 MHz, $CDCl_3$) of **1-4**. The spectrum contains residual water and solvent signals.

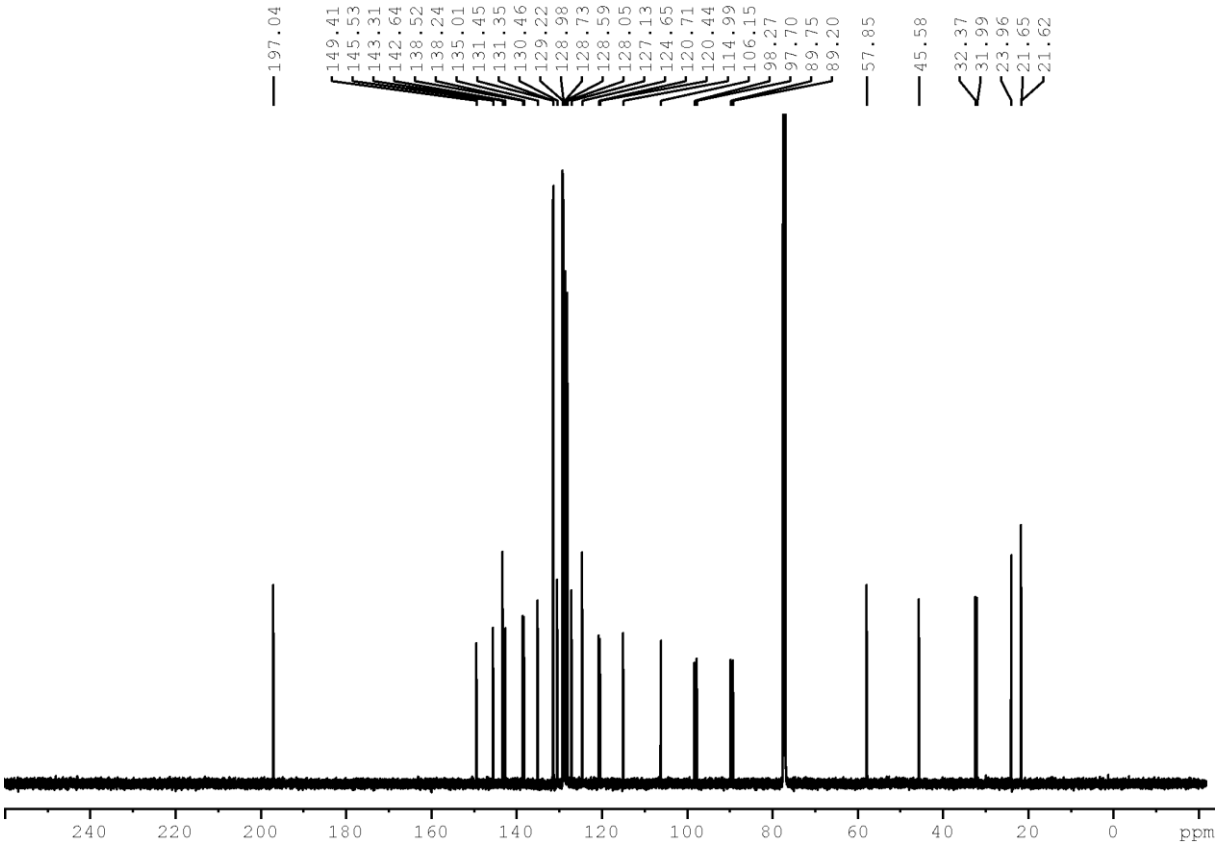

^{13}C{^{1}H} NMR spectrum (125 MHz, $CDCl_3$) of **1-4.**

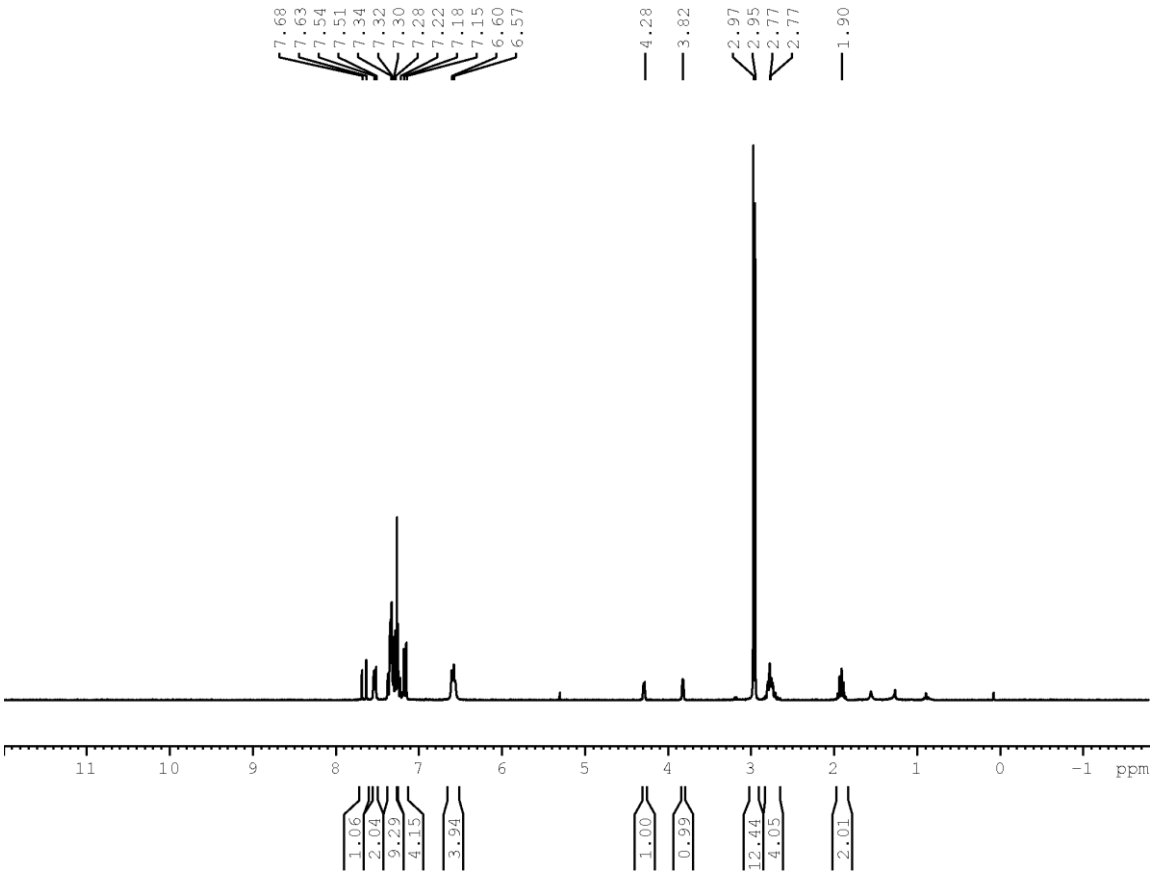

^{1}H NMR spectrum (300 MHz, $CDCl_3$) of **1-8**. The spectrum contains residual water and solvent signals.

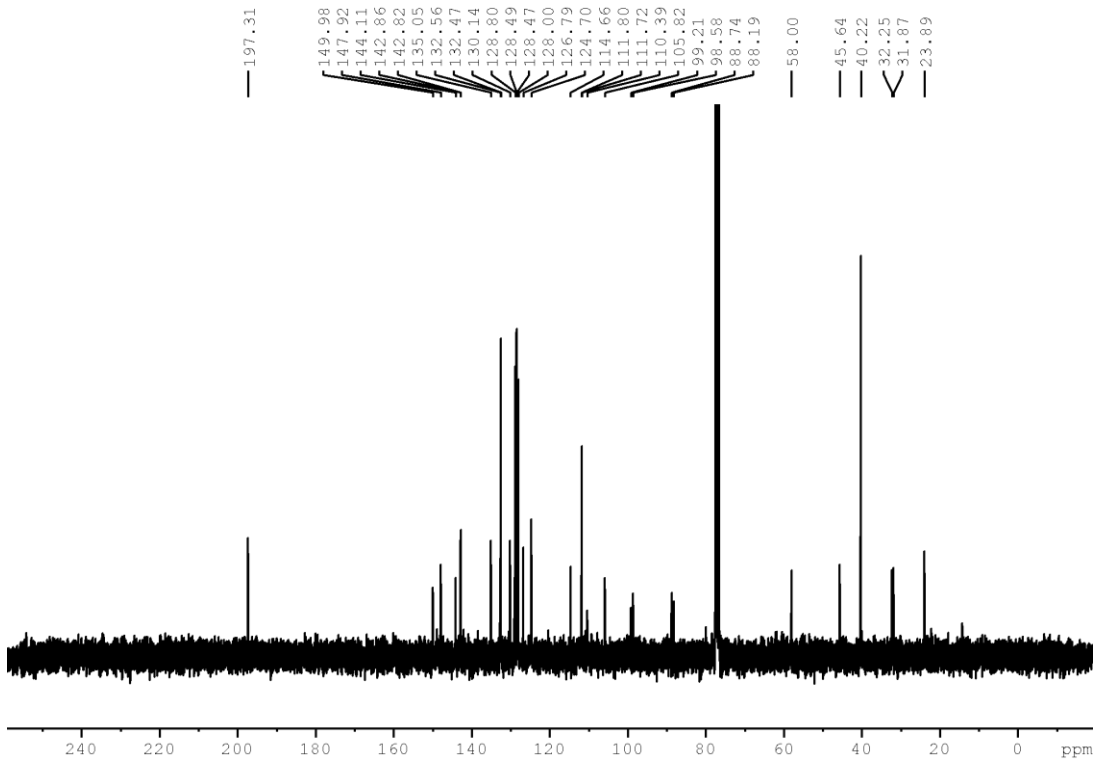

^{13}C{^{1}H} NMR spectrum (75 MHz, $CDCl_3$) of **1-8.**

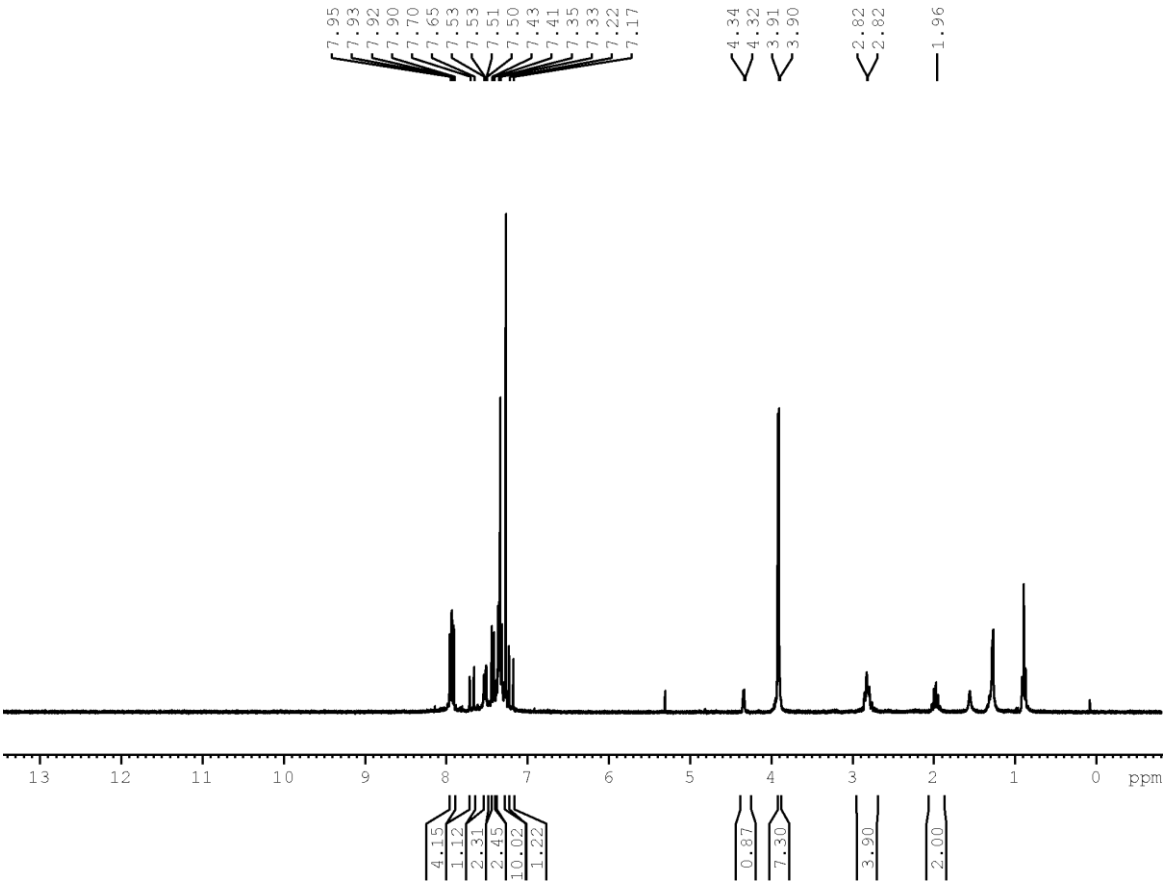

^{1}H NMR spectrum (300 MHz, $CDCl_3$) of **1-10**. The spectrum contains residual water and solvent signals.

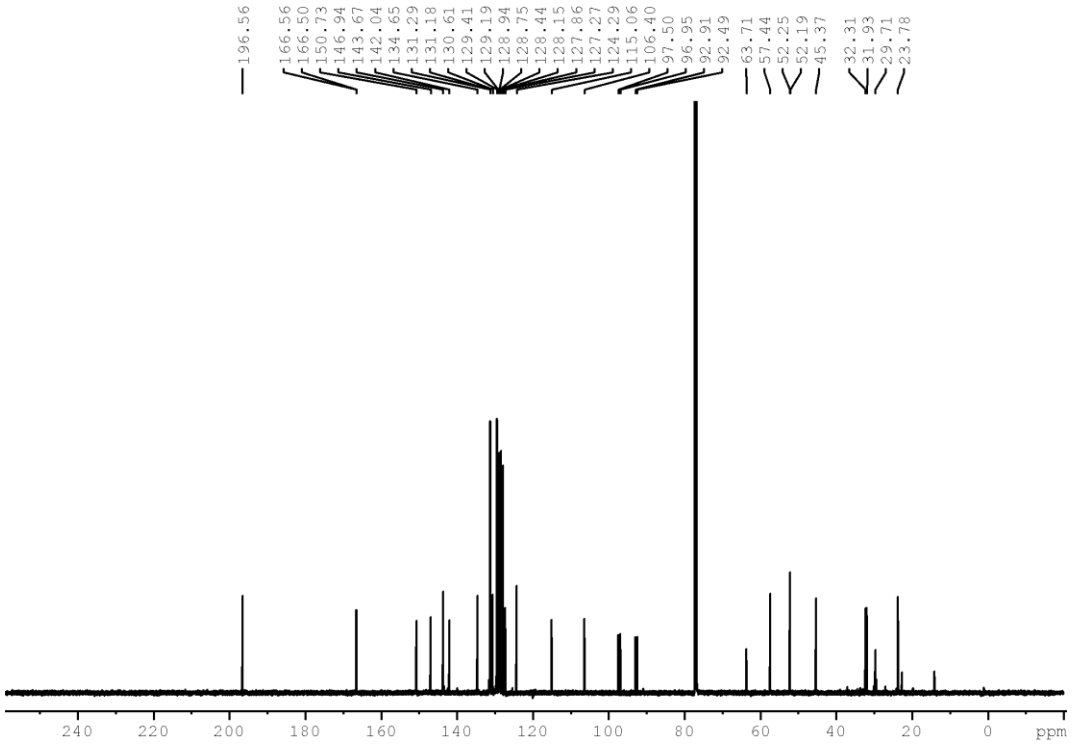

^{13}C{^{1}H} NMR spectrum (75 MHz, $CDCl_3$) of **1-10.**

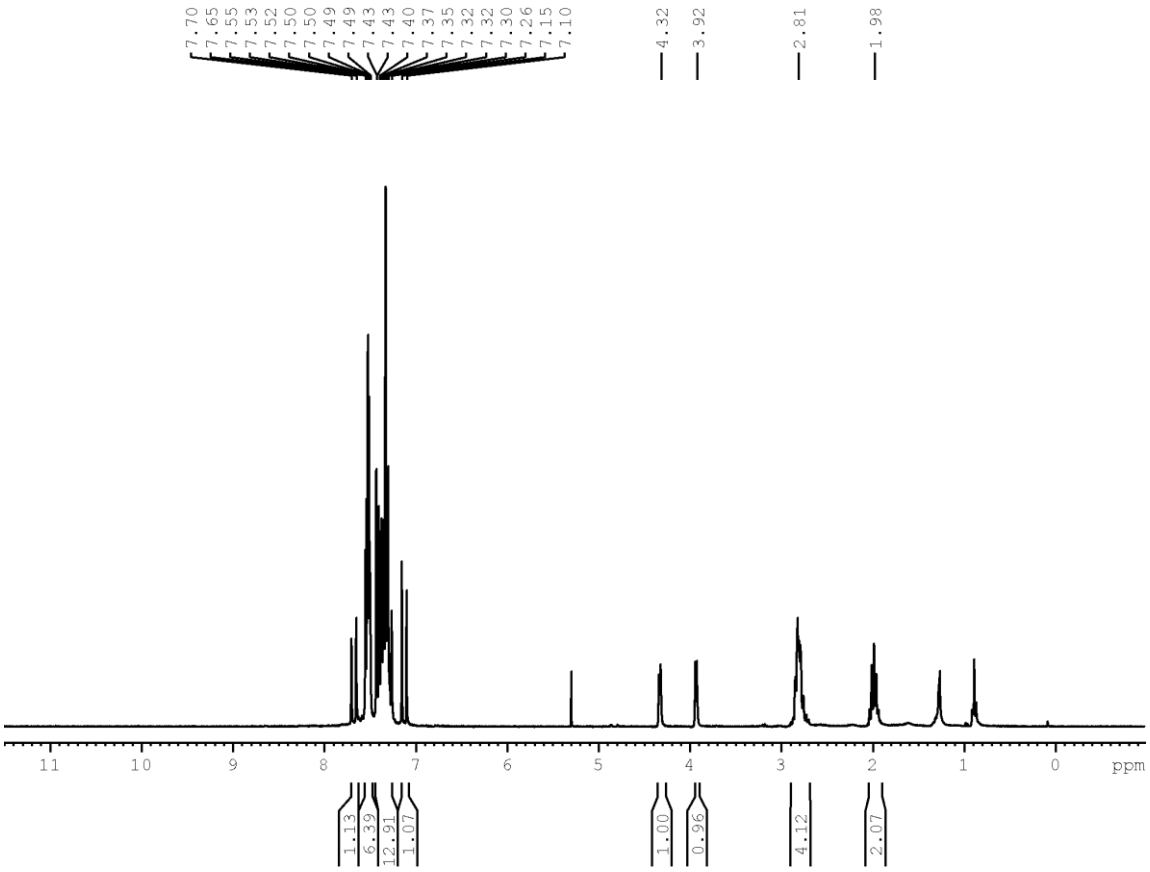

^{1}H NMR spectrum (300 MHz, $CDCl_3$) of **1-11**. The spectrum contains residual water and solvent signals.

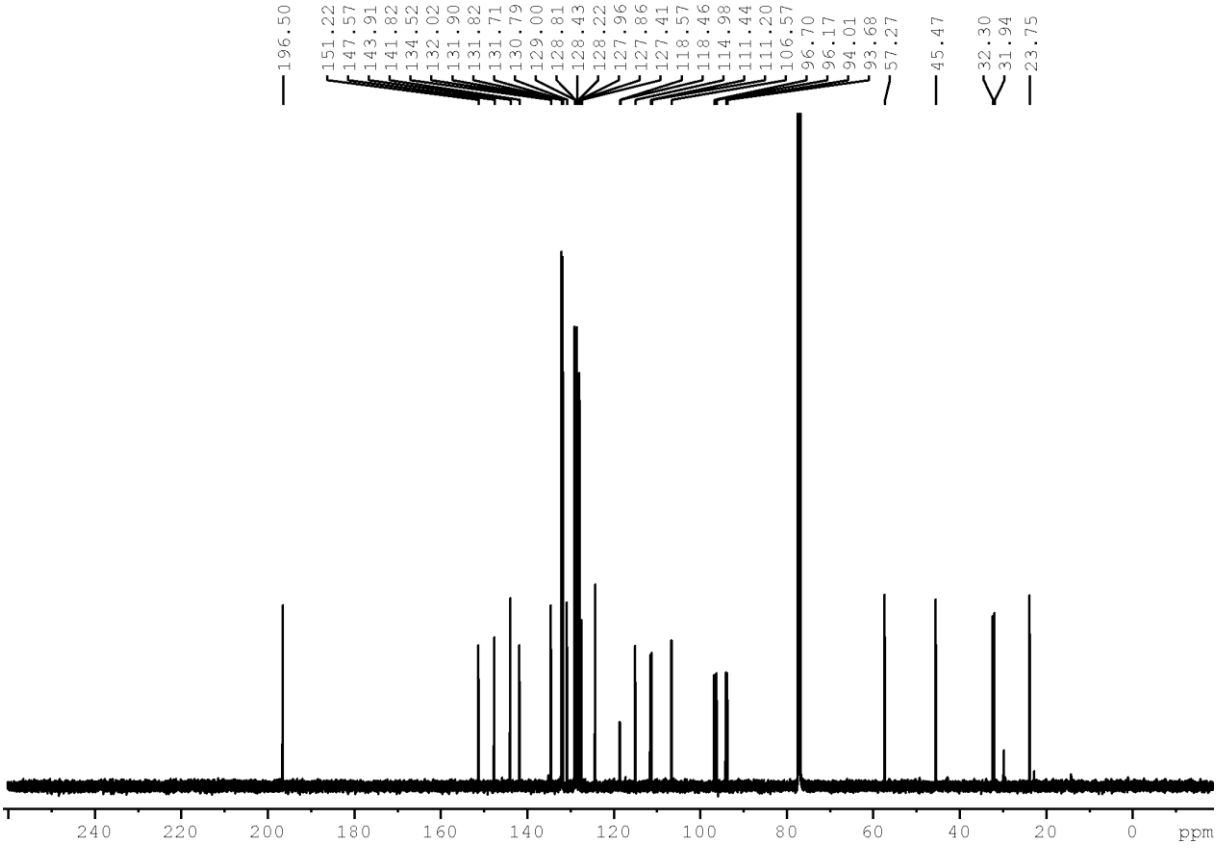

^{13}C{^{1}H} NMR spectrum (75 MHz, $CDCl_3$) of **1-11.**

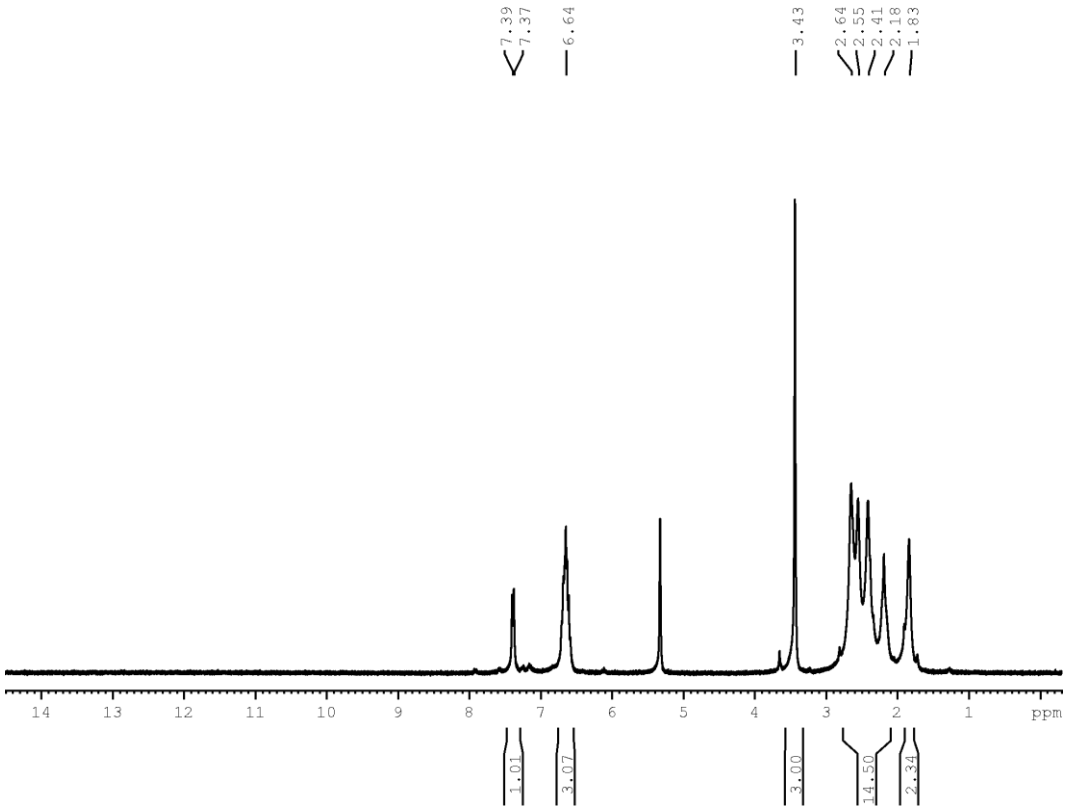

^{1}H NMR spectrum (300 MHz, CD_2Cl_2) of [(TMEDA)Ni(o-tolyl)Cl]

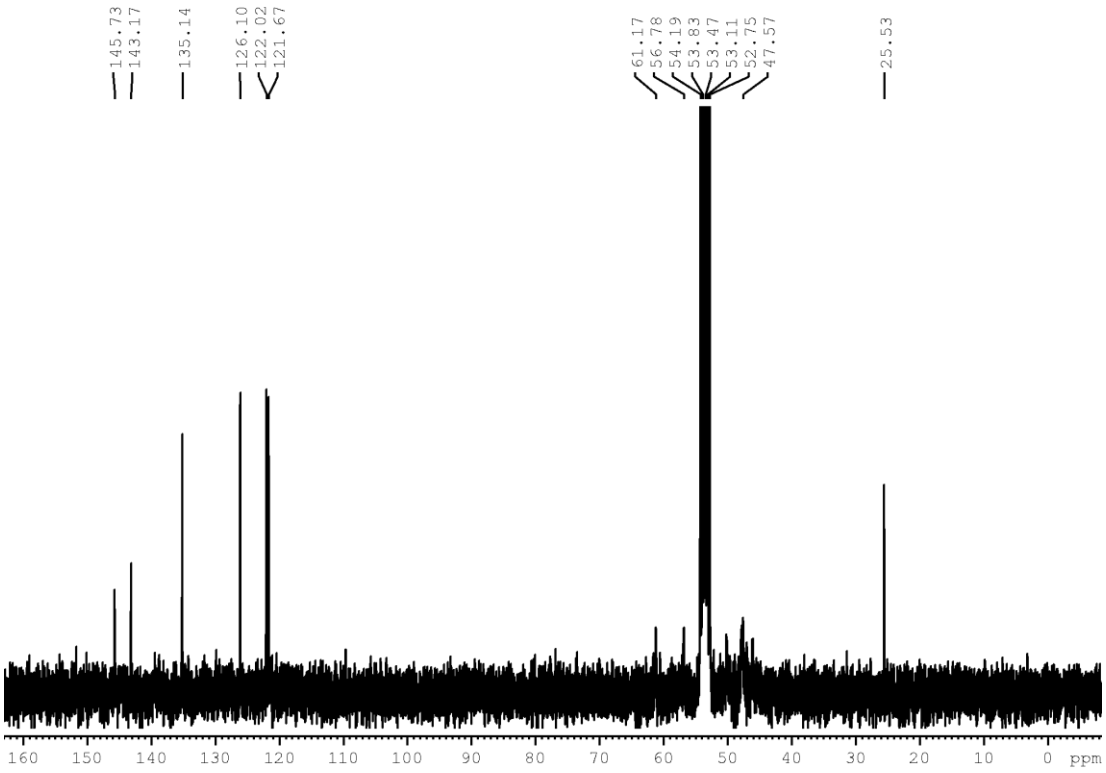

^{13}C{^{1}H} NMR spectrum (75 MHz, CD_2Cl_2) of [(TMEDA)Ni(o-tolyl)Cl].

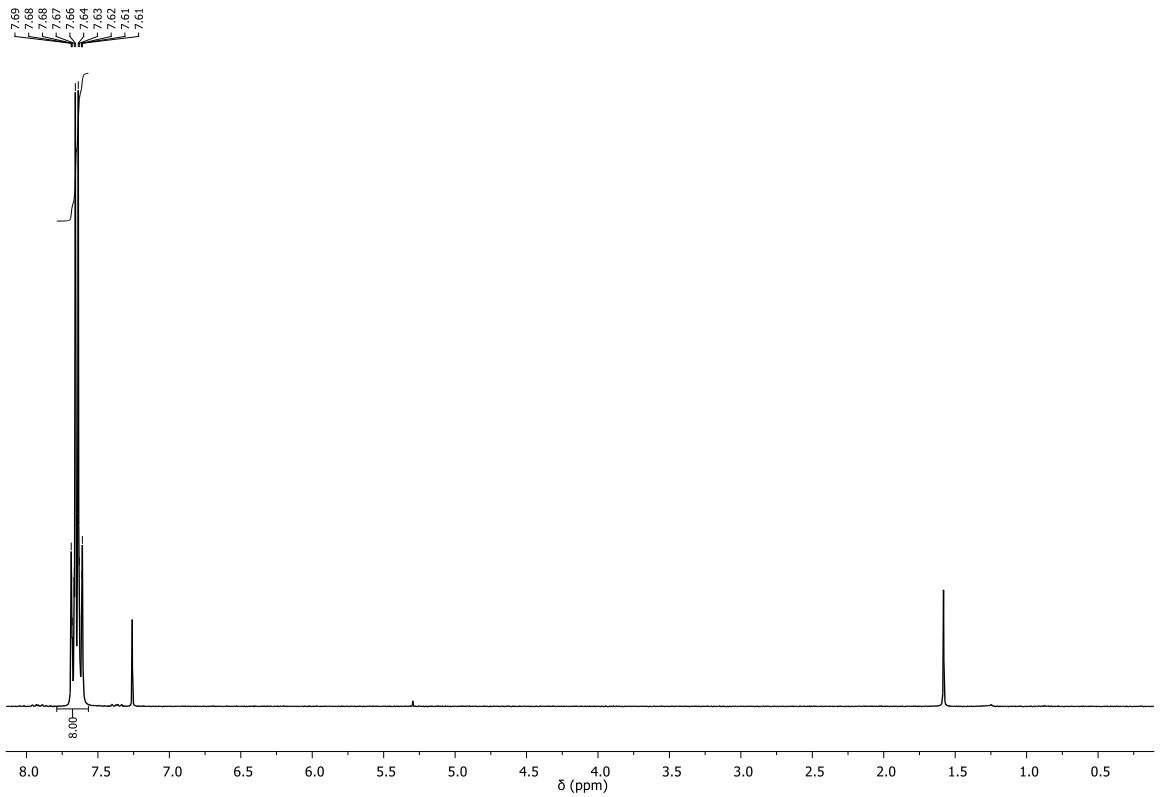

^{1}H NMR spectrum (300 MHz, $CDCl_3$) of 4,4′-(ethyne-1,2-diyl) benzonitrile.

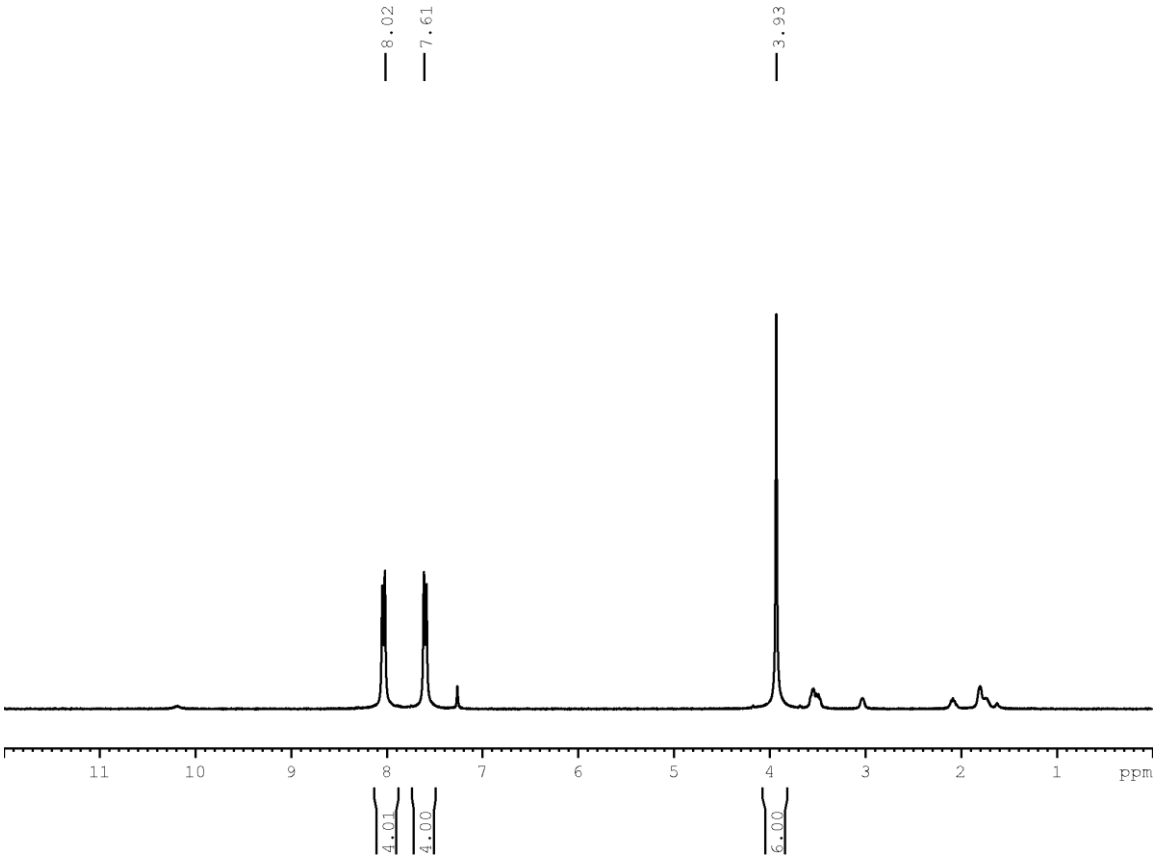

^{1}H NMR spectrum (300 MHz, $CDCl_3$) of dimethyl 4,4'-(ethyne-1,2-diyl)dibenzoate.

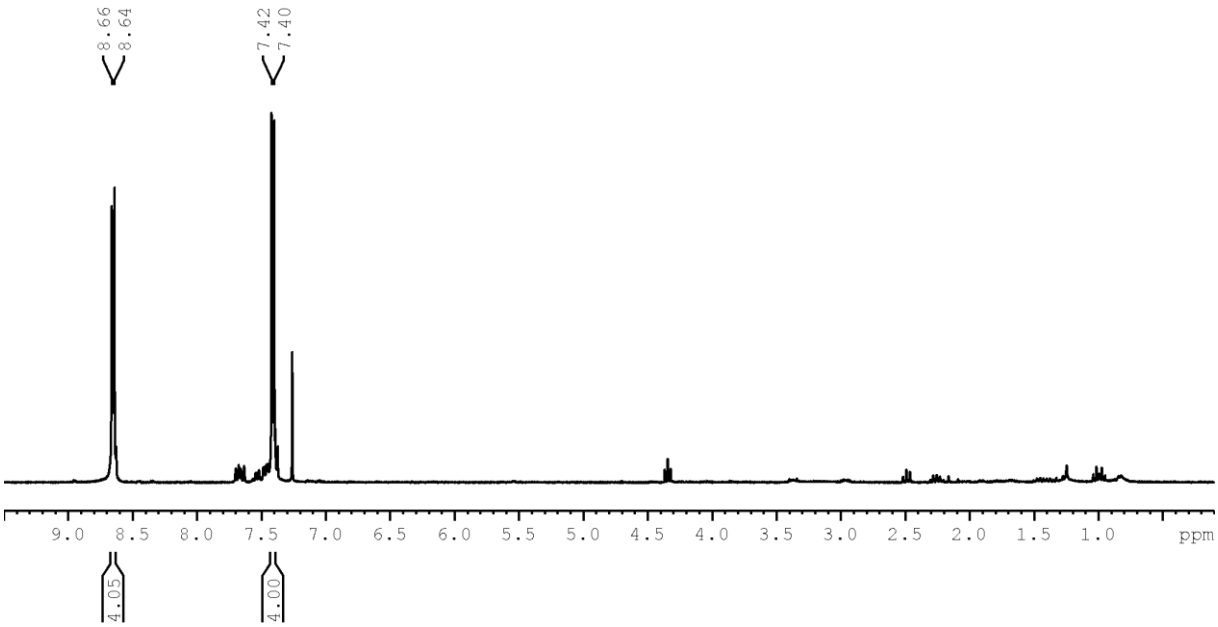

^{1}H NMR spectrum (300 MHz, $CDCl_3$) of 1,2-di(pyridine-4-yl)ethyne.

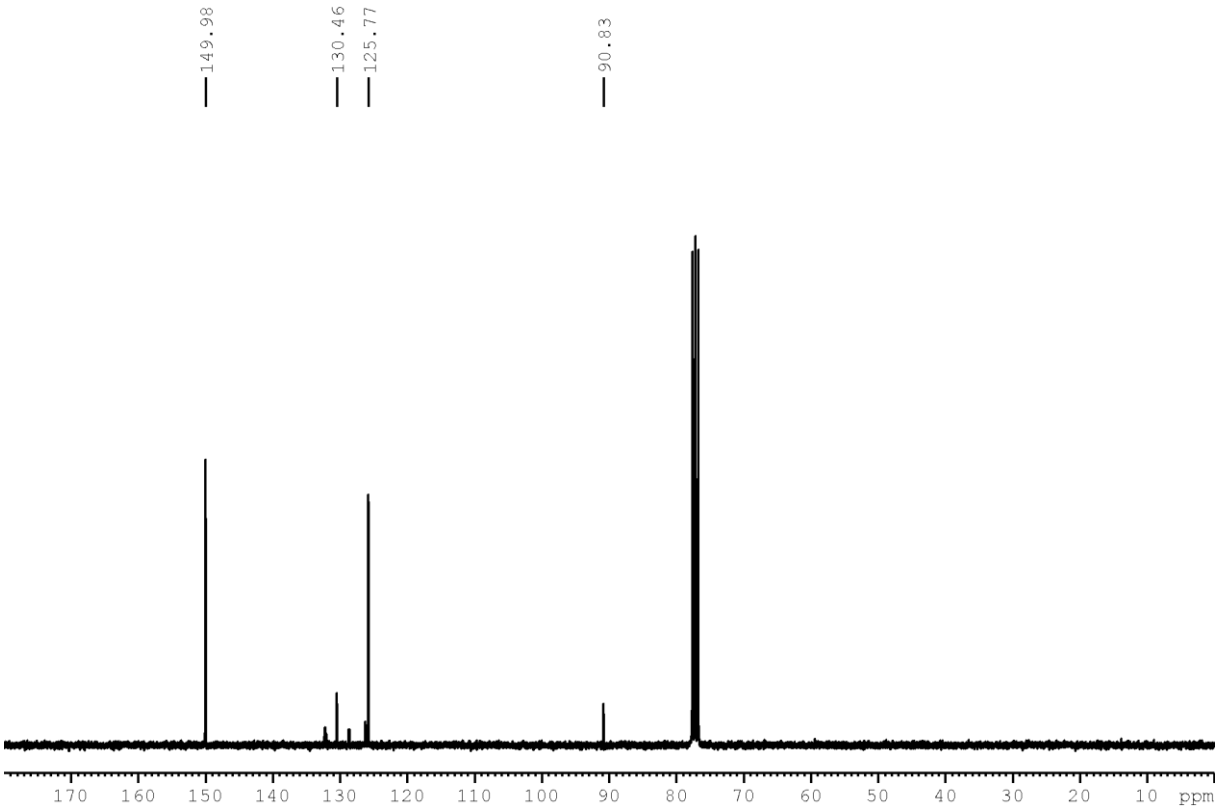

$^{13}C\{^{1}H\}$ NMR spectrum ($CDCl_3$, 75 MHz) of 1,2-di(pyridine-4-yl)ethyne.

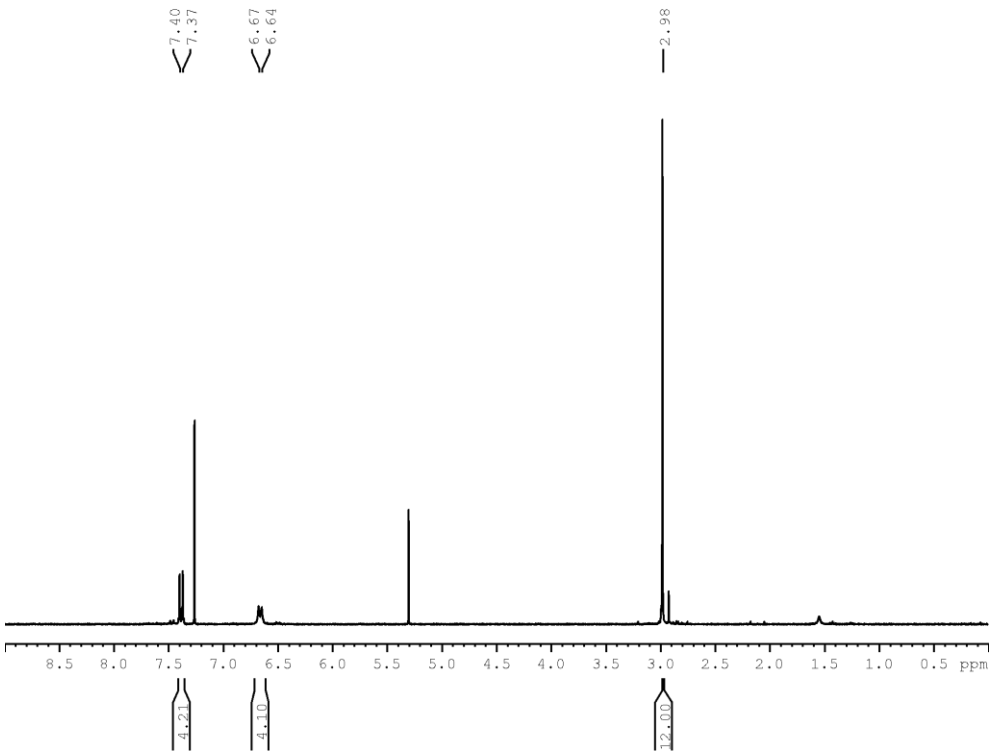

^{1}H NMR spectrum (300 MHz, $CDCl_3$) 4,4'-(ethyne-1,2-diyl)bis(N,N-dimethylaniline)

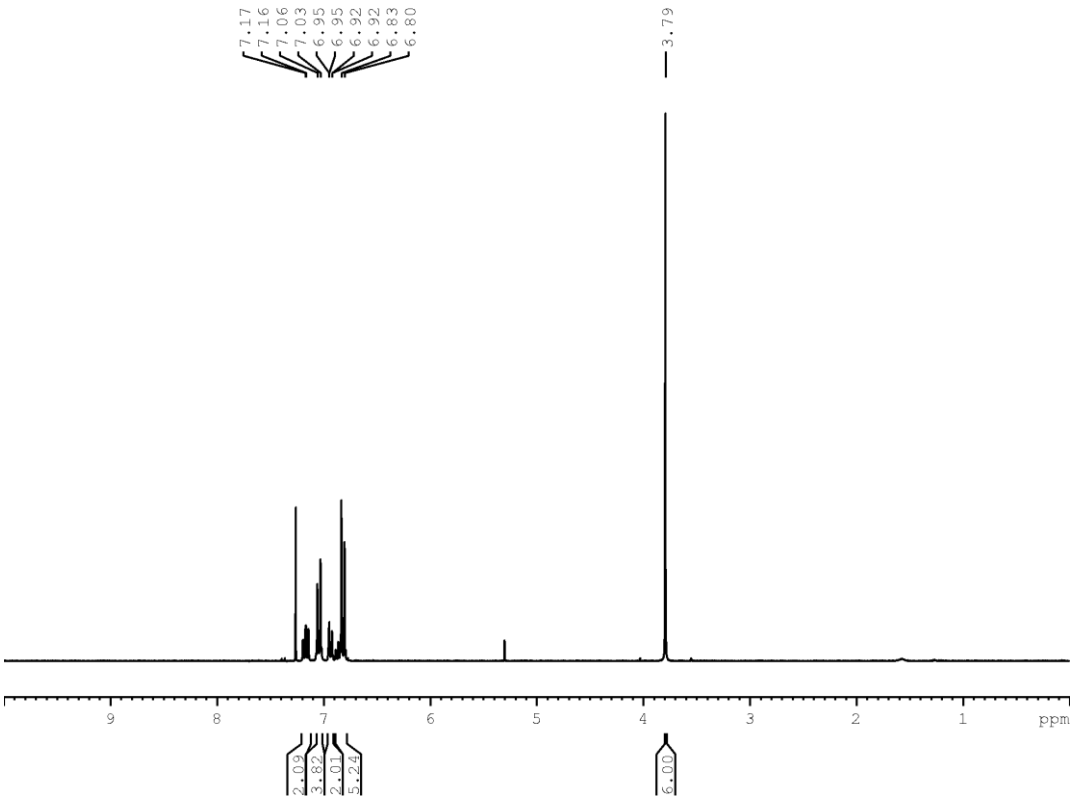

^{1}H NMR spectrum (300 MHz, $CDCl_3$) of 4-methoxy-N-(4-methoxyphenyl)-N-phenylaniline.

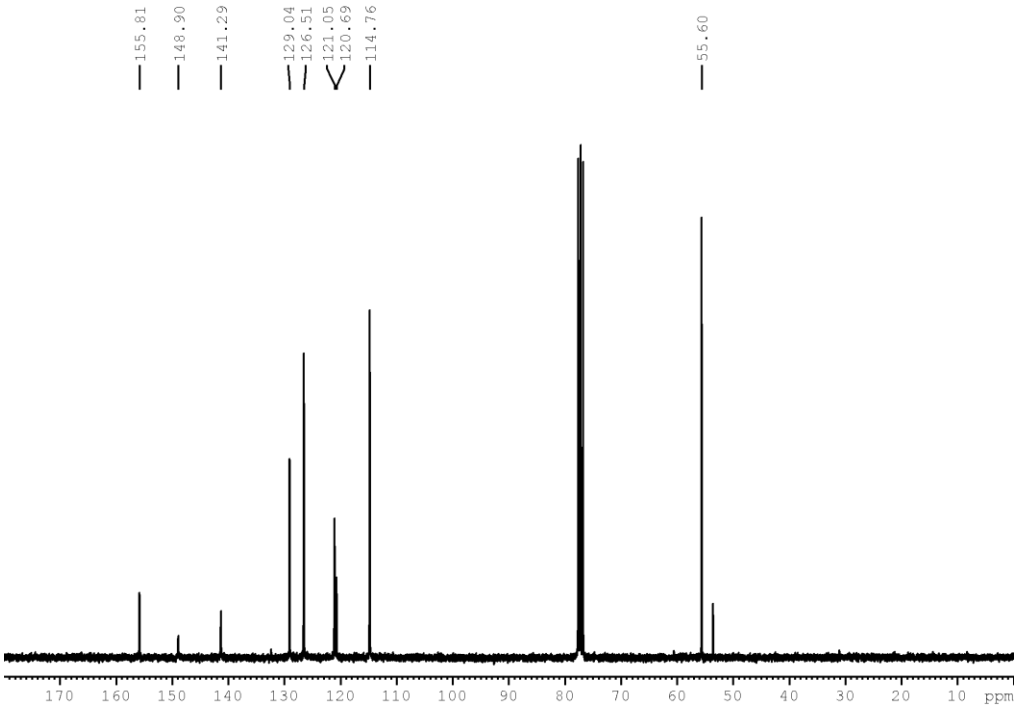

$^{13}C\{^{1}H\}$ NMR spectrum ($CDCl_3$, 75 MHz) of 4-methoxy-N-(4-methoxyphenyl)-N-phenylaniline.

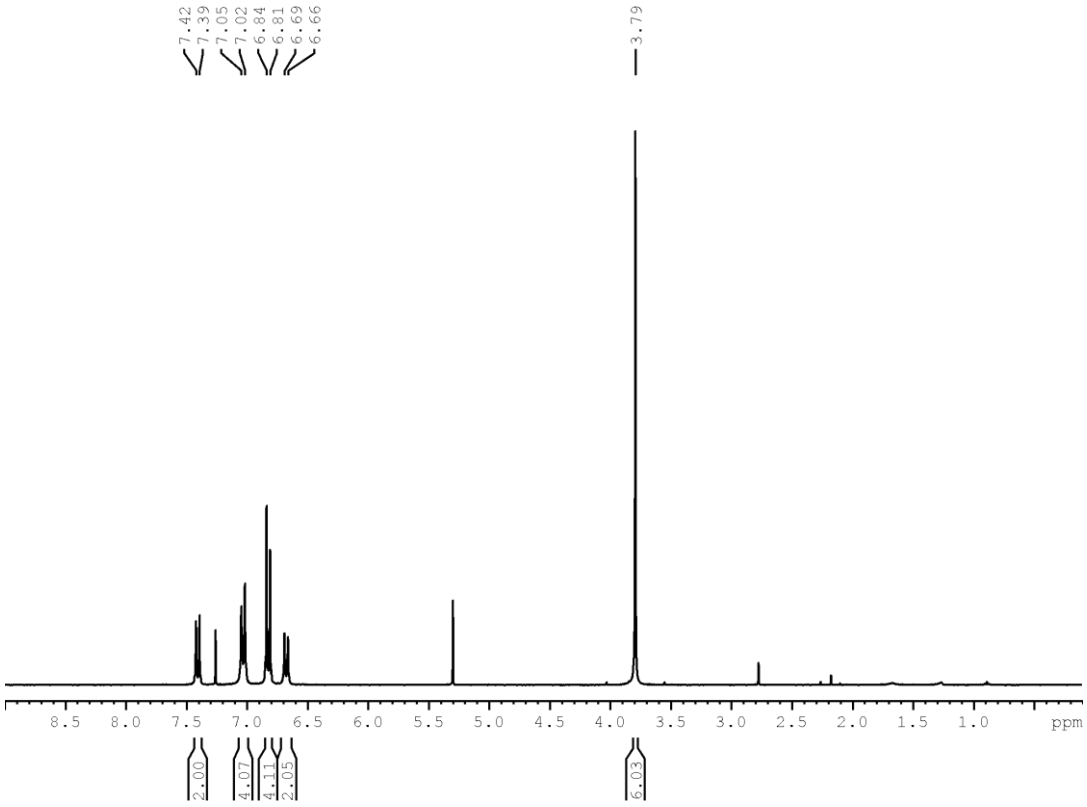

^{1}H NMR spectrum (300 MHz, $CDCl_3$) of 4-Iodo-*N,N*-bis(4-methoxyphenyl)aniline.

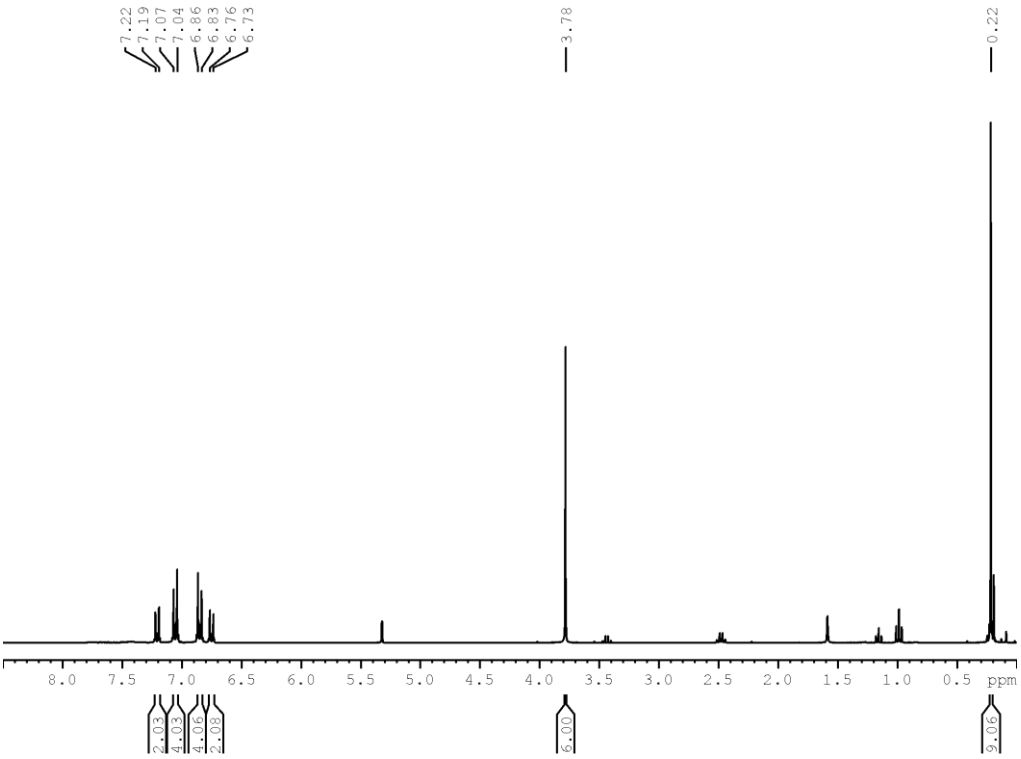

^{1}H NMR spectrum (300 MHz, CD_2Cl_2) of 4-methoxy-N-(4-methoxyphenyl)-N-(4-((trimethylsilyl)-ethynyl)phenyl)aniline.

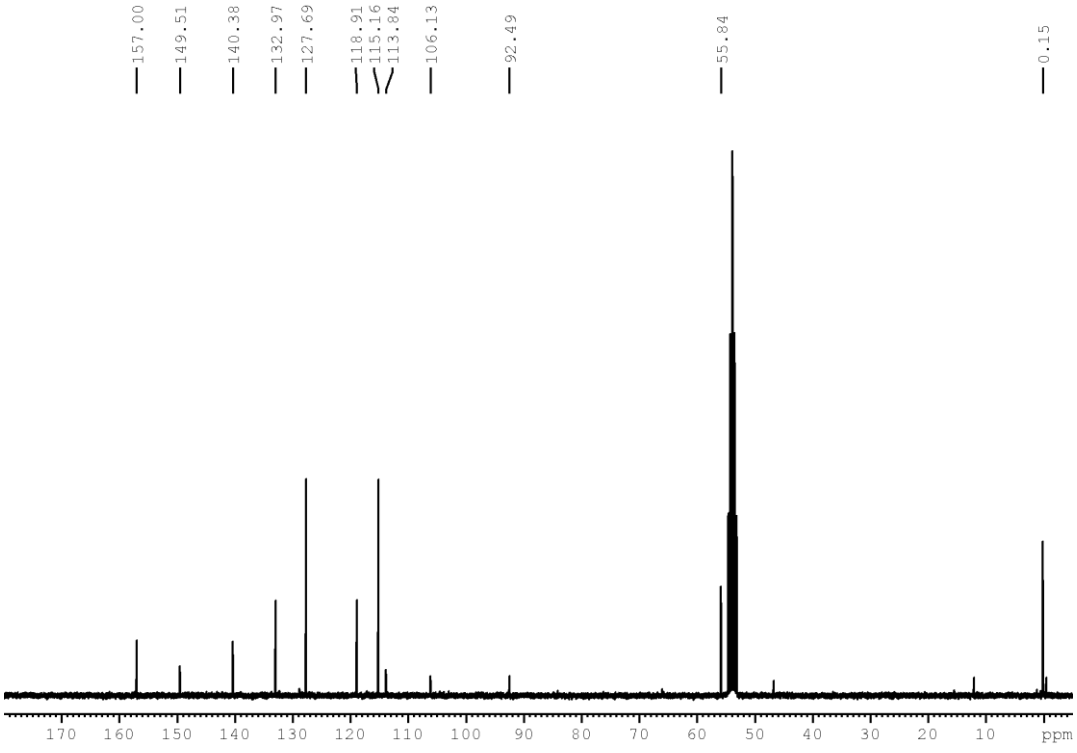

^{13}C{^{1}H} NMR spectrum (75 MHz, CD_2Cl_2) of 4-methoxy-N-(4-methoxyphenyl)-N-(4-((trimethylsilyl)-ethynyl)phenyl)aniline.

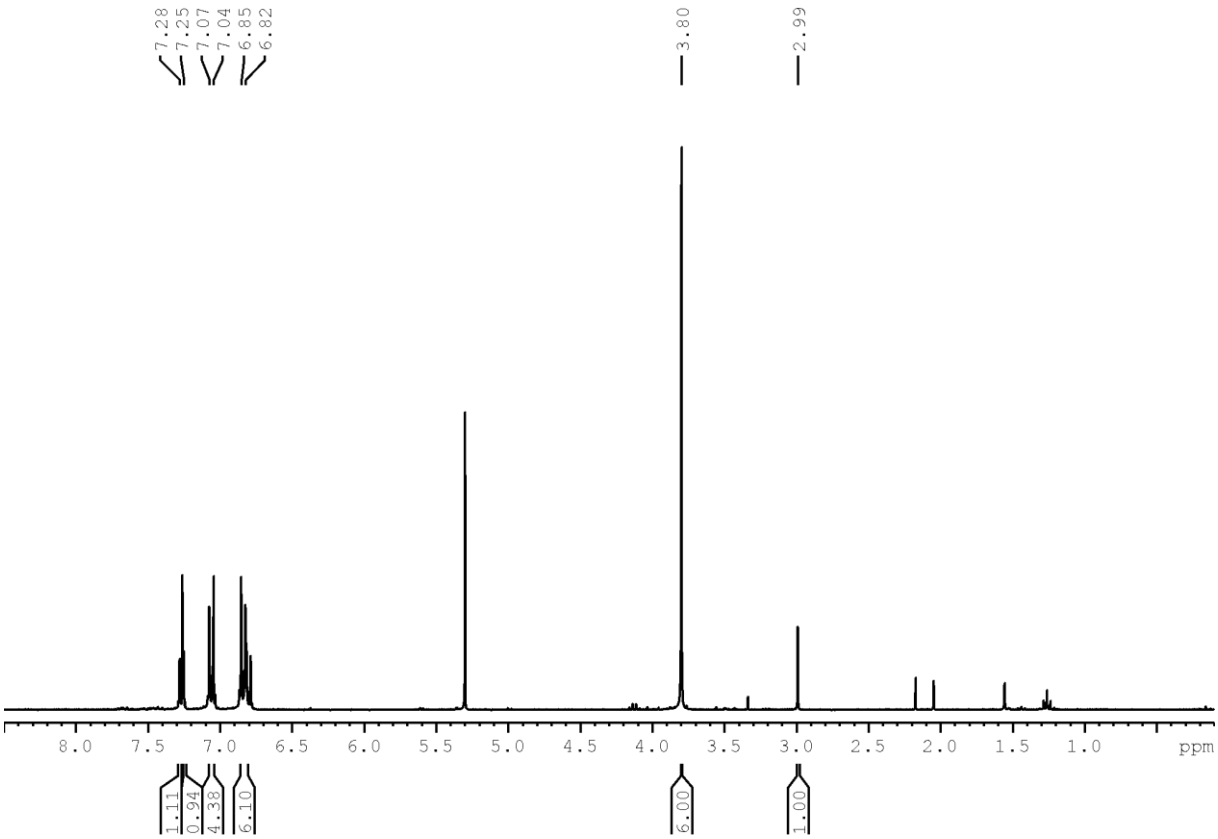

^{1}H NMR spectrum (300 MHz, $CDCl_3$) of 4-ethynyl-*N,N*-bis(4-methoxyphenyl)aniline.

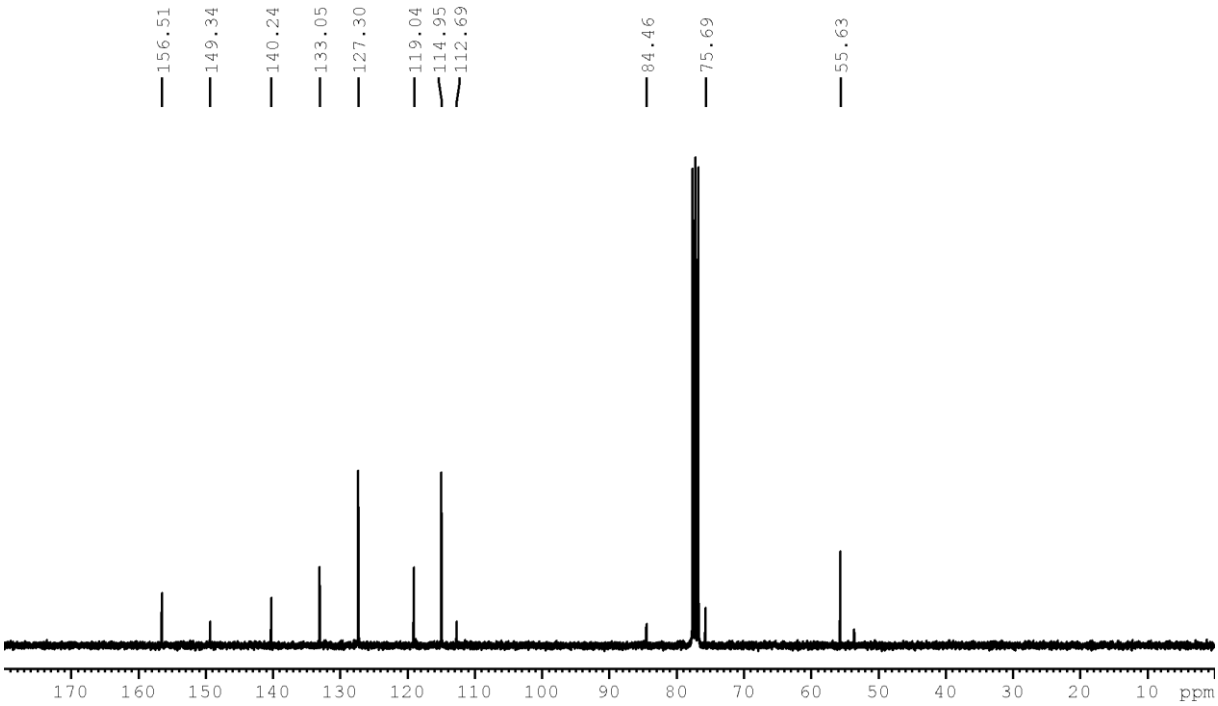

$^{13}C\{^{1}H\}$ NMR spectrum (75 MHz, $CDCl_3$) of 4-ethynyl-*N,N*-bis(4-methoxyphenyl)aniline.

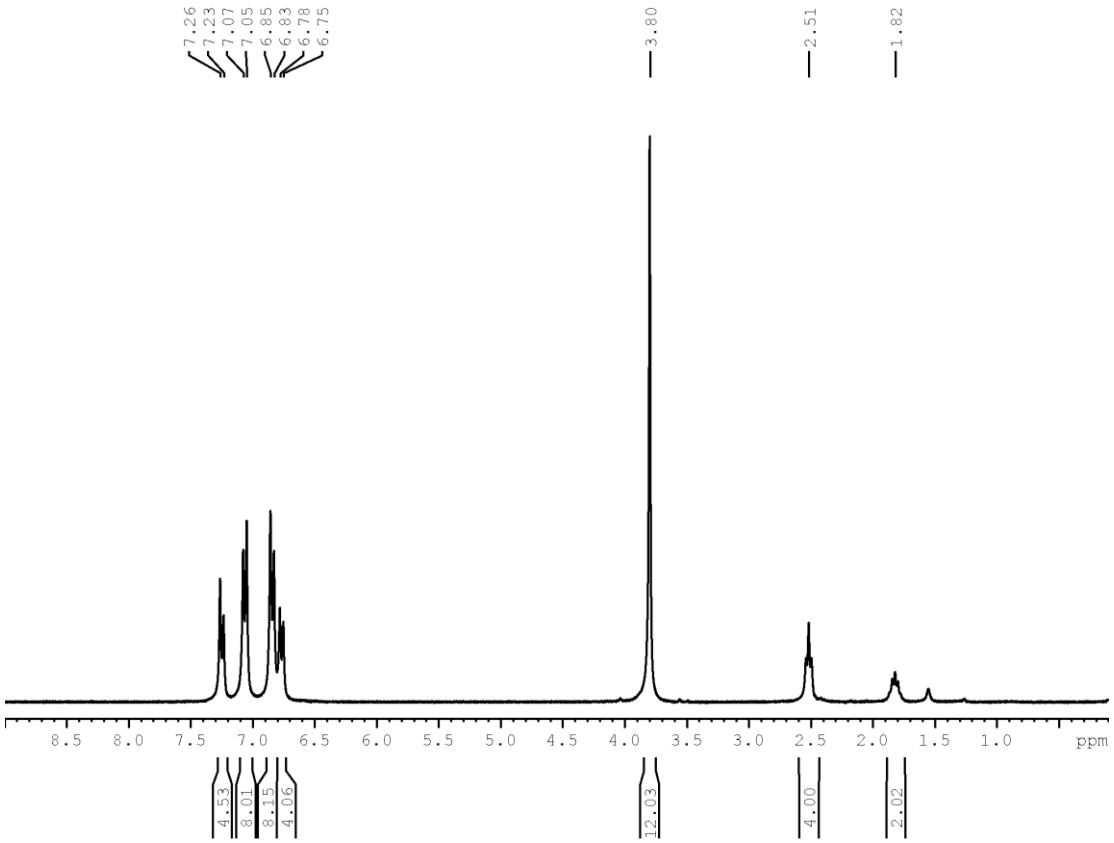

^{1}H NMR spectrum (300 MHz, $CDCl_3$) of 4,4’-(undeca-1,3,8,10-tetrayne-1,11-diyl)bis(N,N-bis(4-methoxyphenyl)aniline).

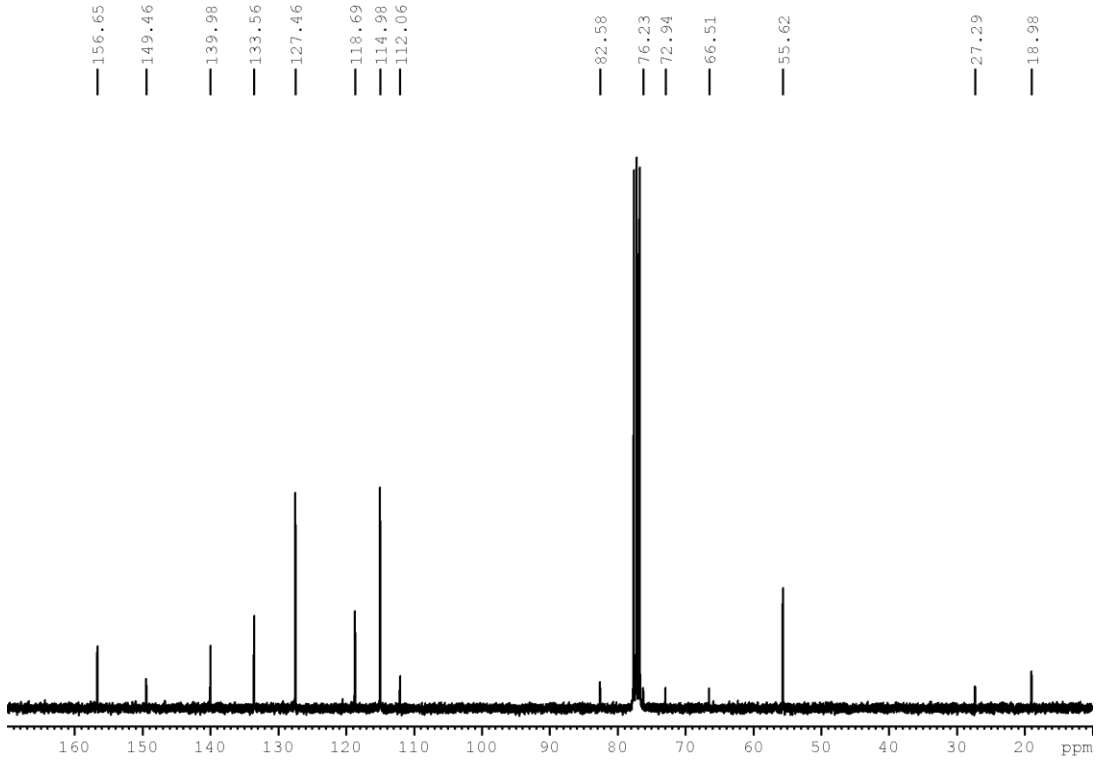

^{13}C{^{1}H} NMR spectrum (75 MHz, $CDCl_3$) of 4,4’-(undeca-1,3,8,10-tetrayne-1,11-diyl)bis(N,N-bis(4-methoxyphenyl)aniline).

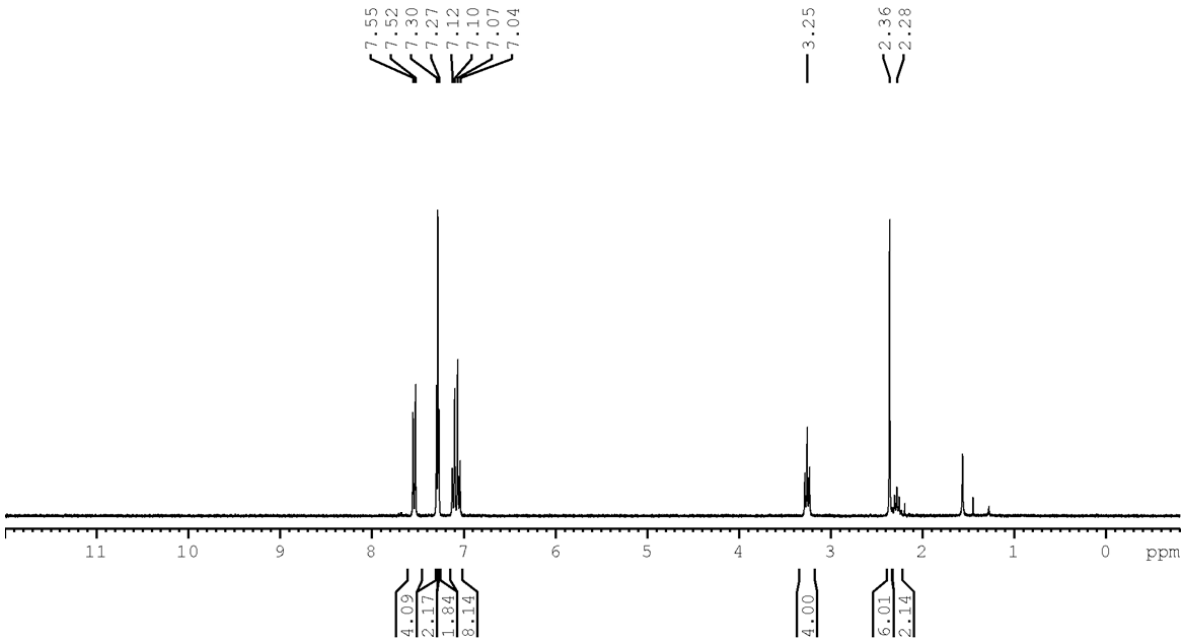

^{1}H NMR spectrum (300 MHz, $CDCl_3$) of **2-4**

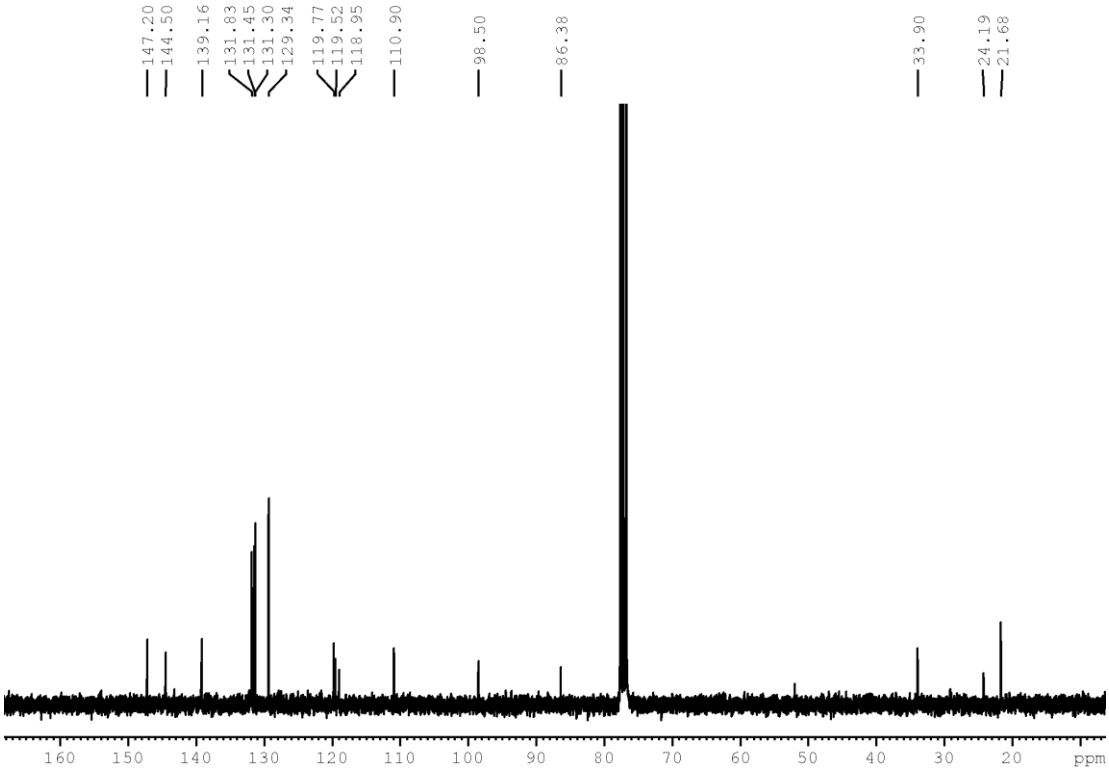

^{13}C{^{1}H} NMR spectrum (75 MHz, $CDCl_3$) of **2-4.**

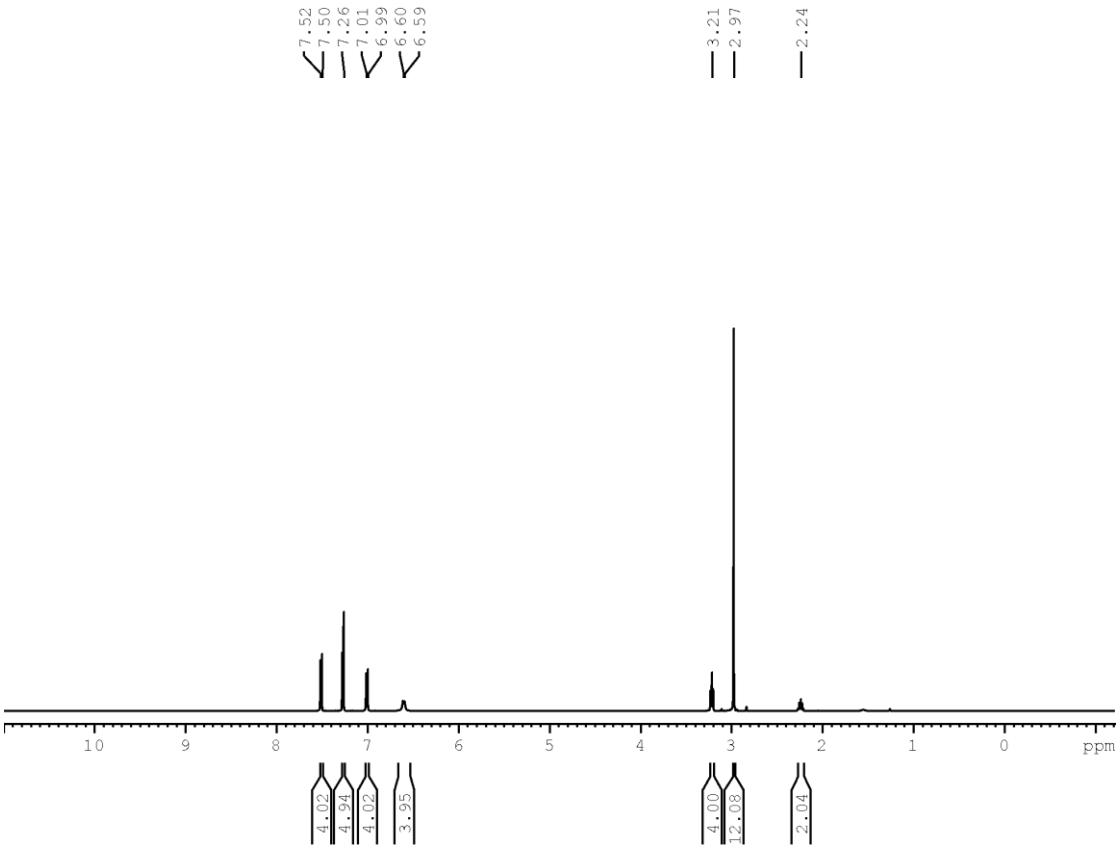

^{1}H NMR spectrum (300 MHz, $CDCl_3$) of **2-5**.

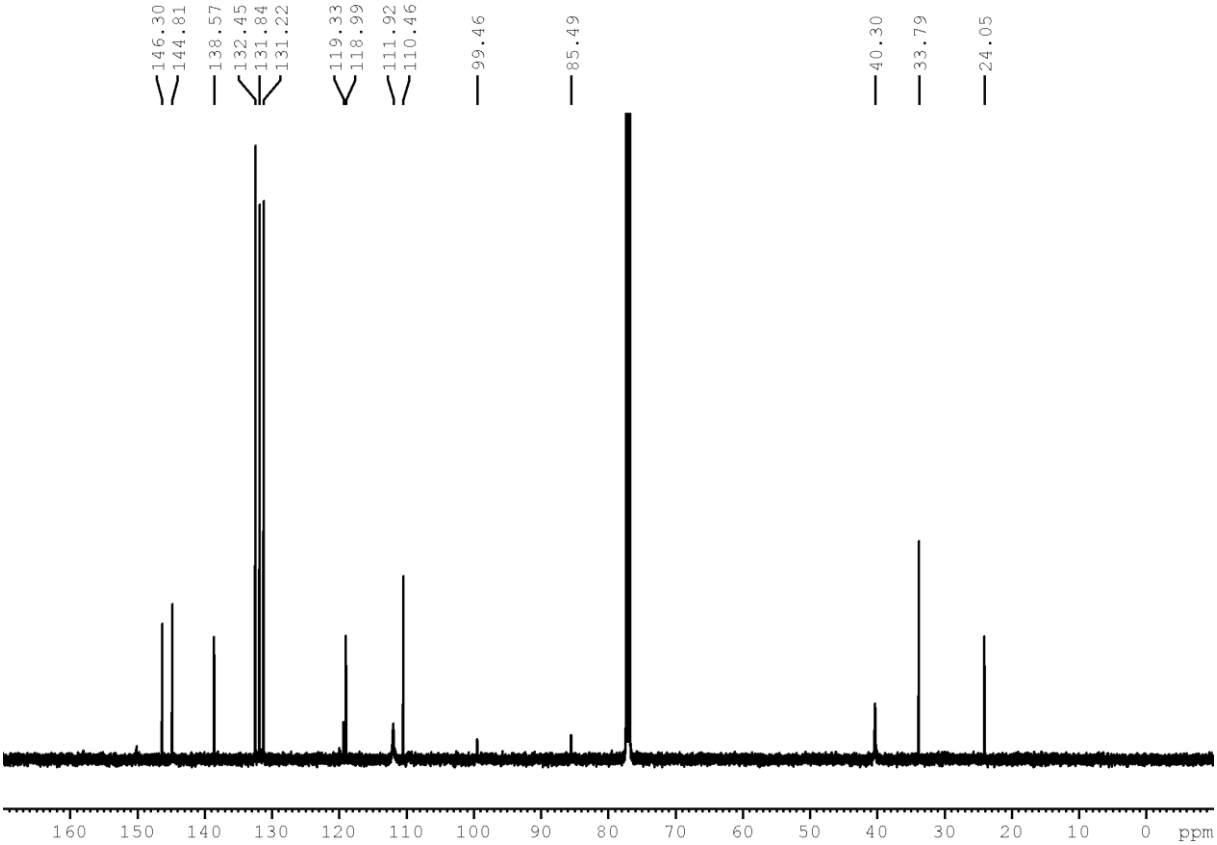

^{13}C{^{1}H} spectrum NMR (75 MHz, $CDCl_3$) of **2-5.**

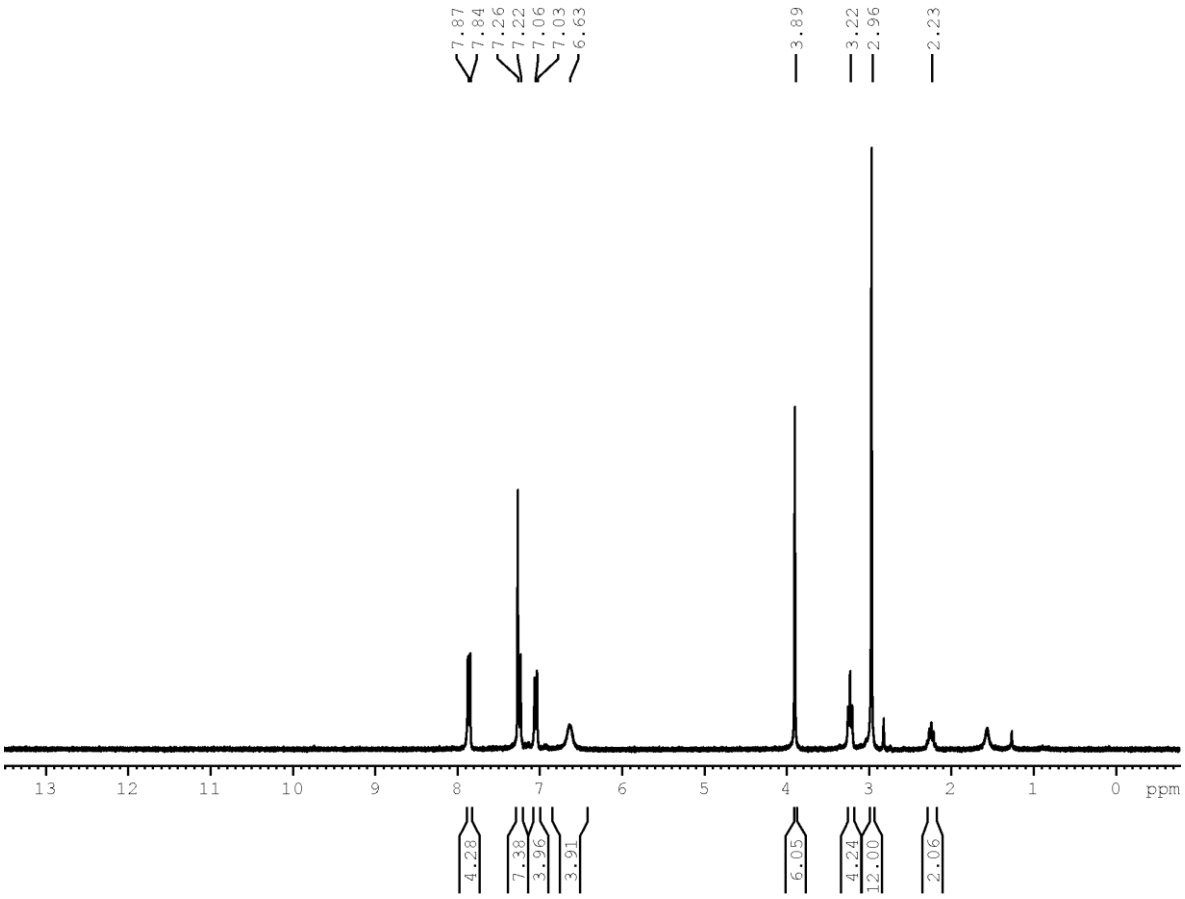

^{1}H NMR spectrum (300 MHz, $CDCl_3$) of **2-6**.

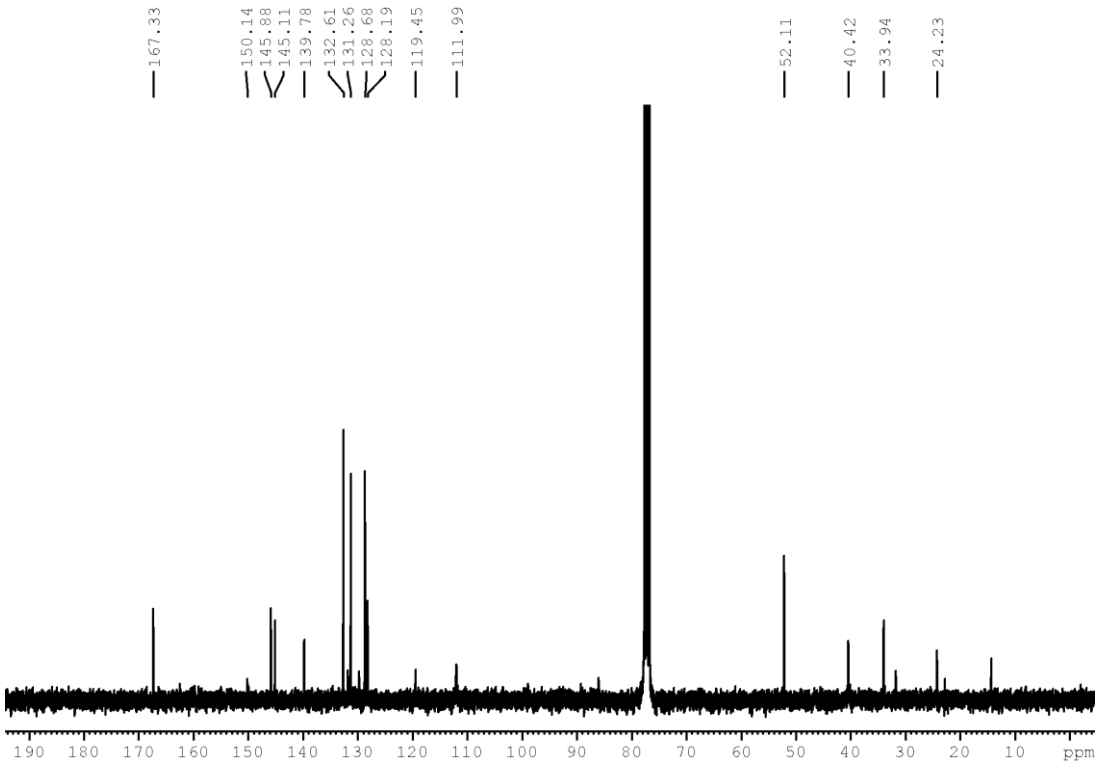

$^{13}C\{^{1}H\}$ NMR spectrum (75 MHz, $CDCl_3$) of **2-6.**

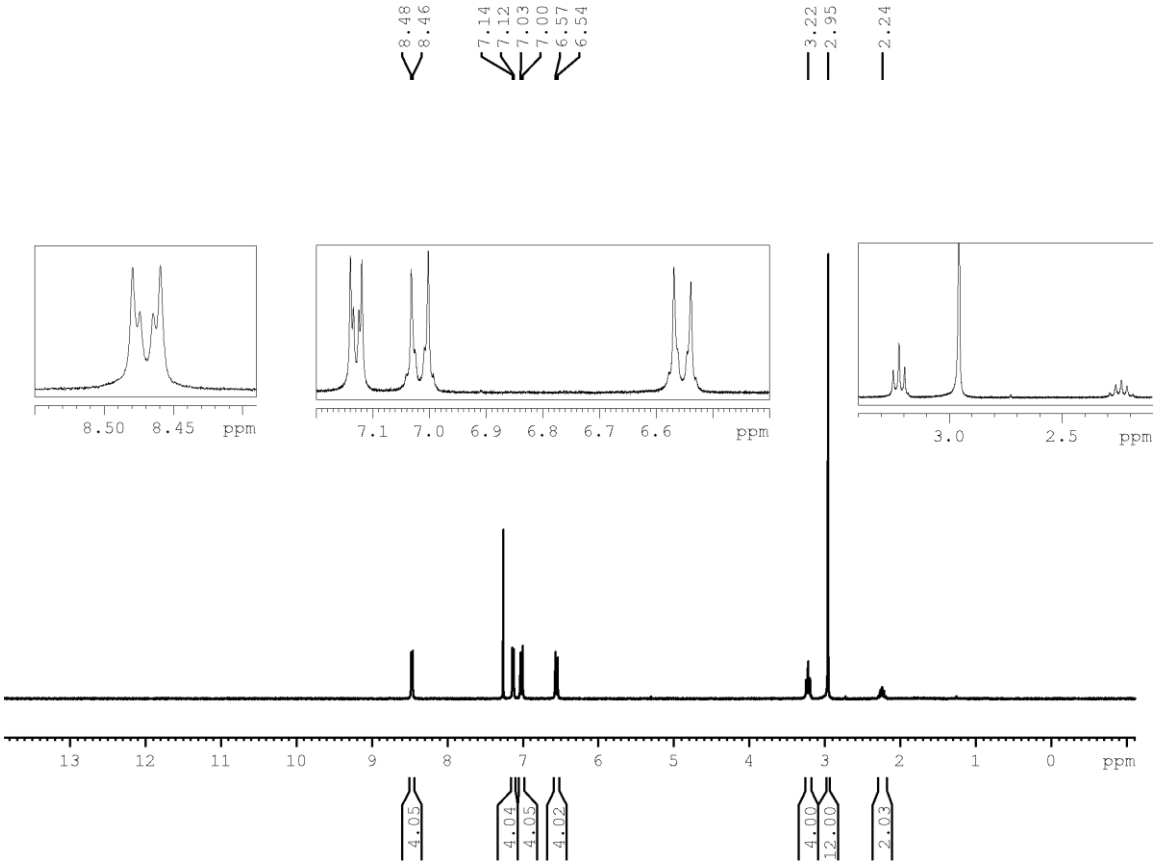

^{1}H NMR spectrum (300 MHz, $CDCl_3$) of compound **2-7.**

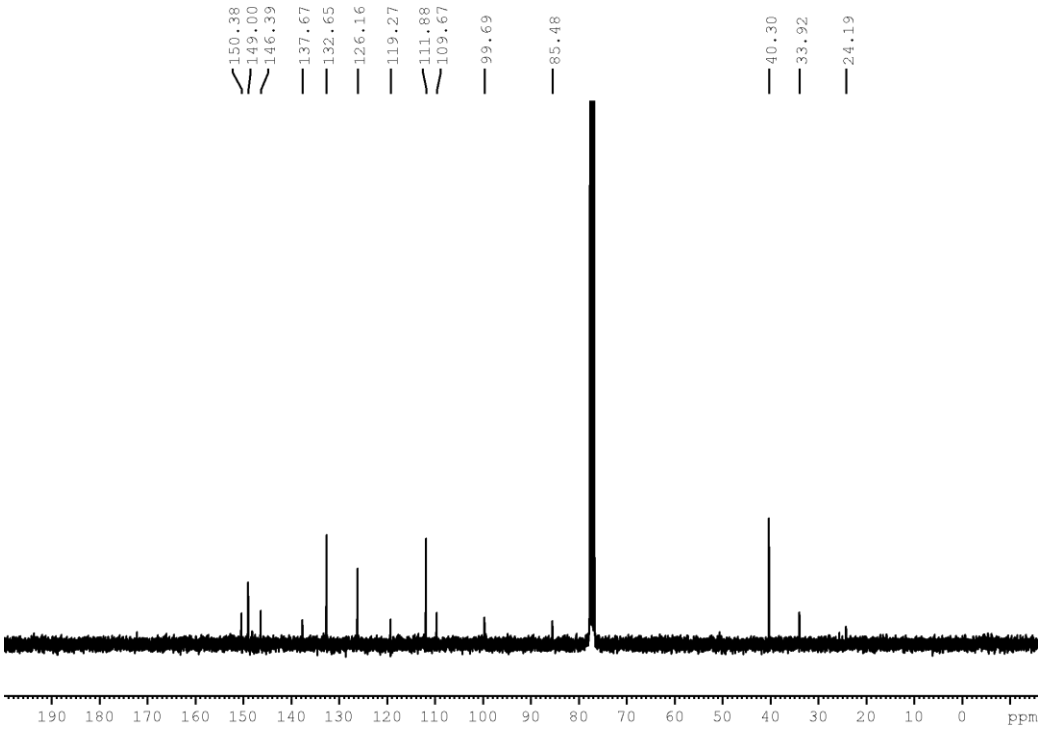

$^{13}C\{^{1}H\}$ NMR spectrum (75 MHz, $CDCl_3$) of **2-7.**

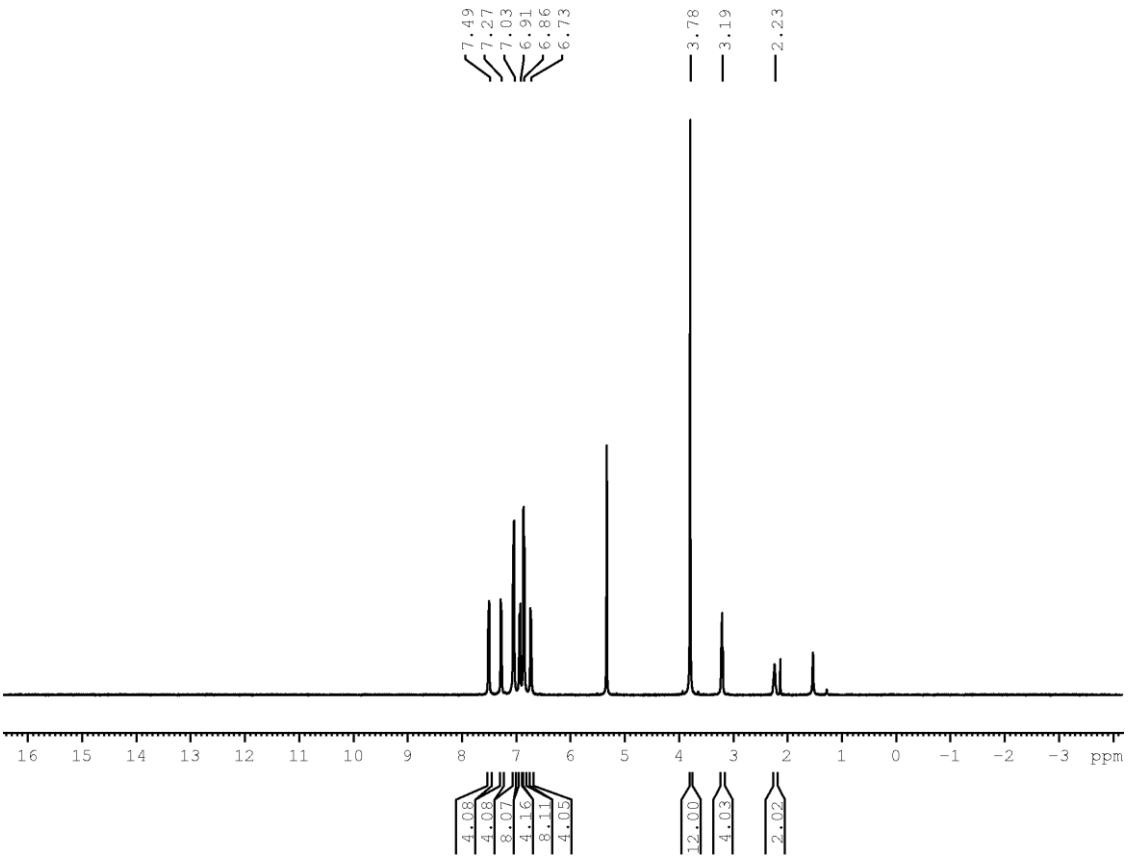

^{1}H NMR spectrum (500 MHz, C_2DCl_2) of **2-8.**

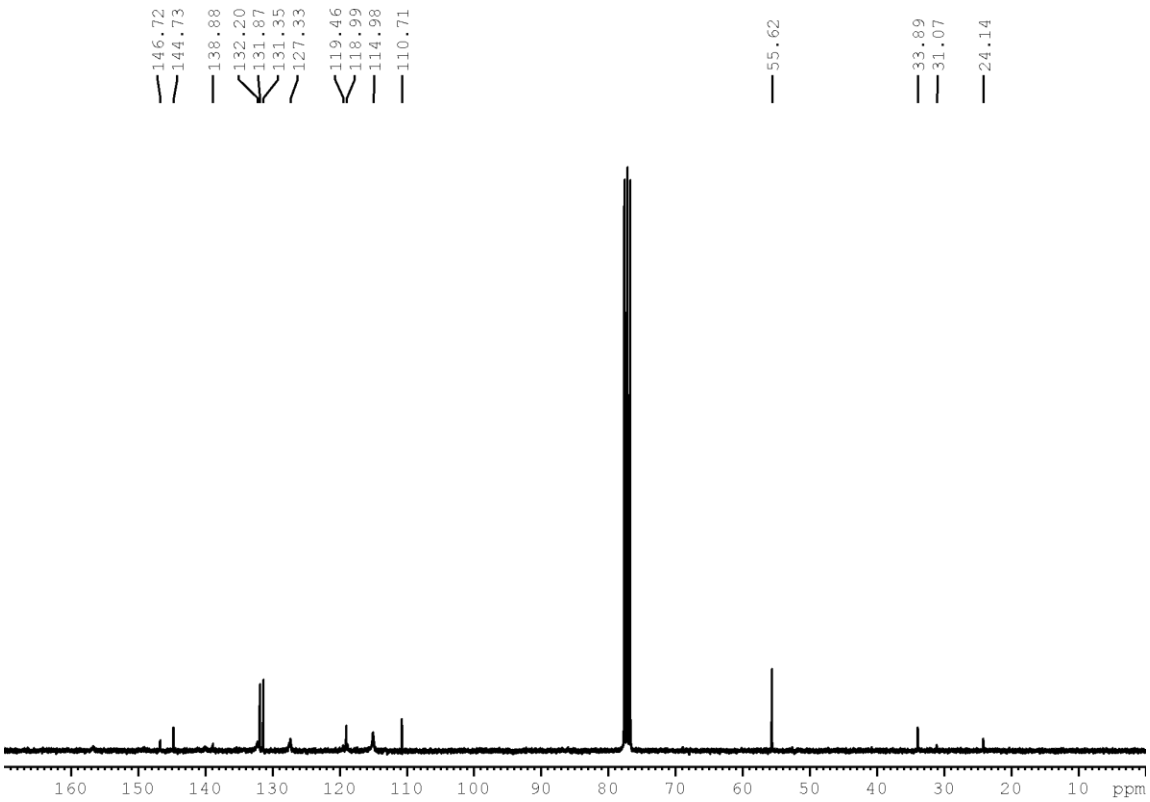

^{13}C{^{1}H} NMR spectrum (125 MHz, C_2DCl_2) of **2-8.**

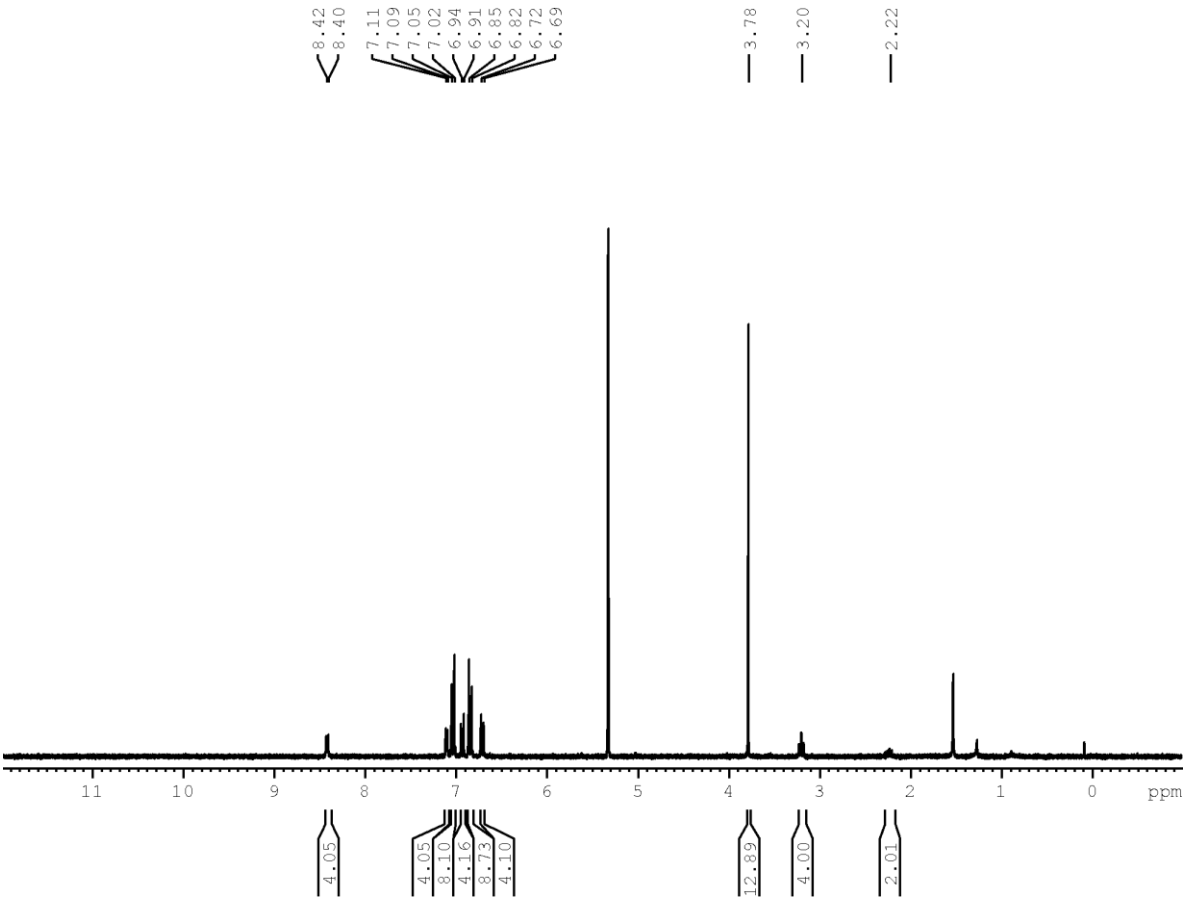

^{1}H NMR spectrum (300 MHz, C_2DCl_2) of **2-9.**

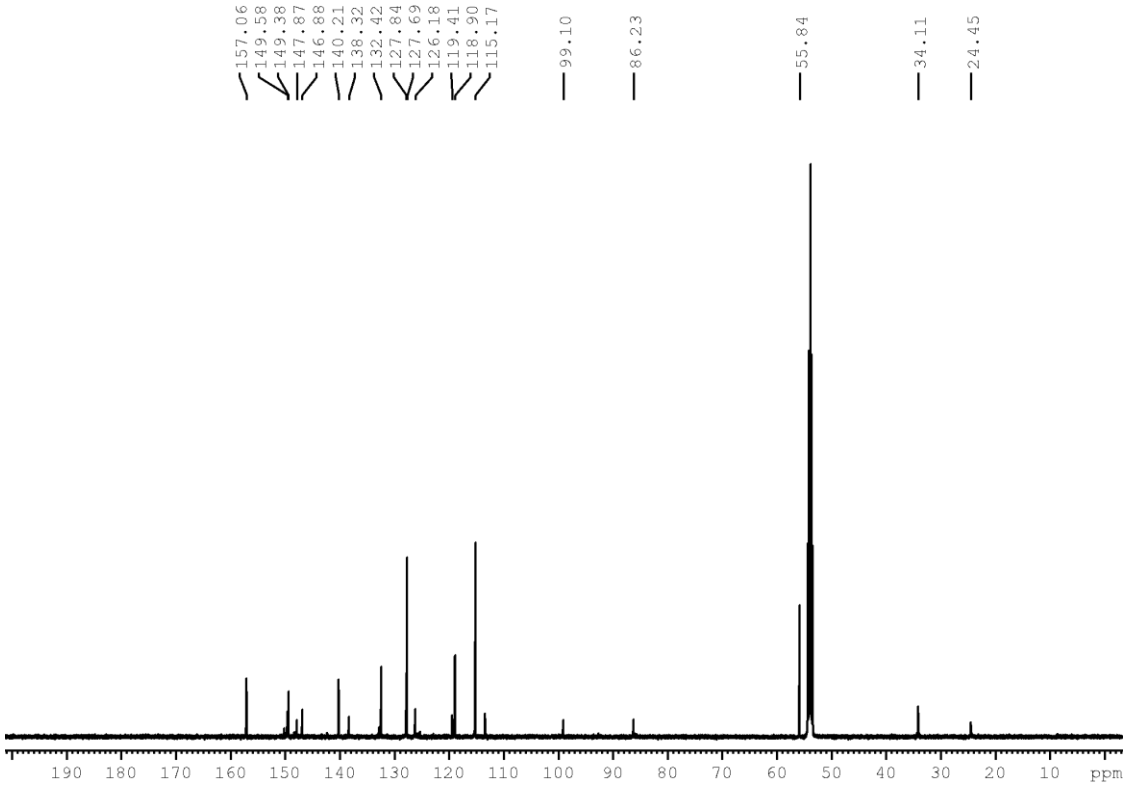

^{13}C{^{1}H} NMR spectrum (75 MHz, C_2DCl_2) of **2-9**.

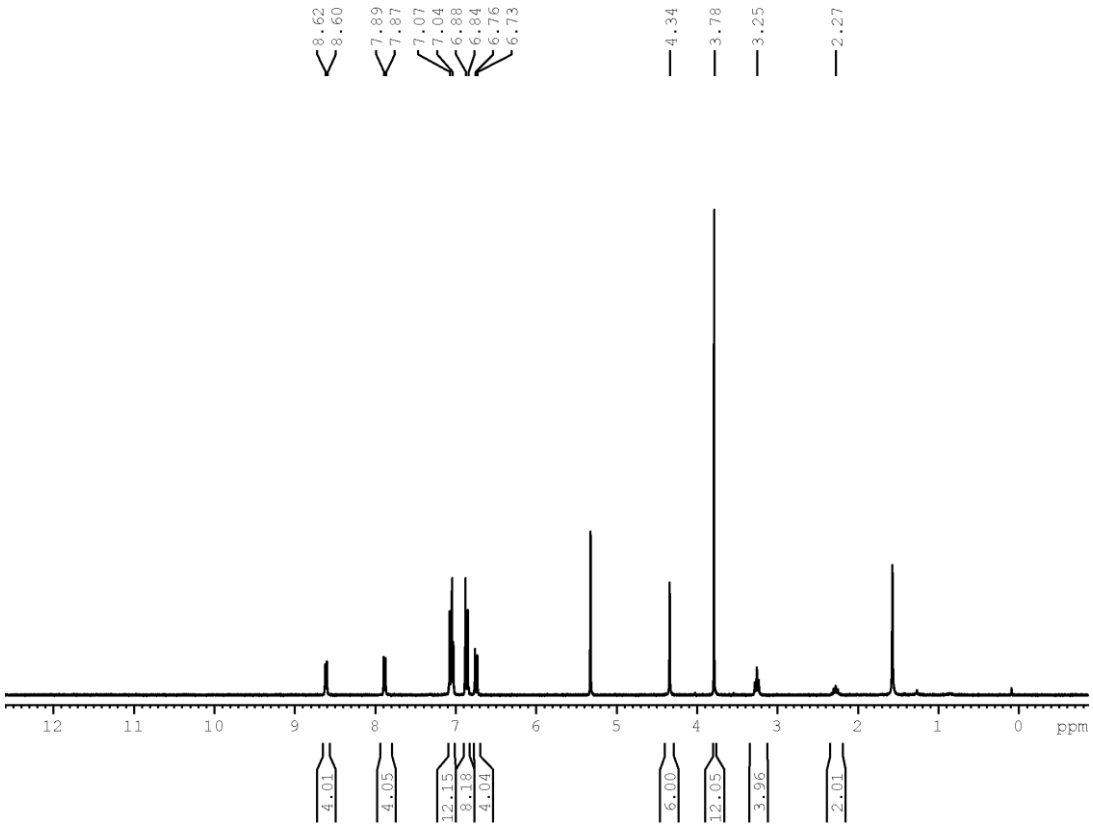

^{1}H NMR spectrum (300 MHz, C_2DCl_2) of **2-10.**

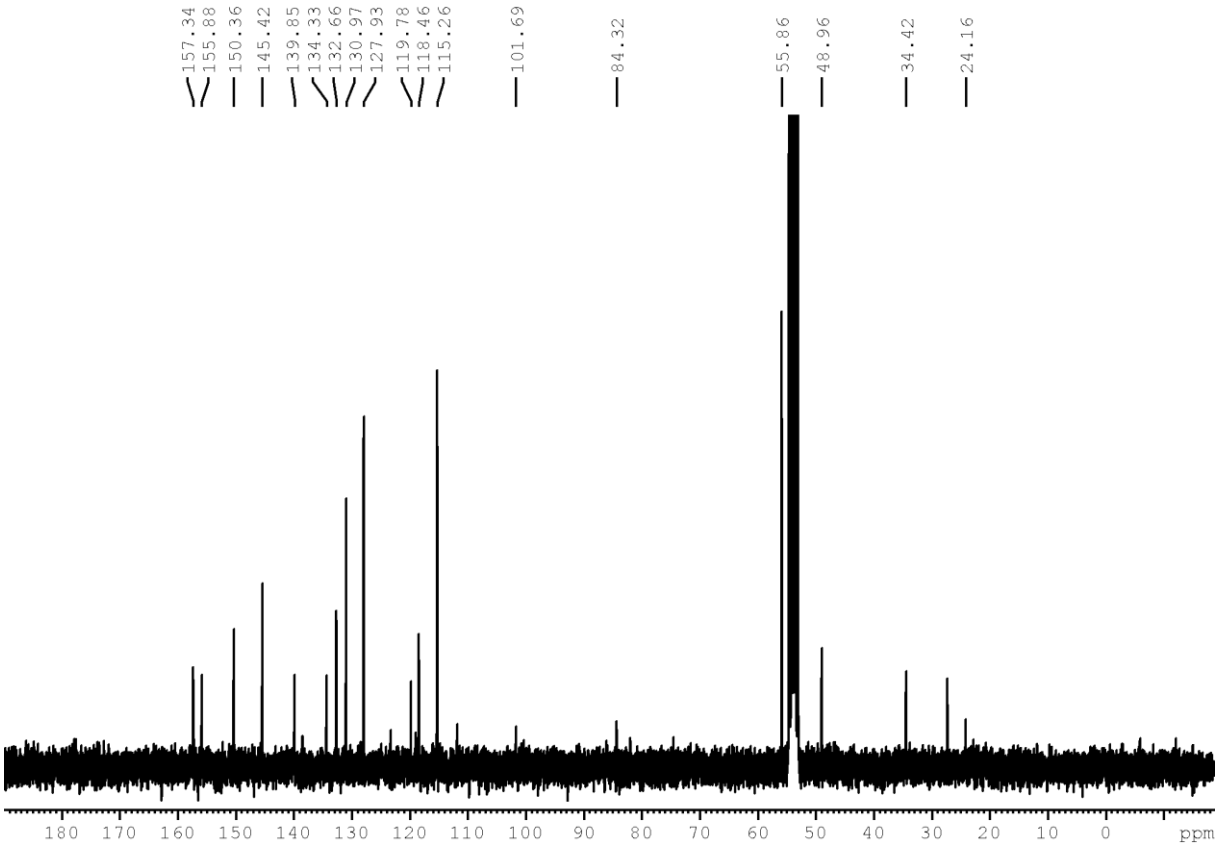

$^{13}C\{^{1}H\}$ NMR spectrum (75 MHz, C_2DCl_2) of **2-10.**

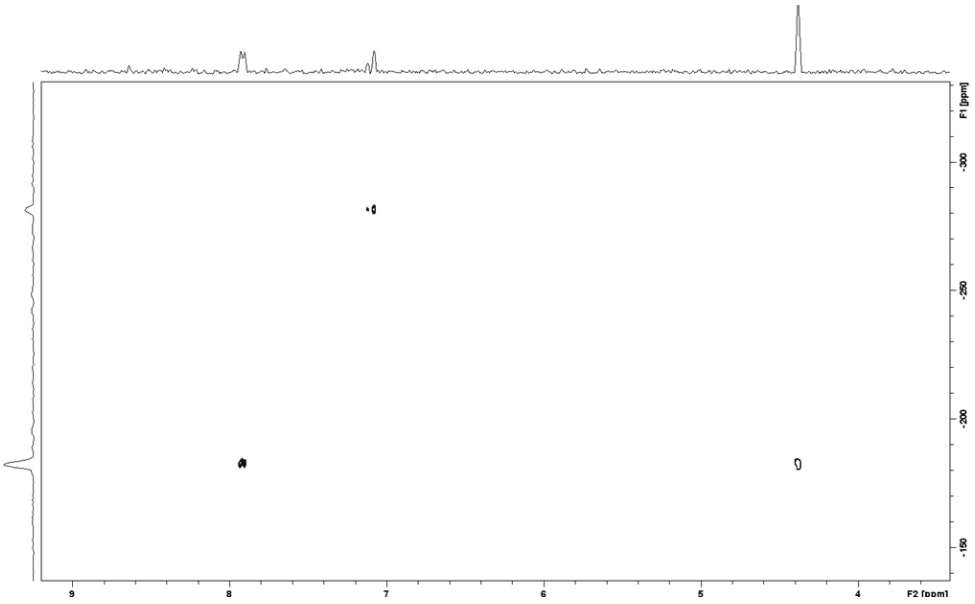

^{15}N-HMBC (300/30 MHz, CD_2Cl_2) spectrum of **2-10**. Left projection: ^{15}N, top projection: ^{1}H.

The signal on the top stems from the coupling of the triphenyl amine nitrogen with the neighboring phenyl hydrogen atoms. The signal on the bottom left of the spectrum stems from the coupling of the pyridine nitrogen with the pyridine hydrogens, while the signal on the bottom right stems from the coupling of pyridine nitrogen with the six methyl hydrogen atoms, which proves that the methylation took place on the pyridine and not on the triphenyl amine nitrogen.

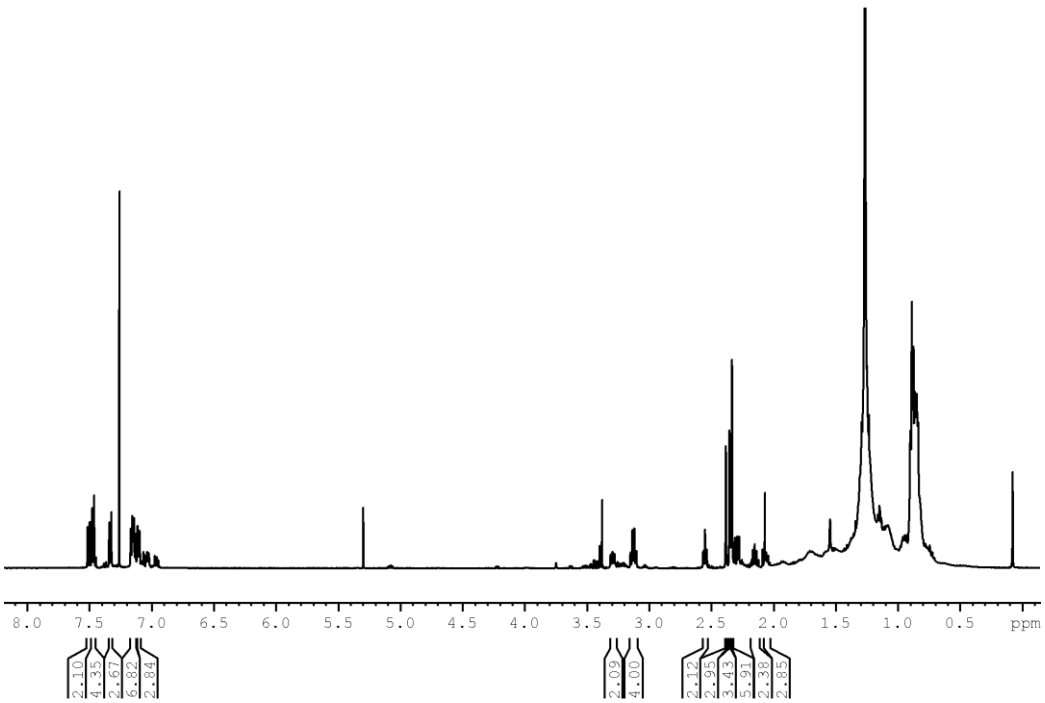

^{1}H NMR spectrum (300 MHz, $CDCl_3$) of **2-2.**

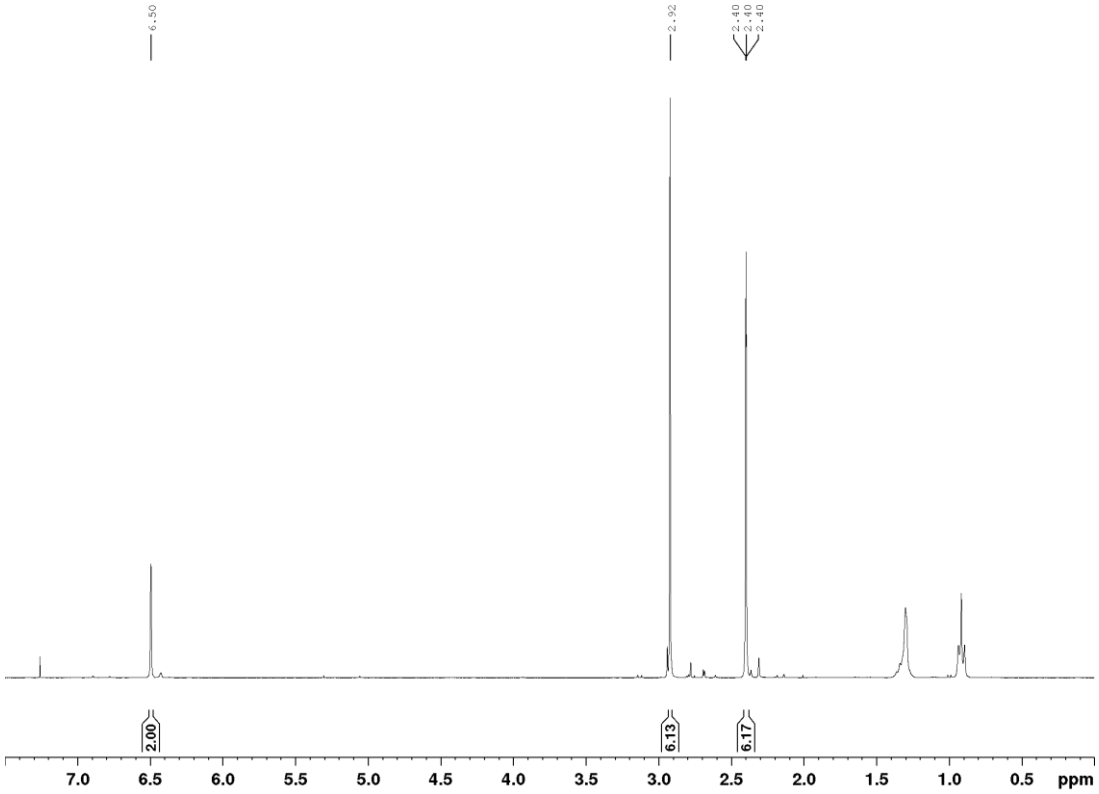

*^{1}H NMR spectrum (300 MHz) of **3-2** in $CDCl_3$. The spectrum was recorded of the crude material and contains solvent & grease signals.*

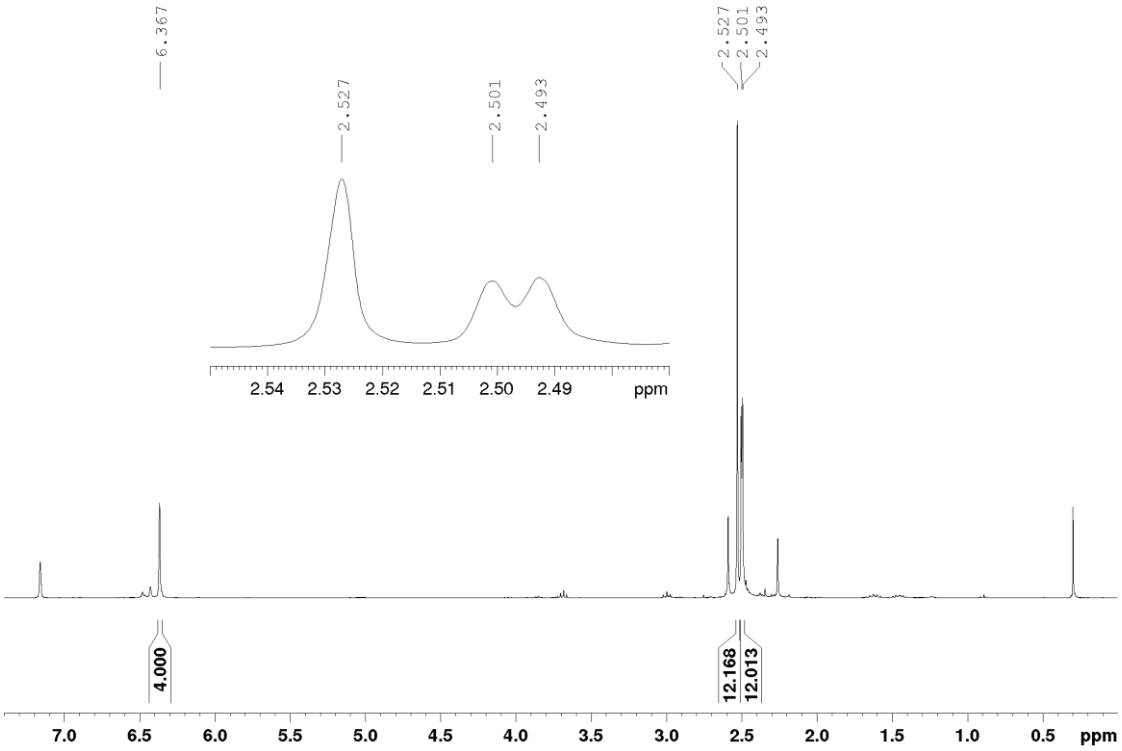

*^{1}H NMR spectrum (300 MHz) of **3-3** in C_6D_6. The spectrum was recorded of the crude material and contains solvent & grease signals.*

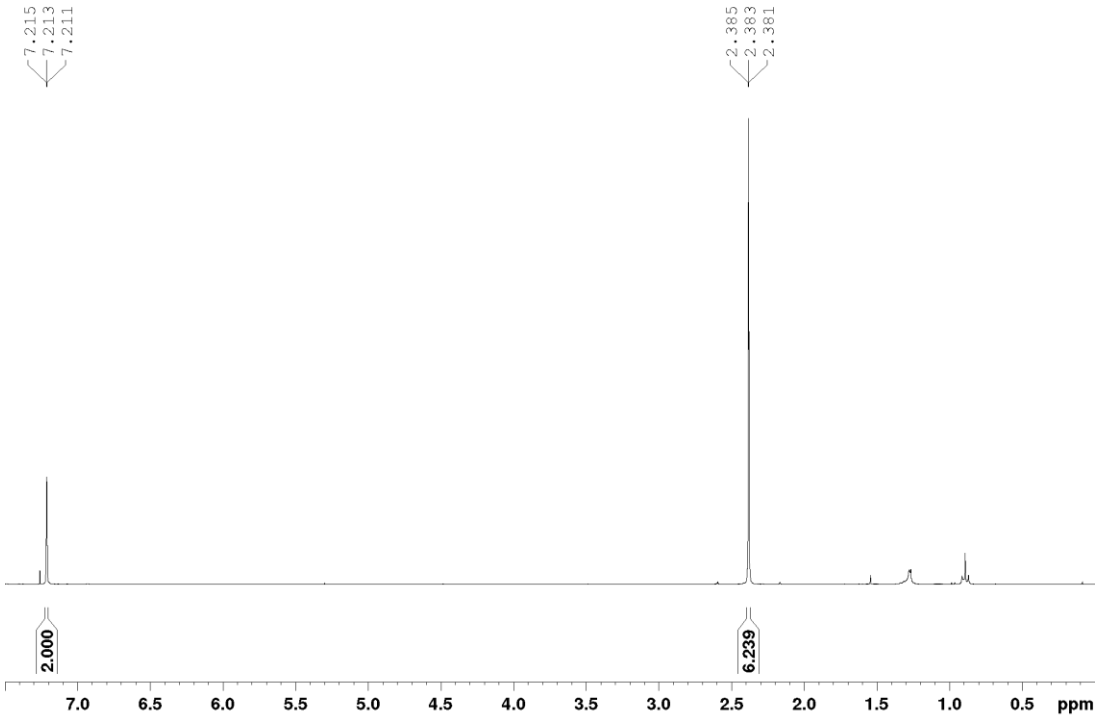

*^{1}H NMR spectrum (300 MHz) of **3-5** in $CDCl_3$. The spectrum was recorded of the crude material and contains solvent signals.*

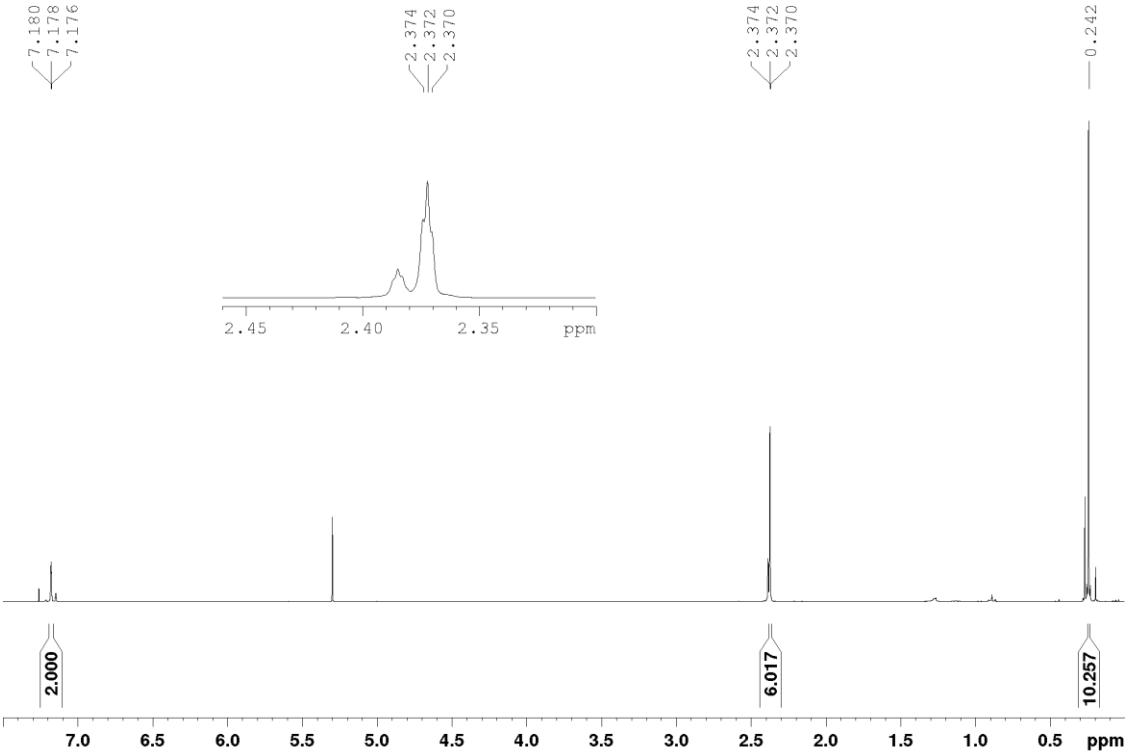

*^{1}H NMR spectrum (300 MHz) of **3-6** in $CDCl_3$. The spectrum was recorded of the crude material and contains solvent signals.*

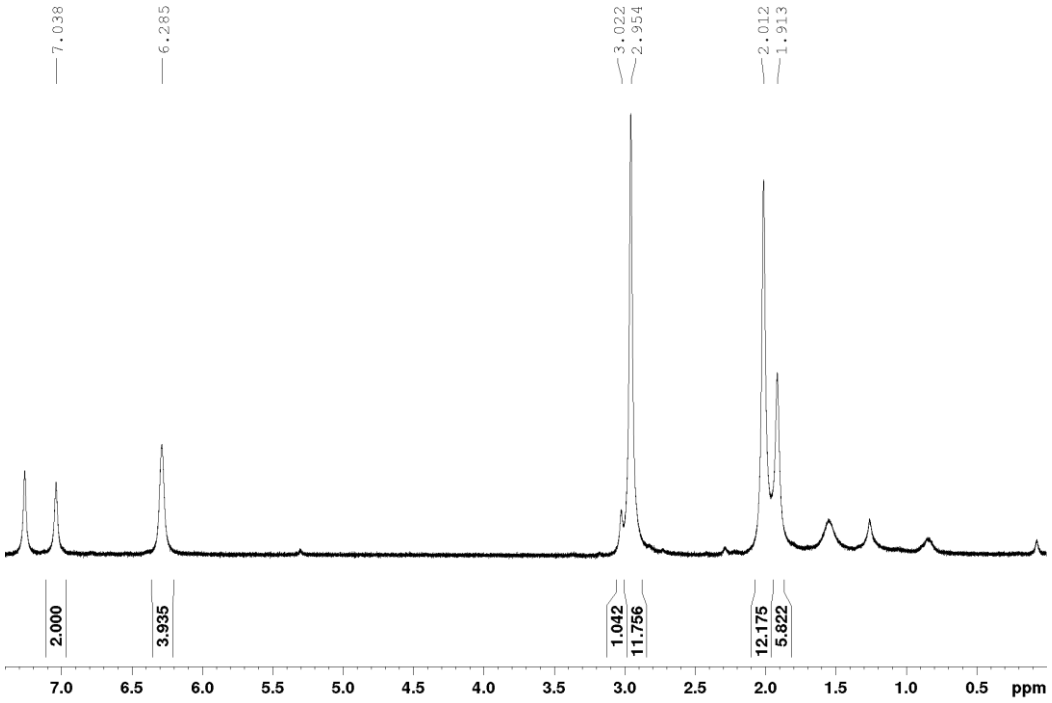

*^{1}H NMR spectrum (300 MHz) of **3-8** in $CDCl_3$. The spectrum was recorded of the crude material and contains solvent signals.*

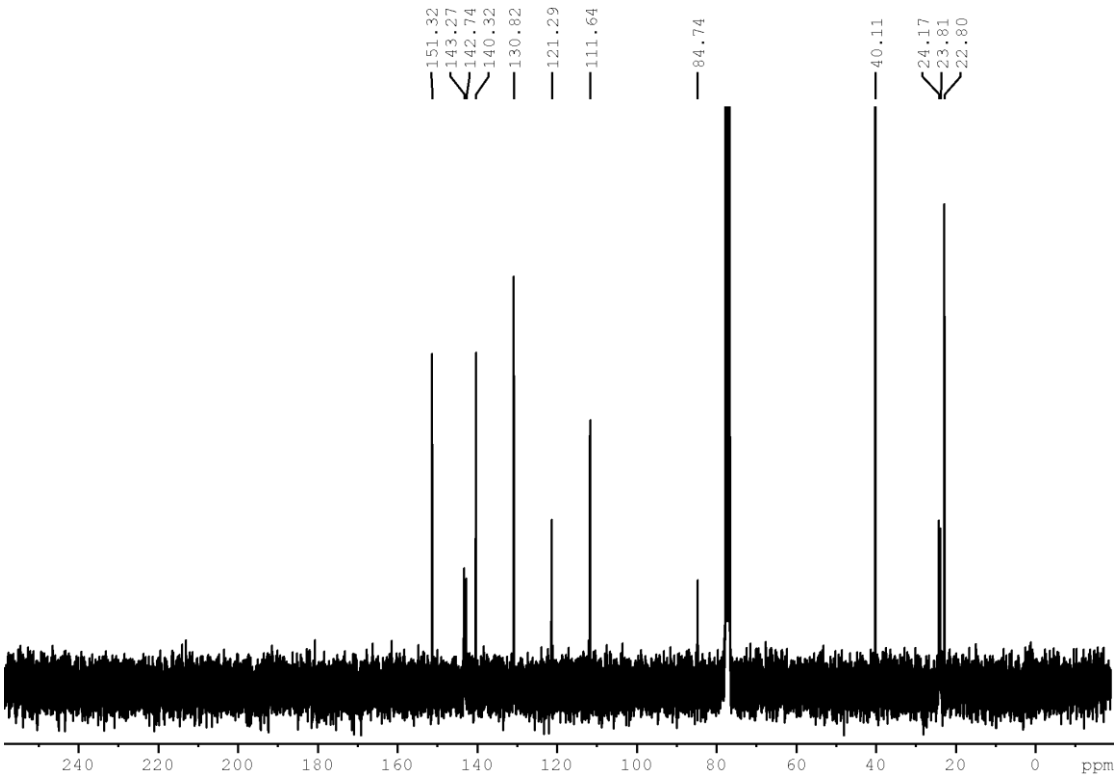

*$^{13}C\{^{1}H\}$ NMR spectrum (75 MHz) of **3-8** in $CDCl_3$.*

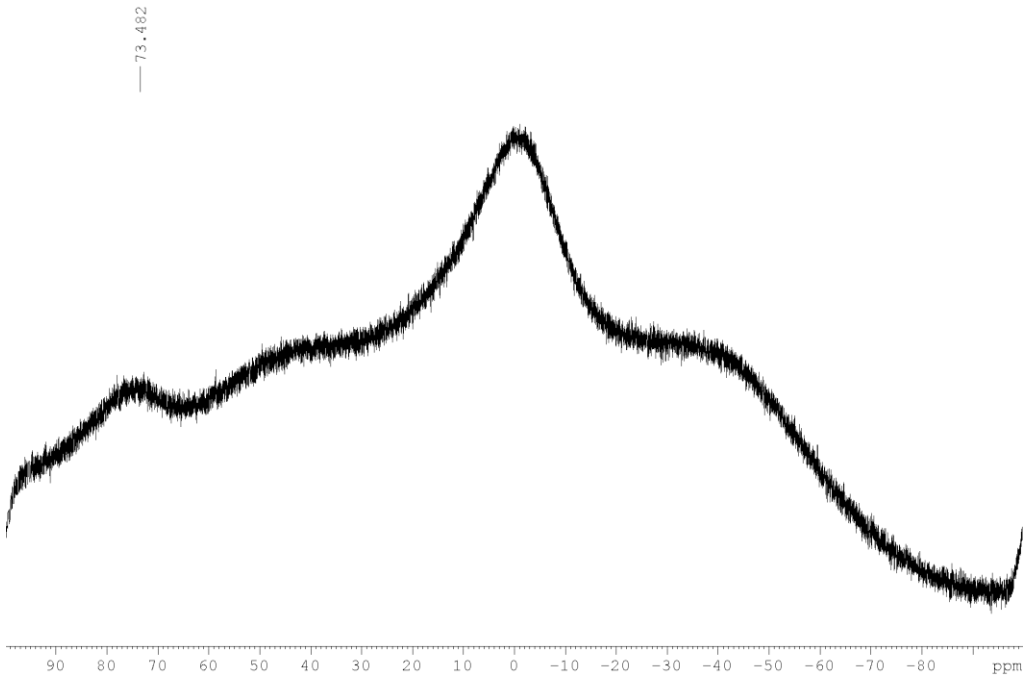

*Figure 121: $^{11}B\{^1H\}$ NMR spectrum (96 MHz) of **3-8** in $CDCl_3$.*

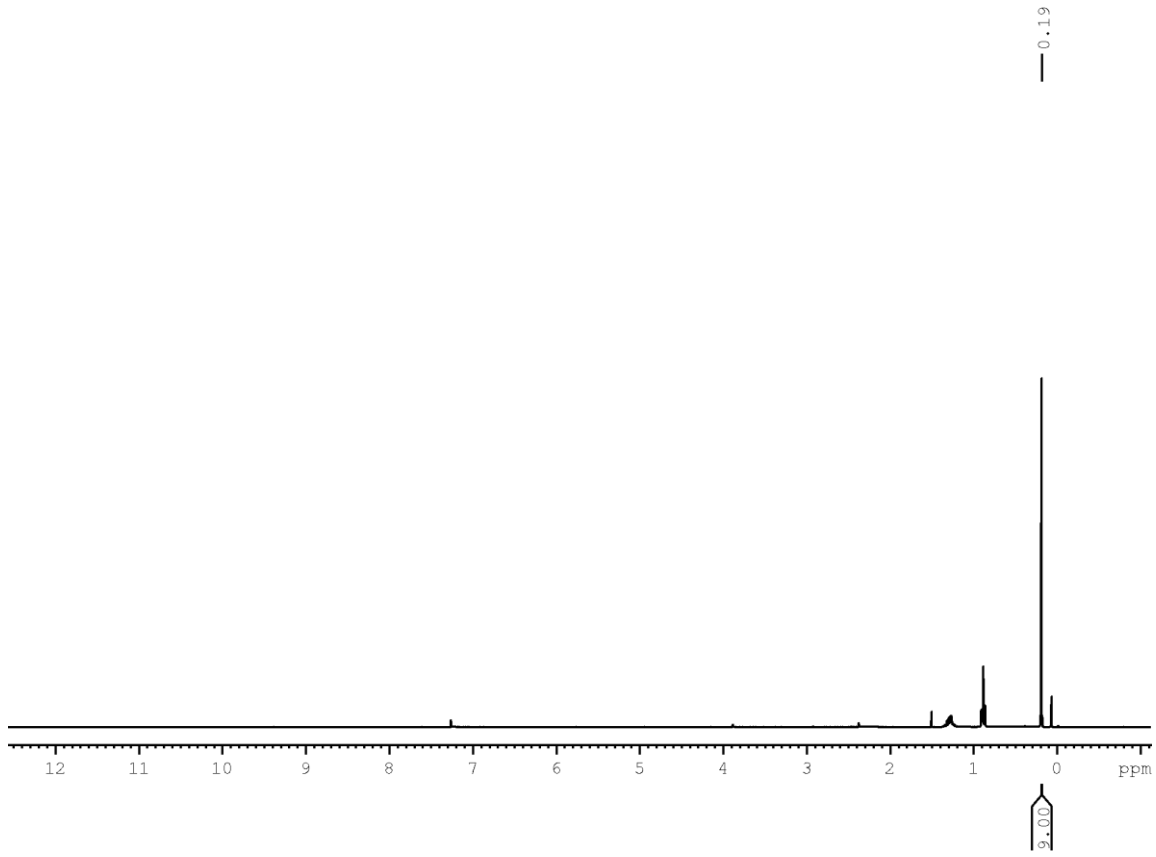

^1H NMR spectrum (300 MHz) of (bromoethynyl)trimethylsilane in $CDCl_3$. The spectrum was recorded of the crude material and contains solvent signals.

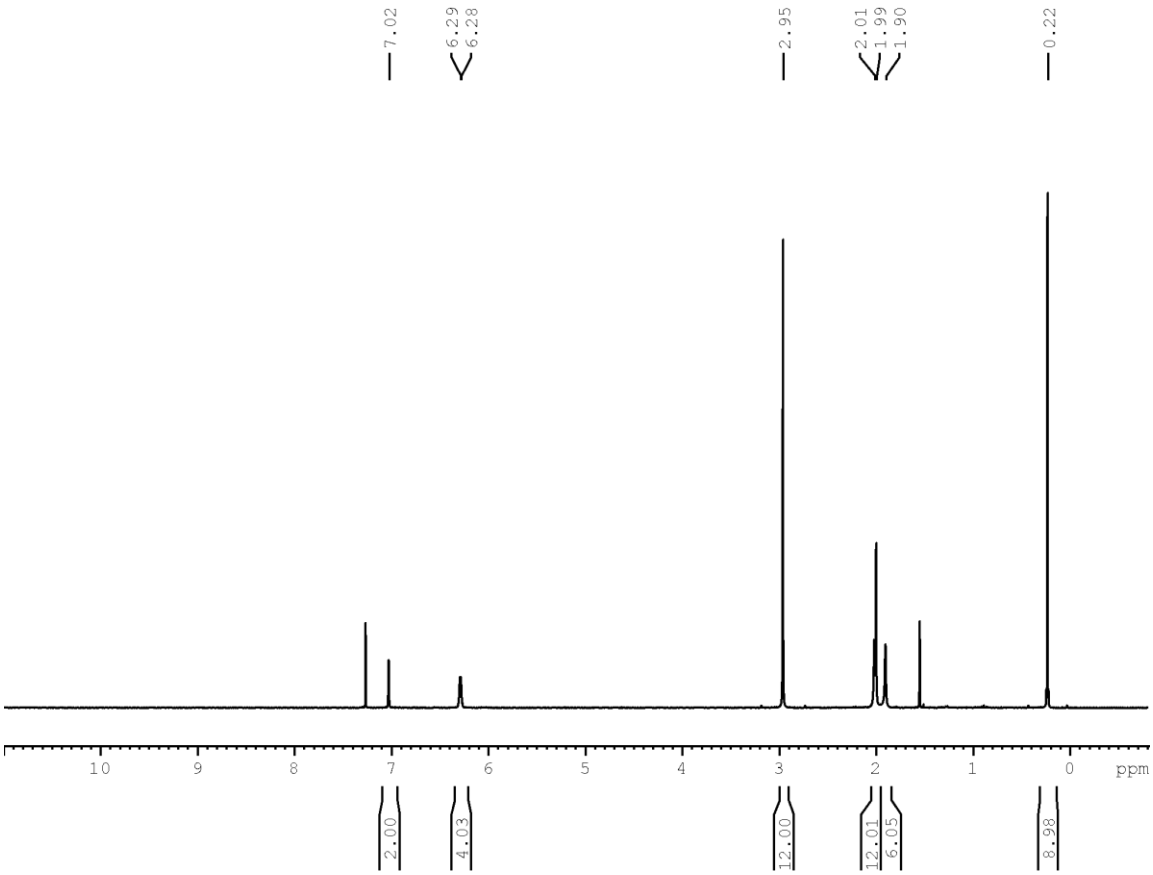

*^{1}H NMR spectrum (300 MHz) of **3-9** in $CDCl_3$.*

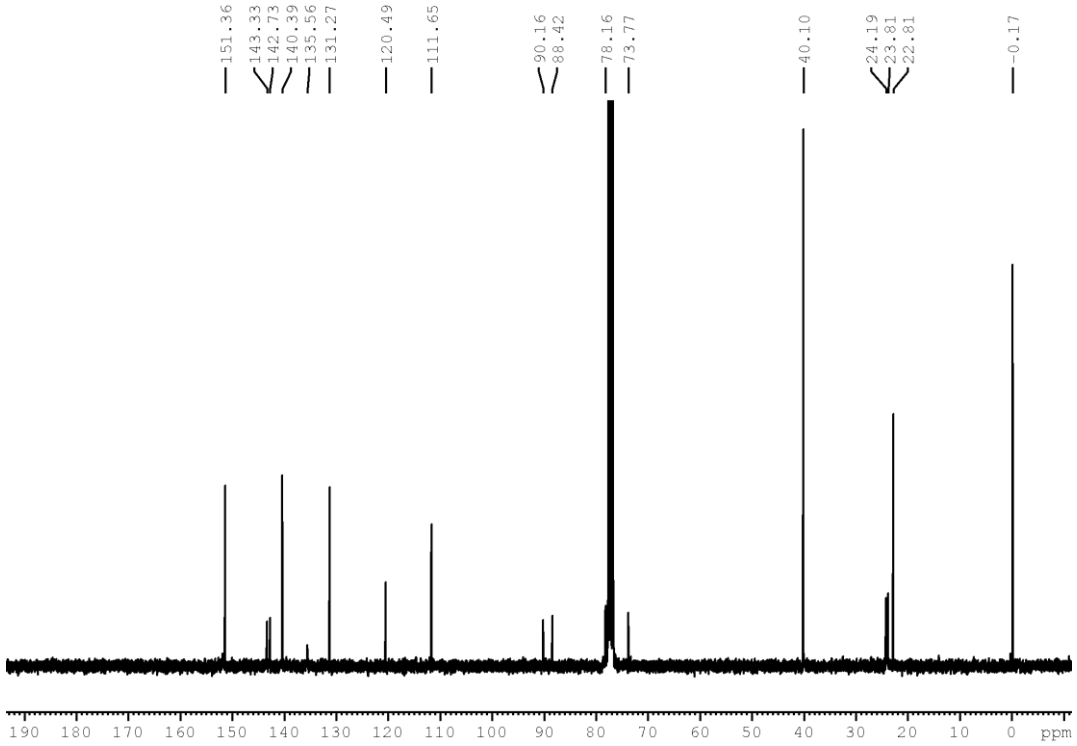

*$^{13}C\{^{1}H\}$ NMR spectrum (75 MHz) of **3-9** in $CDCl_3$.*

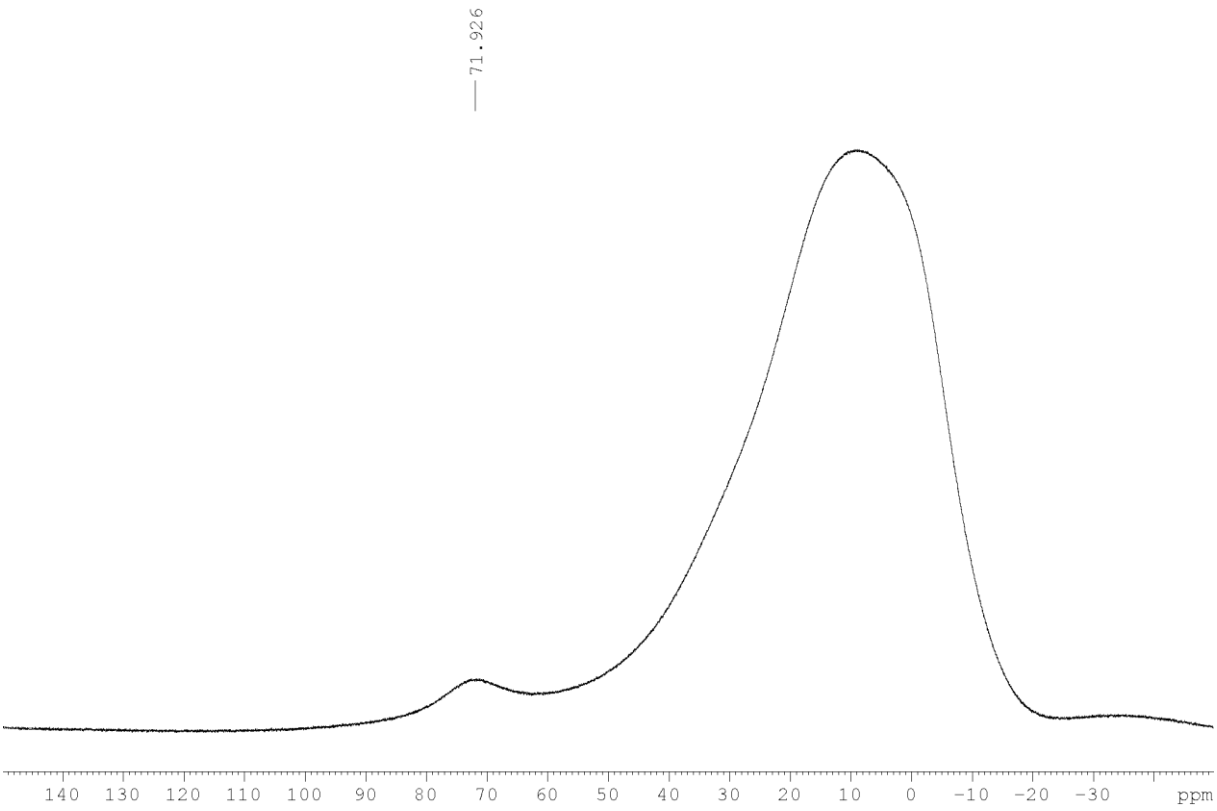

*Figure 122: $^{11}B\{^1H\}$ NMR spectrum (192 MHz) of **3-9** in $CDCl_3$.*

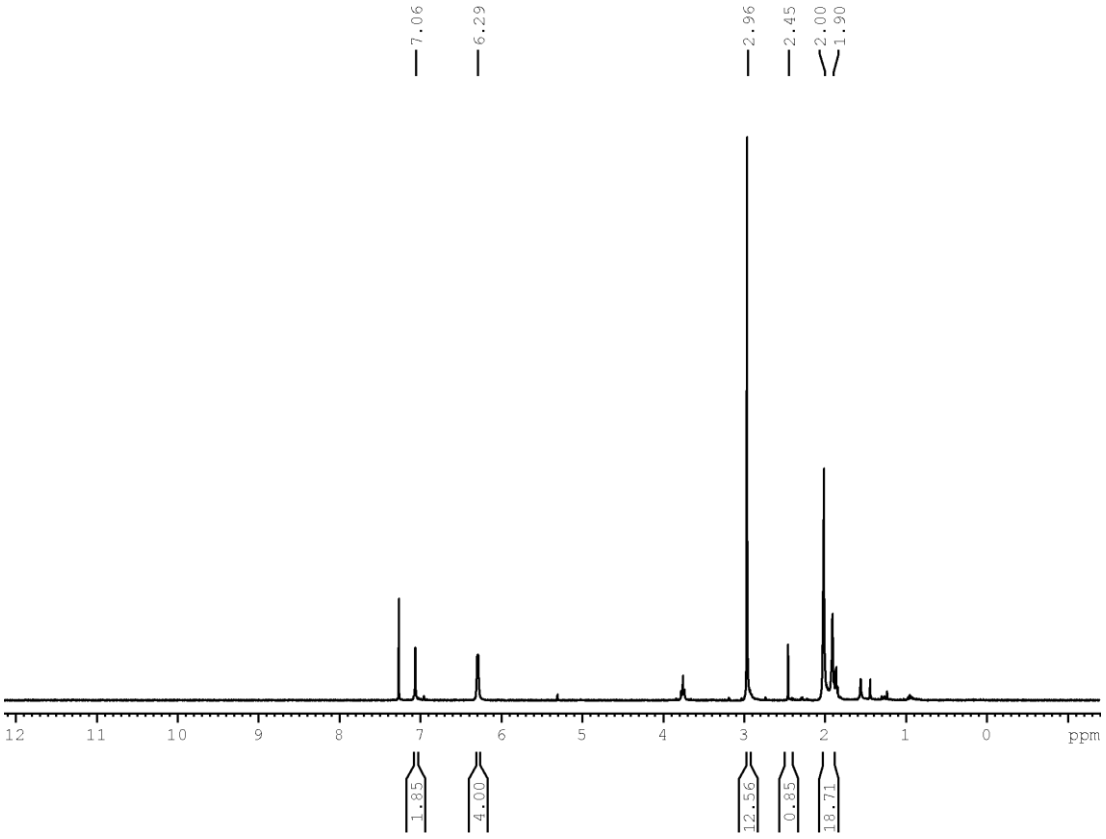

*^1H NMR spectrum (300 MHz) of **3-10** in $CDCl_3$.*

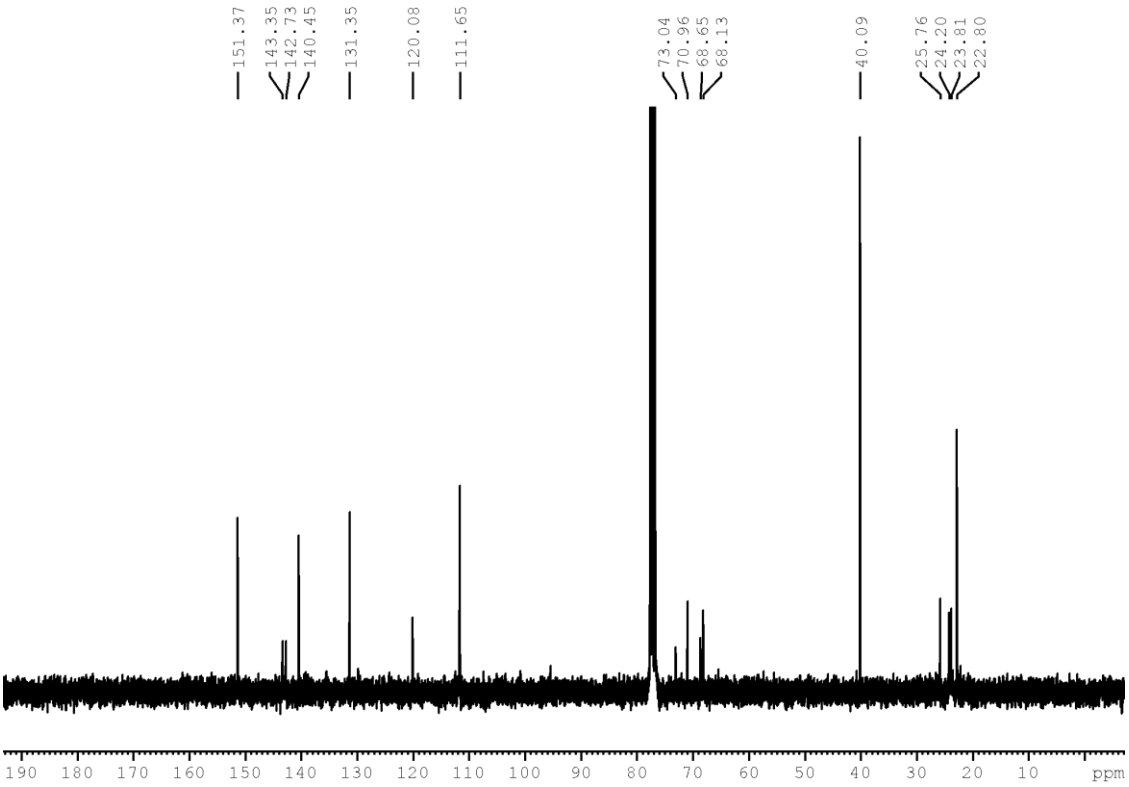

*$^{13}C\{^{1}H\}$ NMR spectrum (75 MHz) of **3-10** in $CDCl_3$.*

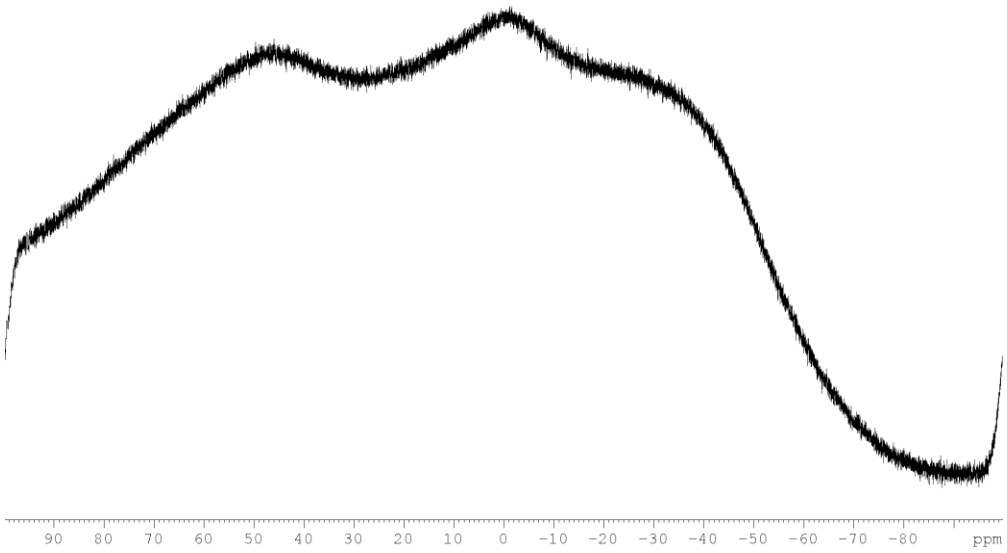

$^{11}B\{^{1}H\}$ NMR *spectrum* (96 MHz) of **3-10** in $CDCl_3$. The signal was too weak and could not be observed.

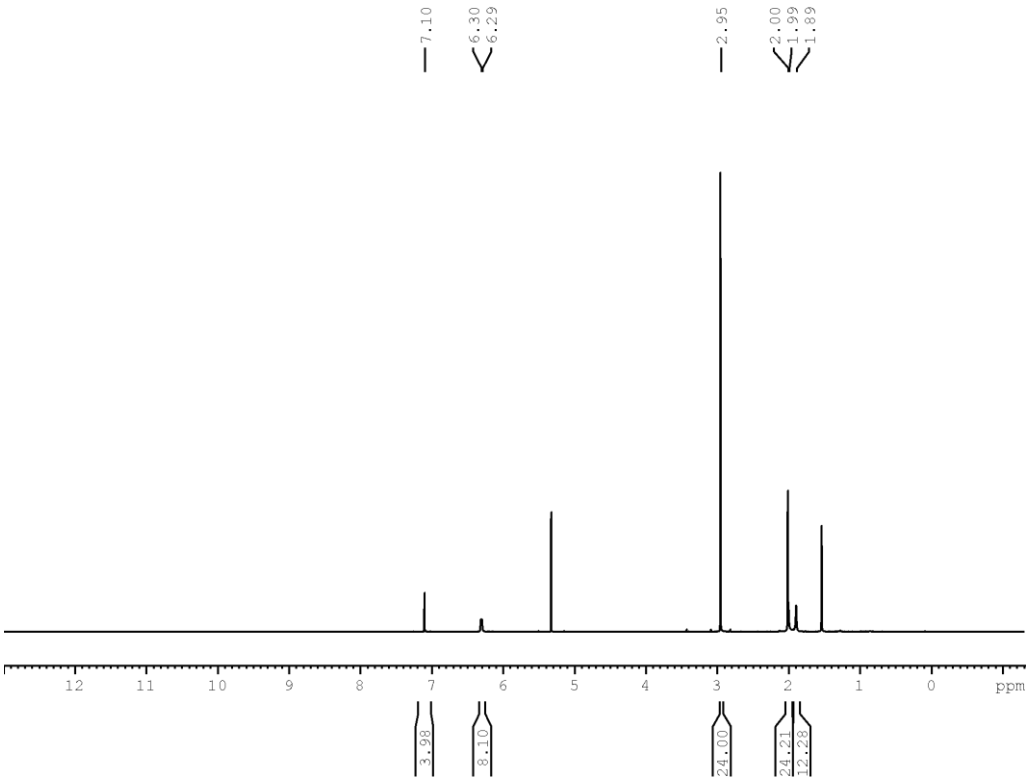

*^{1}H NMR spectrum (500 MHz) of **3-11** in CD_2Cl_2.*

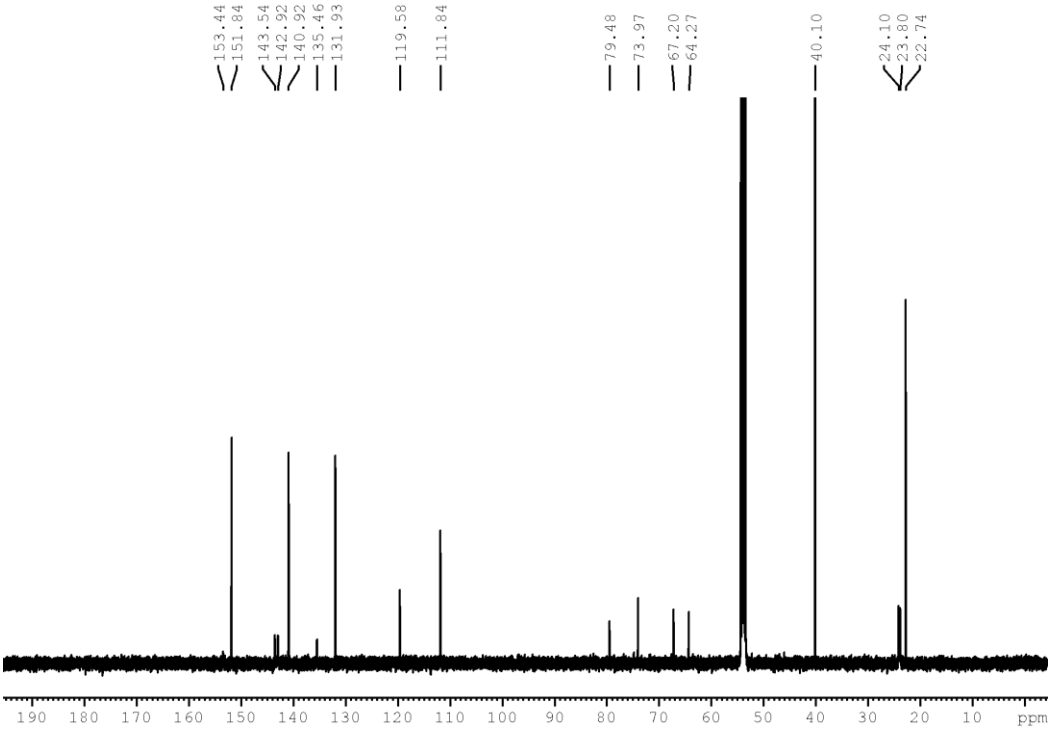

*$^{13}C\{^{1}H\}$ NMR spectrum (125 MHz) of **3-11** in CD_2Cl_2.*

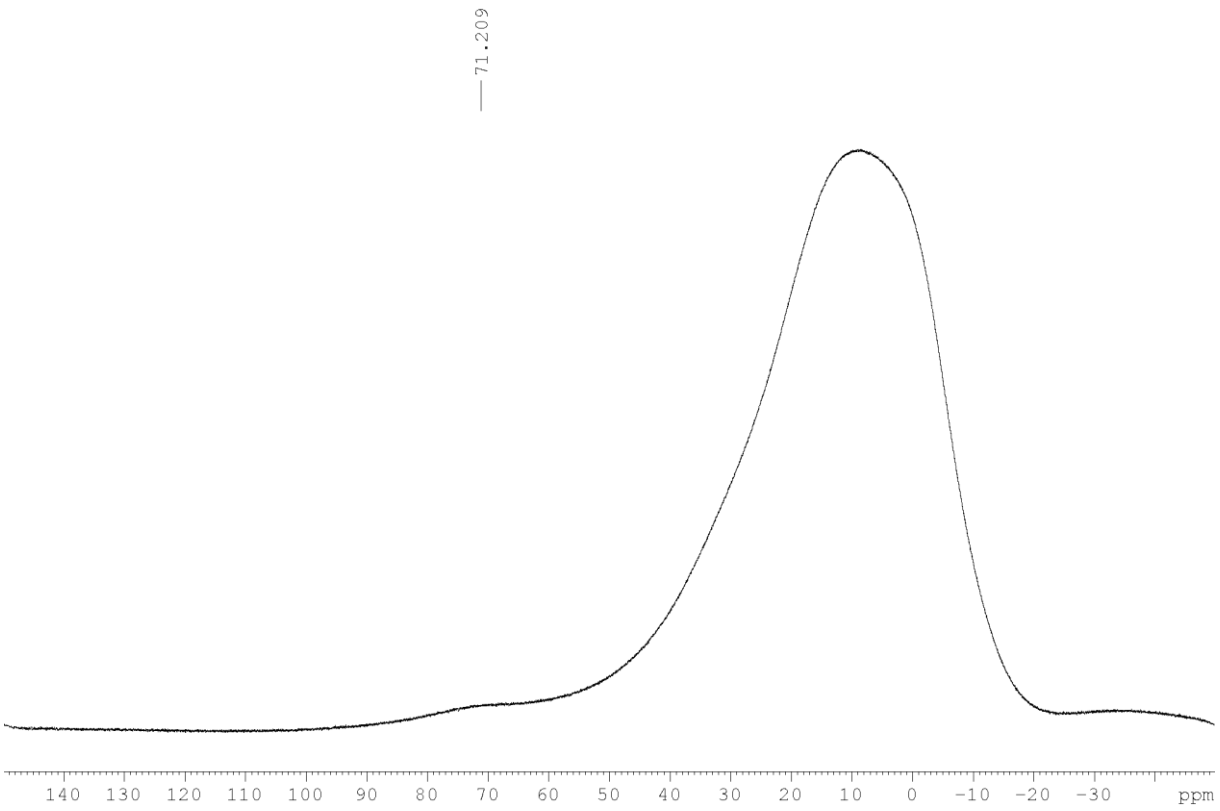

*$^{11}B\{^1H\}$ NMR spectrum (192 MHz) of **3-11** in $CDCl_3$.*

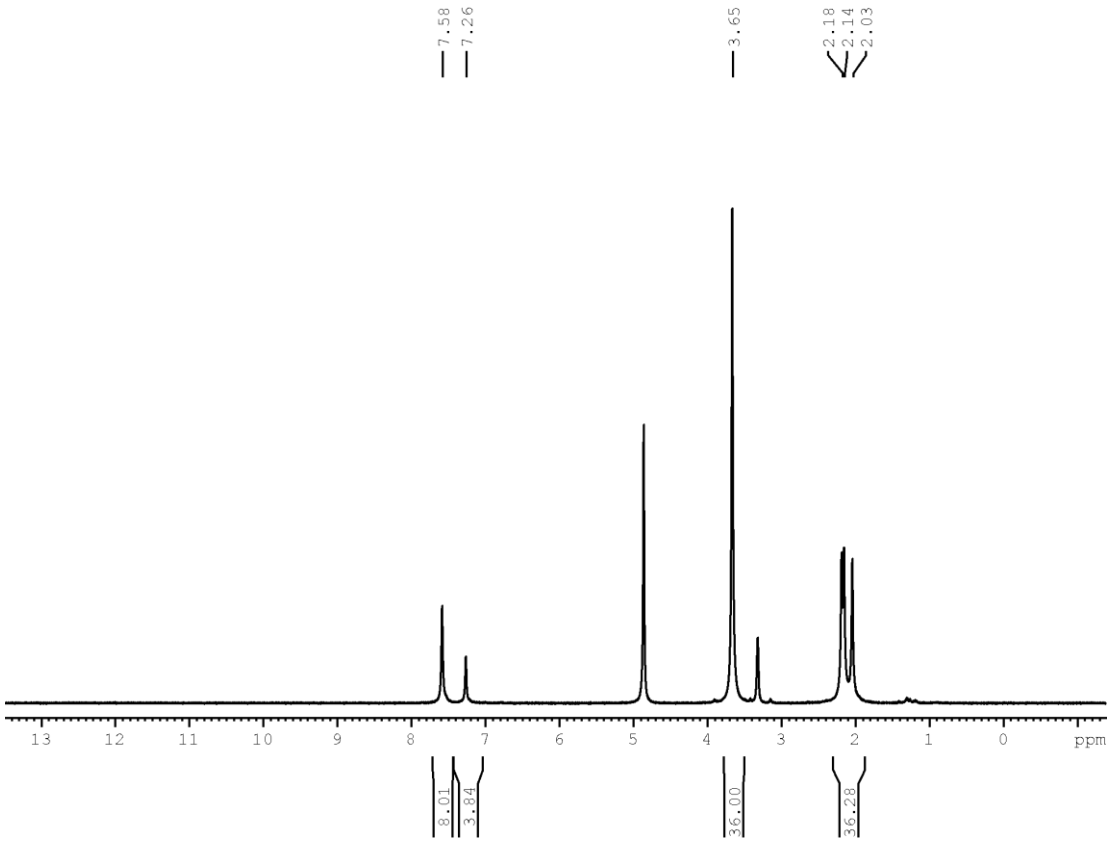

*^1H NMR spectrum (300 MHz) of **3-12** in MeOD.*

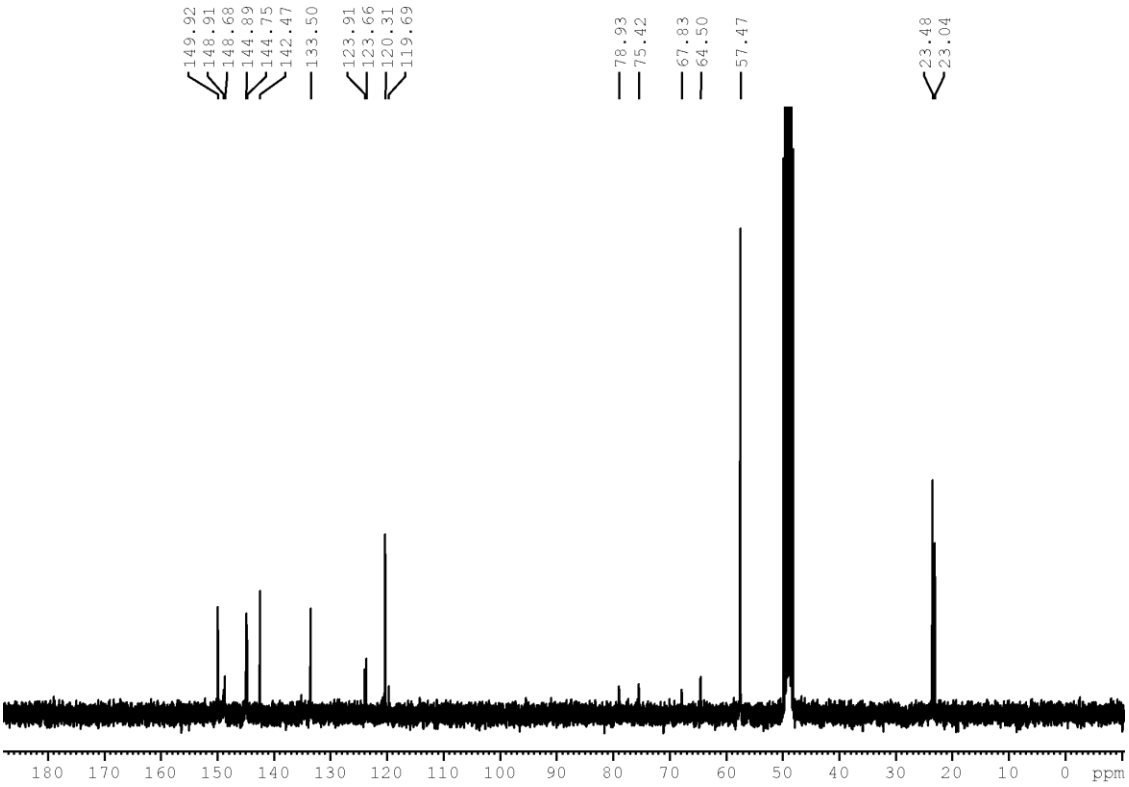

*$^{13}C\{^{1}H\}$ NMR spectrum (75 MHz) of **3-12** in MeOD.*

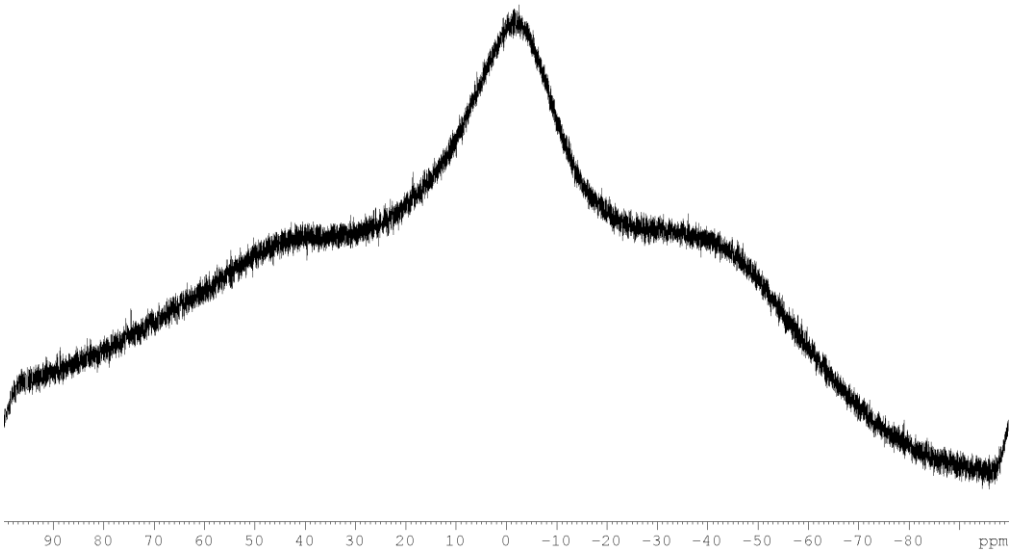

*$^{11}B\{^{1}H\}$ NMR spectrum (96 MHz) of **3-12** in MeOD. The signal was too weak and could not be observed.*

Cartesian Coordinates

Chapter 1

Cartesian coordinates (Å), for all intermediates and transition states (B3LYP-D3(BJ).

1-4

C	0.73526	-2.09247	-1.18519
C	-0.71445	-2.02615	-1.23514
C	-1.4361	-1.19644	-0.43125
C	-0.70756	-0.30352	0.57843
C	0.76383	0.0056	0.12665
C	1.47551	-1.18749	-0.4896
C	1.21551	-3.25263	-2.02829
C	-0.06511	-4.08491	-2.28034
C	-1.22067	-3.05665	-2.21877
H	-0.19008	-4.82105	-1.47654
H	-0.03524	-4.63427	-3.22636
H	1.62404	-2.86893	-2.97444
H	2.01863	-3.82279	-1.54897
H	-2.18056	-3.49183	-1.92381
H	-1.3682	-2.58744	-3.20284
C	0.73442	1.19252	-0.86915
O	0.79224	1.02767	-2.07735
C	0.59638	2.53856	-0.25484
C	0.5165	3.64083	-1.02751
H	0.57787	2.59555	0.831
H	0.54375	3.46831	-2.10318
C	0.40303	5.03591	-0.60513
C	0.30398	6.03251	-1.59427
C	0.39109	5.43668	0.74597
C	0.19463	7.37895	-1.25181
H	0.31331	5.73851	-2.64096
C	0.28303	6.78034	1.08834
H	0.47057	4.69128	1.53175
C	0.18395	7.75759	0.09156
H	0.119	8.13107	-2.03227
H	0.27698	7.07047	2.13556
H	0.10009	8.80629	0.36328
C	-2.84742	-1.17045	-0.43308
C	-4.0664	-1.11729	-0.41574
C	2.88239	-1.24305	-0.40957
C	4.09846	-1.2669	-0.30826
C	-5.48662	-1.06537	-0.40442
C	-6.24768	-1.85865	-1.28778
C	-6.1738	-0.21496	0.4868
C	-7.63719	-1.79949	-1.27364
H	-5.73487	-2.51488	-1.98442
C	-7.56344	-0.1667	0.48892
H	-5.60309	0.40538	1.17111
C	-8.32307	-0.95795	-0.38585
H	-8.20284	-2.41802	-1.96702
H	-8.07112	0.4996	1.18302
C	5.51494	-1.29986	-0.19865
C	6.20993	-0.29364	0.50407
C	6.26422	-2.34204	-0.78366
C	7.5959	-0.33387	0.61143
H	5.64831	0.51355	0.96442
C	7.64962	-2.36896	-0.66706
H	5.7446	-3.12742	-1.3241
C	8.3435	-1.36713	0.0278
H	8.11008	0.45171	1.16077
H	8.20619	-3.18475	-1.12327
C	-9.83264	-0.92349	-0.35355
H	-10.23112	-1.62568	0.39165
H	-10.20641	0.07222	-0.0907
H	-10.26116	-1.20141	-1.32239
C	9.85082	-1.38715	0.12196
H	10.31014	-0.86791	-0.73044
H	10.2027	-0.88925	1.03192
H	10.23924	-2.41141	0.12383
H	1.31031	0.33824	1.01618
C	-0.76388	-0.86184	2.00078
C	-1.05516	-0.00273	3.0688
C	-0.49618	-2.20859	2.28214
C	-1.07236	-0.46932	4.38452
H	-1.27813	1.04329	2.86686
C	-0.50955	-2.67789	3.59585
H	-0.28232	-2.89239	1.467
C	-0.79681	-1.81079	4.6525
H	-1.30734	0.21364	5.19697
H	-0.29816	-3.72557	3.79399
H	-0.81105	-2.17924	5.67481
H	-1.23681	0.6569	0.60269

dba

C	0.	-0.90561	0.00003
O	0.	-2.14009	0.00007
C	-1.25769	-0.1201	0.00001
C	-2.4575	-0.73641	0.00002
H	-1.17074	0.96343	-0.00002
H	-2.43329	-1.82557	0.00005
C	1.25769	-0.1201	0.
C	2.4575	-0.73641	0.00002
H	1.17074	0.96343	-0.00004
H	2.43329	-1.82557	0.00007
C	-3.78766	-0.13015	0.

C	-4.91094	-0.97945	0.00003
C	-4.00612	1.26276	-0.00003
C	-6.20461	-0.4617	0.00001
H	-4.75728	-2.05542	0.00006
C	-5.29762	1.77899	-0.00005
H	-3.16057	1.94378	-0.00005
C	-6.40247	0.92002	-0.00003
H	-7.05664	-1.13548	0.00003
H	-5.44731	2.85497	-0.00008
H	-7.40931	1.32769	-0.00004
C	3.78766	-0.13015	0.
C	4.91094	-0.97945	0.0001
C	4.00612	1.26276	-0.00012
C	6.20461	-0.4617	0.00009
H	4.75728	-2.05542	0.00019
C	5.29762	1.77899	-0.00013
H	3.16057	1.94378	-0.0002
C	6.40247	0.92002	-0.00003
H	7.05664	-1.13548	0.00017
H	5.44731	2.85497	-0.00022
H	7.40931	1.32769	-0.00003

A

C	2.03144	-2.65013	-2.13869
C	1.03023	-1.8404	-1.59601
C	1.26937	-1.09988	-0.42858
C	2.53052	-1.19099	0.18396
C	3.53244	-1.99024	-0.3655
C	3.28384	-2.72509	-1.52767
H	1.82915	-3.22225	-3.04009
H	0.06188	-1.79064	-2.08332
H	2.71697	-0.63697	1.10058
H	4.50281	-2.04811	0.1198
H	4.06012	-3.35673	-1.9505
P	0.00034	0.0001	0.35574
C	-1.58655	-0.5497	-0.43001
C	-2.10588	0.02349	-1.60086
C	-2.29896	-1.5922	0.18627
C	-3.30773	-0.4393	-2.14321
H	-1.57729	0.83424	-2.09184
C	-3.49245	-2.0602	-0.36246
H	-1.91458	-2.02766	1.10526
C	-4.0017	-1.48212	-1.52823
H	-3.70018	0.01858	-3.04713
H	-4.03024	-2.86795	0.12628
H	-4.93719	-1.83848	-1.95032
C	0.31881	1.64827	-0.43006
C	-0.23217	2.78604	0.18309
C	1.07852	1.81142	-1.59854
C	-0.04278	4.05323	-0.36718
H	-0.80387	2.67077	1.1006
C	1.27693	3.08338	-2.14218
H	1.51991	0.94841	-2.08676
C	0.71558	4.2053	-1.53085
H	-0.47738	4.92239	0.11882
H	1.87207	3.19442	-3.04451
H	0.87315	5.19334	-1.95425
Pd	0.00006	0.0013	2.56656

B

C	-6.8715	1.56106	-0.57922
C	-5.63115	0.93198	-0.54694
C	-5.52413	-0.41721	-0.1522
C	-6.70359	-1.10436	0.20281
C	-7.93611	-0.46076	0.16691
C	-8.0454	0.88289	-0.22012
H	-6.93166	2.60159	-0.89131
H	-4.73366	1.47042	-0.83411
H	-6.63825	-2.14609	0.50214
H	-8.83274	-1.01177	0.44245
C	-9.38257	1.58539	-0.22573
H	-10.20292	0.88646	-0.42152
H	-9.58631	2.06146	0.74331
H	-9.41909	2.37272	-0.98651
C	-4.26306	-1.0744	-0.11452
C	-3.20125	-1.67742	-0.06968
C	-2.00706	-2.35406	-0.00523
C	-1.27065	-3.38189	0.04147
C	-1.06677	-4.84707	0.06383
H	-1.09039	-5.19096	1.10943
H	-1.91809	-5.32539	-0.43986
C	1.49373	-4.77502	0.12582
H	1.48626	-5.11818	1.1719
H	2.39392	-5.2037	-0.33595
C	1.60835	-3.29982	0.10767
C	2.29538	-2.2348	0.07335
C	3.48695	-1.55116	0.01533
C	4.56172	-0.97362	-0.04754
C	5.83846	-0.35081	-0.12074
C	6.90919	-0.80759	0.67547
C	6.07232	0.7326	-0.99282
C	8.15933	-0.20198	0.59726
H	6.74493	-1.63869	1.35476
C	7.3294	1.3245	-1.06321
H	5.25562	1.10405	-1.603
C	8.39684	0.87001	-0.27488
H	8.96893	-0.56914	1.22436
H	7.4867	2.15915	-1.74329
C	9.76633	1.49857	-0.38183
H	10.33364	1.38507	0.54823
H	10.35766	1.03235	-1.18191
H	9.70112	2.56802	-0.61088

C	0.24442	-5.32118	-0.58529
H	0.26141	-5.018	-1.63921
H	0.27315	-6.41725	-0.56035
C	-2.56198	2.82557	-2.39297
C	-1.86582	2.39676	-1.2605
C	-1.09019	1.22792	-1.30171
C	-1.03607	0.49466	-2.49749
C	-1.72768	0.92707	-3.63042
C	-2.49261	2.09346	-3.58073
H	-3.1581	3.73355	-2.34607
H	-1.93336	2.97315	-0.34306
H	-0.45794	-0.42544	-2.53205
H	-1.6755	0.34634	-4.54748
H	-3.0368	2.42792	-4.46
P	-0.09285	0.60818	0.12843
C	-0.94119	1.28864	1.62961
C	-0.7933	2.62669	2.03422
C	-1.75362	0.43896	2.39517
C	-1.45599	3.10425	3.16564
H	-0.14687	3.29453	1.4729
C	-2.41642	0.91872	3.52666
H	-1.86361	-0.6	2.10404
C	-2.2709	2.2514	3.91362
H	-1.32938	4.14126	3.46585
H	-3.04245	0.24627	4.10708
H	-2.78324	2.62295	4.79725
C	1.41644	1.67944	0.06893
C	2.35927	1.54637	1.10224
C	1.65201	2.62178	-0.94181
C	3.49072	2.35862	1.14058
H	2.20578	0.80466	1.88148
C	2.79446	3.42716	-0.9087
H	0.94062	2.74053	-1.7523
C	3.711	3.30455	0.13542
H	4.20863	2.24338	1.94775
H	2.95888	4.15635	-1.6981
H	4.59681	3.93329	0.16385
Pd	0.13772	-1.78867	0.09212

TS_{BC}

C	7.47543	-0.03536	-0.69405
C	6.10685	0.21339	-0.6856
C	5.58824	1.34598	-0.02278
C	6.4943	2.20765	0.63013
C	7.85943	1.94114	0.61898
C	8.37824	0.82059	-0.04608
H	7.85264	-0.91547	-1.21057
H	5.42234	-0.46355	-1.18816
H	6.11139	3.08162	1.14853
H	8.53794	2.61703	1.13507
C	9.86526	0.55838	-0.08583
H	10.36466	0.94002	0.81133
H	10.08216	-0.51242	-0.16496
H	10.33331	1.0487	-0.95055
C	4.19051	1.6057	-0.01182
C	2.98779	1.83519	-0.01273
C	1.61789	2.00825	-0.01101
C	0.76439	3.01066	-0.02687
C	0.97884	4.50272	-0.05838
H	1.11153	4.86578	0.97245
H	1.90757	4.71727	-0.59816
C	-1.43392	4.44175	-0.04618
H	-1.56773	4.79096	0.9893
H	-2.37936	4.6161	-0.57081
C	-1.15392	2.9587	-0.03072
C	-1.97297	1.92668	-0.02947
C	-3.34137	1.74185	-0.03789
C	-4.53997	1.48917	-0.03778
C	-5.93304	1.2062	-0.04349
C	-6.79478	1.76465	0.92406
C	-6.49568	0.35775	-1.02122
C	-8.15575	1.47735	0.91203
H	-6.3818	2.42571	1.68004
C	-7.86055	0.08661	-1.02441
H	-5.84891	-0.07613	-1.77798
C	-8.71686	0.634	-0.05814
H	-8.79889	1.92148	1.6689
H	-8.27085	-0.56397	-1.79395
C	-10.19147	0.30653	-0.04655
H	-10.78335	1.13554	0.35669
H	-10.56164	0.08488	-1.05339
H	-10.40055	-0.57359	0.57719
C	-0.24868	5.16643	-0.67951
H	-0.2506	5.01674	-1.76603
H	-0.27416	6.24367	-0.48457
C	3.18494	-3.55223	-1.61454
C	2.18674	-3.09864	-0.74959
C	1.43202	-1.95993	-1.07118
C	1.70275	-1.2797	-2.26813
C	2.6962	-1.7376	-3.13438
C	3.43982	-2.87481	-2.80894
H	3.76495	-4.43315	-1.35203
H	2.00279	-3.62802	0.18066
H	1.14285	-0.37965	-2.50782
H	2.89606	-1.19976	-4.05722
H	4.21778	-3.22835	-3.4806
P	0.09148	-1.31533	0.02483
C	0.56843	-1.93056	1.69996
C	-0.04859	-3.03196	2.30927
C	1.5956	-1.25728	2.38415
C	0.35379	-3.4528	3.57996
H	-0.84538	-3.56106	1.79654
C	1.99984	-1.68631	3.64732
H	2.07402	-0.39576	1.92623

C	1.37778	-2.78338	4.2501
H	-0.13694	-4.30477	4.04331
H	2.79617	-1.15772	4.16446
H	1.68825	-3.11118	5.2387
C	-1.38818	-2.32504	-0.42825
C	-2.65425	-1.84714	-0.05371
C	-1.29626	-3.54583	-1.1153
C	-3.80285	-2.58429	-0.34528
H	-2.74302	-0.88916	0.44868
C	-2.44842	-4.27666	-1.41273
H	-0.32788	-3.92673	-1.42379
C	-3.70232	-3.79975	-1.02599
H	-4.77527	-2.19711	-0.0536
H	-2.36353	-5.2181	-1.94937
H	-4.59774	-4.36942	-1.26087
Pd	-0.13832	0.91394	-0.02545

C

C	1.98636	2.13512	0.08185
C	-0.67803	2.17221	0.08717
C	-0.03514	3.37817	0.15003
C	1.40881	3.36973	0.15012
C	-0.54141	4.80317	0.19611
C	0.70002	5.62293	-0.25066
C	1.92956	4.78884	0.20188
H	-1.42126	4.97392	-0.43213
H	-0.82693	5.06707	1.22492
H	0.7033	6.64098	0.15086
H	2.21289	5.05154	1.23174
H	0.70258	5.70071	-1.34413
H	2.81377	4.95244	-0.42239
C	-2.05677	1.9914	0.04187
C	-3.27341	1.82925	-0.00249
C	3.33787	1.80703	0.04745
C	4.49889	1.40413	0.00907
Pd	0.63062	0.59018	0.05526
C	-4.68697	1.69345	-0.04314
C	-5.29779	0.44895	-0.31315
C	-5.52411	2.80634	0.19153
C	-6.68289	0.33302	-0.34396
H	-4.67442	-0.41996	-0.49703
C	-6.90821	2.67295	0.15509
H	-5.0743	3.77115	0.4048
C	-7.51694	1.43829	-0.11438
H	-7.12886	-0.63699	-0.55157
H	-7.53035	3.54519	0.34143
C	5.85868	0.99765	-0.03287
C	6.21076	-0.36253	-0.16993
C	6.90178	1.94579	0.06594
C	7.54678	-0.74898	-0.20577
H	5.42446	-1.10755	-0.24462
C	8.23157	1.54345	0.02746
H	6.65153	2.99639	0.17635
C	8.5832	0.19142	-0.11133
H	7.79212	-1.8033	-0.30988
H	9.01562	2.29283	0.108
C	10.0302	-0.2297	-0.18449
H	10.15742	-1.28119	0.09054
H	10.4279	-0.1084	-1.20075
H	10.65853	0.37306	0.47958
C	-9.01843	1.30557	-0.18371
H	-9.37529	1.36727	-1.22032
H	-9.35611	0.34319	0.21493
H	-9.5184	2.09967	0.37922
P	-0.62642	-1.4828	0.04796
C	-1.74901	-1.84458	-1.36385
C	-2.75772	-2.81954	-1.31049
C	-1.56617	-1.11278	-2.54844
C	-3.56147	-3.0616	-2.42624
H	-2.92001	-3.38715	-0.39959
C	-2.3668	-1.36265	-3.66367
H	-0.80106	-0.34208	-2.59049
C	-3.36577	-2.33619	-3.60381
H	-4.3408	-3.81677	-2.37394
H	-2.21637	-0.78883	-4.57352
H	-3.99433	-2.52509	-4.46945
C	0.74329	-2.71442	-0.10865
C	1.7843	-2.64661	0.83692
C	0.83127	-3.65159	-1.14844
C	2.87943	-3.50589	0.74895
H	1.73474	-1.92626	1.65052
C	1.93322	-4.50612	-1.23624
H	0.04159	-3.71914	-1.88966
C	2.95705	-4.43674	-0.29041
H	3.67148	-3.44482	1.48986
H	1.98747	-5.22857	-2.04584
H	3.81151	-5.10356	-0.36195
C	-1.52956	-2.0224	1.56044
C	-1.50395	-3.34871	2.02199
C	-2.26213	-1.06261	2.27742
C	-2.20558	-3.70749	3.17405
H	-0.93013	-4.1004	1.48883
C	-2.9663	-1.42737	3.42588
H	-2.28305	-0.03271	1.93517
C	-2.93846	-2.74843	3.87666
H	-2.17637	-4.73587	3.52323
H	-3.53011	-0.67553	3.97055
H	-3.48128	-3.02921	4.77486

TS_{CA}

C	1.27639	-1.99011	-0.57968
C	-0.88996	-0.55267	-0.95639
C	-0.73961	-1.64397	-1.8201
C	0.44438	-2.36528	-1.68787

C	-1.6221 -2.22128 -2.90368	H	-2.1285 2.49863 3.97053
C	-0.87349 -3.52122 -3.32909	H	-2.75477 4.89368 3.7307
C	0.56847 -3.41922 -2.75082	C	2.56456 2.83947 0.77234
H	-2.63712 -2.42644 -2.55021	C	3.68551 2.21242 0.19797
H	-1.71385 -1.50854 -3.73486	C	2.75209 3.69081 1.87093
H	-0.87512 -3.66164 -4.41452	C	4.96378 2.43817 0.70704
H	1.2928 -3.09238 -3.51281	H	3.56029 1.54552 -0.65171
H	-1.36817 -4.37723 -2.86862	C	4.03411 3.91152 2.38098
H	0.9338 -4.37292 -2.35762	H	1.90181 4.18369 2.33045
C	-2.04942 0.21191 -0.86853	C	5.14011 3.28773 1.80219
C	-3.08583 0.86106 -0.75866	H	5.81688 1.9407 0.2552
C	2.68295 -2.08885 -0.69389	H	4.16505 4.57362 3.23236
C	3.90617 -2.05287 -0.767	H	6.13466 3.45862 2.20422
Pd	0.88916 0.03138 -0.17152	C	0.83118 3.40118 -1.49976
C	-4.32101 1.55271 -0.65591	C	1.65514 4.51214 -1.74061
C	-5.52682 0.91504 -1.02288	C	-0.08514 3.00324 -2.48722
C	-4.38219 2.88402 -0.1903	C	1.55934 5.21309 -2.94455
C	-6.73909 1.58826 -0.92296	H	2.37671 4.82839 -0.99393
H	-5.49776 -0.10996 -1.37845	C	-0.18189 3.71083 -3.6857
C	-5.60272 3.54389 -0.10323	H	-0.72267 2.1413 -2.31805
H	-3.46592 3.39134 0.09309	C	0.6409 4.81505 -3.91767
C	-6.8037 2.91235 -0.46272	H	2.20508 6.06878 -3.12082
H	-7.65462 1.07657 -1.2093	H	-0.89511 3.39256 -4.44063
H	-5.62601 4.57128 0.25226	H	0.57 5.36009 -4.85469
C	5.32417 -2.01452 -0.87393	C	-1.65238 -3.45459 0.50172
C	6.13524 -1.87404 0.27212	O	-1.30979 -4.26723 -0.40026
C	5.95803 -2.10753 -2.13247	C	-3.08607 -3.22537 0.82222
C	7.52123 -1.82785 0.15515	C	-4.06946 -3.9157 0.21313
H	5.6649 -1.80245 1.24753	H	-3.30578 -2.47639 1.5802
C	7.34364 -2.06159 -2.23199	H	-3.75136 -4.66477 -0.51101
H	5.34899 -2.21471 -3.02486	C	-0.69205 -2.70909 1.23791
C	8.15336 -1.92288 -1.09335	C	0.70108 -2.91188 0.98695
H	8.12624 -1.71743 1.05185	H	-1.02168 -1.99601 1.98568
H	7.80917 -2.13442 -3.21204	H	0.89403 -3.90687 0.58517
C	9.6573 -1.90352 -1.21161	C	-5.51519 -3.79109 0.41742
H	10.05897 -2.91976 -1.31725	C	-6.373 -4.71535 -0.21013
H	9.98411 -1.33734 -2.09023	C	-6.10226 -2.78375 1.21081
H	10.12435 -1.45886 -0.32779	C	-7.75557 -4.64835 -0.04496
C	-8.1259 3.62637 -0.33108	H	-5.94016 -5.49651 -0.83016
H	-8.02301 4.70043 -0.51597	C	-7.48285 -2.71613 1.3749
H	-8.86781 3.22989 -1.03093	H	-5.47241 -2.04362 1.69492
H	-8.53887 3.51077 0.67978	C	-8.31826 -3.64838 0.75033
P	0.90588 2.43324 0.06758	H	-8.3935 -5.37708 -0.5379
C	-0.29119 3.25812 1.19804	H	-7.91164 -1.92988 1.9906
C	-0.65813 4.60639 1.06215	H	-9.39537 -3.59198 0.88063
C	-0.83489 2.50555 2.2511	C	1.66989 -2.53458 2.06648
C	-1.54095 5.1909 1.97278	C	1.57861 -1.31863 2.7659
H	-0.25785 5.20092 0.247	C	2.6994 -3.42103 2.41632
C	-1.71304 3.09339 3.16225	C	2.4828 -1.00296 3.78102
H	-0.57781 1.45471 2.34851	H	0.78655 -0.61843 2.51371
C	-2.06656 4.43723 3.025	C	3.60072 -3.11243 3.4373
H	-1.8173 6.23535 1.85854	H	2.78699 -4.36667 1.8881

C	3.49856	-1.89969	4.12247
H	2.39065	-0.05783	4.30979
H	4.38162	-3.82203	3.69758
H	4.19879	-1.65745	4.91712

D

C	1.63456	-0.27039	-1.74681
C	-1.06633	-0.72196	-1.70601
C	-0.32495	-1.26954	-2.71707
C	1.09219	-1.02999	-2.74506
C	-0.726	-2.1206	-3.90358
C	0.61943	-2.7431	-4.35861
C	1.70067	-1.7073	-3.95604
H	-1.48939	-2.86651	-3.66091
H	-1.14703	-1.48544	-4.69679
H	0.63755	-2.98765	-5.42526
H	1.85023	-0.97302	-4.76143
H	0.79032	-3.6747	-3.80608
H	2.67814	-2.15709	-3.75456
C	-2.45222	-0.93987	-1.70394
C	-3.65276	-1.17139	-1.79457
C	3.00917	0.00015	-1.76337
C	4.21395	0.24288	-1.76439
Pd	0.12877	0.35351	-0.33824
C	-5.03346	-1.48175	-1.93631
C	-6.04124	-0.58334	-1.52445
C	-5.43602	-2.70511	-2.51591
C	-7.38574	-0.90365	-1.68441
H	-5.75678	0.36935	-1.09074
C	-6.7842	-3.01006	-2.67009
H	-4.67702	-3.40894	-2.84341
C	-7.78681	-2.12049	-2.25582
H	-8.14223	-0.19111	-1.36303
H	-7.06597	-3.9583	-3.12214
C	5.61154	0.50283	-1.80521
C	6.23264	1.33432	-0.84784
C	6.4238	-0.06289	-2.81363
C	7.60068	1.58176	-0.90144
H	5.63011	1.78938	-0.06754
C	7.78963	0.1933	-2.85332
H	5.96633	-0.70067	-3.5638
C	8.40812	1.01666	-1.89936
H	8.05208	2.22912	-0.15328
H	8.39052	-0.25315	-3.64234
C	9.89639	1.26294	-1.93344
H	10.16104	2.19459	-1.42405
H	10.44528	0.45269	-1.43542
H	10.27111	1.32014	-2.96071
C	-9.24771	-2.47203	-2.3961
H	-9.62798	-2.96433	-1.49104
H	-9.86228	-1.58091	-2.55988
H	-9.41746	-3.15834	-3.23172
P	-1.86585	0.8394	1.04401
C	-2.66524	-0.75621	1.53375
C	-4.00812	-0.86836	1.92364
C	-1.84748	-1.89561	1.58675
C	-4.52059	-2.09331	2.35052
H	-4.66757	-0.0095	1.88531
C	-2.35981	-3.11826	2.02534
H	-0.81081	-1.82974	1.27041
C	-3.69765	-3.22025	2.4063
H	-5.56584	-2.16601	2.63745
H	-1.712	-3.98965	2.0588
H	-4.09963	-4.17263	2.74049
C	-1.78515	1.717	2.68073
C	-1.88257	3.11801	2.75149
C	-1.59001	0.99747	3.86995
C	-1.80183	3.77696	3.97971
H	-2.03638	3.69962	1.84902
C	-1.5095	1.6593	5.09596
H	-1.49746	-0.08141	3.84368
C	-1.6166	3.04909	5.1566
H	-1.89132	4.85935	4.01419
H	-1.36195	1.08268	6.00463
H	-1.55732	3.56151	6.11267
C	-3.07543	1.90234	0.13328
C	-4.2661	2.37371	0.71571
C	-2.75333	2.32002	-1.16694
C	-5.12263	3.21297	0.0024
H	-4.5159	2.11623	1.73939
C	-3.60777	3.16623	-1.87702
H	-1.83012	1.97891	-1.62476
C	-4.7968	3.60866	-1.29771
H	-6.03845	3.56643	0.46795
H	-3.34001	3.47628	-2.88293
H	-5.46229	4.2662	-1.85001
C	1.91829	-0.19864	2.05618
O	1.21912	-0.09977	3.06748
C	2.00521	0.89417	1.03967
C	1.30872	2.06914	1.17656
H	2.81686	0.81767	0.32941
H	0.65255	2.14235	2.03872
C	2.75014	-1.39016	1.77453
C	2.79037	-2.42608	2.63857
H	3.31572	-1.38757	0.84773
H	2.18954	-2.32451	3.54163
C	1.50408	3.3142	0.42269
C	0.97722	4.50484	0.96091
C	2.2165	3.38603	-0.79225
C	1.15766	5.72591	0.31422
H	0.4356	4.46442	1.90083
C	2.3893	4.6068	-1.43803
H	2.62866	2.48634	-1.23453
C	1.86166	5.7806	-0.89016

H	0.74936	6.63325	0.75021
H	2.93865	4.64256	-2.37442
H	2.00015	6.73019	-1.39933
C	3.54529	-3.67114	2.51315
C	3.47029	-4.61106	3.55924
C	4.34504	-3.98051	1.39367
C	4.16815	-5.81538	3.49515
H	2.85633	-4.38525	4.42739
C	5.04055	-5.18329	1.33066
H	4.41902	-3.27803	0.56939
C	4.95614	-6.10547	2.37997
H	4.09691	-6.52629	4.31343
H	5.65109	-5.40604	0.46023
H	5.50115	-7.04358	2.32559

TS_{DE}

C	0.70992	-2.7037	0.2574
C	-1.83814	-1.93291	-0.23161
C	-1.61426	-3.28802	0.04347
C	-0.28257	-3.70118	0.18623
C	-2.55426	-4.47788	0.09636
C	-1.63341	-5.63476	0.57329
C	-0.18889	-5.20766	0.19179
H	-3.40921	-4.32044	0.76255
H	-2.96683	-4.67837	-0.90222
H	-1.91324	-6.60387	0.14932
H	0.07978	-5.56964	-0.81189
H	-1.70034	-5.72132	1.66314
H	0.5714	-5.59222	0.87913
C	-3.13827	-1.43274	-0.28525
C	-4.28216	-0.98362	-0.31265
C	1.99063	-2.90053	-0.28211
C	3.11038	-2.99369	-0.76918
Pd	-0.11432	-0.79944	-0.0801
C	-5.63136	-0.54025	-0.31134
C	-5.9836	0.75494	-0.74803
C	-6.66486	-1.39741	0.13053
C	-7.3114	1.16882	-0.7357
H	-5.20639	1.42287	-1.10373
C	-7.98687	-0.9699	0.13522
H	-6.41254	-2.39899	0.46473
C	-8.33762	0.32043	-0.29336
H	-7.55942	2.17003	-1.07979
H	-8.76489	-1.64829	0.47703
C	4.42927	-3.0497	-1.29473
C	4.80151	-4.01185	-2.25493
C	5.40359	-2.12336	-0.856
C	6.10079	-4.045	-2.75452
H	4.06482	-4.73057	-2.60096
C	6.69322	-2.16788	-1.37146
H	5.12015	-1.38363	-0.11386
C	7.0695	-3.12613	-2.32794
H	6.36824	-4.79766	-3.49228
H	7.42971	-1.44732	-1.02231
C	8.47227	-3.15046	-2.88382
H	8.66667	-2.27334	-3.51419
H	9.22093	-3.139	-2.08333
H	8.64709	-4.0408	-3.49479
C	-9.77183	0.78585	-0.25371
H	-10.46522	-0.03005	-0.48171
H	-10.03686	1.1648	0.74219
H	-9.95176	1.59528	-0.96757
P	-0.61821	1.35685	-1.02521
C	-1.10055	2.7146	0.12892
C	-2.19003	2.4763	0.98737
C	-0.41993	3.93709	0.22061
C	-2.59899	3.44769	1.90009
H	-2.72335	1.53052	0.93699
C	-0.83001	4.90635	1.1415
H	0.43162	4.13789	-0.42062
C	-1.91913	4.66636	1.97982
H	-3.44619	3.25074	2.55104
H	-0.29317	5.84904	1.19875
H	-2.23596	5.42173	2.69338
C	0.85087	1.97232	-1.96526
C	2.08529	1.32788	-1.79695
C	0.75974	3.03362	-2.88262
C	3.20678	1.73776	-2.52151
H	2.17505	0.49926	-1.10207
C	1.88264	3.44766	-3.59831
H	-0.19043	3.53137	-3.0493
C	3.10813	2.79964	-3.42004
H	4.1508	1.21944	-2.38163
H	1.79801	4.27074	-4.30245
H	3.97929	3.11873	-3.98539
C	-1.9315	1.40539	-2.32521
C	-2.76044	2.51948	-2.52918
C	-2.04777	0.30379	-3.18681
C	-3.68193	2.5311	-3.57974
H	-2.69019	3.38056	-1.872
C	-2.96611	0.32008	-4.2365
H	-1.42336	-0.57073	-3.02692
C	-3.78567	1.43319	-4.43545
H	-4.31658	3.40061	-3.72789
H	-3.04621	-0.54142	-4.89335
H	-4.5041	1.44304	-5.25027
C	2.43822	0.24482	1.62652
O	3.47815	-0.35524	1.31337
C	1.1424	-0.42612	1.81046
C	1.12646	-1.84789	2.06431
H	0.37633	0.17849	2.29096
H	2.11913	-2.2897	2.07397
C	2.453	1.70915	1.90163
C	3.61014	2.39969	1.87609

H	1.50694	2.18256	2.14995
H	4.49737	1.83017	1.60209
C	0.19912	-2.45665	3.04693
C	0.6083	-3.61485	3.73325
C	-1.06932	-1.92366	3.33664
C	-0.21597	-4.21619	4.68208
H	1.58721	-4.03734	3.52062
C	-1.89558	-2.52773	4.2846
H	-1.4143	-1.03747	2.81486
C	-1.47448	-3.6749	4.96042
H	0.12471	-5.10407	5.20763
H	-2.87224	-2.10013	4.49441
H	-2.11904	-4.14154	5.70007
C	3.82846	3.81644	2.17206
C	5.10839	4.36099	1.95281
C	2.82456	4.66698	2.67815
C	5.37642	5.70341	2.21463
H	5.89558	3.71697	1.56923
C	3.09342	6.00668	2.94217
H	1.83127	4.27438	2.87123
C	4.36897	6.53277	2.7104
H	6.37156	6.10063	2.03509
H	2.30753	6.64491	3.33707
H	4.57463	7.57863	2.92022

E

C	-0.80979	-0.59586	0.64623
C	-2.06218	-0.95788	-0.18665
C	-2.84813	0.0631	-1.03678
C	-2.41603	1.06592	-1.8665
C	0.10961	1.19244	-1.60903
C	-1.06949	1.54552	-2.17442
H	-0.49391	-1.53047	1.11214
H	-2.79052	-1.25952	0.57932
C	-3.40334	1.8777	-2.70494
H	-4.30846	2.13442	-2.14772
C	-2.60924	3.1073	-3.1764
H	-2.65326	3.89455	-2.41434
C	-1.17083	2.58323	-3.29122
H	-1.02394	2.09085	-4.26412
H	-0.40739	3.36135	-3.20443
H	-2.9911	3.52876	-4.11111
H	-3.72936	1.2758	-3.56568
Pd	0.98357	-0.02322	-0.27828
P	2.5718	-1.33607	1.02658
C	3.74822	-2.25544	-0.062
C	3.79952	-1.9379	-1.42732
C	4.58394	-3.27302	0.42956
C	4.677	-2.60962	-2.28145
H	3.14216	-1.16984	-1.82501
C	5.45925	-3.94348	-0.42474
H	4.54673	-3.54696	1.47957
C	5.50862	-3.61189	-1.78149
H	4.70291	-2.35264	-3.33656
H	6.09926	-4.72841	-0.03149
H	6.18819	-4.13833	-2.44584
C	1.99001	-2.66214	2.17093
C	2.33497	-2.71751	3.52791
C	1.15762	-3.66078	1.63717
C	1.85907	-3.75394	4.33483
H	2.97146	-1.95327	3.96096
C	0.68845	-4.69602	2.44491
H	0.87474	-3.63182	0.58877
C	1.0369	-4.74438	3.79684
H	2.13374	-3.78379	5.38558
H	0.04574	-5.46009	2.01694
H	0.66706	-5.54828	4.42714
C	3.62923	-0.2333	2.06362
C	5.02995	-0.21787	1.99166
C	2.97741	0.67233	2.92201
C	5.76688	0.68192	2.76641
H	5.55102	-0.90199	1.3306
C	3.72036	1.56034	3.70042
H	1.89196	0.67319	2.98667
C	5.11554	1.57052	3.62252
H	6.85138	0.68386	2.69892
H	3.20576	2.24966	4.36406
H	5.69051	2.26868	4.22462
C	-1.80227	-2.23782	-0.9945
C	-2.14332	-3.48073	-0.44393
C	-1.20944	-2.2145	-2.26516
C	-1.89317	-4.66973	-1.13441
H	-2.61249	-3.51796	0.53649
C	-0.95792	-3.40005	-2.95795
H	-0.94804	-1.26353	-2.71611
C	-1.29565	-4.63347	-2.39503
H	-2.17395	-5.62091	-0.68962
H	-0.50156	-3.35902	-3.94365
H	-1.10305	-5.55482	-2.93778
C	-0.89055	0.41404	1.75182
O	-0.31853	0.18197	2.82949
C	-1.64239	1.68327	1.56794
C	-1.74509	2.56855	2.57954
H	-2.10872	1.85825	0.60717
H	-1.23107	2.30822	3.50375
C	-2.46014	3.84597	2.58497
C	-2.32671	4.68996	3.70409
C	-3.28429	4.27558	1.52517
C	-2.97788	5.92099	3.76091
H	-1.69996	4.37046	4.53287
C	-3.93661	5.50313	1.58332
H	-3.42355	3.63722	0.65846
C	-3.78515	6.33324	2.69939
H	-2.85706	6.55646	4.63381

H	-4.57034	5.81473	0.75757
H	-4.2972	7.29044	2.74089
C	1.3906	1.64179	-1.95018
C	2.60185	1.86051	-2.05433
C	-4.24777	-0.18473	-0.9777
C	-5.43717	-0.44399	-0.88281
C	3.96183	2.21076	-2.28345
C	4.48585	2.239	-3.59387
C	4.81631	2.54546	-1.21175
C	5.81192	2.59342	-3.81493
H	3.84173	1.98125	-4.42893
C	6.14107	2.89414	-1.45044
H	4.43012	2.52693	-0.19787
C	6.66451	2.92923	-2.75186
H	6.19571	2.6088	-4.83207
H	6.78276	3.14462	-0.60946
C	-6.82411	-0.74471	-0.7809
C	-7.78437	-0.00381	-1.50054
C	-7.27636	-1.79263	0.0491
C	-9.13829	-0.30441	-1.39049
H	-7.45627	0.80913	-2.14095
C	-8.63257	-2.08174	0.14792
H	-6.55157	-2.37092	0.61365
C	-9.59032	-1.34762	-0.56906
H	-9.86051	0.2829	-1.95244
H	-8.9572	-2.8925	0.79584
C	-11.05698	-1.6895	-0.47714
H	-11.3159	-2.51083	-1.15824
H	-11.3319	-2.01119	0.53269
H	-11.68627	-0.83515	-0.74423
C	8.09307	3.34235	-3.00406
H	8.50396	2.84825	-3.89002
H	8.16596	4.42464	-3.17384
H	8.73659	3.10456	-2.15153

TS_{EA}

C	0.36979	-1.47555	-0.50259
C	1.9024	-1.42987	-0.58331
C	2.68056	-1.42435	0.73658
C	2.13472	-1.56117	1.98052
C	-0.32406	-1.40831	1.4673
C	0.72398	-1.72464	2.28599
H	-0.0212	-2.4882	-0.41403
H	2.147	-0.49776	-1.10242
C	2.93695	-1.71391	3.26492
H	3.66989	-0.91095	3.39387
C	1.8747	-1.74727	4.38467
H	1.68654	-0.73072	4.74897
C	0.6029	-2.28228	3.69469
H	0.62084	-3.38245	3.6619
H	-0.3243	-1.98704	4.19218
H	2.1803	-2.35403	5.2419
H	3.50771	-2.65201	3.23425
Pd	-0.40403	0.39747	0.52303
P	-0.63921	2.74809	0.23178
C	-2.10653	3.32358	-0.72895
C	-3.2887	2.57157	-0.63308
C	-2.09174	4.46558	-1.5438
C	-4.43593	2.9619	-1.32377
H	-3.30231	1.67157	-0.02386
C	-3.23956	4.85017	-2.24057
H	-1.1848	5.05372	-1.64135
C	-4.41299	4.10222	-2.13009
H	-5.34154	2.36746	-1.24389
H	-3.21361	5.73432	-2.87162
H	-5.30323	4.40121	-2.6764
C	0.79196	3.6001	-0.56642
C	1.27447	4.84558	-0.1364
C	1.41657	2.95872	-1.65021
C	2.36028	5.44231	-0.78116
H	0.80828	5.35029	0.70378
C	2.49563	3.56458	-2.29524
H	1.0647	1.98573	-1.98478
C	2.97109	4.80449	-1.86214
H	2.7278	6.40484	-0.43589
H	2.97113	3.05994	-3.1317
H	3.81725	5.26875	-2.36115
C	-0.81173	3.60144	1.86404
C	-1.67512	4.68585	2.07839
C	-0.03871	3.12631	2.93744
C	-1.76055	5.28313	3.33866
H	-2.28511	5.06479	1.2647
C	-0.11819	3.73081	4.1917
H	0.62322	2.27702	2.78663
C	-0.98235	4.80945	4.39588
H	-2.43709	6.11949	3.49145
H	0.48691	3.35306	5.01114
H	-1.05218	5.27436	5.37527
C	2.37789	-2.57695	-1.48641
C	2.75795	-2.32506	-2.81107
C	2.41009	-3.8992	-1.01848
C	3.16595	-3.36733	-3.64628
H	2.71682	-1.30804	-3.18801
C	2.81445	-4.94203	-1.85227
H	2.12876	-4.11227	0.00961
C	3.19586	-4.67921	-3.17018
H	3.45827	-3.15261	-4.6708
H	2.83689	-5.95958	-1.47112
H	3.5133	-5.49047	-3.8196
C	-0.3149	-0.79598	-1.67117
O	0.31379	-0.11993	-2.50294
C	-1.74838	-1.13733	-1.86902
C	-2.42566	-0.70766	-2.95286
H	-2.21418	-1.76015	-1.11071

H	-1.87494	-0.07906	-3.65056
C	-3.82202	-0.97702	-3.30077
C	-4.37905	-0.32015	-4.41489
C	-4.64269	-1.86751	-2.57852
C	-5.70487	-0.53256	-4.78896
H	-3.75864	0.36621	-4.98541
C	-5.96625	-2.07945	-2.95262
H	-4.24016	-2.40354	-1.72475
C	-6.50511	-1.41286	-4.05847
H	-6.11219	-0.01248	-5.65156
H	-6.57992	-2.77155	-2.38244
H	-7.53798	-1.58333	-4.34891
C	-1.64703	-1.82806	1.69699
C	-2.79993	-2.20598	1.8647
C	4.08325	-1.28118	0.59831
C	5.28634	-1.14905	0.43914
C	-4.13722	-2.6426	2.07924
C	-5.21988	-2.01392	1.42761
C	-4.4153	-3.71963	2.94729
C	-6.5228	-2.45251	1.6388
H	-5.02572	-1.18489	0.75445
C	-5.72398	-4.14342	3.15153
H	-3.59421	-4.21832	3.45289
C	-6.80248	-3.52059	2.50494
H	-7.34069	-1.95471	1.12356
H	-5.91432	-4.97669	3.82356
C	6.686	-0.99867	0.23822
C	7.56545	-0.82565	1.32863
C	7.23	-1.01399	-1.06257
C	8.93071	-0.67453	1.11728
H	7.16296	-0.80686	2.33674
C	8.59928	-0.86069	-1.25756
H	6.5661	-1.14701	-1.91103
C	9.47609	-0.68985	-0.17669
H	9.58952	-0.53934	1.97197
H	8.99642	-0.87352	-2.26956
C	10.96308	-0.54731	-0.38891
H	11.38054	0.26017	0.22262
H	11.49333	-1.46696	-0.10949
H	11.20123	-0.33668	-1.43552
C	-8.22146	-3.96797	2.7534
H	-8.8525	-3.81319	1.87247
H	-8.26661	-5.02776	3.02254
H	-8.67418	-3.40347	3.57909

A + 1-4

C	1.29505	1.64649	-0.02894
C	-0.18677	1.79775	-0.47753
C	2.19832	1.17064	-1.171
C	-0.68019	0.62933	-1.35857
C	0.26883	-0.02284	-2.17121
C	1.6805	0.33748	-2.11914
C	2.40816	-0.30889	-3.28053
H	2.63131	0.44979	-4.04529
H	3.36965	-0.74363	-2.98648
C	1.40207	-1.35085	-3.8228
H	1.52577	-1.5418	-4.89348
H	1.53472	-2.30255	-3.29518
C	0.01723	-0.76506	-3.47702
H	-0.77237	-1.51657	-3.41346
H	-0.28902	-0.03403	-4.24352
C	-2.06591	0.59666	-1.68424
C	-3.25953	0.61083	-1.94055
C	3.57485	1.48162	-1.14306
C	4.76105	1.76738	-1.11175
C	-4.65151	0.61546	-2.2322
C	-5.55678	1.33374	-1.42329
C	-5.16527	-0.09794	-3.33503
C	-6.91704	1.33426	-1.71374
H	-5.18031	1.88228	-0.5653
C	-6.52855	-0.08896	-3.61079
H	-4.48295	-0.65954	-3.96619
C	-7.4307	0.62812	-2.81136
H	-7.59608	1.8921	-1.07252
H	-6.90202	-0.65097	-4.46416
C	6.13319	2.13044	-1.04876
C	7.07781	1.58212	-1.94027
C	6.58417	3.06204	-0.08885
C	8.41714	1.95217	-1.86852
H	6.74681	0.86842	-2.68889
C	7.92596	3.42094	-0.02995
H	5.86619	3.49943	0.59825
C	8.86931	2.87335	-0.91302
H	9.12739	1.5183	-2.56911
H	8.25034	4.1435	0.71598
C	10.32966	3.24747	-0.81874
H	10.84837	2.6439	-0.06119
H	10.84717	3.08846	-1.77075
H	10.45765	4.29824	-0.53543
C	-8.90536	0.65933	-3.13704
H	-9.51309	0.78401	-2.23422
H	-9.14837	1.49389	-3.80923
H	-9.22583	-0.26151	-3.6364
C	3.50235	-4.46675	2.837
C	2.16905	-4.29467	2.45979
C	1.84419	-3.55484	1.31167
C	2.88138	-2.98116	0.55938
C	4.214	-3.15847	0.93445
C	4.52687	-3.90198	2.0742
H	3.73932	-5.03773	3.73112
H	1.3803	-4.72762	3.06811
H	2.63401	-2.37869	-0.31076
H	5.00483	-2.70198	0.3453
H	5.56372	-4.03195	2.37306

P	0.10599	-3.28278	0.74146
C	-0.88035	-3.38799	2.30263
C	-1.38783	-4.59193	2.81478
C	-1.12704	-2.1919	2.99883
C	-2.11558	-4.60232	4.00698
H	-1.22288	-5.52228	2.27906
C	-1.84849	-2.2084	4.19329
H	-0.76906	-1.24565	2.59895
C	-2.34361	-3.41204	4.70013
H	-2.50587	-5.54135	4.39121
H	-2.03318	-1.27571	4.71951
H	-2.91253	-3.42159	5.62628
C	-0.32883	-4.84403	-0.1493
C	-1.49053	-4.8329	-0.94045
C	0.43368	-6.01929	-0.08555
C	-1.88989	-5.9749	-1.63352
H	-2.07464	-3.9185	-1.01635
C	0.03859	-7.15935	-0.79128
H	1.34094	-6.04748	0.51
C	-1.12409	-7.14185	-1.56235
H	-2.79283	-5.95019	-2.23806
H	0.64302	-8.06116	-0.73588
H	-1.42905	-8.02932	-2.11064
Pd	-0.29579	-1.30726	-0.40299
C	1.77809	2.92809	0.63857
C	2.00526	4.09443	-0.10764
C	1.98595	2.97148	2.02252
C	2.43029	5.26946	0.51212
H	1.86645	4.07695	-1.18591
C	2.41305	4.14572	2.64695
H	1.80442	2.07828	2.61409
C	2.63686	5.29914	1.89385
H	2.6057	6.1609	-0.08491
H	2.56928	4.15717	3.72268
H	2.96916	6.21401	2.37773
H	1.29776	0.84631	0.72775
H	-0.27722	2.7119	-1.0853
C	-1.09333	1.95744	0.7597
O	-0.93083	1.25503	1.75212
C	-2.15849	2.98255	0.68701
C	-2.98112	3.20251	1.73382
H	-2.24348	3.54487	-0.23821
H	-2.80485	2.59053	2.61777
C	-4.07831	4.16418	1.82903
C	-4.7851	4.2629	3.04268
C	-4.46927	4.99858	0.76199
C	-5.83958	5.16174	3.1909
H	-4.49628	3.62422	3.87381
C	-5.52299	5.89459	0.90927
H	-3.94604	4.94245	-0.18777
C	-6.21226	5.98122	2.124
H	-6.37002	5.22195	4.13727
H	-5.81038	6.52888	0.07509
H	-7.03462	6.6827	2.23506

I would like to thank ….

Todd Marder for giving me the opportunity to work on this thesis and for advice. Alexandra Friedrich for teaching me how to do crystallography & collecting data, solving structures and recording the Raman spectrum in chapter 1. Xiaoling Luo for conducting the DFT calculations on Chapter 1. My interns Johannes Schneider, Leon Euringer, Luise Kersting, Paul Mentzel, Michelle Kalizki and Alena Neudert for assistance in the lab. The elemental analysis team of the IAC: Liselotte Michels and Sabine Timmroth. Christoph Mahler and Stephan Wagner for teaching me, how to do HRMS. Rüdiger Bertermann, Marie-Luise Schäfer and Laura Wolz for NMR measurements and discussion. Sabine Lorenzen for helping me with problems in the lab & synthesis in chapters 2 and 3. Johannes Krebs for collecting and solving X-Ray structures. Florian Rauch for advice on photophysics. Nils Schopper for measuring Raman spectra in chapter 2 and 3. Ludwig Zapf for conducting the CV experiments in chapter 2. Leon Schneider for advice on technical issues. Florian Kerner for collecting and solving X-Ray structures. Udo Radius for advice. The present and past members of the Marder Group for discussions, help and support: Eva Wittenberg, Jianhua Han, Sharvan Kumar, Weipeng Li, Jiefeng Hu, Xiaolei Zhang, Zhu Wu, Maria-Victoria Benicke-Rojas, Julie Borel, Hamad Al Mamari, Matthias Ferger, Jörn Nitsch, Julia Merz, Laura Kuehn, Jiang He, Shishir Gosh, Xiaoning Guo, Yudha Budiman, Goutam Kumar Kole, Hua Wang, Xiangqing Jia, Stefanie Griesbeck, Jian Zhao, Lei Ji, Hashem Amini, Mingming Huang, Hildegard Holzinger, Zhiqiang Liu, Sarina Berger, Jan Maier, Jiang He, Yaming Tian , Laura Kuehn, Xiaocui Liu, Wenbo Ming. And the technical and workshop staff of the institute: Stephan Köper, Alfred Schertzer, Cornelia Walter, Gertrud Wunderling, Wolfgang Obert & Manfred Reinhardt.

References

1. Chopade, P. R.; Louie, J., [2+2+2] Cycloaddition reactions catalyzed by transition metal complexes. *Adv. Synth. Catal.* **2006**, *348*, 2307-2327.
2. Domínguez, G.; Pérez-Castells, J., Alkenes in [2+2+2] Cycloadditions. *Chem. Eur. J.* **2016**, *22*, 6720-6739.
3. Aubert, C.; Gandon, V.; Han, S.; Johnson, B. M.; Malacria, M.; Schömenauer, S.; Vollhardt, K. P. C.; Whitener, G. D., Cyclopentadienylcobalt-Mediated Intermolecular Cycloaddition of α, ω-Diynes to (Cyclo) alkenes: Synthesis of Linearly Fused Oligocycles and Extension to Enantiomerically Pure (6aR, 10aR)-Dihydroanthracyclinones. *Synthesis* **2010**, *13*, 2179-2200.
4. A Worlikar, S.; C Larock, R., Pd-catalyzed reactions involving arynes. *Curr. Org. Chem.* **2011**, *15*, 3214-3232.
5. Agenet, N.; Buisine, O.; Slowinski, F.; Gandon, V.; Aubert, C.; Malacria, M., Cotrimerizations of acetylenic compounds. *Org. React.* **2004**, *68*, 1-302.
6. Roglans, A.; Pla-Quintana, A.; Solà, M., Mechanistic Studies of Transition-Metal-Catalyzed [2+ 2+ 2] Cycloaddition Reactions. *Chem. Rev.* **2020**, *121*, 1894–1979.
7. Yamamoto, Y., Theoretical Study of the Mechanism of Palladium(0)-Catalyzed Intramolecular [2+2+2] Cycloaddition of Ester-Substituted Alkynes. *Eur. J. Org. Chem.* **2020**, *48*, 7455-7465.
8. Gandon, V.; Agenet, N.; Vollhardt, K. P. C.; Malacria, M.; Aubert, C., Cobalt-mediated cyclic and linear 2:1 cooligomerization of alkynes with alkenes: A DFT study. *J. Am. Chem. Soc.* **2006**, *128*, 8509-8520.
9. Yamamoto, K.; Nagae, H.; Tsurugi, H.; Mashima, K., Mechanistic understanding of alkyne cyclotrimerization on mononuclear and dinuclear scaffolds: [4 + 2] cycloaddition of the third alkyne onto metallacyclopentadienes and dimetallacyclopentadienes. *Dalton Trans.* **2016**, *45*, 17072-17081.
10. Rourke, J. P.; Batsanov, A. S.; Howard, J. A. K.; Marder, T. B., Regiospecific high yield reductive coupling of diynes to give a luminescent rhodium complex. *Chem. Commun.* **2001**, 2626-2627.
11. Steffen, A.; Ward, R. M.; Tay, M. G.; Edkins, R. M.; Seeler, F.; van Leeuwen, M.; Pålsson, L.-O.; Beeby, A.; Batsanov, A. S.; Howard, J. A. K.; Marder, T. B., Regiospecific Formation and Unusual Optical Properties of 2,5-Bis(arylethynyl)rhodacyclopentadienes: A New Class of Luminescent Organometallics. *Chem. Eur. J.* **2014**, *20*, 3652-3666.
12. Steffen, A.; Tay, M. G.; Batsanov, A. S.; Howard, J. A. K.; Beeby, A.; Vuong, K. Q.; Sun, X.-Z.; George, M. W.; Marder, T. B., 2,5-Bis(p-R-arylethynyl)rhodacyclopentadienes Show Intense Fluorescence: Denying the Presence of a Heavy Atom. *Angew. Chem.* **2010**, *122*, 2399-2403.
13. Steffen, A.; Costuas, K.; Boucekkine, A.; Thibault, M.-H.; Beeby, A.; Batsanov, A. S.; Charaf-Eddin, A.; Jacquemin, D.; Halet, J.-F.; Marder, T. B., Fluorescence in Rhoda- and Iridacyclopentadienes Neglecting the Spin–Orbit Coupling of the Heavy Atom: The Ligand Dominates. *Inorg. Chem.* **2014**, *53*, 7055-7069.
14. Sieck, C.; Tay, M. G.; Thibault, M.-H.; Edkins, R. M.; Costuas, K.; Halet, J.-F.; Batsanov, A. S.; Haehnel, M.; Edkins, K.; Lorbach, A.; Steffen, A.; Marder, T. B., Reductive Coupling of Diynes at Rhodium Gives Fluorescent Rhodacyclopentadienes or Phosphorescent Rhodium 2,2'-Biphenyl Complexes. *Chem. Eur. J.* **2016**, *22*, 10523-10532.

15. Sieck, C.; Sieh, D.; Sapotta, M.; Haehnel, M.; Edkins, K.; Lorbach, A.; Steffen, A.; Marder, T. B., Convenient synthetic access to fluorescent rhodacyclopentadienes via ligand exchange reactions. *J. Organomet. Chem.* **2017**, *847*, 184-192.
16. Kerner, F. Reactions of rhodium(I) with diynes and studies of the photophysical behavior of the luminescent products, Ph.D. Thesis. Julius-Maximilians-Universität Würzburg, Würzburg, **2020**.
17. Maier, J. R. Investigations of Metal-free Cannibalistic Hexadehydro-Diels-Alder and Pt-catalyzed Dimerization Reactions of Linked Aryl Bisdiynes, Ph.D. Thesis. Julius-Maximilians-Universität Würzburg, Würzburg, **2021**.
18. Xin, H.; Gao, X., Application of azulene in constructing organic optoelectronic materials: new tricks for an old dog. *ChemPlusChem* **2017**, *82*, 945-956.
19. Haley, M. M.; Tykwinski, R. R., *Carbon-rich compounds: from molecules to materials*. John Wiley & Sons, Weinheim: **2006**.
20. Huy Do, H.; Villinger, A.; Lochbrunner, S.; Ehlers, P.; Langer, P., Palladium-Catalyzed Synthesis and Fluorescence Study of Ethynylated Naphthalene Derivatives. *Eur. J. Org. Chem.* **2017**, 2238-2244.
21. Lee, H. W.; Kim, H. J.; Kim, Y. S.; Kim, J.; Lee, S. E.; Lee, H. W.; Kim, Y. K.; Yoon, S. S., Emitting materials based on phenylanthracene-substituted naphthalene derivatives for organic light-emitting diodes. *J. Lumin.* **2015**, *165*, 99-104.
22. Wang, C.; Dong, H.; Hu, W.; Liu, Y.; Zhu, D., Semiconducting π-conjugated systems in field-effect transistors: a material odyssey of organic electronics. *Chem. Rev.* **2012**, *112*, 2208-2267.
23. Jiang, H.-F.; Shen, Y.-X.; Wang, Z.-Y., A simple $PdCl_2/O_2$/DMF catalytic system for highly regioselective cyclotrimerization of olefins with electron-withdrawing groups. *Tetrahedron Lett.* **2007**, *48*, 7542-7545.
24. Liu, Y.-L.; Liang, Y.; Pi, S.-F.; Huang, X.-C.; Li, J.-H., Palladium-catalyzed cocyclotrimerization of allenes with arynes: Selective synthesis of phenanthrenes. *J. Org. Chem.* **2009**, *74*, 3199-3202.
25. Shen, Y.; Jiang, H.; Chen, Z., $PdCl_2(HNMe_2)_2$-catalyzed highly selective cross [2+2+2] cyclization of Alkynoates and alkenes under molecular oxygen. *J. Org. Chem.* **2010**, *75*, 1321-1324.
26. Yamamoto, Y.; Kuwabara, S.; Ando, Y.; Nagata, H.; Nishiyama, H.; Itoh, K., Palladium (0)-catalyzed cyclization of electron-deficient enynes and enediynes. *J. Org. Chem.* **2004**, *69*, 6697-6705.
27. Zhou, P.; Huang, L.; Jiang, H.; Wang, A.; Li, X., Highly Chemoselective Palladium-Catalyzed Cross-Trimerization between Alkyne and Alkenes Leading to 1,3,5-Trienes or 1,2,4,5-Tetrasubstituted Benzenes with Dioxygen. *J. Org. Chem.* **2010**, *75*, 8279-8282.
28. Zhou, P.; Zheng, M.; Jiang, H.; Li, X.; Qi, C., An aerobic [2+2+2] Cyclization via Chloropalladation: From 1,6-Diynes and Acrylates to Substituted Aromatic Carbocycles. *J. Org. Chem.* **2011**, *76*, 4759-4763.
29. Berlman, I. B., *Handbook of fluorescence spectra of aromatic molecules*. Academic Press: New York, **1971**.
30. Woodward, R. B.; Hoffmann, R., Stereochemistry of Electrocyclic Reactions. *J. Am. Chem. Soc.* **1965**, *87*, 395-397.
31. Woodward, R. B.; Hoffmann, R., *The conservation of orbital symmetry*. Verlag Chemie, Weinheim: **1970**.
32. Zhu, G.-D.; Okamura, W. H., Synthesis of Vitamin D (Calciferol). *Chem. Rev.* **1995**, *95*, 1877-1952.

33. Lin-Vien, D.; Colthup, N. B.; Fateley, W. G.; Grasselli, J. G., *The handbook of infrared and Raman characteristic frequencies of organic molecules. Chapter 7 - Acetylenes*. Academic Press: San Diego, CA: **1991**.
34. Trost, B. M.; Li, C.-J., *Modern alkyne chemistry: Catalytic and atom-economic transformations*. John Wiley & Sons, Weinheim: **2015**.
35. Nishiwaki, N., *Methods and applications of cycloaddition reactions in organic syntheses*. John Wiley & Sons, Weinheim: **2013**.
36. Tron, G. C.; Pirali, T.; Billington, R. A.; Canonico, P. L.; Sorba, G.; Genazzani, A. A., Click chemistry reactions in medicinal chemistry: Applications of the 1,3-dipolar cycloaddition between azides and alkynes. *Med. Res. Rev.* **2008**, *28*, 278-308.
37. Broere, D. L. J.; Ruijter, E., Recent advances in transition-metal-catalyzed [2+2+2]-cyclo(co) trimerization reactions. *Synthesis* **2012**, *44*, 2639-2672.
38. Domínguez, G.; Pérez-Castells, J., Recent advances in [2+2+2] cycloaddition reactions. *Chem. Soc. Rev.* **2011**, *40*, 3430-3444.
39. Kotha, S.; Brahmachary, E.; Lahiri, K., Transition metal catalyzed [2+2+2] cycloaddition and application in organic synthesis. *Eur. J. Org. Chem.* **2005**, 4741-4767.
40. Hara, H.; Hirano, M.; Tanaka, K., A new route to substituted phenols by cationic rhodium (I)/BINAP complex-catalyzed decarboxylative [2+ 2+ 2] cycloaddition. *Org. Lett.* **2009**, *11*, 1337-1340.
41. Dachs, A.; Torrent, A.; Pla-Quintana, A.; Roglans, A.; Jutand, A., Rates and mechanism of Rhodium-catalyzed [2+2+2] cycloaddition of bisalkynes and a monoalkyne. *Organometallics* **2009**, *28*, 6036-6043.
42. Yamamoto, Y.; Ishii, J.-i.; Nishiyama, H.; Itoh, K., Ru(II)-catalyzed chemo-and regioselective cyclotrimerization of three unsymmetrical alkynes through boron temporary tether. One-pot four-component coupling via cyclotrimerization/Suzuki-Miyaura coupling. *J. Am. Chem. Soc.* **2004**, *126*, 3712-3713.
43. Lübtow, M.; Helmers, I.; Stepanenko, V.; Albuquerque, R. Q.; Marder, T. B.; Fernández, G., Self-Assembly of 9,10-Bis (phenylethynyl) Anthracene (BPEA) Derivatives: Influence of π–π and Hydrogen-Bonding Interactions on Aggregate Morphology and Self-Assembly Mechanism. *Chem. Eur. J.* **2017**, *23*, 6198-6205.
44. Bunz, U. H.; Rubin, Y.; Tobe, Y., Polyethynylated cyclic π-systems: scaffoldings for novel two and three-dimensional carbon networks. *Chem. Soc. Rev.* **1999**, *28*, 107-119.
45. Breiten, B.; Biaggio, I.; Diederich, F., Nonplanar push–pull chromophores for opto-electronic applications. *Chimia* **2010**, *64*, 409-413.
46. Zhang, J.; Smith, Z. C.; Thomas III, S. W., Electronic effects of ring fusion and alkyne substitution on acene properties and reactivity. *J. Org. Chem.* **2014**, *79*, 10081-10093.
47. Diederich, F.; Stang, P. J.; Tykwinski, R. R., *Acetylene chemistry: chemistry, biology and material science*. John Wiley & Sons, Weinheim: **2006**.
48. Piao, M. J.; Chajara, K.; Yoon, S. J.; Kim, H. M.; Jeon, S.-J.; Kim, T.-H.; Song, K.; Asselberghs, I.; Persoons, A.; Clays, K., First hyperpolarizabilities of hexa(ethynyl)benzene derivatives: effect of conjugation length. *J. Mater. Chem.* **2006**, *16*, 2273-2281.
49. Bui, T.-T.; Goubard, F.; Ibrahim-Ouali, M.; Gigmes, D.; Dumur, F., Thermally activated delayed fluorescence emitters for deep blue organic light emitting diodes: A review of recent advances. *Appl. Sci.* **2018**, *8*, 494.
50. Xu, Y.; Xu, P.; Hu, D.; Ma, Y., Recent progress in hot exciton materials for organic light-emitting diodes. *Chem. Soc. Rev.* **2021**, *50*, 1030-1069.
51. Maier, J.; Deutsch, M.; Merz, J.; Ye, Q.; Diamond, O.; Schilling, M.-T.; Friedrich, A.; Engels, B.; Marder, T. B., Highly Conjugated π-Systems Arising from Cannibalistic

Hexadehydro-Diels-Alder Couplings: Cleavage of C–C Single and Triple Bonds. *Chem. Eur. J.* **2020**, *26*, 15989-16000.
52. Diamond, O. J.; Marder, T. B., Methodology and applications of the hexadehydro-Diels-Alder (HDDA) reaction. *Org. Chem. Front.* **2017**, *4*, 891-910.
53. Schwenk, N. Seeing the Light: Synthesis of Luminescent Rhodacyclopentadienes and Investigations of their Optical Properties and Catalytic Activity, Ph.D. Thesis. Julius-Maximilians-Universität Würzburg, Würzburg, **2018**.
54. Tasker, S. Z.; Standley, E. A.; Jamison, T. F., Recent advances in homogeneous nickel catalysis. *Nature* **2014**, *509*, 299-309.
55. Doyle, A. G.; Shields, J. D.; Gray, E. E.; Doyle, A. G., A modular, air-stable nickel precatalyst. *Org. Lett.* **2015**, *17*, 2166-2169.
56. Magano, J.; Monfette, S., Development of an air-stable, broadly applicable nickel source for nickel-catalyzed cross-coupling. *ACS Catal.* **2015**, *5*, 3120-3123.
57. Goswami, A.; Ito, T.; Okamoto, S., Efficient Activation of 2-Iminomethylpyridine/Cobalt-Based Alkyne [2+2+2] Cycloaddition Catalyst by Addition of a Silver Salt. *Adv. Synth. Catal.* **2007**, *349*, 2368-2374.
58. Orian, L.; Van Stralen, J. N. P.; Bickelhaupt, F. M., Cyclotrimerization reactions catalyzed by rhodium(I) half-sandwich complexes: A mechanistic density functional study. *Organometallics* **2007**, *26*, 3816-3830.
59. Varela, J. A.; Saá, C., CpRuCl- and CpCo-catalyzed or mediated cyclotrimerizations of alkynes and [2+2+2] cycloadditions of alkynes to alkenes: A comparative DFT study. *J. Organomet. Chem.* **2009**, *694*, 143-149.
60. Sauer, J., Diels-Alder Reactions II: The Reaction Mechanism. *Angew. Chem. Int. Ed.* **1967**, *6*, 16-33.
61. Arjona-Esteban, A.; Lenze, M. R.; Meerholz, K.; Würthner, F., *Donor–acceptor dyes for organic photovoltaics*. Springer, Basel: **2017**; p 193-214.
62. Ahn, D. H.; Kim, S. W.; Lee, H.; Ko, I. J.; Karthik, D.; Lee, J. Y.; Kwon, J. H., Highly efficient blue thermally activated delayed fluorescence emitters based on symmetrical and rigid oxygen-bridged boron acceptors. *Nature Photonics* **2019**, *13*, 540-546.
63. Giordano, L.; Shvadchak, V. V.; Fauerbach, J. A.; Jares-Erijman, E. A.; Jovin, T. M., Highly solvatochromic 7-aryl-3-hydroxychromones. *J. Phys. Chem. Lett.* **2012**, *3*, 1011-1016.
64. Do, J.; Huh, J.; Kim, E., Solvatochromic fluorescence of piperazine-modified bipyridazines for an organic solvent-sensitive film. *Langmuir* **2009**, *25*, 9405-9412.
65. Valeur, B.; Berberan-Santos, M. N., *Molecular fluorescence: principles and applications*. John Wiley & Sons, Weinheim: **2012**.
66. Zhou, C.; Cong, D.; Gao, Y.; Liu, H.; Li, J.; Zhang, S.; Su, Q.; Wu, Q.; Yang, B., Enhancing the Electroluminescent Efficiency of Acridine-Based Donor–Acceptor Materials: Quasi-Equivalent Hybridized Local and Charge-Transfer State. *J. Phys. Chem. Lett.* **2018**, *122*, 18376-18382.
67. Van Mullekom, H.; Vekemans, J.; Havinga, E.; Meijer, E., Developments in the chemistry and band gap engineering of donor–acceptor substituted conjugated polymers. *Mater. Sci. Eng. Rep.* **2001**, *32*, 1-40.
68. Englman, R.; Jortner, J., The energy gap law for radiationless transitions in large molecules. *Mol. Phys.* **1970**, *18*, 145-164.
69. Lin-Vien, D.; Colthup, N.; Fateley, W.; Grasselli, J., *The handbook of infrared and Raman characteristic frequencies of organic molecules. Chapter 8 The–C≡N and–N≡C Groups*. Academic Press: San Diego: **1991**.

70. Chalifoux, W. A.; Tykwinski, R. R., Synthesis of polyynes to model the sp-carbon allotrope carbyne. *Nat. Chem.* **2010**, *2*, 967.
71. Shi Shun, A. L.; Tykwinski, R. R., Synthesis of naturally occurring polyynes. *Angew. Chem. Int. Ed.* **2006**, *45*, 1034-1057.
72. Zidorn, C.; Jöhrer, K.; Ganzera, M.; Schubert, B.; Sigmund, E. M.; Mader, J.; Greil, R.; Ellmerer, E. P.; Stuppner, H., Polyacetylenes from the Apiaceae vegetables carrot, celery, fennel, parsley, and parsnip and their cytotoxic activities. *J. Agric. Food Chem.* **2005**, *53*, 2518-2523.
73. Pan, Y.; Lowary, T. L.; Tykwinski, R. R., Naturally occurring and synthetic polyyne glycosides. *Can. J. Chem.* **2009**, *87*, 1565-1582.
74. Bryce, M. R., A review of functional linear carbon chains (oligoynes, polyynes, cumulenes) and their applications as molecular wires in molecular electronics and optoelectronics. *J. Mater. Chem. C* **2021**, *9*, 10524-10546.
75. Casari, C. S.; Tommasini, M.; Tykwinski, R. R.; Milani, A., Carbon-atom wires: 1-D systems with tunable properties. *Nanoscale* **2016**, *8*, 4414-4435.
76. Thiele, C.; Gerhard, L.; Eaton, T. R.; Torres, D. M.; Mayor, M.; Wulfhekel, W.; Löhneysen, H. V.; Lukas, M., STM study of oligo(phenylene-ethynylene)s. *New. J. Phys* **2015**, *17*.
77. Zhao, Z.; Su, H.; Zhang, P.; Cai, Y.; Kwok, R. T.; Chen, Y.; He, Z.; Gu, X.; He, X.; Sung, H. H., Polyyne bridged AIE luminogens with red emission: design, synthesis, properties and applications. *J. Mater. Chem. B* **2017**, *5*, 1650-1657.
78. Cataldo, F., *Polyynes: synthesis, properties, and applications*. CRC Press, Boca Raton: **2005**.
79. Pigulski, B.; Gulia, N.; Szafert, S., Reactivity of polyynes: complex molecules from simple carbon rods. *Eur. J. Org. Chem.* **2019**, *2019*, 1420-1445.
80. Akhtar, R.; Zahoor, A. F., Transition metal catalyzed Glaser and Glaser-Hay coupling reactions: Scope, classical/green methodologies and synthetic applications. *Synth. Commun.* **2020**, 1-32.
81. Deperasińska, I.; Szemik-Hojniak, A.; Osowska, K.; Rode, M.; Szczepanik, A.; Lis, T.; Szafert, S., Synthesis, photophysics and excited state structure of 1,8-di (p-tolyl)-1,3,5,7-octatetrayne. *J. Photochem. Photobiol.* **2011**, *217*, 299-307.
82. Gulia, N.; Osowska, K.; Pigulski, B.; Lis, T.; Galewski, Z.; Szafert, S., Mori–Hiyama versus Hay coupling for higher polyynes. *Eur. J. Org. Chem.* **2012**, *2012*, 4819-4830.
83. Batsanov, A. S.; Collings, J. C.; Fairlamb, I. J.; Holland, J. P.; Howard, J. A.; Lin, Z.; Marder, T. B.; Parsons, A. C.; Ward, R. M.; Zhu, J., Requirement for an oxidant in Pd/Cu co-catalyzed terminal alkyne homocoupling to give symmetrical 1,4-disubstituted 1,3-diynes. *J. Org. Chem.* **2005**, *70*, 703-6.
84. Radhika, S.; Harry, N. A.; Neetha, M.; Anilkumar, G., Recent trends and applications of the Cadiot–Chodkiewicz reaction. *Org. Biomol. Chem.* **2019**, *17*, 9081-9094.
85. Luu, T.; Morisaki, Y.; Cunningham, N.; Tykwinski, R. R., One-pot formation and derivatization of di-and triynes based on the Fritsch−Buttenberg−Wiechell rearrangement. *J. Org. Chem.* **2007**, *72*, 9622-9629.
86. Curbet, I.; Colombel-Rouen, S.; Manguin, R.; Clermont, A.; Quelhas, A.; Müller, D. S.; Roisnel, T.; Baslé, O.; Trolez, Y.; Mauduit, M., Expedient synthesis of conjugated triynes via alkyne metathesis. *Chem. Sci.* **2020**, *11*, 4934-4938.
87. Eisler, S.; Chahal, N.; McDonald, R.; Tykwinski, R. R., Alkyne migration in alkylidene carbenoid species: A new method of polyyne synthesis. *Chem. Eur. J.* **2003**, *9*, 2542-2550.
88. Springborg, M.; Kavan, L., On the stability of polyyne. *Chem. Phys.* **1992**, *168*, 249-258.

89. Cataldo, F., Stability of polyynes in air and their degradation by ozonolysis. *Polym. Degrad. Stab.* **2006**, *91*, 317-323.
90. Gulcur, M.; Moreno-García, P.; Zhao, X.; Baghernejad, M.; Batsanov, A. S.; Hong, W.; Bryce, M. R.; Wandlowski, T., The Synthesis of Functionalised Diaryltetraynes and Their Transport Properties in Single-Molecule Junctions. *Chem. Eur. J.* **2014**, *20*, 4653-4660.
91. Gibtner, T.; Hampel, F.; Gisselbrecht, J. P.; Hirsch, A., End-cap stabilized oligoynes: model compounds for the linear sp carbon allotrope carbyne. *Chem. Eur. J.* **2002**, *8*, 408-432.
92. Glen, A.; Hutchinson, S., Contribution of triacetylene to the biological effects of Fomes annosus. *Trans. Brit. Mycol. Soc.* **1973**, *61*, 583-585.
93. Baughman, R. H., Dangerously seeking linear carbon. *Science* **2006**, *312*, 1009-1110.
94. Lesley, G.; Nguyen, P.; Taylor, N. J.; Marder, T. B.; Scott, A. J.; Clegg, W.; Norman, N. C., Synthesis and Characterization of Platinum(II)−Bis(boryl) Catalyst Precursors for Diboration of Alkynes and Diynes: Molecular Structures of cis-$[(PPh_3)_2Pt(B\text{-}4\text{-}Bu^tcat)_2]$, cis-$[(PPh_3)_2Pt(Bcat)_2]$, cis-$[(dppe)Pt(Bcat)_2]$, cis-$[(dppb)Pt(Bcat)_2]$, (E)-(4-$MeOC_6H_4$)C(Bcat)CH(Bcat), (Z)-($C_6H_5$)C(Bcat)C($C_6H_5$)(Bcat), and (Z,Z)-(4-$MeOC_6H_4$)C(Bcat)C(Bcat)C(Bcat)C(4-$MeOC_6H_4$)(Bcat) (cat = 1,2-$O_2C_6H_4$; dppe = $Ph_2PCH_2CH_2PPh_2$; dppb = $Ph_2P(CH_2)4PPh_2$). *Organometallics* **1996**, *15*, 5137-5154.
95. Berger, S. M.; Ferger, M.; Marder, T. B., Synthetic Approaches to Triarylboranes from 1885 to 2020. *Chem. Eur. J.* **2021**, *27*, 7043-7058.
96. Berger, S. M.; Marder, T. B., Applications of triarylborane materials in cell imaging and sensing of bio-relevant molecules such as DNA, RNA, and proteins. *Mater. Horiz.* **2022**, *9*, 112-120.
97. Entwistle, C. D.; Marder, T. B., Applications of three-coordinate organoboron compounds and polymers in optoelectronics. *Chem. Mater.* **2004**, *16*, 4574-4585.
98. Hudson, Z. M.; Wang, S., Metal-containing triarylboron compounds for optoelectronic applications. *Dalton Trans.* **2011**, *40*, 7805-7816.
99. Turkoglu, G.; Cinar, M. E.; Ozturk, T., Triarylborane-based materials for OLED applications. *Molecules* **2017**, *22*, 1522.
100. Sun, Z.-B.; Li, S.-Y.; Liu, Z.-Q.; Zhao, C.-H., Triarylborane π-electron systems with intramolecular charge-transfer transitions. *Chin. Chem. Lett.* **2016**, *27*, 1131-1138.
101. Chiu, C.-W.; Kim, Y.; Gabbaï, F. P., Lewis acidity enhancement of triarylboranes via peripheral decoration with cationic groups. *J. Am. Chem. Soc.* **2009**, *131*, 60-61.
102. Berger, S. M.; Rühe, J.; Schwarzmann, J.; Phillipps, A.; Richard, A. K.; Ferger, M.; Krummenacher, I.; Tumir, L. M.; Ban, Ž.; Crnolatac, I., Bithiophene-Cored, mono-, bis-, and tris-(Trimethylammonium)-Substituted, bis-Triarylborane Chromophores: Effect of the Number and Position of Charges on Cell Imaging and DNA/RNA Sensing. *Chem. Eur. J.* **2021**, *27*, 14057-14072.
103. Griesbeck, S.; Ferger, M.; Czernetzi, C.; Wang, C.; Bertermann, R.; Friedrich, A.; Haehnel, M.; Sieh, D.; Taki, M.; Yamaguchi, S.; Marder, T. B., Optimization of Aqueous Stability versus π-Conjugation in Tetracationic Bis(triarylborane) Chromophores: Applications in Live-Cell Fluorescence Imaging. *Chem. Eur. J.* **2019**, *25*, 7679-7688.
104. Fu, G.-L.; Pan, H.; Zhao, Y.-H.; Zhao, C.-H., Solid-state emissive triarylborane-based BODIPY dyes: Photophysical properties and fluorescent sensing for fluoride and cyanide ions. *Org. Biomol. Chem.* **2011**, *9*, 8141-8146.
105. Yao, C.; Tian, Z.; Jin, D.; Zhao, F.; Sun, Y.; Yang, X.; Zhou, G.; Wong, W.-Y., Platinum(II) acetylide complexes with star-and V-shaped configurations possessing good trade-off between optical transparency and optical power limiting performance. *J. Mater. Chem. C* **2017**, *5*, 11672-11682.

106. Lam, S.-T.; Zhu, N.; Yam, V. W.-W., Synthesis and characterization of luminescent rhenium(I) tricarbonyl diimine complexes with a triarylboron moiety and the study of their fluoride ion-binding properties. *Inorg. Chem.* **2009**, *48*, 9664-9670.
107. Ferger, M.; Ban, Ž.; Krošl, I.; Tomić, S.; Dietrich, L.; Lorenzen, S.; Rauch, F.; Sieh, D.; Friedrich, A.; Griesbeck, S., Bis (phenylethynyl) arene Linkers in Tetracationic Bis-triarylborane Chromophores Control Fluorimetric and Raman Sensing of Various DNAs and RNAs. *Chem. Eur. J.* **2021**, *27*, 5142-5159.
108. Ban, Ž.; Griesbeck, S.; Tomić, S.; Nitsch, J.; Marder, T. B.; Piantanida, I., A quadrupolar bis-triarylborane chromophore as a fluorimetric and chirooptic probe for simultaneous and selective sensing of DNA, RNA and proteins. *Chem. Eur. J.* **2020**, *26*, 2195-2203.
109. Demeunynck, M.; Bailly, C.; Wilson, W. D., *Small molecule DNA and RNA binders: from synthesis to nucleic acid complexes*. John Wiley & Sons, Weinheim: **2006**.
110. Hashem Amini, D.; Ban, Ž.; Ferger, M.; Lorenzen, S.; Rauch, F.; Friedrich, A.; Crnolatac, I.; Kenđel, A.; Miljanić, S.; Piantanida, I., Tetracationic Bis-Triarylborane 1,3-Butadiyne as a Combined Fluorimetric and Raman Probe for Simultaneous and Selective Sensing of Various DNA, RNA, and Proteins. *Chem. Eur. J.* **2020**, *26*, 6017.
111. Langer, J.; Jimenez de Aberasturi, D.; Aizpurua, J.; Alvarez-Puebla, R. A.; Auguié, B.; Baumberg, J. J.; Bazan, G. C.; Bell, S. E.; Boisen, A.; Brolo, A. G., Present and future of surface-enhanced Raman scattering. *ACS Nano* **2019**, *14*, 28-117.
112. Cialla, D.; Pollok, S.; Steinbrücker, C.; Weber, K.; Popp, J., SERS-based detection of biomolecules. *Nanophotonics* **2014**, *3*, 383-411.
113. Hu, F.; Zeng, C.; Long, R.; Miao, Y.; Wei, L.; Xu, Q.; Min, W., Supermultiplexed optical imaging and barcoding with engineered polyynes. *Nat. Meth.* **2018**, *15*, 194-200.
114. Tommasini, M.; Milani, A.; Fazzi, D.; Lucotti, A.; Castiglioni, C.; Januszewski, J. A.; Wendinger, D.; Tykwinski, R. R., π-conjugation and end group effects in long cumulenes: Raman spectroscopy and DFT calculations. *J. Phys. Chem. C* **2014**, *118*, 26415-26425.
115. Lin-Vien, D.; Colthup, N. B.; Fateley, W. G.; Grasselli, J. G., *The Handbook of Infrared and Raman Characteristic Frequencies of Organic Molecules. Chapter 10: Compounds Containing –NH_2, –NHR, and –NR_2 Groups*. Academic Press: San Diego: **1991**.
116. Brown, D. G.; Bostrom, J., Analysis of past and present synthetic methodologies on medicinal chemistry: where have all the new reactions gone? Miniperspective. *J. Med. Chem.* **2016**, *59*, 4443-4458.
117. Sandford, C.; Aggarwal, V. K., Stereospecific functionalizations and transformations of secondary and tertiary boronic esters. *Chem. Commun.* **2017**, *53*, 5481-5494.
118. Hall, D. G., *Boronic acids: preparation, applications in organic synthesis and medicine, 2nd Ed.* John Wiley & Sons, Weinheim: **2011**.
119. Rej, S.; Das, A.; Panda, T. K., Overview of Regioselective and Stereoselective Catalytic Hydroboration of Alkynes. *Adv. Synth. Catal.* **2021**, *363*, 4818-4840.
120. Burgess, K.; Ohlmeyer, M. J., Transition-metal promoted hydroborations of alkenes, emerging methodology for organic transformations. *Chem. Rev.* **1991**, *91*, 1179-1191.
121. Obligacion, J. V.; Chirik, P. J., Earth-abundant transition metal catalysts for alkene hydrosilylation and hydroboration. *Nat. Rev. Chem.* **2018**, *2*, 15-34.
122. Sundararaju, B.; Fürstner, A., A trans-Selective Hydroboration of Internal Alkynes. *Angew. Chem. Int. Ed.* **2013**, *52*, 14050-14054.
123. Bowen, J.; Slebodnick, C.; Santos, W. L., Phosphine-catalyzed hydroboration of propiolonitriles: access to (E)-1,2-vinylcyanotrifluoroborate derivatives. *Chem. Commun.* **2022**, *58*, 5984-5987.

124. Zi, Y.; Schömberg, F.; Seifert, F.; Görls, H.; Vilotijevic, I., trans-Hydroboration vs. 1, 2-reduction: divergent reactivity of ynones and ynoates in Lewis-base-catalyzed reactions with pinacolborane. *Org. Biomol. Chem.* **2018**, *16*, 6341-6349.
125. Nagao, K.; Yamazaki, A.; Ohmiya, H.; Sawamura, M., Phosphine-Catalyzed Anti-Hydroboration of Internal Alkynes. *Org. Lett.* **2018**, *20*, 1861-1865.
126. Li, D.; Kim, Y. E.; Yun, J., Highly regio-and stereoselective synthesis of boron-substituted enynes via copper-catalyzed borylation of conjugated diynes. *Org. Lett.* **2015**, *17*, 860-863.
127. Sang, H. L.; Wu, C.; Phua, G. G. D.; Ge, S., Cobalt-catalyzed regiodivergent stereoselective hydroboration of 1, 3-diynes to access boryl-functionalized enynes. *ACS Catal.* **2019**, *9*, 10109-10114.
128. Sokolnicki, T.; Szyling, J.; Franczyk, A.; Walkowiak, J., Regio-and Stereoselective Synthesis of Enynyl Boronates via Ruthenium-Catalyzed Hydroboration of 1,4-Diaryl-Substituted 1,3-Diynes. *Adv. Synth. Catal.* **2020**, *362*, 177-183.
129. Walkowiak, J.; Szyling, J.; Franczyk, A.; Melen, R. L., Hydroelementation of diynes. *Chem. Soc. Rev.* **2022**, *51*, 869-994.
130. Zweifel, G.; Polston, N. L., Selective hydroboration of conjugated diynes with dialkylboranes. A convenient route to conjugated cis-enynes, alpha,beta-acetylenic ketones, and cis, cis-dienes. *J. Am. Chem. Soc.* **1970**, *92*, 4068-4071.
131. Takahashi, K.; Geib, S. J.; Maeda, K.; Curran, D. P.; Taniguchi, T., Radical trans-hydroboration of substituted 1,3-diynes with an N-heterocyclic carbene borane. *Org. Lett.* **2021**, *23*, 1071-1075.
132. Bage, A. D.; Nicholson, K.; Hunt, T. A.; Langer, T.; Thomas, S. P., The Hidden Role of Boranes and Borohydrides in Hydroboration Catalysis. *ACS Catal.* **2020**, *10*, 13479-13486.
133. Westcott, S. A.; Blom, H. P.; Marder, T. B.; Baker, R. T.; Calabrese, J. C., Nucleophile promoted degradation of catecholborane: consequences for transition metal-catalyzed hydroborations. *Inorg. Chem.* **1993**, *32*, 2175-2182.
134. Zalesskiy, S. S.; Ananikov, V. P., $Pd_2(dba)_3$ as a Precursor of Soluble Metal Complexes and Nanoparticles: Determination of Palladium Active Species for Catalysis and Synthesis. *Organometallics* **2012**, *31*, 2302–2309.
135. Eglinton, G.; McCrae, W., 427. Reactive acetylenic intermediates: the synthesis of 1-bromoacetylenes and mercury acetylides. *J. Chem. Soc.* **1963**, 2295-2299.
136. Wierzbicka, M.; Bylińska, I.; Czaplewski, C.; Wiczk, W., Experimental and theoretical studies of the spectroscopic properties of simple symmetrically substituted diphenylacetylene derivatives. *RSC Adv.* **2015**, *5*, 29294-29303.
137. Yang, Y.; Xu, Y.; Jones, C. R., A Ring Expansion Route to Benzofused N-Heterocycles via Aryne Insertion into 1,3-Diaza-heterocycles. *Eur. J. Org. Chem.* **2019**, *0*.
138. Frisch, M. J.; Trucks, G. W.; Schlegel, H. B.; Scuseria, G. E.; Robb, M. A.; Cheeseman, J. R.; Scalmani, G.; Barone, V.; Petersson, G. A.; Nakatsuji, H.; Li, X.; Caricato, M.; Marenich, A. V.; Bloino, J.; Janesko, B. G.; Gomperts, R.; Mennucci, B.; Hratchian, H. P.; Ortiz, J. V.; Izmaylov, A. F.; Sonnenberg, J. L.; Williams; Ding, F.; Lipparini, F.; Egidi, F.; Goings, J.; Peng, B.; Petrone, A.; Henderson, T.; Ranasinghe, D.; Zakrzewski, V. G.; Gao, J.; Rega, N.; Zheng, G.; Liang, W.; Hada, M.; Ehara, M.; Toyota, K.; Fukuda, R.; Hasegawa, J.; Ishida, M.; Nakajima, T.; Honda, Y.; Kitao, O.; Nakai, H.; Vreven, T.; Throssell, K.; Montgomery Jr., J. A.; Peralta, J. E.; Ogliaro, F.; Bearpark, M. J.; Heyd, J. J.; Brothers, E. N.; Kudin, K. N.; Staroverov, V. N.; Keith, T. A.; Kobayashi, R.; Normand, J.; Raghavachari, K.; Rendell, A. P.; Burant, J. C.; Iyengar, S. S.; Tomasi, J.; Cossi, M.; Millam, J. M.; Klene, M.; Adamo, C.; Cammi, R.;

Ochterski, J. W.; Martin, R. L.; Morokuma, K.; Farkas, O.; Foresman, J. B.; Fox, D. J. *Gaussian 16 Rev. C.01*, Wallingford, CT, **2016**.
139. Becke, A. D., Density-functional thermochemistry. III. The role of exact exchange. *J. Chem. Phys.* **1993**, *98*, 5648-5652.
140. Lee, C.; Yang, W.; Parr, R. G., Development of the Colle-Salvetti correlation-energy formula into a functional of the electron density. *Phys. Rev. B* **1988**, *37*, 785.
141. Dolg, M.; Wedig, U.; Stoll, H.; Preuss, H., Energy-adjusted abinitio pseudopotentials for the first row transition elements. *J. Chem. Phys.* **1987**, *86*, 866-872.
142. Andrae, D.; Huermann, U.; Dolg, M.; Stoll, H.; Preu, H., Energy-adjustedab initio pseudopotentials for the second and third row transition elements: Molecular test for M2 (M=Ag, Au) and MH (M=Ru, Os). *Theor. Chim. Acta* **1991**, *78*, 247-266.
143. Marenich, A. V.; Cramer, C. J.; Truhlar, D. G., Universal Solvation Model Based on Solute Electron Density and on a Continuum Model of the Solvent Defined by the Bulk Dielectric Constant and Atomic Surface Tensions. *J. Phys. Chem. B* **2009**, *113*, 6378-6396.
144. Roy, L. E.; Hay, P. J.; Martin, R. L., Revised basis sets for the LANL effective core potentials. *J. Chem. Theory. Comput.* **2008**, *4*, 1029-1031.
145. Legault CY. CYLView, b., Université de Sherbrooke, Canada, 2009.
146. Sheldrick, G., SHELXT - Integrated space-group and crystal-structure determination. *Acta Crystallogr. A.* **2015**, *71*, 3-8.
147. Sheldrick, G., A short history of SHELX. *Acta Crystallogr. A.* **2008**, *64*, 112-122.
148. Brown, A. E.; Eichler, B. E., Symmetric diarylacetylenes: one-pot syntheses and solution photoluminescence. *Tetrahedron Lett.* **2011**, *52*, 1960-1963.
149. Zhang, J.; Hoye, T. R., Divergent Reactivity during the Trapping of Benzynes by Glycidol Analogs: Ring Cleavage via Pinacol-Like Rearrangements vs Oxirane Fragmentations. *Org. Lett.* **2019**, *21*, 2615-2619.
150. Nguyen, P. T.; Nguyen, H. T.; Pham, H. Q.; Kim, J.; Cordova, K. E.; Furukawa, H., Synthesis and Selective CO2 Capture Properties of a Series of Hexatopic Linker-Based Metal–Organic Frameworks. *Inorg. Chem.* **2015**, *54*, 10065-10072.
151. Zhou, Z.; Yu, J.; Colell, J. F.; Laasner, R.; Logan, A.; Barskiy, D. A.; Shchepin, R. V.; Chekmenev, E. Y.; Blum, V.; Warren, W. S., Long-lived $^{13}C_2$ nuclear spin states hyperpolarized by parahydrogen in reversible exchange at microtesla fields. *J. Phys. Chem. Lett.* **2017**, *8*, 3008-3014.
152. Vogt, A. Aufbau neuer, funktionaler Chromophore aus Acetylenen. ETH Zurich, **2009**.
153. Yamaguchi, Y.; Ochi, T.; Matsubara, Y.; Yoshida, Z.-i., Highly Emissive Whole Rainbow Fluorophores Consisting of 1,4-Bis (2-phenylethynyl) benzene Core Skeleton: Design, Synthesis, and Light-Emitting Characteristics. *J. Phys. Chem. A* **2015**, *119*, 8630-8642.
154. Tydlitát, J.; Fecková, M.; Le Poul, P.; Pytela, O.; Klikar, M.; Rodríguez-López, J.; Robin-le Guen, F.; Achelle, S., Influence of Donor-Substituents on Triphenylamine Chromophores Bearing Pyridine Fragments. *Eur. J. Org. Chem.* **2019**, *2019*, 1921-1930.
155. Hubschle, C. B.; Sheldrick, G. M.; Dittrich, B., ShelXle: a Qt graphical user interface for SHELXL. *J. Appl. Crystallogr.* **2011**, *44*, 1281-1284.
156. Ferger, M.; Berger, S. M.; Rauch, F.; Schönitz, M.; Rühe, J.; Krebs, J.; Friedrich, A.; Marder, T. B., Synthesis of Highly Functionalizable Symmetrically and Unsymmetrically Substituted Triarylboranes from Bench-Stable Boron Precursors. *Chem. Eur. J.* **2021**, *27*, 9094-9101.
157. Ladouceur, S.; Fortin, D.; Zysman-Colman, E., Role of substitution on the photophysical properties of 5,5′-Diaryl-2,2′-bipyridine (bpy*) in $[Ir(ppy)_2(bpy^*)]$ PF_6 complexes: A combined experimental and theoretical study. *Inorg. Chem.* **2010**, *49*, 5625-5641.

158. Chiu, C.-W.; Gabbaï, F. P., Diarylborenium Cations: Synthesis, Structure, and Electrochemistry. *Organometallics* **2008**, *27*, 1657-1659.
159. Mellerup, S. K.; Yuan, K.; Nguyen, C.; Lu, Z. H.; Wang, S., Donor-Appended N, C-Chelate Organoboron Compounds: Influence of Donor Strength on Photochromic Behaviour. *Chem. Eur. J.* **2016**, *22*, 12464-12472.
160. Ji, L.; Lorbach, A.; Edkins, R. M.; Marder, T. B., Synthesis and photophysics of a 2,7-disubstituted donor–acceptor pyrene derivative: An example of the application of sequential Ir-catalyzed C–H borylation and substitution chemistry. *J. Org. Chem.* **2015**, *80*, 5658-5665.
161. Fujihara, T.; Tomike, Y.; Ohtake, T.; Terao, J.; Tsuji, Y., Ruthenium-catalyzed ring-closing metathesis accelerated by long-range steric effect. *Chem. Commun.* **2011**, *47*, 9699-9701.
162. Chen, Z.; Jiang, H.; Li, Y.; Qi, C., Highly efficient two-step synthesis of (Z)-2-halo-1-iodoalkenes from terminal alkynes. *Chem. Commun.* **2010**, *46*, 8049-8051.